Design of porous materials with biomass for the methanol conversion into olefins

Qianwen Zheng

UNIVERSITÉ DE STRASBOURG

ÉCOLE DOCTORALE DES SCIENCES CHIMIQUES

Institut de Chimie et Procédés pour l'Energie, l'Environnement et la Santé, UMR 7515

THÈSE

présentée par :

Qianwen Zheng

soutenue le : **14 Décembre 2021**

pour obtenir le grade de : **Docteur de l'Université de Strasbourg**

Discipline / Spécialité : Chimie / Catalyse Hétérogène

Design of porous materials with biomass for the methanol conversion into olefins

THÈSE dirigée par :

M. LOUIS Benoît	Directeur de Recherche CNRS, Université de Strasbourg

RAPPORTEURS :

Mme. IVANOVA Svetlana	Professeur, Université de Séville
M. MUSYOKA Nicholas	Directeur de recherches, CSIR–Université Prétoria (Afrique du Sud)

AUTRES MEMBRES DU JURY :

Mme. ROGER Anne-Cécile	Professeur, Université de Strasbourg

“When work is a pleasure, life is a joy. When work is a duty, life is slavery!”

— Maxim Gorky

Acknowledgements

I am honored to spend my three years of my PhD period in such a beautiful city with a group of professional people. I would like to extend my deep gratitude to all those who have offered me a lot of help and support in the process of my thesis writing.

My deepest gratitude is first to my supervisor Dr. Benoît Louis, who has offered me numerous valuable comments and suggestions during my studies, especially when the investigation of mechanism puzzled me. And he always encouraged me profoundly throughout my Ph. D study. I have to say that without his insightful advice and encouragement, the completion of this Thesis would have been impossible.

Secondly, I would like to express my heartfelt thanks to colleagues in our lab. I would like to thank Anne-Cécile Roger, and it is a great pleasure to conduct my experiment in your lab. Besides, I would also like to thank my colleagues and the permanent staff: Ksenia, Sébastien, Clémence, Claire, Rogéria, Cristina, Lola, Arno, Camila, Diego, Morvan and Olesia for all the help, the beers after work, the international lunch, the skiing, …. I am especially grateful to Thierry Romero for all the SEM sessions and all colleagues who taught me to utilize the equipments. To Rogéria, she is my first friend in Strasbourg and really help me a lot before I came. And with Rogéria, Cristina and Renata, we had many happy times together both in Beijing and Strasbourg.

Special thanks to my boyfriend Liang Huang, who accompanies me every day both in life and work, even though we are far apart, also with a six-hour jet lag. He has supported every time and shared with my worries, frustrations and happiness. This Thesis however also could not have been possible without the support of him. With your concern by my side, I never feel alone.

Many thanks also go to all my friends, especially for Yu Zhang, dingkai Chen, Xiong Zhang, Han Peng, Jiang Jing, Liping Zhong, Xiaoxiao He, Jinming Zhang, Kaiyan Jin, for your friendship and support. We had lots of fun and shared many interesting things, and make me feel warm and happy every day.

Last but never, ever, least, I am deeply indebted to my family, who showed their concern and support when I pursued my study. Your support is unconditional, and I know I will always have a safe place to come back to if everything goes wrong. It is for you all the sacrifice and hard work. Love you.

Table of contents

List of abbreviations

AHFS	Ammonium Hexafluorosilicate
ANA	Analcime
BET	Brunauer-Emmet-Teller
BJH	Barrett-Joyner-Halenda
BPs	Biomass Pretreatment
BSST	Bio-Sourced Secondary Template
CNTs	Carbon Nanotubes
CS	Coffee Silverskin
DME	Dimethyl Ether
EDS	Energy Dispersive Spectrometer
EDTA	Ethylenediaminetetraacetic Acid
EFAl	Extra-framework Aluminum
EXAFS	Extended X-ray Absorption Fine Structure
FAU	Faujasite
FCC	Fluid Catalytic Cracking
FID	Flame Ionization Detector
FT-IR	Fourier Transformed Infrared Spectroscopy
FTS	Fischer-Tropsch synthesis
GC	Gas Chromatography
HTLcs	Hydrotalcite-like Compounds
ICPF	Institute of Chemical Process Fundamentals
IZA	International Zeolite Association
JCPDS	Joint Committee on Powder Diffraction Standards
LC-MS	Liquid Chromatography-Mass Spectrometry
LDHs	Layered Double Hydroxides
LDOs	Layered Double Oxides
LTA	Linde type A
MOFs	Metal-Organic Frameworks

MTG	Methanol-To-Gasoline
MTH	Methanol-To-Hydrocarbons
MTO	Methanol-To-Olefins
NBA	n-Butylamine
n-MR	n-Membered ring
OHL	Oxidized Hydrolysed Lignin
OSDAs	Organic Structure-directing Agents
PBU	Primary Building Units
PSS	Product shape selectivity
RSS	Reactant shape selectivity
SBUs	Secondary Building Units
SCG	Spent Coffee Grounds
SCR	Selective Catalytic Reduction
SDA	Structure-Directing Agent
SE	Secondary Electrons
SEM	Scanning Electron Microscopy
SSA	Specific Surface Area
STI	Stilbite Zeolite
TCD	Thermal Conductivity Detector
TEOS	Tetraethyl Orthosilicate
TETA	Triethylenetetramine
TGA	Thermogravimetric Analysis
TMA^+	Tetramethylammonium
TOS	Time-On-Stream
TPA^+	Tetrapropylammonium Amines
TPABr	Tetrapropylammonium Bromide
TPAOH	Tetrapropylammonium hydroxide
TPD	Temperature-Programmed Desorption
TSSS	Transition State Shape Selectivity

USMD	Umbrella Sampling Molecular Dynamics
VPT	Vapor Phase transport
WHSV	Weight Hourly Space Velocity
XRD	X-ray diffraction
ZGM	Zeolite Growth Modifier

Résumé en français

I. Introduction

Les défis sociétaux et environnementaux actuels conduisent les gens à revoir la nature de l'énergie à consommer et la manière de l'utiliser. Le lauréat du prix Nobel, George A. Olah, a proposé une alternative très intéressante pour utiliser plus efficacement les ressources disponibles en pétrole, charbon et gaz naturel et, à terme, libérer l'humanité de sa dépendance aux combustibles fossiles. Cette approche, basée sur la synthèse et la transformation du méthanol, est appelée le concept d'*économie du méthanol*. Le méthanol peut être une réelle solution du mix énergétique du XXI^{è} siècle. En effet, cette molécule simple peut être utilisée comme carburant à combustion propre ou comme matière première pour la production de nombreux intermédiaires de la chimie industrielle clés, tels que les mousses, les résines, les plastiques, les peintures, les polyesters et divers produits pharmaceutiques et de santé.[1, 2]

Le marché mondial exige que les industries chimiques et des matériaux réduisent le temps entre la recherche et le développement. Les zéolithes sont importantes dans de nombreux procédés, allant de l'adsorption et de l'échange d'ions à la catalyse. En termes de quantité, la catalyse représente de loin le plus grand marché pour les zéolithes, environ 60% du marché total et promet des taux de croissance élevés.

Bien qu'il existe de nombreux types de zéolithes acides susceptibles d'être utilisés dans le processus de conversion du méthanol, la ZSM-5 (de structure cristalline MFI), l'une des candidates potentielles, attire une attention particulière grâce à la topologie spécifique de sa structure, comme le diamètre des pores et la taille de la cage.[3] Aujourd'hui, de nombreux scientifiques ont cherché des stratégies pour ajuster les caractéristiques de cette zéolithe afin d'obtenir de meilleures performances catalytiques en raison de sa faible sélectivité.

Grâce à une recherche intensive, Rimer et ses collègues ont proposé une méthode bio-inspirée pour adapter la cristallisation des zéolithes en utilisant des modificateurs de croissance des zéolites (ZGM), qui sont capables de s'auto-assembler en s’adsorbant

sur des faces cristallines définies, régulant ainsi un mode de croissance anisotrope, permettant d'adapter la taille des particules et la morphologie des cristaux des zéolithes.[4, 5] S'inspirant de cette idée, B. Louis *et al*. ont mis au point une autre stratégie pour la synthèse de plusieurs structures de zéolithe, appelée stratégie du « template » secondaire bio-sourcé (BSST).[6] L'approche BSST consiste à modifier et à adapter les propriétés intrinsèques des zéolithes, comme la texture, la porosité et l'acidité, en utilisant des résidus de biomasse (déchets) bon marché. La compréhension du processus de synthèse des zéolithes et la connaissance approfondie de la nature des biomasses font défaut en raison de la complexité de ces deux processus. En outre, les interactions entre les BSST et les précurseurs inorganiques peuvent encore accroître la difficulté.[7] Récemment, notre groupe a présenté des zéolithes ZSM-5 présentant le plus faible rapport Si/Al = 8 connu à ce jour, en utilisant la bagasse de canne à sucre bon marché comme modificateurs de croissance cristalline. Par conséquent, des études approfondies sont menées dans cette thèse sur l'impact de l'utilisation de plusieurs types de biomasses dans la synthèse de type de zéolithe ZSM-5 pour améliorer la sélectivité envers les oléfines : on utilisera par exemple : la lignine (oxydée ou non), la bagasse de café usée, les déchets du thé et diverses algues (Figure 1). Toutes les algues que nous avons utilisées ont été obtenues auprès de « Institute of Chemical Process Fundamentals (ICPF) », Prague, République tchèque. Parmi elles, deux échantillons de biomasse de déchets à base d'algues d'eau douce (Trachydiscus minutus et Bracteacoccus bullatus, dénommés respectivement algaTM et algaBB) et le dernier échantillon consiste en un mélange de cyanobactéries d'eau douce (algaCM).

Figure 1. Différentes biomasses utilisées pour la synthèse des zéolithes.

Cette thèse se compose de 7 chapitres, commençant par une revue de la littérature sur les zéolithes, la valorisation de la biomasse et les applications choisies, et se terminant par des conclusions générales et des perspectives. Les synthèses de ZSM-5 assistées par biomasse ont été effectuées via la méthode hydrothermale avec deux rapports molaires différents, dénommées méthode A et méthode B, respectivement. Afin d'évaluer si les matériaux tels que synthétisés sont satisfaisants, tous les échantillons ont été caractérisés par DRX, MEB, BET et analyse NH_3-TPD en solution liquide, etc. Les performances catalytiques de la transformation du méthanol en oléfines (MTO) catalysée par des zéolithes acide ont été étudiées en utilisant un réacteur à lit fixe à pression atmosphérique et ont été analysées par GC.

II. Résultats et discussions

i. Synthèse et caractérisation des zéolithes ZSM-5 assistées par la biomasse

a. Influence de différentes biomasses et du temps hydrothermique sur la synthèse de ZSM-5

Avant de déterminer les méthodes, nous devons préciser que le processus

hydrothermique de synthèse des zéolithes avec des biomasses est assez complexe, et qu'il est affecté par de nombreux facteurs, tels que: la nature des réactifs, le rapport Si/Al, le type et la quantité de biomasse, la durée et la température du processus, la durée et la température de la calcination, etc. Heureusement, sur la base des données de ma littérature, notamment des travaux réalisés au sein de notre équipe, nous pouvons principalement nous focaliser sur l'influence de la biomasse et du temps hydrothermique sur la synthèse de la ZSM-5. Par conséquent, une série de zéolithes ZSM-5 obtenue avec de la lignine oxydée a été préparée en optimisant le temps hydrothermique entre 2 et 7 jours, ainsi que la quantité de lignine oxydée de 200, 300 et 500 mg. Il s'avère que la quantité optimale de biomasse est de 300 mg.

D'après les études de cristallographie décrites en Figure 2, il est possible de confirmer la seule présence de la structure MFI. Il est intéressant de mentionner que la plupart des zéolithes produites via l'assistance de biomasse ont montré des intensités plus élevées pour les réflexions principales (101), (200), (501), (151), (313) par rapport aux échantillons de référence. Par conséquent, cela a démontré que la stratégie BSST joue un rôle positif dans la synthèse des zéolithes et n'entraînera pas de cristallisation vers d'autres structures.

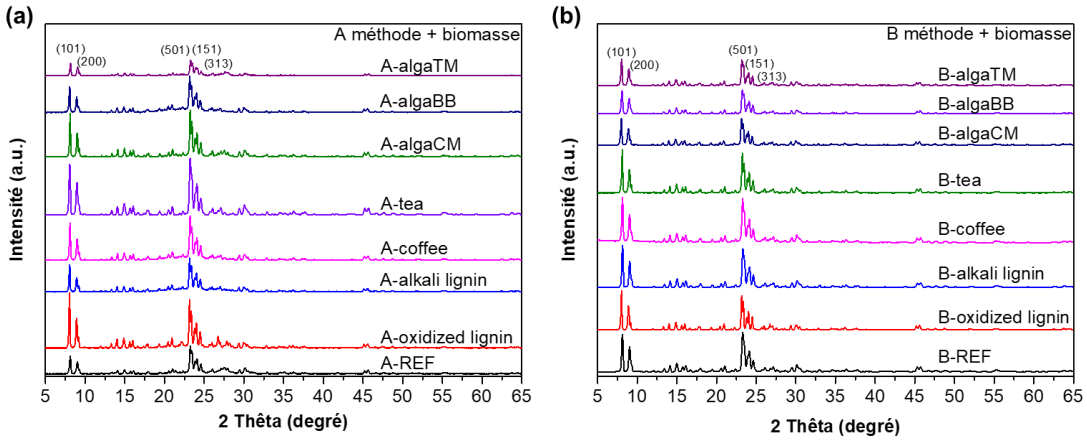

Figure 2. Diffractogrammes sur poudre de ZSM-5 parente (sans biomasse) et des matériaux ZSM-5 préparés avec différentes biomasses par la (a) méthode A et (b) méthode B.

Ces matériaux ont également été caractérisés par des mesures de physisorption de N_2, de MEB, de l'ATG et d'acidité et les résultats sont soigneusement décrits dans le présent chapitre. Il apparaît que les surfaces totales et la surface des micropores des ZSM-5 augmentent lors de la présence de biomasse. En outre, les morphologies des cristaux sont différentes en raison de l'effet du BSST et d'une cristallisation bimodale, mais pour la plupart d'entre eux sont montrés les cristaux caractéristiques en forme de « cercueil » (coffin-shape), associés au type de zéolite ZSM-5 avec des tailles de cristaux de 4-10 μm ou des cristaux cubiques avec une surface rugueuse pour les zéolites assistées par le thé. L'acidité des catalyseurs ZSM-5 et ZSM-5 dérivés de biomasses a été déterminée par NH_3-TPD. Les pics aux alentours de <250 °C, 250-350 °C, et 350-500 °C correspondaient à la désorption de NH_3 en position acide faible, acide moyen et acide fort.[8] Chaque échantillon a montré des résultats différents pour ses propriétés acides par l'assistance de diverses biomasses. En raison de la complexité de la biomasse, il est difficile de tirer des conclusions de ces seules données et de préciser comment les biomasses impactent l'acidité.

b. Influence de la quantité de TPAOH

Les gabarits organiques tels que l'hydroxyde de tétrapropylammonium (TPAOH) ont généralement été utilisés pour la préparation de la zéolithe ZSM-5, qui joue un rôle important à la fois dans l'orientation de la structure et le remplissage des micropores. Cependant, l'utilisation extensive et abondante des gabarits a causé une série de problèmes, tels que (1) la plupart des gabarits organiques sont chers, et leur prix limite leur application dans l'industrie, (2) les gabarits organiques sont toxiques et peu respectueux de l'environnement, (3) l'élimination des gabarits organiques se fait normalement par calcination à haute température, ce qui entraîne un grand nombre de gaz polluants (par exemple, NO_x et CO_2).[9] Dans ce chapitre, nous avons également étudié l'influence de la quantité de gabarit TPAOH pendant le processus de synthèse de la ZSM-5, et nous avons essayé de réduire l'utilisation de ce gabarit afin de réduire davantage le coût de la synthèse.

Comme le montre la Figure 3, il est facile d'observer que les pics caractéristiques de la structure MFI sont plus évidents avec l'augmentation de la quantité de gabarit pour un même temps hydrothermique (2 jours). Il n'y a presque pas de cristallisation, principalement une phase amorphe dans A-tea-0%TPAOH. Cela indique que le structurant organique est nécessaire pour le processus de synthèse et ne peut être totalement remplacé par la biomasse. Lorsque la quantité atteint 50%, l'intensité des pics est supérieure à celle de la zéolithe de référence avec 100% de TPAOH, ce qui signifie que les feuilles de thé usées ont organisé et mélangé les réactifs dans des dispositions favorables à la nucléation et à la croissance des particules de ZSM-5. Bien que les résidus de thé ne puissent pas remplacer complètement le rôle du gabarit organique, ils peuvent promouvoir efficacement le processus de cristallisation, réduire l'utilisation du gabarit et réduire le temps de synthèse.

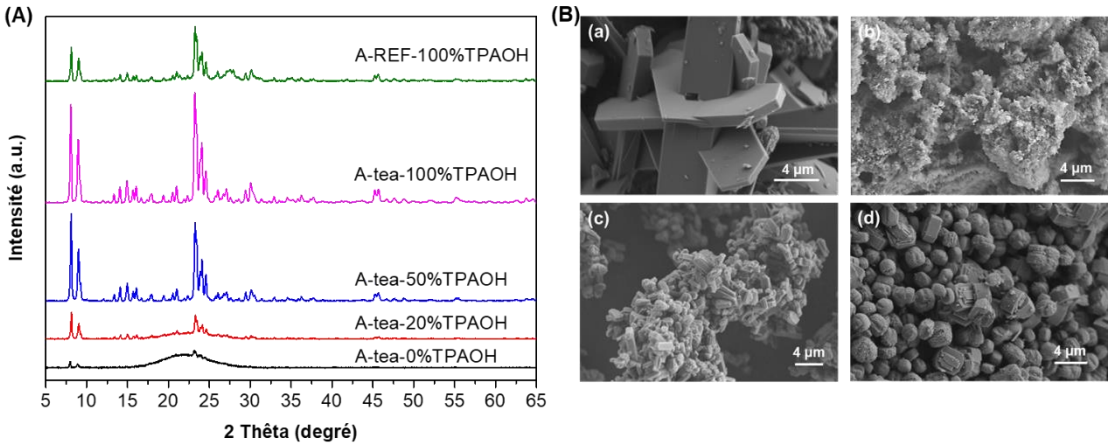

Figure 3. (A) Diffractogrammes sur poudre des zéolithes de référence ZSM-5 et A-tea avec 0, 20, 50 et 100% de TPAOH. (B). Images MEB de (a) A-REF, (b-d) A-tea-2d-300 avec 20, 50 et 100% TPAOH.

ii. Conversion du méthanol en oléfines légères sur des zéolithes ZSM-5 assistées par la biomasse

La réaction du méthanol en oléfines (MTO) est l'une des options idéales pour valoriser les réserves de gaz naturel, suscitant un intérêt industriel considérable. En outre, la demande du marché mondial pour l'éthylène et du propylène augmente progressivement

et les taux de croissance prévus lors des prochaines décennies devraient rester élevés. Par conséquent, notre objectif est de tester la performance catalytique de la ZSM-5 de référence et de toutes les ZSM-5 assistées par la biomasse et d'évaluer leur performance catalytique en termes de taux de conversion, de sélectivité et de stabilité.

Les performances catalytiques des zéolithes à base de feuilles de thé par la méthode A sont présentées dans la Figure 4(a). Par rapport à la ZSM-5 de référence, nous pouvons voir que les zéolithes à base de feuilles de thé (100% TPAOH) ont présenté des bonnes performances de conversion et de stabilité. La durée de vie du catalyseur ZSM-5 à base de feuilles de thé a augmenté à plus de 60 h et peut maintenir la conversion presque complète du méthanol et de l'éther diméthylique pendant cette période. En outre, la sélectivité envers les oléfines légères (C_2-C_4) peut atteindre 83% (augmentation d'environ 31%), et la sélectivité du propylène est d'environ 50%, comme le montre la Figure 4(b et c). Pour les zéolithes synthétisées par la méthode B, il y a des améliorations évidentes dans la performance catalytique (taux de conversion, stabilité, et sélectivité) en ajoutant différentes algues. Même si le taux de conversion de 3 types de ZSM-5 assistées par des algues n'atteint pas 100%, leur stabilité est améliorée de manière significative. Après environ 80-150 h, le taux de conversion est encore de 50%, comme le montre la Figure 4(d). De même, dans la Figure 4(f), l'amélioration significative de la sélectivité (C_2-C_4) peut également être observée sur B-algaCM, B-algaBB et B-algaTM, qui sont de 59%, 60% et 62% (augmentation de 61%, 66% et 71%, respectivement).

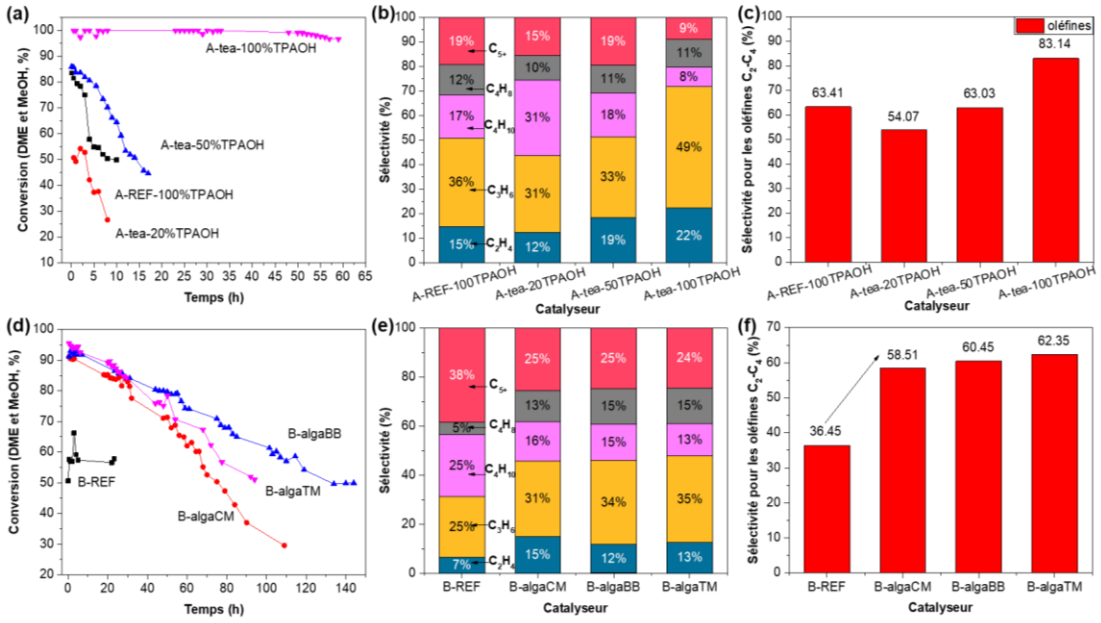

Figure 4. (a, d) Conversion du méthanol et du DME en hydrocarbures en fonction du temps de réaction en continu (time-on-stream, TOS), (b, e) Sélectivité envers les différents hydrocarbures. (C_2H_4, C_3H_6, C_4H_{10}, C_4H_8 et C_5^+), (c, f) Sélectivité vers les oléfines (C_2-C_4). (450 °C, TOS = 1 h, et WHSV = 2 h^{-1})

iii. Proposition de mécanisme de l'impact des gabarits secondaires biosourcés (BSST) sur la formation des cristaux de zéolithe ZSM-5

La caractérisation et la performance catalytique des zéolithes ZSM-5 ont démontré que l'utilisation de résidus de biomasse peut avoir un impact sur la construction des sous-unités cristallines et modifier la taille et la morphologie des cristaux, ce qui permet d'améliorer le taux de conversion, la stabilité et la sélectivité dans la réaction MTO. Cependant, le mécanisme impliquant le BSST sur la formation des cristaux n'est pas encore clairement établi en raison de la complexité de la structure et de la composition des biomasses organiques. Par conséquent, l'un des objectifs de ce travail est de proposer un mécanisme rationnel sur la nature des interactions entre les dérivés de la biomasse et les précurseurs inorganiques construisant la charpente de la zéolithe.

Grâce à de nombreuses techniques de caractérisation, tant sur les biomasses que sur les zéolithes, nous déduisons que les performances catalytiques sont améliorées par modulation des propriétés acido-acides des ZSM-5 (Figure 5).

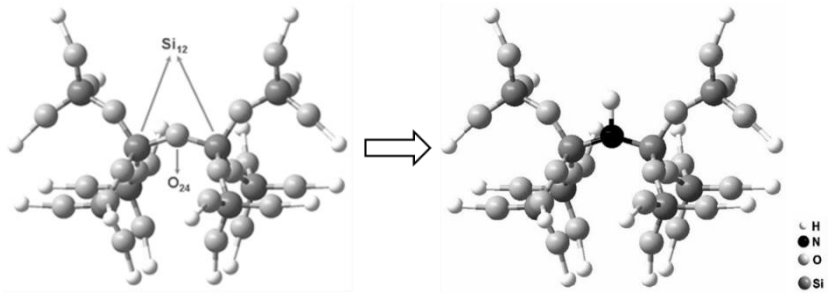

Figure 5. Modèle d'amas de zéolite ZSM-5 et de zéolite ZSM-5 incorporée à l'azote.[10]

III. Performance catalytique des matériaux dérivés des hydroxydes doubles lamélaires (LDHs) dans les réactions en phase gaz-solide et liquide-solide

Les catalyseurs à base de LDHs pour la conversion du méthanol, en tant que matériaux multifonctionnels adaptables à la composition, n'ont été que rarement étudiés. Notre étude visait à comparer le comportement catalytique de différents types de LDHs. Les LDHs ont été préparés par une méthode conventionnelle de co-précipitation avec différents cations M^{2+} (Mg, Cu, Ni, Zn) et M^{3+} (Al, Fe, Co). Tous les LDHs synthétisés ont été soigneusement caractérisés par la DRX, ATG, MEB, FT-IR et les analyses d'adsorption-désorption d'azote. Enfin, leurs performances catalytiques ont été évaluées dans la conversion du méthanol en hydrocarbures mais aussi dans l'oxydation en phase liquide de l'alcool benzylique afin d'évaluer la versatilité de ces matériaux dans différents environnements réactionnels.

Alors que $CuAlO_x$ a démontré une haute sélectivité dans le DME (Figure 6), $NiFeO_x$ a montré une sélectivité de 100% pour le CH_4 à conversion complète et une haute stabilité (supérieure à 30 h), suggérant que $NiFeO_x$ pourrait être un candidat potentiel pour la réaction réversible extrêmement importante d'oxydation du CH_4 en méthanol.

Enfin, ces matériaux dérivés de la LDH ont également été testés avec succès dans l'oxydation en phase liquide de l'alcool benzylique avec de l'oxygène, ce qui renforce encore leurs applications en catalyse et pourquoi pas pour cibler des synthèses vertes de produits chimiques à haute valeur ajoutée.

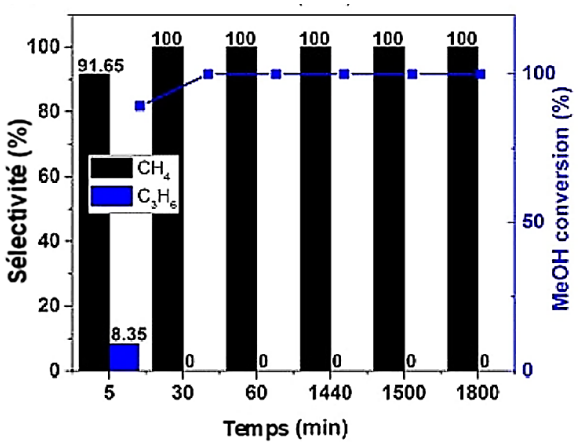

Figure 6. Conversion du méthanol et sélectivités pour le système $NiFeO_x$.

IV. Conclusion générale

Une caractérisation approfondie a confirmé que l'une des zéolithes produites par assistance de la biomasse (feuilles de thé) présente d'excellentes performances catalytiques, avec une longue durée de vie et une conversion presque totale du méthanol durant 60 h. Une sélectivité élevée pour les oléfines légères et le propylène a également été obtenue. Le mécanisme possible de l'impact des feuilles de thé usées et d'autres biomasses sur la construction de la sous-unité cristalline et sur la composition morphologique et chimique ainsi que sur les propriétés de surface a également été étudié.

De plus, ce travail offre non seulement d'excellents catalyseurs ZSM-5 pour la conversion du méthanol, mais implique également une stratégie appelée modèle secondaire bio-sourcé (BSST) pour les synthèses de zéolithes et la valorisation de déchets de différentes biomasses.

General Introduction

1. Goal and scope of the Thesis

Actual societal and environmental challenges lead mankind to revise the nature of the energy as well as its consumption patterns. Nobel Prize laureate, Olah suggested a very attractive alternative to use more efficiently available oil, coal and natural gas resources and, eventually, to free humankind from its dependence on fossil fuels. This approach is based on methanol synthesis and its transformation, being so-called the "Methanol economy" concept.[11] Indeed, this simple molecule has the versatility to be used as clean-burning, biodegradable fuel or as a feedstock for the production of numerous key petrochemical building blocks, such as foams, resins, plastics, paints, polyesters and a variety of health and pharmaceutical products. Therefore, the methanol-to-olefins (MTO) reaction becomes even more prominent in C_1 chemistry, providing a chance to fabricate basic petrochemicals from non-oil resources such as coal and natural gas.[12]

Besides, zeolites are important in many processes, ranging from adsorption and ion-exchange to catalysis. In value terms, catalysis represents by far the largest market for zeolites, approximately 55% of the total and promising high rates of market growth.[13] Although there are many kinds of acidic zeolites with potential to be used in the MTO reaction, ZSM-5 (MFI framework) as one of potential candidates, draws considerable attention thanks to its specific framework topology, such as the pore diameter and cage size. Nowadays, many scientists have looking for strategies to tune the characteristics of this zeolite to reach higher catalytic performance.

Through a comprehensive research and experimental proof, Rimer and co-workers have proposed a novel method for tailoring zeolite morphology by using "zeolite growth modifiers" (ZGMs), considering organic molecules interacting with soluble silicate or aluminate species (monomers) during the self-assembly process and tailoring their growth.[4] Inspired by this, our group developed a related strategy, named as "bio-sourced secondary templates" (BSST) for the synthesis of zeolites.[6] However, since this strategy has only been put forward in recent years, the related study is still at the early

stages of exploration, and there are wide unknown areas waiting to be explored.

The work described in this Thesis aims therefore in the design of ZSM-5 zeolites with biomass, supposed to act as BSST, for the MTO reaction. Through rational design of biomass-assisted zeolite, significant progress on catalytic activity, selectivity and longer lifetime could be achieved in the MTO reaction.

Firstly, to achieve this goal, a series of ZSM-5 zeolites have been synthesized by hydrothermal reaction via the addition of different kinds of biomasses. Herein, the study of several biomasses (*i.e.* oxidized lignin, Russian lignin, sugarcane bagasse, ecoshell, coffee, tea residues, algae and a commercial Kraft lignin, denoted as alkali lignin) not only helps to summarize the regularity of my research, but also contributes to provide a large database for future investigation of BSST strategy. Besides, the rational design of an "optimal" catalyst should combine several factors in order to exhibit a proper morphology, structure and acid site strength and density. Hence, the optimal hydrothermal duration and biomass composition and quantity were studied for the synthesis of ZSM-5 zeolites. Moreover, three different preparation methods (Z-LO-07, A and B methods) and the influence of the amount of TPAOH template were also evaluated. Detailed characterizations of as-synthesized ZSM-5 zeolites in terms of textural, structural and their surface acidic properties have been conducted to explore the effects of biomasses extra-addition on zeolite crystals.

For the MTO reaction, all as-prepared zeolites were tested to assess their catalytic performance. We mainly focus on how the alkaline hydrolysates of biomass used as bio-sourced secondary templates (BSST) impacted the catalysts performance: activity, selectivity and stability. From our studies, one promising biomass-assisted zeolite, tested in the MTO reaction, led to an excellent catalytic performance and was therefore compared with two benchmark zeolites.

To explain aforementioned experimental results, and gain further understanding on BSST strategy, we also attempted to investigate the mechanism(s) of bio-sourced secondary templates (BSST) impact on zeolite crystal formation and further effect the catalytic performance in the MTO reaction. The main active ingredients in the biomass involved in the zeolite growth and a tentative mechanism were proposed in this Thesis.

In addition, the structure-activity relationships of ZSM-5 catalysts in the presence of biomass were studied to further illustrate the reason for catalytic performance changes. Through the discussion of a tentative self-assembly mechanism, we suggest therefore that the MTO catalytic performance enhancement can be achieved by the judicious selection of BSST nature.

In addition, the preparation of layered double hydroxides (LDHs) and their application in the methanol conversion were presented. Series of detailed characterization were conducted over as-prepared LDHs.

Finally, we hope that some promising zeolites with high performance could be found and applied in the MTO reaction. Through further studies, the tentative self-assembly mechanism between biomass molecules and T-monomers is put forward and helps to deepen the understanding of the BSST strategy. Therefore, a facile and cheap route for zeolite synthesis, the improvement of catalytic performance in the MTO reaction as well as valorization of bio-wastes could achieved at the same time with the guidance of BSST strategy.

2. Outline of the Thesis

The Thesis consists of 6 chapters, starting with a literature review on zeolites, biomasses and the MTO reaction, ending with catalytic performance of LDHs derived materials in methanol conversion reaction, preceded by this general introduction and a summary in French, and the last part gives general conclusions and future prospects.

Chapter 1 presents an overview of the background and current research progress on zeolites, biomasses and the MTO reaction.

Chapter 2 describes the materials and synthesis methods used to accomplish this work. Besides, the characterization techniques, operating conditions and the experimental set-up used for the MTO reaction were also performed in this Chapter.

Chapter 3 relates a series of biomass-assisted ZSM-5 zeolites synthesis by optimizing the hydrothermal duration, biomass composition and quantity, gel composition and the TPAOH amount. Herein, 8 different kinds of biomasses from Europe, South America and Asia and a commercial alkali lignin were selected as BSSTs

in the zeolite crystallization process. Then, as-synthesized biomass-assisted ZSM-5 zeolites were characterized by XRD, SEM, BET, and NH_3-TPD techniques to investigate the effects of biomass extra-addition.

Chapter 4 addresses the catalytic performance of ZSM-5 catalysts in the presence of biomass in the MTO reaction. For comparison, three different preparation methods (Z-LO-07, A and B methods) were evaluated. The results show the higher catalytic performances of ZSM-5 zeolites reached via the addition of oxidized lignin, tea residues and three algae. Among them, tea-assisted ZSM-5 catalyst also compared with two benchmark zeolites and other reported biomass-assisted zeolites, exhibiting higher activity, selectivity towards C_2-C_4 olefins and stability. ZSM-5 zeolites using three algae (algaCM, algaBB and algaTM) also showed prolonged lifetime.

Chapter 5 investigates the tentative mechanism(s) of biomass acting as bio-sourced secondary templates (BSST) and how they interact with T-monomers. Further, how the BSST species modify the zeolite and then impact the catalytic performance in the MTO reaction were also explored. It indicates that BSST acted both as "inhibitor" for the zeolite crystal growth in the b-axis direction and as "promoter" to accelerate the kinetics of crystallization due to an interaction between hydroxyl, carboxyl and amino groups of BSST with aluminates and silicates species. In summary, this study elucidates the tentative mechanisms and suggests a feasible way to tailor zeolite morphology and further promote the catalytic performance.

Chapter 6 reports the preparation of layered double hydroxides (LDHs) and their application in the methanol conversion. The results indicate that LDH derived materials act as selective catalysts towards dimethyl ether (DME), methane or light olefins formation, depending on their chemical composition.

General conclusions summarize the most promising results and propose future prospects for this work.

3. List of scientific contributions

1) **Qianwen Zheng**, Liang Huang, Ziyi Zhong, Benoît Louis, Qiang Wang, Synthesis of $K_xNa_{2-x}TiO_3$ as a novel CO_2 sorbent for high-temperature CO_2 sorption with fast sorption rate, ***Chem. Eng. J.***, 380(2020)122444.
2) Liang Huang, Cristina Megías-Sayago, Rogeria Bingre, **Qianwen Zheng**, Qiang Wang*, Benoit Louis*, Catalytic performance of layered double hydroxides (LDHs) derived materials in gas-solid and liquid-solid phase reactions, ***ChemCatChem***, 11(2019)3279-3286.
3) Wanlin Gao, Shuyu Liang, Rujie Wang, Qian Jiang, Yu Zhang, **Qianwen Zheng**, Bingqiao Xie, Cui Ying Toe, Xuancan Zhu, Junya Wang, Liang Huang, Yanshan Gao, Zheng Wang, Changbum Jo, Qiang Wang, Lidong Wang, Yuefeng Liu, Benoit Louis, Jason Scott, Anne-Cecile Roger, Rose Amal, Hong He, Sang-Eon Park, Industrial carbon dioxide capture and utilization: State of the art and future challenges, ***Chem. Soc. Rev.***, 49(2020)8584-8686.
4) Qiang Wang, Liang Huang, **Qianwen Zheng**. A carbon dioxide adsorption material and its preparation method, Chin. Pat. Appl. Publ., (2020) No. ZL201710239197.8.

Chapter 1. Literature review

Abstract

The literature background presented in this chapter is divided into three main parts:

(1) The zeolite will be defined along with some generalities and details regarding their structure, main features and properties, different modification methods, and their main applications.

(2) This part briefly introduces six kinds of biomasses which we used in the synthesis of ZSM-5 zeolite catalysts. Then, a focus is given for Bio-Sourced Secondary Template (BSST) concept and the current progresses on zeolite synthesis from biomass waste were also summarized in this section.

(3) The last section mainly discussed the ZSM-5 application in the Methanol-To-Olefins (MTO) reaction.

1.1 General description of zeolites

1.1.1 What are zeolites?

In recent decades, porous materials arose wider attention all over the world and are extensively used in chemical industry and daily life due to their common features of regular and uniform porous structures. Among them, zeolites act as one of the leaders, the research on their synthesis, modification and applications is still expanding.

The term zeolite was first proposed by a Swedish mineralogist, Axel Fredrik Crønstedt in 1756, by rapidly heating the minerals in a copper mine in Lappmark.[14] He observed that the material released huge amounts of vapor it had previously absorbed within its pores. Therefore, he named this material as zeolite, which derived from two Greek roots, the Greek ζέω (zéō), meaning to boil, and λίθος (líthos), meaning "stone", literally “boiling stone”. Zeolites can be classified either as natural and synthetic. Since Crønstedt's initial discovery of stilbite, approximately 50 zeolites have been found in nature. Raw zeolites crystallize from glass-rich volcanic ashes and rocks reacting with the high-pH alkaline groundwater after several thousands to million years in post-depositional environments.[15] Natural zeolites are abundant, low-cost materials, especially when local deposits can be used. However, naturally occurring zeolites are rarely pure and therefore barely suitable for industrial and commercial applications in numerous cases.[16] Due to this reason, natural zeolites mostly appear in geological research, jewelry and as construction material, just like people used them to build pyramids and temples in Mexico and of houses and churches in Cappadoccia.[17] Figure 1.1 presents a beautiful zeolite crystal to illustrate the natural occurrence of those amazing materials.

Figure 1.1 Crystal of a natural zeolite.

Fortunately, with the improvement of material science and emerging characterization techniques, zeolite could be prepared in laboratory. In 1948, Richard M. Barrer synthesized the first zeolite[18, 19] by putting one unknown natural mineral in a strong salt solution at high temperature, which was considered to have the KFI topological structure and subsequently named ZK-5 zeolite.[20-22] After this milestone discovery, his friend, Robert Milton in the Linde Division of Union Carbide Corporation attempted to use more reactants under milder conditions to prepare zeolites, and finally such as Na-P and X type zeolites were successfully synthesized.[23, 24] Up to date, more than 240 different zeolite frameworks have been identified and classified by the International Zeolite Association (IZA) database, and about 40 natural zeolites are known. Each framework can be classified according to its symmetry and characteristic X-ray powder diffraction pattern, will be named by IZA referring by a three-capital-letter code according to the rules set up by IUPAC Commission.[25] For example, the LTA code corresponds to Linde Type A, CHA is derived from Chabazite, and FAU is employed for Faujasite, etc.

1.1.2 Nomenclature and topological structure

Zeolites, also called molecular sieves, are microporous crystalline hydrated aluminosilicates with a framework constructed by a 3D porous network of TO_4 tetrahedra units, most commonly SiO_4^{4-} or AlO_4^{5-} by sharing oxygen atoms,[26] as shown in Figure 1.2. The tetrahedron unit mainly consisted of silicon, aluminum and oxygen,

but other elements like boron, phosphorus, zinc, gallium, germanium, titanium, iron, … may also occupy certain T-positions in tetrahedral sites.[27] Due to the presence of trivalent Al^{3+} cations, each AlO_4^{5-} tetrahedron introduces one negative charge inside the zeolite framework which needs to be compensated by cations, such as alkali or alkaline-earth metals. The cations are mobile and have exchange capability in solution. It is widely known that acid sites are closely related to Al atom and Brønsted acid sites consist in tetra-coordinated Al located at different T positions with bridging -OH groups.[28] This part is detailed later in the Thesis. The general unit formula of zeolites can be written by equation (1):

$$M_{x/n}(AlO_2)_x(SiO_2)_y \cdot zH_2O \quad (1)$$

where M is the cation which counter-balances the negative charges mentioned before (*e.g.* H^+, Na^+, Ca^{2+}, Mg^{2+}), and the characteristic to exchange by monovalent or multivalent cations is also well known as the functional cation-exchange properties of zeolites, x is the number of Al per unit cell, n is the valence of the cation M, and the ratio of y/x represents an important ratio of SiO_2/Al_2O_3 (SAR), z defining the number of molecules of water. Besides, the direct linkage of Al-O-Al is not allowed according to Loewenstein's rule.[29]

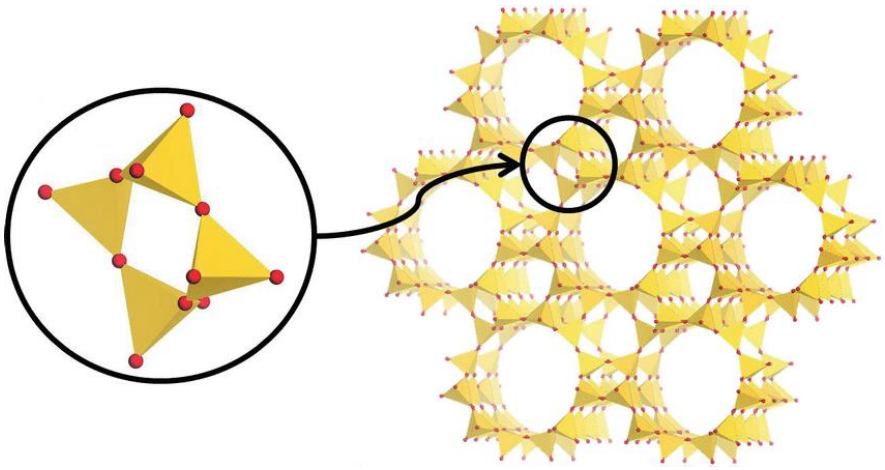

Figure 1.2 TO_4 tetrahedra units' self-assembly to generate a 3D framework.

Many primary building units (PBUs, i.e., TO_4 tetrahedra) combine with each other by sharing oxygen bridges and generate the secondary building units (SBUs),[30] and

allow for the formation of channels and cages in different 3D arrangements, subsequently.[31] As shown in Figure 1.3, there are some different secondary building units which self-arrange by aluminosilicates (TO_4 tetrahedra), and used for building desired zeolite frameworks. More details like the oxygen atoms are not described in this representation, only the atoms links between these members. Because of the limitation of the reasonable connections between primary building units, 23 types of possible SBUs are currently known.[32]

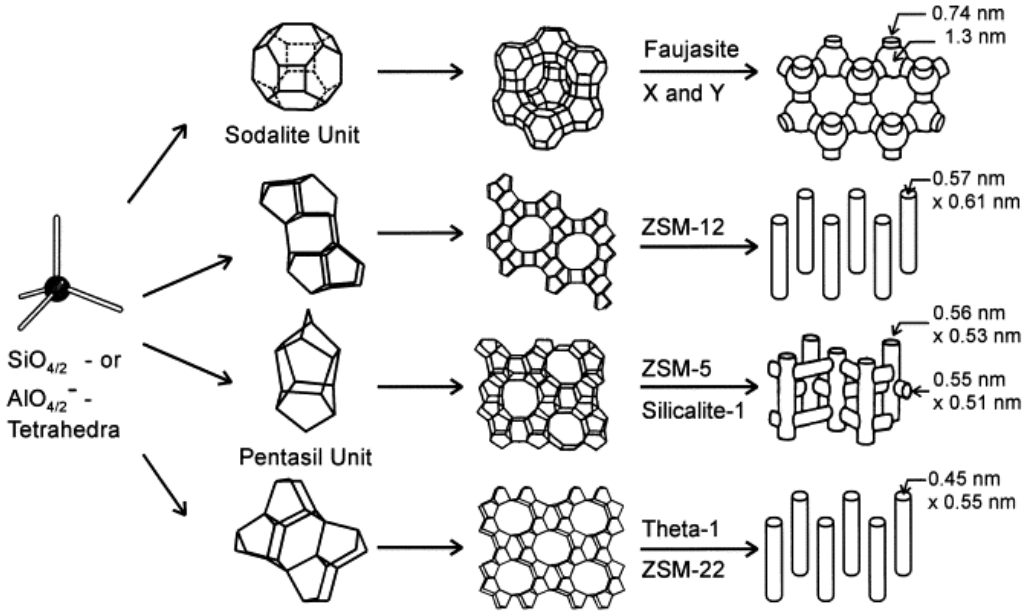

Figure 1.3 Development of zeolite framework from PBU.

Moreover, thanks to the interconnection between secondary building units, the various types of channel systems are formed by 6-, 8-, 9-, 10-, 12-, 14-, 18-, and 20-membered ring pores.[33] The number of T-atoms defines the ring, called n-membered ring (n-MR). Hence, zeolites can be classified into four types by their channel systems and pore sizes:[34]

a. Small pore zeolites: 8-MR with a pore diameter less than 4 Å, such as LTA.
b. Medium pore zeolites: 10-MR with a pore diameter around 5.5 Å (MFI).
c. Large pore zeolites: 12-MR with a pore of approximately 7.5 Å, like FAU.
d. Extra-large pore zeolites: > 12-MR having a pore diameter larger than 7.5 Å, like CFI.

Although zeolites with extra-large pores are difficult to synthesize, this field remains still attractive because of the unique applications of extra-large pore zeolites. They can be used in hydrocracking, catalysis and separation of large molecules.[35, 36] Up to now, few extra-large-pore zeolites have been proposed among the ~250 zeolites in the whole zeolite family,[37] such as aluminophosphate / gallophosphate zeolites (*e.g.,* VPI-5,[38] $AlPO_4$-8,[39] ITQ-51[40]), pure silicates (*e.g.,* UTD-1,[41] CIT-5[42]), substituted silicates (*e.g.,* OSB-1,[43] SSZ-53, SSZ-59,[44] EMM-23,[45] ECR-34[46]) and germanosilicates (*e.g.,* ITQ-15,[47] NUD-1[48]). Besides, there is another classification to define zeolites in 1D (*e.g.,* AFI type), 2D (*e.g.,* MOR type) or 3D (*e.g.,* MFI type) channel systems according to their pores' connecting way.[49]

1.1.3 Zeolite synthesis

The history of zeolite synthesis can be traced back to 1862. Most of the explorations in early stage imitated the formation conditions of natural zeolites with high temperature (more than 200 ^oC) and high pressure (higher than 100 bar). Until the late 1940s, the methodologies were developed by Milton's team under mild conditions by using alkali metal aluminosilicate gels at low temperature and autogenous pressure.[50]

Besides conventional hydrothermal approach, novel routes for synthesizing zeolites have been explored, like solvothermal synthesis,[51] vapor phase transport (VPT) synthesis,[52] transformation route,[53] solid-state technique,[54] microwave-assisted synthesis[55] and topotactic condensation of a layered precursor.[56] There is no doubt that hydrothermal process still remains the most common method, however each route exhibits its own advantages.[57]

Due to their regular framework, pure crystallization and adjustability, synthetic zeolites are generally used in several fields in contrast to natural zeolites. The common synthesis of zeolites mainly uses hydrothermal method, involving the source of silicon, aluminum, template, mineralizing agent and usually water. Thanks to its inherent advantages, like easy operation, fully crystallization, low energy consumption, etc., this conventional synthesis strategy is more appropriate than others. A brief description of each reactant role is given hereunder as follow, along with the schematic diagram

(Figure 1.6):

- *silicon source*

The source of silicon is a critical parameter during the synthesis. The major silicon sources are sodium silicate, fumed silica, colloidal silica, tetraethyl orthosilicate (TEOS), etc.[58] Many studies show that the nature of the silicon source will affect the particle morphology, crystallization rate and size of zeolite crystals as well as other factors, thus the choice of silicon source plays an important role in the synthesis protocol. For example, the silicon source with high specific surface area is easier to nucleate and form smaller particles than that with lower specific surface area.

The syntheses are not eco-friendly and costs a lot because of the reactants. In order to develop more environmentally friendly strategies and reduce the cost, several natural raw silicon sources were investigated, such as clay minerals,[59] fly ash,[60] diatomite,[61] etc. This kind of source is abundant, exploited at low price. Usually, it can be regarded as a mean of utilization of wastes and to realize a new recycling of resources. However, it should be noted that most of natural materials are not very pure. For example, the diatomite may include iron, potassium, calcium and non-metallic constituents, which may have a positive or negative effect on the crystallization process. Therefore, purification treatment may be needed before using bulk silicon sources.

- *aluminum source*

Likewise, the source of aluminum also has an influence on the nucleation phenomenon. The main concern is to select a proper aluminum source among sodium aluminate, aluminum hydroxide, metallic aluminum, aluminum nitrate, aluminum sulfate, pseudo-boehmite, aluminum isopropoxide, ….[62, 63] Moreover, the appearance of $Al(OH)_4^-$ in a basic solution facilitates the nucleation process.

The SiO_2/Al_2O_3 molar ratio (SAR) becomes therefore an undeniable parameter in properly controlling the structure and composition of as-prepared zeolites in the solution. When the SiO_2/Al_2O_3 molar ratio ≤ 5, zeolites as LTA, FAU, SOD are obtained from strongly alkaline solutions. In contrast, zeolites which SAR higher

than 10 can be produced at milder alkalinity or in neutral F^- medium (BEA, MFI and MEL-types). The Si/Al molar ratio become the main parameter used for the classification of zeolites.

- *Structure-directing agent (SDA)*

The structure directing agents can be alkali metal cations or positively charged organic molecules, which provide a surface with positive charges to arrange AlO_4^- and SiO_4^- tetrahedra around during the nucleation stage. Actually, the structure-directing agent not only plays the role as a template to guide the formation of certain framework, but also provide an alkali environment during the reaction and acts as a charge-compensation cation.

The structure directing agents are usually organic molecules.[64] Barrer and Kerr reported the organic molecules in zeolite synthesis by using tetramethylammonium (TMA^+) cations in the gel mixture, which led to achieve a high Si/Al ratio zeolite.[65, 66] G. Kerr at Mobil company introduced quaternary ammonium cations in the synthesis mixtures.[67] After, many attempts have been made to produce high silica zeolites and novel framework structures.

The organic structure-directing agents (OSDAs) can also be referred to as "templates". Various kinds of organic species can be used as OSDAs, like tetrapropylammonium hydroxide (TPAOH), tetrapropylammonium bromide (TPABr) or even crown ethers. However, from an economic and eco-friendly perspective, n-butylamine (NBA) seems to be a good alternative to SDAs owing to its low cost.[68]

Although the mechanism of zeolite formation is still far from being understood, due to the numerous physical and chemical steps, equilibria and solubility variations of reactants; Fortunately, the auto-assembly mechanism between the hydrophobic silicate and organic template has been investigated and reported, as shown in Figure 1.4.[69]

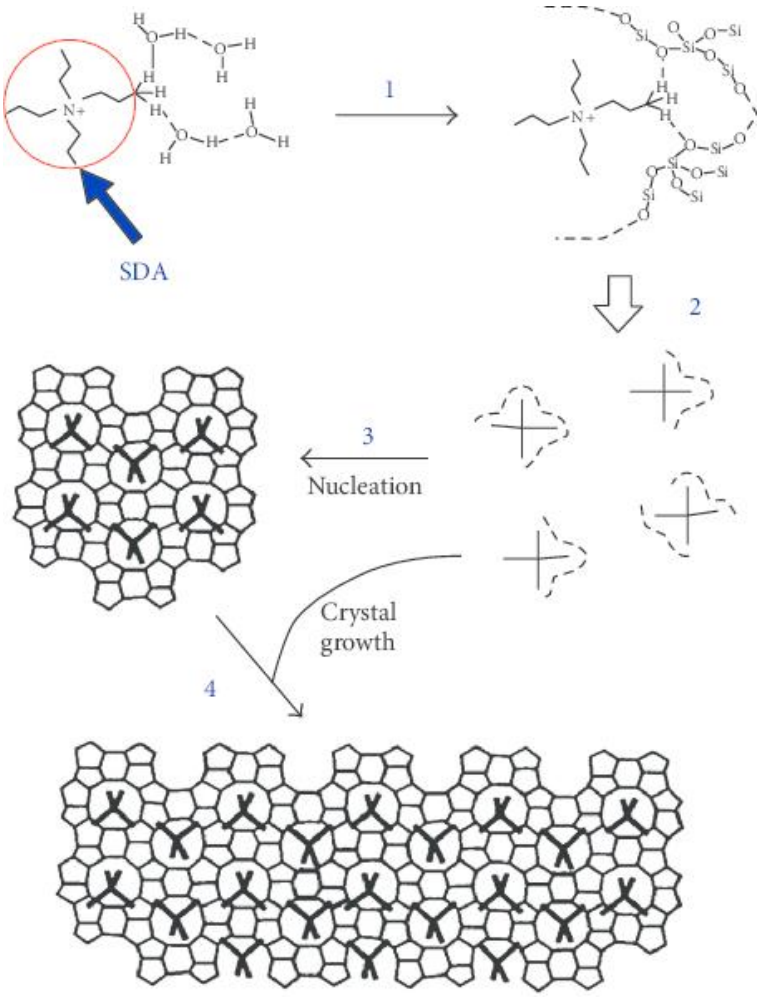

Figure 1.4 Schematic diagram of the zeolite crystallization mechanism involving TPA^+ as structure-directing agent.[69]

The crystallization process can be divided into the following four steps: (1) the replacement of H_2O from structure directing agent by silicon or aluminum sources to form hydrogen bonds; (2) the oligomerization of Si and Al sources, causing the formation of primary units; (3) silicate-template condensation to give birth to a stable nucleus, with a particle size of about 5-10 nm; (4) crystal growth processes. Therefore, it is crucial to select a proper template for preparing the desired size and topology of zeolites. In other words, different templates will lead to unique topological structures. Finally, the removal of organic structure-directing agents from as-synthesized zeolites is quite easy, and requires only a single calcination of the zeolites for few hours. The OSDAs also favors the high pH and supersaturation level of the precursors' nucleation process.

The OSDAs, especially quaternary ammonium ions, are usually expensive, therefore many studies were devoted to reduce their concentration or find other cheaper templates. To solve this problem, some experiments have been also conducted and the results have been discussed in this Thesis.

The concept of "structure-directing agent" further extends to inorganic metal cations. Metal-amine compounds, where M can be Cu, Pd and Pt, also have positive charges to interact with silicates, aluminates and form specific geometries, such as square, linear, etc.[70]

Based on many researches, inorganic alkali-metal cations can also contribute and generate the nucleation and crystallization stages of zeolites as well as organic templates in some cases. The two main functions of inorganic alkali-metal cations are (1) play a structure-directing role to interact with water molecules; (2) contribute to the concentration of OH^- for the solubilization of Si and Al reactants. With the presence of alkali-metal cations, water molecules will surround the alkali cation and arrange in order, as shown in Figure 1.5. The well-ordered water molecules which can be substituted by silicon and aluminum tetrahedra lead to the constitution of cages surrounding the cations.

Alkali-metal cations are often used in the high Al-content zeolites synthesis processes to form an aluminosilicate gel. Sodium ion species are the most common cations to form zeolites, like CHA, ANA, LTA-type topologies. The second are potassium-containing species, crystallizing the BEA, etc., zeolites.[71] Other alkali-metal or alkaline earth metal cations, such as Ba^{2+}, Rb^+, can also be used as SDAs.

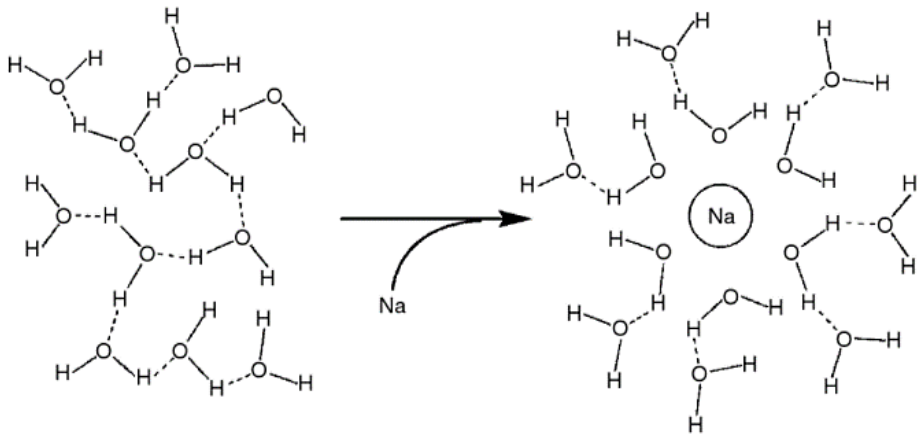

Figure 1.5 Scheme of the interaction between inorganic alkali-metal cation and water molecules (the dotted lines represent hydrogen bonds).

Up to date, organic template mediated routes have been broadly applied in the synthesis process. Nevertheless, the use of OSDAs has its own drawbacks, such as high cost, additional separation and purification steps, and may cause serious environmental issues. To address this problem, it is necessary to find a way out of the conventional synthesis method. Organic template-free synthesis as an eco-friendly sustainable approach raises great concern in recent years. The main ideas are to optimize the reaction conditions without any template use, such as hydrothermal duration, temperature, Si or Al sources, molar ratio, etc., or introduce seeds to guide the synthesis.[72] This method is more attractive and capable for large-scale production in industry, whereas the modulation of each reaction factors is very strict.

- *Mineralizing agent*

Generally, the role of the mineralizing agent is to modulate the solubilization and depolymerization of silica and alumina species at a proper rate and then convert the aluminosilicate species into smaller units. The interaction process usually occurs in alkaline solution at pH ranging between 9 and 13 with the mineralizing agent of OH^-, but in some cases, F^- can replace OH^- mineralizer to create an acidic or near neutral environment.[73]

The solubilization mechanism can be explained via two steps: (1) the

hydrolysis of the silicon and aluminum sources and (2) the silanol condensation in the presence of OH^- (nucleophilic addition). The T-O-T structure is therefore formed as a result of the condensation reaction.

The first use of F^- as a mineralizer was proposed by E. M. Flanigen and R. L. Patton in 1978 to prepare a silicalite zeolite. The fluoride anion mineralizing agent is mainly used to synthesize large-crystals, or novel structures and hetero-substituted materials. However, the development involving of F^- medium, in particular HF, is slow because they are toxic and harmful to our environment and not suitable for large scale production.[74]

- *Solvents*

For most of the synthesis methods, zeolites are prepared from large amounts of solvents such as water (mainly), ethanol, hexane, and toluene with the other necessary components in sealed autoclaves under autogenous pressure. Solvents have been regarded as essential to synthesize zeolites for mass transfer of different reactants and related to the nucleation step especially. The change of the H_2O/SiO_2 ratio in the mixture may dilute the concentration of reactants therefore affecting the pore architecture and crystallization size of zeolites during the hydrothermal treatment.

With regard to organic solvents, they not only play a role as mass transfer but also interact with reactants, in particular the structure-directing agent, to form hydrogen bonds. However, the hydrogen bonds will lead to a shielding effect to framework species interacting with the SDAs. Besides, the viscosity of organic solvents can influence the rate of diffusion thus affecting the size and morphology of the zeolite crystals. In general, the organic solvents with both intermediate hydrogen-bonding ability with template and intermediate viscosity are considered as an appropriate alternative, especially for the large-size zeolite synthesis.

In other words, zeolite synthesis is a complicated process, which needs adequate understanding of the fundamentals of the above-mentioned parameters (Figure 1.6) to direct the synthesis toward targeted zeolites.

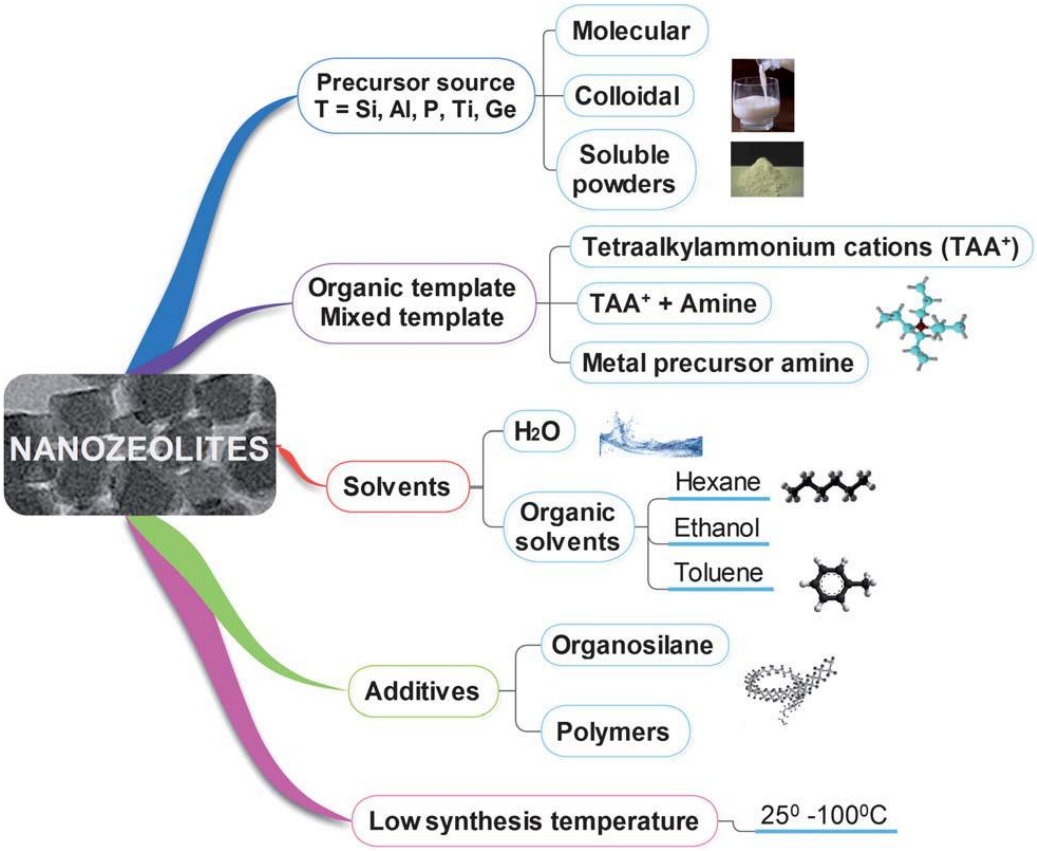

Figure 1.6 Summary of the key parameters controlling the formation of zeolite frameworks.[75]

Crystallization process of zeolites can be described by a typical S-shaped curve (Figure 1.7). It is clearly seen that the synthesis process is divided into 4 different stages: induction time, nucleation, crystal growth and ripening stage. During the induction stage, silicates and aluminates are dissolved and condensate in the alkali mixture, thus forming a gel. The nucleation rate will reach the summit at the second stage and then decreases to zero at the end of nucleation. The most obvious change in the crystal growth stage is the raise in the size of the particles. The precursors begins to aggregate together and form an amorphous phase, which will suffer ripening to get the final products. It is widely believed that there are two major systems of crystallization, which are: (1) homogeneous system, and (2) heterogeneous system.[76] The homogeneous system also called "clear solution system", because the particles in colloidal or sub-colloidal dimensions cannot be identified by naked eyes. The heterogeneous system is also referred to a "hydrogel system", and the gel is visible with a certain degree of

stiffness. The second system is often applied for large-scale production of zeolites.

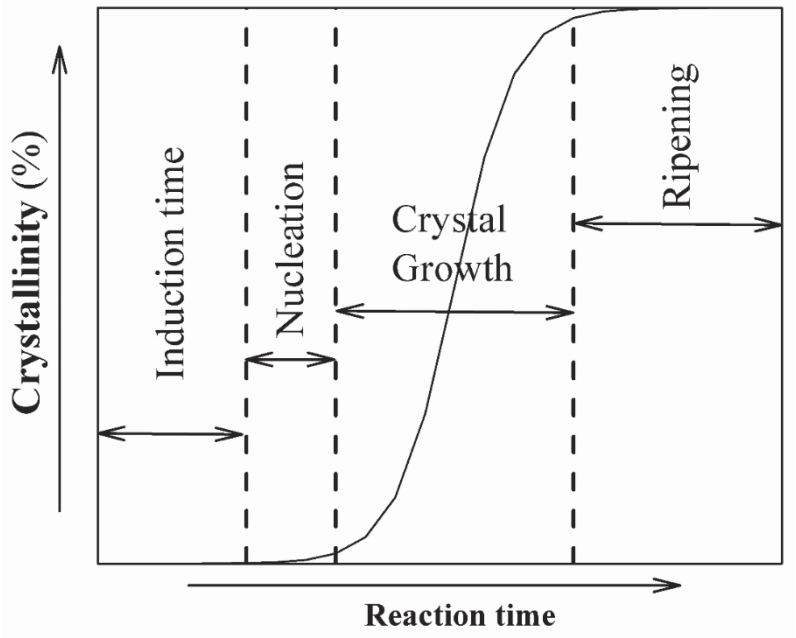

Figure 1.7 Evolution of the degree of crystallinity as a function of time.

1.1.4 Modification of zeolites

Both natural and synthetic zeolites can be modified to further improve their properties, such as acidic properties, and purposeful control opening pore size, topological structure, etc. The term "modification of zeolites" can include a variety of methods from ion-exchange of zeolites, metal supported on zeolites, dealumination of zeolites, to the insertion into the zeolite framework, etc. The detailed description of each method will be discussed in coming sections.

1.1.4.1 Ion exchange of zeolites

AlO_4 tetrahedron carries a negative charge, which will be balanced by a positive charge associated with an extra-framework cation.[77] The cationic exchange reaction occurs most frequently in the solution mixtures between the solid phase and cations. Not all the zeolites can be directly ion exchanged with cations. Barrer first proposed an ion exchange of aluminum by strong mineral acid in 1968.[78] The ion exchange usually takes place with monovalent cations (*e.g.,* Na^+, K^+ and quaternary ammonium ions), divalent ions (*e.g.,* Cu^{2+}, Zn^{2+}, Ni^{2+} and Ca^{2+}), and also trivalent ions (*e.g.,* La^{3+}, Fe^{3+}).[79] For

example, stilbite zeolite (STI) was immersed and modified with $FeCl_3$ solution for the removal of fluoride from drinking water. Ion exchange method was used to prepare Cu-modified SAPO-34 for the selective catalytic reduction (SCR) of NO with NH_3 (NH_3-SCR).[80] Ikeda investigated the topological structure and hydrothermal stability of NH_4^+ exchanged LIT-type zeolite.[81] Silver ions as effective biological antibacterial components were loaded into the zeolites by ion exchange method for both inhibiting microbial growth and improving sterilizing effect.[82] The ion exchange mechanism of active ingredients (silver ions) is shown in Figure 1.8.

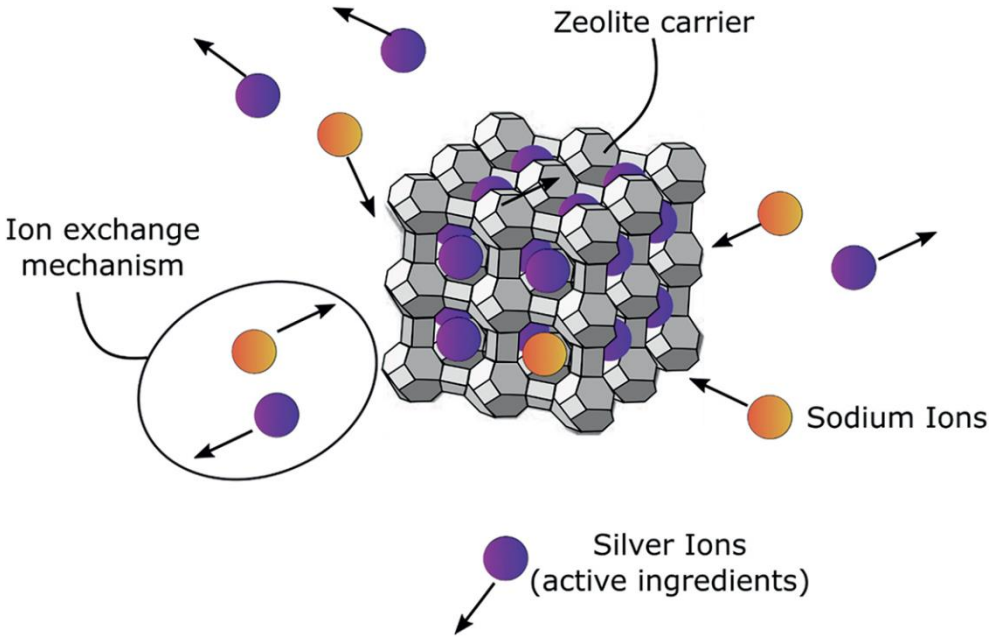

Figure 1.8 Scheme of silver ion exchange mechanism in zeolites as inorganic antimicrobial agents.

The ion exchange rates among various cations are different, which depending on their ionic diameter, the concentration of exchangeable cations, temperature and the impact of co-solvent in some cases. It should be noted that the cations may form a hydration shell in the solution and change their actual size. For instance, a hydrated K^+ may be smaller than a hydrated Na^+. Besides, the hydrated cations can penetrate the open pore by losing H_2O molecules from themselves, even turning into bare ions.

The cations seriously impact the acidic properties of zeolites' surface and could

block the pore for selecting different size molecules efficiently. In view of this, ion exchanged zeolites with specific cations have a great potential in the field of catalysis and adsorption. In addition, due to the ion exchange capacity of zeolites, the latter are widely used as water softeners, removing toxic or heavy metal ions from wastewater, like Pb^{2+}, Cd^{2+}, Zn^{2+} and Mn^{2+},[83, 84] and biological bacteriostasis, etc.

1.1.4.2 Metal doping on zeolites

Except the ion exchange methodology, metals doping is another approach to introduce cations into zeolite crystals. Metal nanoparticles supported zeolites exhibit potential research and application value in the fields of nanoelectronics, energy storage and conversion, biomimetic chemistry,[85] and heterogeneous catalysis. Metals are often supported on the external surface of zeolites, but the disadvantage is that metal particles may migrate or ripen.[86] Therefrom, a novel strategy to design metal doped zeolites, to overcome this problem, is urgent and necessary. Inspiration from other materials is mandatory, for instance, Bao *et al*. investigated metal or metal oxide nanoparticles dispersion inside carbon nanotubes (CNTs) which significantly improved the surface charge and catalytic performance of Fe nanoparticles in the Fischer-Tropsch synthesis (FTS).[87] A considerable amount of work on metals supported on zeolites have been carried out, and many research groups have reported zeolites encapsulated metal complexes as catalysts applying in many important catalytic reactions recent years.

There are three ways for the encapsulation of metal complexes in zeolites according to the size, which are isolated metal sites, nanoclusters and nanoparticles. Ion exchange in solution mixtures does not work for the cations with high barrier for simultaneously exchanging three positive charges, thus high temperature metals dispersion at the solid-state could address this issue. The metals interact with the oxygen species from the zeolites. The post-treatment could allow inserting noble metals into the shallow layers of zeolites. In-situ encapsulation during the crystallization can acquire more uniform and well-dispersed metals supported zeolites. For example, RuO_2 clusters were encapsulated within FAU-type pores and tested in aerobic alcohol oxidation.[88] The key point of these metals supported zeolites is to stabilize the metal

species and enhance the interactions between metal-precursors and zeolite units.[89] The metals supported zeolite catalysts exhibit outstanding activity and shape selectivity in many industrial reactions, especially for the transformation of C_1 reagents (CO, CO_2, CH_4, etc.). Figure 1.9 shows a general summary of the metals supported on zeolites for catalysis.[90]

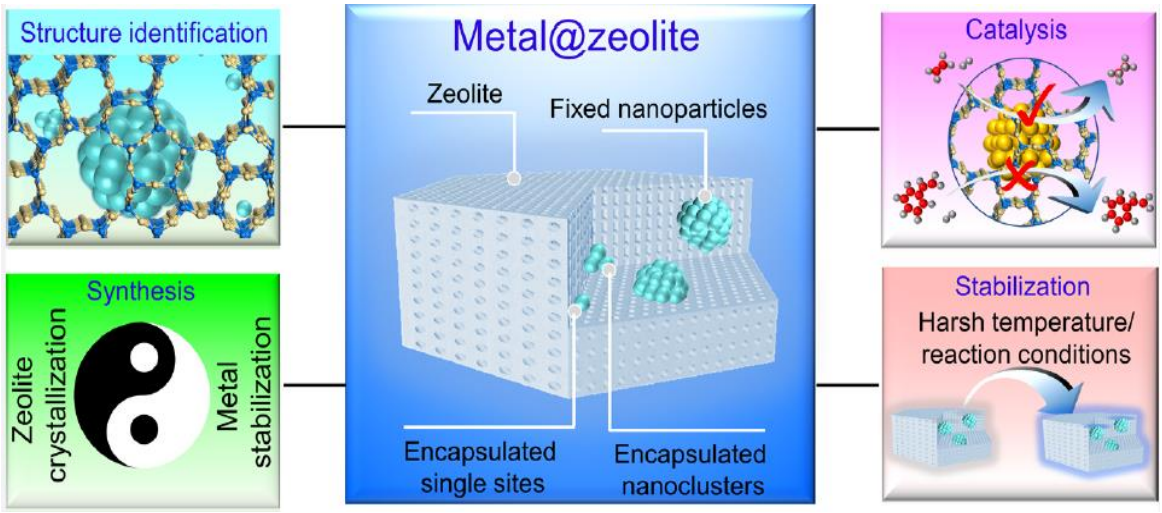

Figure 1.9 Summary of metals supported zeolites from their synthesis processes to catalytic applications.[90]

1.1.4.3 Dealumination of zeolites

Dealumination is considered as one of the most universal and effective treatment in the area of demetallation in industry. Typical dealumination is known as a post-synthesis method of removing aluminum from the zeolite structure by using physical methods, chemical agents or by hydrothermal treatments.[91] Barrer first used acid in the high temperature to expel aluminum from clinoptilolite in 1960s, and then the dealumination technique was not only used to synthesis high SAR zeolites with enhanced stability, but also applied to generate mesoporosity.[92] Before a detailed description of dealumination of zeolites, Figure 1.10 summarizes various synthesis routes towards generating mesopores within microporous zeolites. Many different approaches can be used to give birth to mesoporous structure. For example, by tailoring the pore architecture with multiple mesoporous templates, zeolite can form a hierarchical structure with ordered

mesoporosity. In addition, there are two strategies that can generate random mesopores of zeolites: one is a top-down approach or so-called “destructive” modification, as well as a bottom-up route, namely “constructive” way.

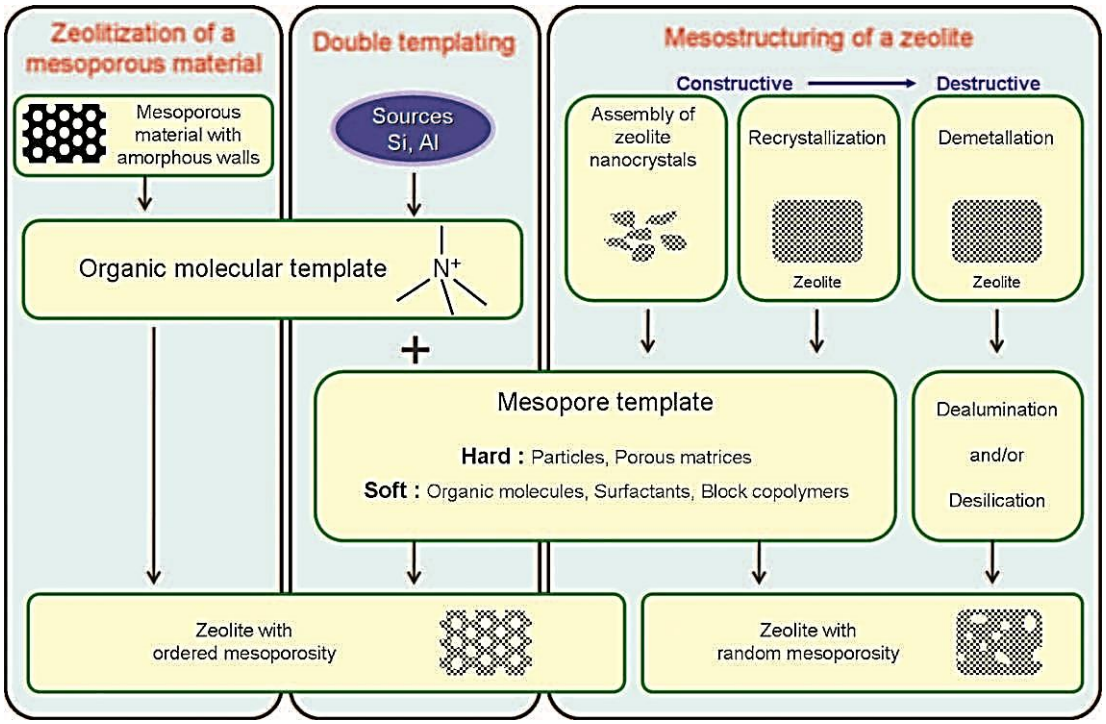

Figure 1.10 Overview of the various synthesis routes towards zeolite materials combining micro- and mesopores.[93]

The dealumination is one of the widely used methods of destructive strategies for already synthesized zeolites. Many attempts were carried out to create hierarchical zeolites by one of the most advanced techniques of “dealumination”. Among them, hydrothermal treatment in the presence of steam[94] and acid leaching[95] are most common and easy to manipulate. Besides, calcination[96] and chemical treatment (*e.g.,* ethylenediaminetetraacetic acid (EDTA), ammonium hexafluorosilicate (AHFS), $(NH_4)_2SiF_6$, NH_4HF_2, etc.)[97-99] can also break the Al-O-Si bonds in the generation of mesoporous materials.

- *Steaming*

Steaming as a hydrothermal treatment usually carried out at temperatures above 500 ºC in the presence of water vapor. Actually, recent studies demonstrated that

the cleavage of Si-O-Al bonds happens at lower temperature when water have access to the opening pores by using in-situ Al K-edge XAS and XRPD Parametric Rietveld Refinement.[100] The steam atmosphere efficiently improves the mobility of aluminum and silicon species, and hydrolyzes Al-O-Si bonds. However, the amorphization of the framework structure and defects formation are still the main drawbacks of this method. Besides, a mild acid treatment to remove extracted extra-framework debris cannot be ignored.

- *Acid leaching*

As mentioned, a mild acid leaching is used as one of the necessary steps after calcination or steaming to remove amorphous species. However, strong concentration acid leaching can also expel aluminum from the framework directly without cooperating with other treatments. The mechanism of this strategy is similar with steaming. The more convenient way to proceed is using acid leaching strategy that can extract the debris at the same time. Nitric acid, hydrochloric acid, sulfuric acid, as well as some organic acids, like oxalic acid, acetic acid and tartaric acid are widely used for the formation of mesopores. The dealumination performance is determined by the nature of the zeolite. For example, MOR exhibits a good resistance to acid decomposition while Al is slowly expelled. The method has strict requirements on pH value, which cannot occur when the pH value becomes higher than 2.3.[101]

- *Calcination*

This thermal treatment without the presence of water vapor for guiding dealumination phenomenon is supposed to be a purely thermal effect. The extra-framework aluminum (EFAl) species, produced by heat treatment at specific calcination conditions, remain located in the zeolite channels.[102] Like hydrothermal treatment, those expelled EFAl species are removed by a mild acid leaching. For instance, the commercial ZSM-5 zeolites were subjected to a heat treatment at about 1000 ºC for few hours to create mesopores.[103] Finally, the hierarchical zeolites with meso-micro porous bimodal system were developed and characterized.

- *Chemical treatment*

Treatment with chemical agents has also been proposed for the extraction of aluminum from the framework in the preparation of mesoporous zeolites. As already mentioned above, the chemical reagents are usually some strong chelating agents, like ethylenediaminetetraacetic acid (EDTA),[104] acetylacetone,[105] silicon tetrachloride,[106] ammonium hexafluorosilicate (AHFS),[107] $(NH_4)_2SiF_6$,[108] NH_4HF_2,[109] etc.

Kerr reported a dealumination mechanism in 1969 that the acidity of all these agents cause the Si-O-Al bonds breaking, which leads to the removal of aluminum from the framework. Subsequently, solubilization and mobilization of extra-framework Al species carried out with specific chemical reagents.[110]

1.1.4.4 Insertion into the zeolite framework

We already know that aluminum can be expelled from the framework by some specific means without structural collapse. However, this process can also be reversed, in other words, aluminum can be inserted into zeolite frameworks by hydrolysis of aluminum, aluminum oxide, aluminum halides and other elements.[111-113] The research shows that mild alkaline treatment allows extra-framework aluminum to return to the vacancy left behind.[114] For some high silica zeolites, increasing the aluminum content is an effective way to promote their catalytic activity. As a result, a considerable amount aluminum species inserted in the framework has been conducted and made some achievement. Breck and Skeels first proposed that non-framework aluminum species were back to their cavities by the treatment of a thermally decomposed NH_4Y with an aqueous solution of NaOH.[115]

The incorporation of tin heteroatoms within framework vacancy defects of dealuminated BEA zeolites in dichloromethane (reflux, 333K) was reported by Vaga-Vila *et al.*[116] Moreover, Dijkmans also realized a detailed study on the electronic structure and redox behavior of Sn with extended X-ray absorption fine structure (EXAFS) spectra.[117] The schematic diagram is shown in Figure 1.11.

Figure 1.11 Visualization of the insertion of Sn heteroatoms into dealuminated BEA zeolites.[117]

1.1.4.5 Other modifications

Other modification methods mainly include the reaction between zeolite OH-groups and oxoacids. Acidic bridging hydroxyls, internal silanol groups and external silanol groups which terminate the zeolite lattice are three types of silanol groups in zeolites. All of them can form hydrogen bonds with water. With an increase in Si/Al ratio, the concentration of acidic OH decreases, while the concentration of internal silanol groups (defect sites) and tetrahedral vacancies increases. However, the latter can be annealed by thermal or steaming treatment.[118] Besides, a higher selectivity can be achieved by modification with certain oxoacids in some specific reactions, such as the isomerization of xylenes,[119] but more evidence should be given to support this conclusion.

1.1.5 Zeolite properties and applications

Zeolites were first used in the sugar industry in 1896. In the following decades, the applications of zeolites have been expanding due to their unique physical and chemical properties. Zeolites are traditionally referred to as a family of aluminosilicates possessing of well-defined topological frameworks and orderly distributed micropores. Meanwhile, with their high specific surface area (more than 300 m^2/g), outstanding hydrothermal stability and low production costs, zeolites got the achievements of their paramount role in many fields. Herein, there are three main applications for zeolites in industry, which are: ion exchange, gas adsorption and separation, and heterogeneous

catalysis, as shown in Figure 1.12. Up to date, besides those traditional utilizations in the chemical industry, zeolites also make great contributions in many sustainable fields, such as renewable energy, and environmental protection.[120]

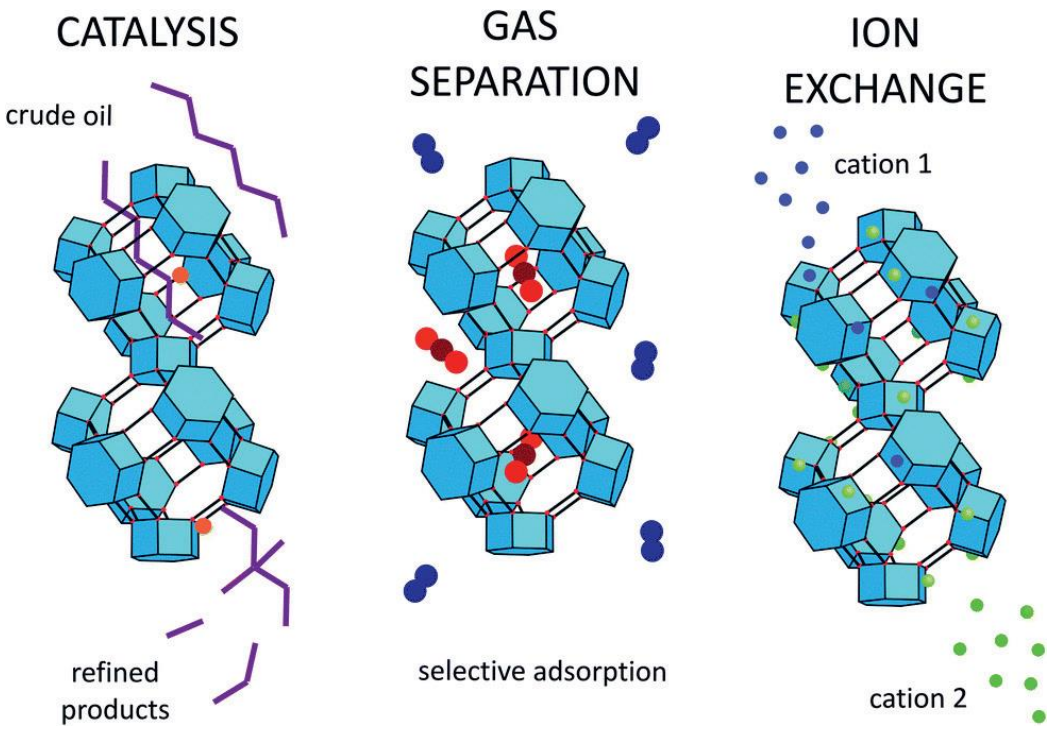

Figure 1.12 Three main application fields of zeolites in chemical industry.[121]

1.1.5.1 Ion exchange

A brief description about the application of zeolites in the field of ion exchange has been made before. As aforementioned, the cations which appearance in the void channels and cages to compensate the negative charge from the aluminum tetrahedron, combine with the framework structure by electrostatically bound. Hence, the non-covalent bonds between cations and the zeolite framework can be easily exchanged with other cations. Further, the replacement of aluminum atoms can directly lead to change the Si/Al ratio and therefore the acid properties of zeolites. In this aspect, zeolites are most commonly used as water softeners. For example, the removal of "hard" ions, such as calcium and magnesium, from domestic water by sodium or potassium cations renders the water softer and more suitable for use in daily life (Figure 1.13).[122] More than that, Na-LTA zeolites also apply to take up phosphate ions from water as

detergent builders, which effectively relieve the water eutrophication phenomenon.[123] Some specific utilizations of zeolites were also carried out, including the removal of radioactive isotopes from mining or nuclear plants, in particular $^{137}Cs^{+}$. For instance, zeolites were used to remove $^{137}Cs^{+}$ from contaminated water and soils after accidents at Chernobyl and Fukushima.[124, 125] Interesting, the characteristic of ion exchange can be applied into organic field, where the zeolites are doped with metal ions and involved in the reactions actively.[126, 127]

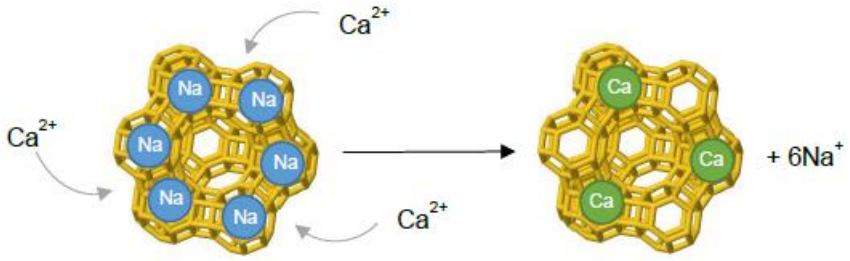

Figure 1.13 Scheme of the exchange of sodium cations by calcium.

1.1.5.2 Gas adsorption and separation

Zeolites are playing an increasing role in the gas adsorption field, including applications in drying, purification and separation. This phenomenon relies on the opening microporous architectures, micropore shape and polarity. As the term "molecular sieves", which means that small molecules can pass through the channel directly, but some molecules have bigger size than channels will be blocked and separated from the mixed system. Here are some examples to demonstrate the applications in the gas adsorption of zeolites:

- *Air drying*

Zeolites have been used in refrigerators to dry and purify gases from water in the late 1950's. Besides, because of the advantage of air drying, zeolites are widely used in the food industry to improve efficiency of air dehumidified than conventional dryers.[128]

- *CO_2 capture*

Numerous materials have been tested to reduce CO_2 emissions, such as activated carbon, metal-organic frameworks (MOFs), mesoporous silica, alkali metal silicates,[129] layered double hydroxides (LDHs),[130] metal oxides, etc.,[131] among which zeolites have attracted much attention because of their unique adsorption and catalytic properties. Zeolites, along with other porous materials, are one of the best inorganic adsorbents for CO_2 adsorption.

It is generally known that the different type of cations (*e.g.,* Li, Na, K, Rb, Cs) are preferred adsorption sites, being especially remarkable for adsorption with polar or easily polarizable molecules, but they also influence the nonpolar molecules adsorption thanks to the electrostatic interactions, such as CO_2 molecule which is a weakly acidic gas and possesses a quadrupole moment. Extra-framework alkali cations play an important role in zeolite for CO_2 adsorption.[132] Recently, the exchange of alkali metal cations in zeolites is considered as an effective method to increase the adsorption capacity of CO_2.

Herein, the mechanism of CO_2 adsorption over pure Si-zeolite (Si/Al→∞) is briefly described. For the pure siliceous zeolite, CO_2 adsorption capacity is dominated by dispersion interaction between CO_2 and the zeolite surface. CO_2 molecules are adsorbed in the vicinity of the channel or cavity wall.[133] However, for the alkali-metal cation exchanged zeolite, excepted physical adsorption, CO_2 molecule can also be captured by these cations through electrostatic interactions and form CO_2 adsorption complexes with them. The adsorption heats of those electrostatic interactions between CO_2 and cations are higher than dispersion interactions between CO_2 and the zeolite framework. It means that the CO_2 reacting with these extra-framework cations are easier and more stable than interacting with the wall of ZSM-5.[134]. Figure 1.14 shows the adsorption mechanism of one CO_2 molecule in Y zeolites (Si/Al ratio = 2.5) which contain Li^+, Na^+, K^+, Cs^+ cations.

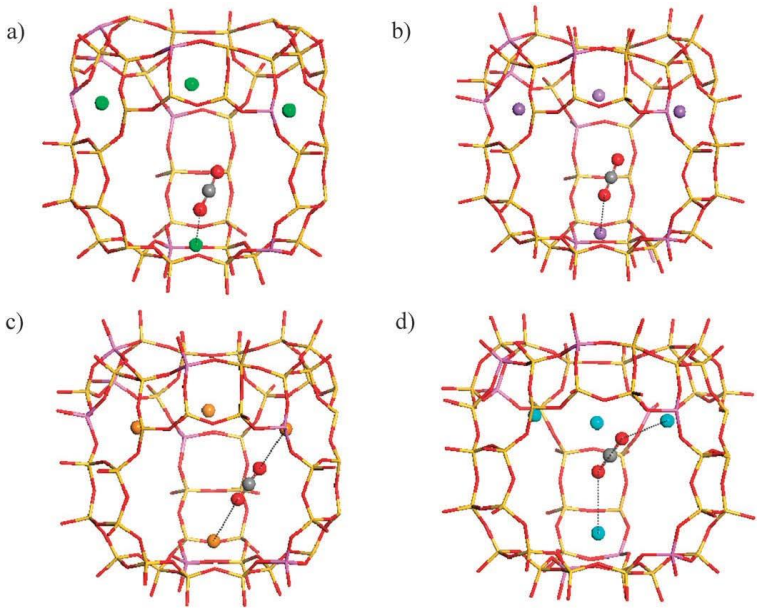

Figure 1.14 Optimized adsorption mode of one CO_2 molecule in Y zeolite where the CO_2 molecule is oriented towards the supercage: (a) M=Li, (b) M=Na, (c) M=K, (d) M=Cs.[134]

1.1.5.3 Heterogeneous catalysis

Thanks to their unique structure and chemical properties, zeolites become ideal heterogeneous catalysts even for reactions carried out at temperatures above 300 ºC.[135] Similarly, heterogeneous catalysis is the most important among all the application fields of zeolites, due to the high added economic value.[136] Specifically, the great catalytic performance is mainly attributed to two aspects: acidity and well-defined micropores. The former enables the zeolites use in a wide range of reactions, by taking advantage of Brønsted acid sites and in some cases, extra-framework Lewis acid sites.[137] The latter can discriminate reactants and products by size and shape, since a variety of topological structures of zeolite will cause the difference on diffusivity and coke formation.[138] The shape selectivity can be divided into 3 types as follows: (1) Reactant shape selectivity (RSS): Relying on the topology of pores and channels, large particles cannot get inside through the opening pores and react with active sites.[139] (2) Product shape selectivity (PSS): Similar to the case of reactants, the products whose dimensions can better match with the channel structure will be easier to diffuse outside the zeolites, thus affect the product distribution.[140] (3) Transition state shape selectivity (TSSS): when the reaction

occurs in the channels or pores, the limited size and certain shape can effectively prevent the formation of bulky transition states and intermediates. One relevant example is the inhibition of coke formation and the cracking of paraffins over MFI-type zeolites, as shown in Figure 1.15.[141] Besides, the largest utilizations in catalysis is the Fluid Catalytic Cracking (FCC) process with zeolite Y for the production of gasoline from heavy fraction of crude oil into shorter chain molecules. In this case, strong Brønsted acids of Y zeolites lead to protolytic cracking and carbonium ion generation, as well as strong Lewis acids forming carbenium anions by hydride abstraction.[142]

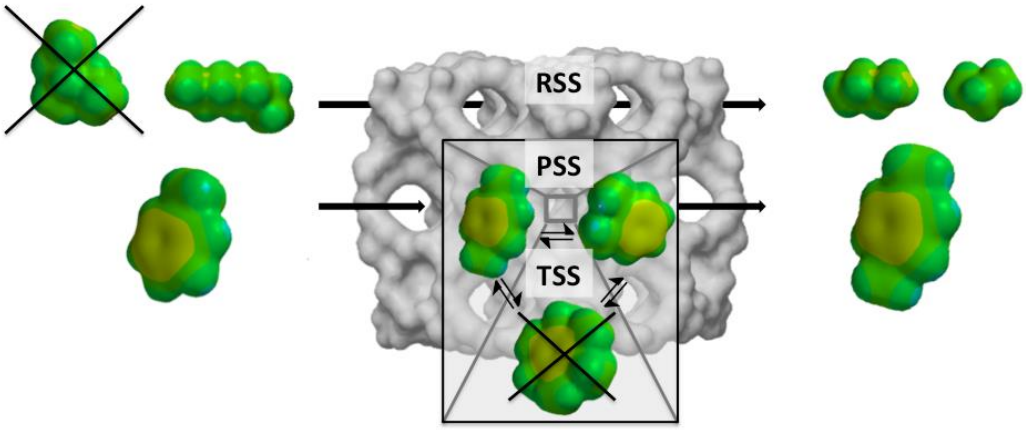

Figure 1.15 Schematic representation of the different shape selectivities for two typically shape selective reactions: *supra*: paraffins cracking, *infra*: toluene methylation to para-xylene.

Among roughly 240 types of zeolites, about 17 kinds of zeolites are applied in industry: AEL, AFI, BEA, CHA, EDI, FAU, FER, GIS, LTA, LTL, MER, MFI, MOR, MTT, MWW, TON, RHO.[143, 144] They are mainly used in chemical industry, such as petroleum refining, synfuels production, and petrochemical production, etc.[145] Among these 17 zeolites, five of them exhibited significant capacities for catalytic applications, called “the Big Five”, being FER, MFI, MOR, BEA and FAU structures,[146] and their structures are presented in Figure 1.16.

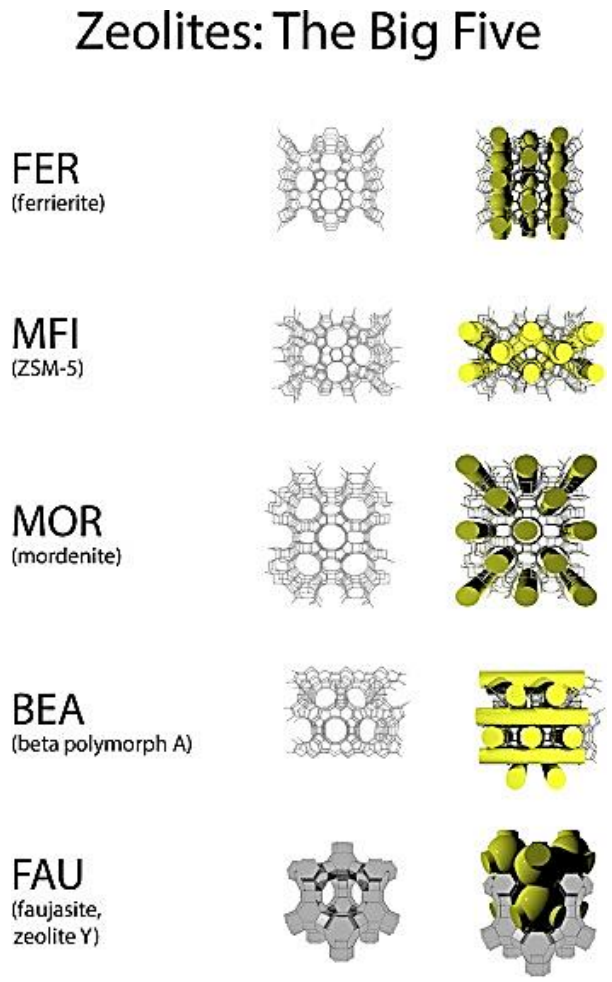

Figure 1.16 The structures of the Big Five zeolites.[147]

1.1.6 Conclusions

In the first section, an overview of the zeolites was proposed, including the historical development of natural and synthetic zeolites, topological structure, different synthesis methodologies, modifications of zeolites and three main applications of zeolites. Through a comprehensive understanding of zeolites, we believe that zeolite have unlimited application possibilities from our daily life to industries through certain modifications.

1.2 Biomass-assisted zeolite synthesis

1.2.1 Biomasses

Biomass, which consists of organic and inorganic matter, is a complicated heterogeneous resource which has a huge potential to be explored and utilized.[148] As

shown in Figure 1.17, there are numerous types of biomasses, including wood waste, agricultural waste, households and industrial waste, commercial waste, aquatic waste, animal and human waste, etc.[60]

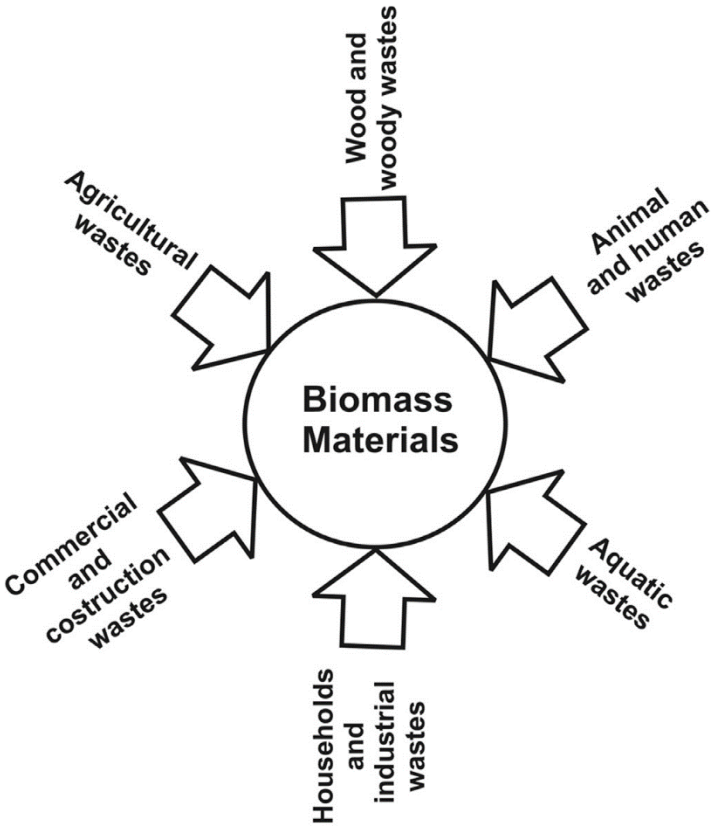

Figure 1.17 Classification of biomass materials.

Since biomass can be technically used as a fuel directly, the term "biomass" is equivalent to biomass energy in some cases. Biomass energy is energy generated or produced by living or once-living organisms. Biomass energy obtained from biomass combustion can be applied to create heat for electricity and fuels for transportation, etc.[149] Up to now, biomass accounts for 8 to 15% of the total world energy consumption, and direct combustion still remains the most common treatment to acquire biomass energy around the world, contributing approximately for 95%.[150] Biomass ash is the product from biomass combustion, which also has a huge potential and needs to be explored and utilized. However, even so, this thermal treatment mode also suffers obvious limitations. For example, the production of biomass ashes will not only contribute to environmental issues, but also threaten human health.[151] Therefore, the

reuse of biomass ash becomes very important, especially in the field of environmental protection. Although many factors, like types of biomass, location, burning conditions, etc., may affect the combustion productions, typically, biomass ashes from neat biomass burning process contains more alkali metals (*e.g.,* sodium, potassium) and less alumina than coal fly ash.[152, 153] Besides, many other oxides, such as SiO_2, Fe_2O_3, CaO, MgO, TiO_2, MnO, and P_2O_5 are also common in biomass ashes.[154] It can be therefore expected that biomass ash has the potential utilization in many other ways.[155] In addition to biomass fly ash, we are also concerned about some organic residues that are closely related to our lives, such as spent coffee grounds and tea waste. Coffee and tea as two of the most widely consumed beverages worldwide, have taken an important place in our daily life. This also leads to a large amount of residual waste generated and then discarded into the trash directly. With the improvement of public awareness of environmental protection, people realize that those wastes can also be very helpful and even turned into a commercial asset due to the chemical and molecular richness of the coffee and tea waste. Generally speaking, coffee and tea waste retains polyphenols, antioxidants, catechins, cellulose, free amino acids, insoluble proteins, caffeine, fiber, sugars, lignin, boron, zinc, and tannic acid, etc.[156] Figure 1.18 presents a collection of 43 coffee aroma compounds that have been repeatedly found in coffee, which including methanethiol, guaiacol, 2-methyl-3-furanthiol, 2-furfurylthiol, acetaldehyde, isobutanal, methional, etc.[157] Major tea factories dispose their tea residue in the plantation area as bio-fertilizer because the tea leaves contain about 4.4% N, 0.24% P and 0.25% K, making it a good NPK fertilizer.[158, 159] However, besides to this most common application, coffee and tea waste have huge potential to apply in agriculture and construction, and why not zeolite manufacturing, etc.[160] Meanwhile, the upgrade and utilization of biomass from feedstocks into activated carbon,[161] value-added materials, renewable energy sources, etc. is becoming very attractive both in environmental issues control, like an accumulation of agricultural waste, which causes air and water pollution during natural degradation process, and economic potential aspect.[120, 162, 163]

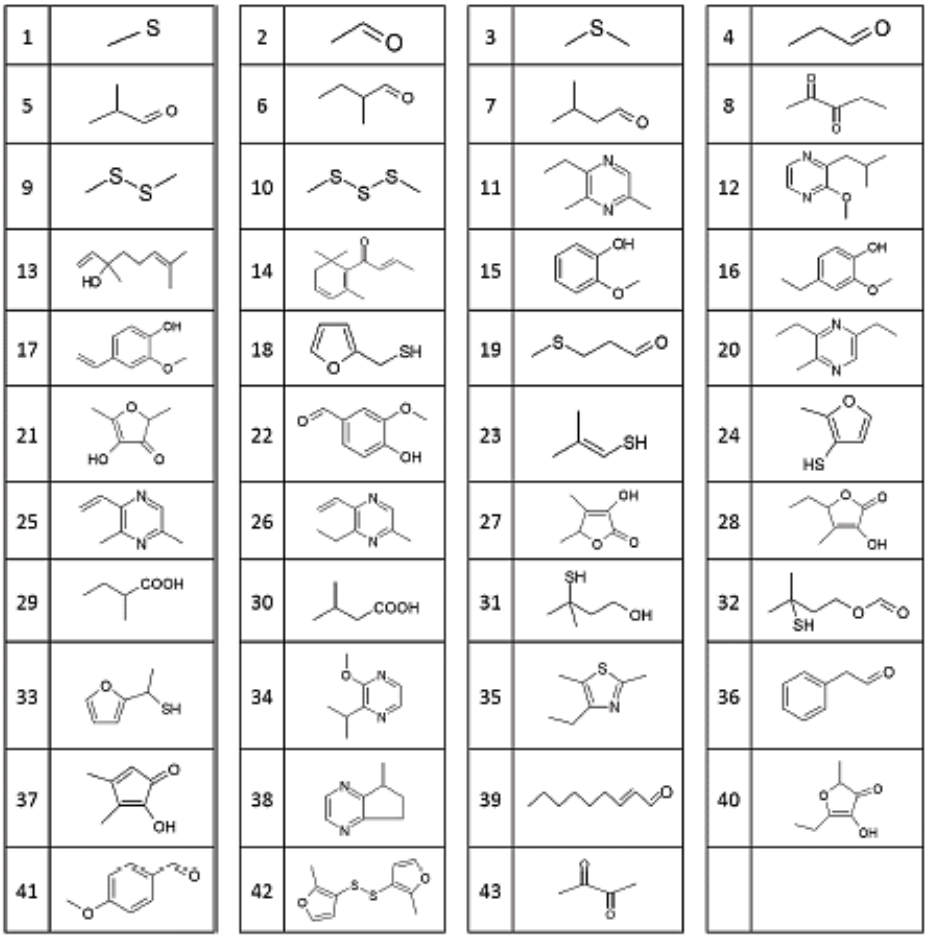

Figure 1.18 The selection of aroma compounds in coffee.[164]

Biomass resources that are available on a renewable basis and are used either directly as a fuel or converted to another form or energy product are commonly referred to "feedstocks". In this Thesis, biomass feedstocks mainly include lignin, ecoshell, sugarcane bagasse, spent tea leaves, spent coffee grounds, and different types of algae, etc.

1.2.1.1 Lignin

Lignin is a complex macromolecule that forms key structural materials in the support of tissues of vascular plants.[165-167] They are abundant in wood and bark, which constitutes the second most abundant organic polymer on earth, after cellulose. Lignin is a three-dimensional polymer and its chemical structure is formed by cross-linked phenolic polymers.[168] Moreover, lignin is a structurally complex, heterogeneous, partly

branched polymer synthesized from three main phenylpropane monolignols: coniferyl, sinapyl, and p-coumaryl alcohols.[169] Raw lignin is also partly solubilized by alkali pre-treatment with different concentrations of lime ($Ca(OH)_2$), sodium hydroxide (NaOH) and potassium hydroxide (KOH), and the pre-treatment allows the degradation of lignin to cellulose and hemicellulose.[170] Figure 1.19 exhibits the structure of lignin and oxidized lignin.

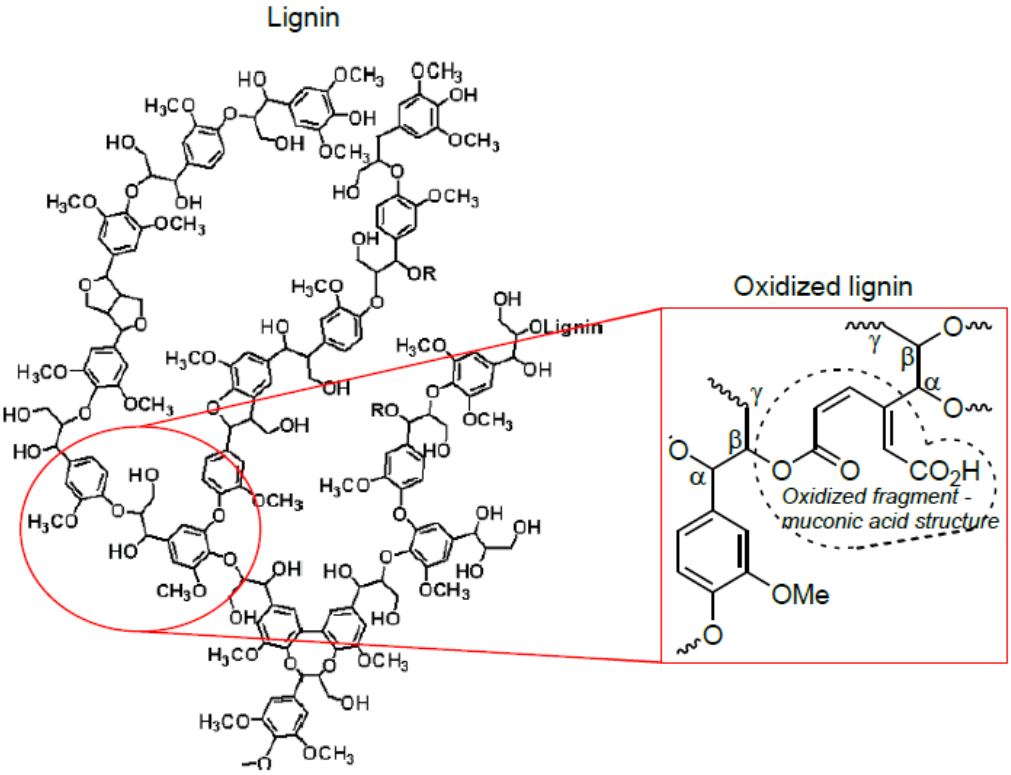

Figure 1.19 Structure of lignin and oxidized lignin.

1.2.1.2 Ecoshell

The biomass source of ecoshell comes from a company, which is the walnut shell and produced as a commodity industrial market around the world. In terms of chemical composition, walnut shells contain approximately 38% lignin and 62% cellulose and hemicellulose on a dry ash-free basis.[171, 172] Ecoshell products are bio-degradable, non-toxic, environmentally safe and cost effective for many industrial uses around the world.

1.2.1.3 Sugarcane bagasse

Sugarcane bagasse is a lignocellulosic fiber residue obtained from sugarcane culm. Sugarcane bagasse as one of the common and abundant agricultural residues has the following composition (by weight): cellulose, 41.8%; hemicellulose (as pentosan), 28.0%; lignin, 21.8%,[173] and enriches with various elements, such as N, Na, Al, Ca, and Mg, etc.[174]

1.2.1.4 Spent tea leaves

Tea waste as a kind of common biomass also causes considerable attentions nowadays.[175] Currently, tea has become one of the most consumed non-alcoholic beverages worldwide.[176] Meanwhile, the disposal of tea residual problem is more and more serious because spent tea leaves are generated in large amounts every year.[177] Most of tea waste has been disposed by composting, incineration or in landfills nowadays. However, tea waste has caused a great pollution hazard because it is difficult to degrade, and resulted in huge loss of beneficial components if left into the environment directly. Some attempts have been made to make full use of spent tea leaves, like removing heavy metal contaminations,[178] synthesis of activated carbon,[179] preparing microcrystalline cellulose,[175] etc. Furthermore, spent tea leaves as one type of bio-templates, are attractive and competitive for synthesis of catalysts because of their numerous amount, multiplex morphology and eco-friendly feature.[180, 181] However, there is a completely new research interest that synthesis of zeolites by using spent tea waste as a bio-template.

1.2.1.5 Spent coffee grounds

Because the huge number of residues generated annually in the consumption of coffee, spent coffee grounds (SCG) and coffee silverskin (CS) become a great pollution hazard if discharged in the environment. Fortunately, spent coffee grounds contain large amounts of organic compounds, such as fatty acids, amino acids, polyphenols, minerals and polysaccharides, which can be used for biodiesel production,[182] precursor for activated carbon production,[183] etc.

1.2.1.6 Algae

Algae as feedstocks for bioenergy refers to a diverse group of highly productive organisms that include microalgae, macroalgae (seaweed), and cyanobacteria (formerly

called “blue-green algae”). Many use sunlight and nutrients to create biomass, which contains key components, including lipids, proteins, and carbohydrates, that can be converted and upgraded to a variety of biofuels and products. Although the composition and category of algae are different, in general, algae are composed of around 50% carbon, 10% nitrogen, and 2% phosphorus, which constitute the protein, carbohydrates, lipids, and nucleic acid of algae. In this Thesis, three kinds of algae were selected for our study, which are Trachydiscus minutus and Bracteacoccus bullatus from freshwater, and a mixture of freshwater cyanobacterium.

1.2.2 Bio-sourced secondary template (BSST) concept

Through a fundamental approach, Rimer and co-workers have proposed a bio-inspired method to tailor zeolite crystallization using zeolite growth modifiers (ZGMs), which are able to self-assemble by selecting crystal faces and regulating the anisotropic growth rates, and thus, tailor the particle size and zeolite crystal morphology.[4, 5] Inspired by this idea, a further strategy for the synthesis of several zeolite structures was developed by Louis *et al.*,[6] which was called bio-sourced secondary template (BSST) strategy. The BSST approach aims to modify and tailor the intrinsic properties of zeolites, like texture, porosity, acidity, by involving cheap biomass residues. The understanding of the synthesis process of zeolites and thorough recognition of biomasses are lacking due to the complexity of both of them. Besides, the interactions between BSST and inorganic precursors may further increase difficulty.[7] People attempt to preliminary rationalize the hypothesis of BSST impact on zeolite crystal formation, and the schematic diagram is shown in Figure 1.20. Here, the effect of sugarcane bagasse-assisted zeolite synthesis is taken as an example. During the hydrolysis process, the surfactant-like-BSST species could interact with the growing and nucleating crystals by electrostatic interactions. Meanwhile, aromatic species via possible π-stacking interactions may elongate the morphology along a- and b-axes. The strategy involving BSST may cause mesopores formation and overcome Si/Al ratio limitation during the synthesis. Herein, BSST may not only play a role as a soft template, but also as a non-soluble species possibly guiding the zeolite formation.

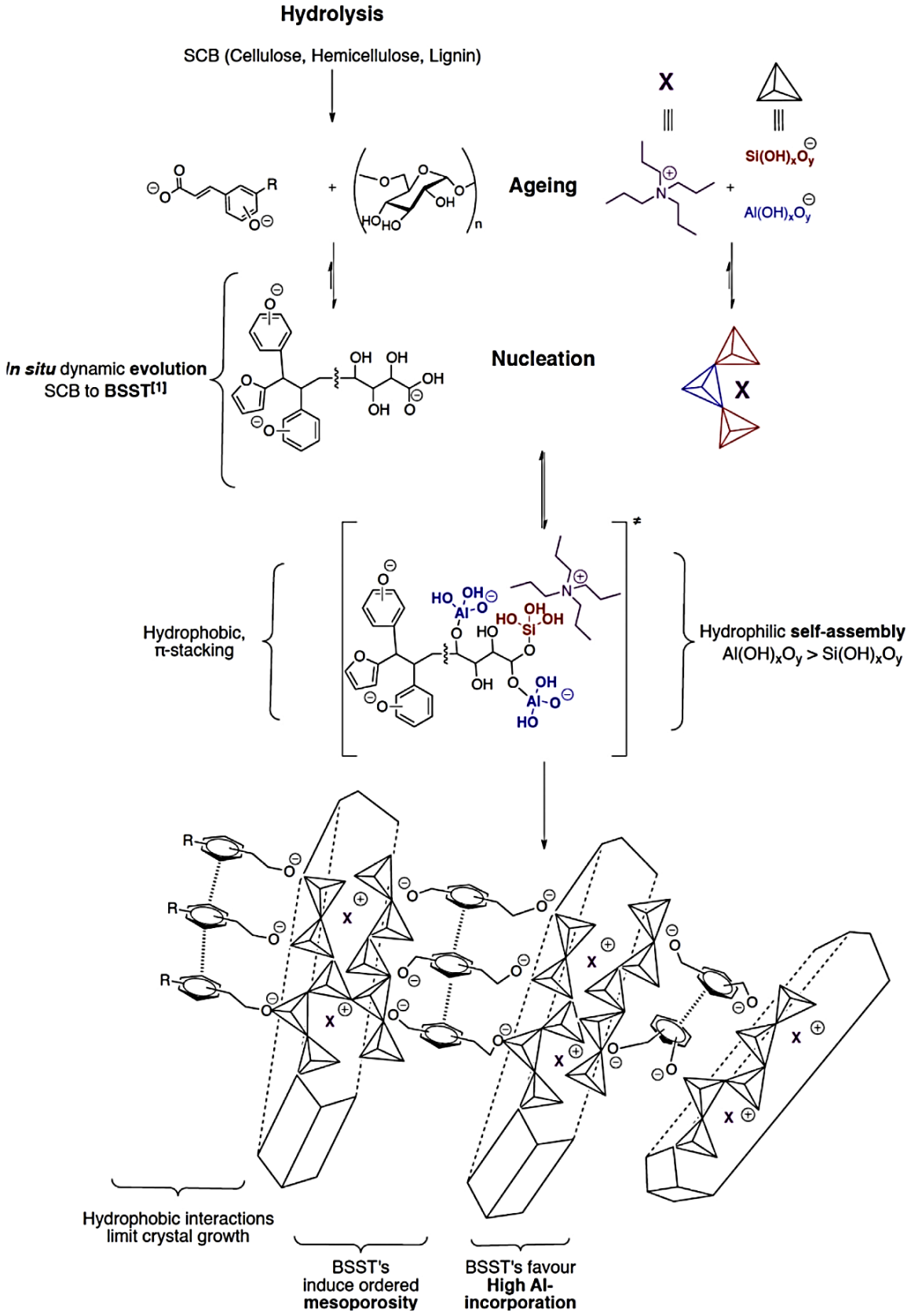

Figure 1.20 Proposed mechanism involving BSST-assisted zeolite synthesis.[6]

1.2.3 Zeolite synthesis from biomass waste

The biomass waste can be considered as silicon source, aluminum source or organic template for zeolite synthesis. For example, the rice husk ashes from biomass power plants are used to synthesize LTA and FAU zeolites for the adsorption of cadmium because they are rich in amorphous silica (83-90%).[184, 185] Up to date, the zeolites that could be synthesized from biomass waste were pointed out, such as MFI, FAU, LTA, BEA, MEL, SOD, EMT, LTL, etc.[186] The preparation methods mainly focused on the hydrothermal process, microwave irradiation, and ultrasonication approach, etc.[60] Various researches have reported that biomass-assisted zeolites can improve the performance in many fields than zeolites without biomass waste. Eng-Poh Ng and co-workers reported that the bamboo leaf biomass-synthesis zeolite LTA exhibited an excellent catalytic performance in solvent-free cyanoethylation reaction of methanol, with ca. 82% conversion and 100% selectivity even after 10 cycles.[187] Zhang *et al.* also used bacteria as organic templates to prepare ordered microporous zeolite fibres.[188] Interestingly, eggshell membrane has also been used to produce zeolite structures.[180, 189]

Recently, several studies from Louis *et al*. have reported the use of biomass as potential template to synthesize zeolites for the methanol-to-olefins (MTO) reaction and the valorization of bio-waste. ZSM-5 zeolites, which is a medium pore zeolite with channels defined by 10-MR, were synthesized in the presence of sugarcane bagasse,[190] lignin,[191] vanillin,[191] coumaric acid,[191] and coal fly ash,[192] and showed quite different structural properties and catalytic performances. For instance, ZSM-5 was prepared by using cheap sugarcane bagasse and exhibited the lowest Si/Al ratio (SAR = 8) ever reported.[193]

The existence of polyamines, proteins and sugars had visible differences and great impact to assembly the crystals allowing them to mimic biomineralization processes and giving unexpected characteristics.[6] Inspired by the features of afore-mentioned biomasses which possess complex organic components and hierarchical structure, purposeful selecting the biomass can be expected to develop the catalytic performance effectively. In particular, spent tea leaves have drown our attention because they also

contain sophisticated organic architectures, including sugars, proteins, lignin, oxyaromatic acids, catechins, polyphenols, etc., and many kinds of metal elements.[162, 194] Therefore, a promising ZSM-5 catalyst for MTO process could be expected through the assistance of certain biomasses (*i.e.* oxidized lignin, Russian lignin, sugarcane bagasse, ecoshell, coffee, tea residues, algae and a commercial Kraft lignin, denoted as alkali lignin). Moreover, this work not only offers an excellent ZSM-5 catalyst for the methanol conversion, but also involves a "bio-sourced secondary template" strategy for zeolite syntheses and biomass waste valorization.

1.3 The Methanol-To-Olefins (MTO) reaction

1.3.1 Introduction

The methanol-to-olefins (MTO) process is a crucial non-petrochemical route to produce ethylene, propylene and other hydrocarbons from C_1 chemical feedstocks,[1, 2] which can first be obtained from coal or natural gas.[195] The production of light olefins has attracted a huge attention during the last decades due to the ever increasing market demands toward ethylene and propylene far from being met by current steam cracking and catalytic cracking of naphtha fraction.[1] Propylene and ethylene are the most important monomers for petroleum industry production worldwide. Propylene is used as a raw material of polypropylene to produce films, fibers, containers, packaging, etc. and can be converted to various common chemicals, such as propylene oxide,[196] isopropanol, acrylonitrile, acrylic acid,[197] etc.[198]

It is well known that the product selectivity is mainly impacted by framework structure, acid site properties and reaction conditions in zeolite catalysis.[199] Therefore, a rational design of acidic zeolites to reach high selectivity to light olefins becomes a great challenge in state-of-the-art catalysis research industrial application.[200] Although there are many kinds of acidic zeolites with potential to be used in methanol conversion process, only two catalysts, which are ZSM-5 [3, 201, 202] (MFI) and SAPO-34 (CHA),[203-205] draw considerable attention thanks to their specific framework topologies, such as pore diameter and cage size. Although great progresses have been achieved with the above two types of catalysts, each of them still offers their own disadvantages, for

instance, a fast coke formation and residue in the cage usually cause a rapid deactivation and a short lifetime of SAPO-34 (silico-aluminophosphate), as shown in Figure 1.21. As a result, ZSM-5 catalyst is more often used in the MTO reaction despite its lower selectivity.[12, 200, 206, 207]

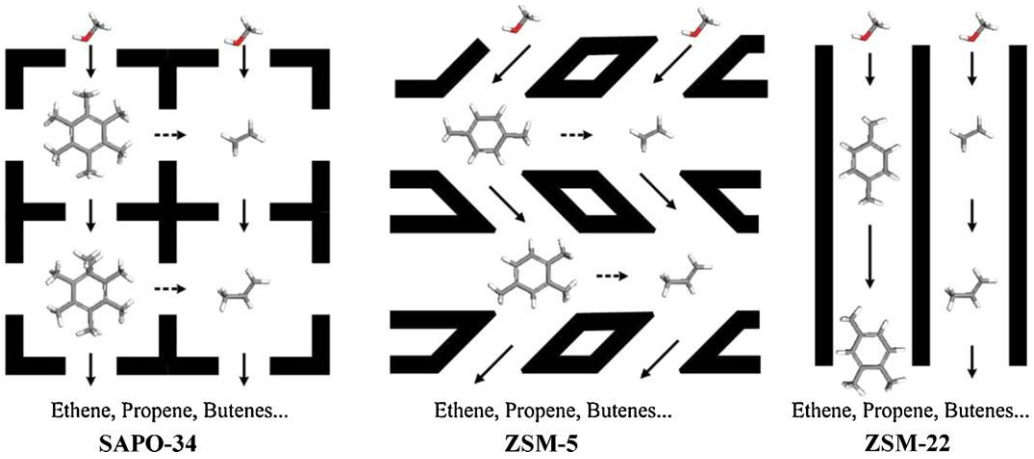

Figure 1.21 Comparison of reaction routes of methanol conversion over zeolites with different pore structures.

1.3.2 Development of ZSM-5 as MTO catalysts

By modifying and developing new ZSM-5 catalysts at nearly full conversion, excellent stability, and high selectivity to light olefins is highly demanded. Several contributions dealing with the ZSM-5 zeolite have been found to enhance catalytic performance in the MTO reaction recently, such as (1) incorporating alkali metals,[208] rare-earth metals,[209] and alkaline earth metals[210] in the framework to modify the acidic property,[142] (2) doping of zeolites by transition metals (Mn, Co, Ni) resulted in the generation of new acid sites,[211] (3) designing special morphology to decrease the diffusion length or enhance the diffusion efficiency,[212, 213] (4) synthesizing nano-sized ZSM-5 crystals with shorter diffusion length,[214, 215] (5) composite zeolites [216, 217] (6) preparing the hierarchical ZSM-5 zeolites by various methods,[218-220]. Besides, it is worth noting that biomass as a bio-sourced secondary template provides a high affinity for inducing morphological and textural changes, chemical composition and surface property modifications in the synthesis of zeolites.[180, 188] However, almost no research yet exists that will allow for a complete and exhaustive characterization of biomasses due to their

complexity and diversity.[168] Furthermore, the mechanism(s) of how the biomass affects the self-assembly processes is still unclear.

Chapter 2. Experimental part

Abstract

This chapter will present in details the materials and methods, the characterization instruments that were used, as well as the reaction equipment. The characterization techniques mainly include: X-ray diffraction (XRD), scanning electron microscopy (SEM), N_2 adsorption-desorption, temperature-programmed desorption of ammonia (NH_3-TPD), elemental microanalysis of C, H, N, liquid chromatography-mass spectrometry (LC-MS). The catalytic performance set-up is described as well as the analytical gas chromatography (GC). The apparatus employed for methanol-to-olefins reaction are also described briefly.

2.1 Preparation of the materials

2.1.1 Reactants and catalysts

Biomasses treatment, ZSM-5 zeolites synthesis and MTO reaction were performed with the following reactants: sodium aluminate anhydrous ($NaAlO_2$, Riedel de Haën), tetrapropylammonium hydroxide (TPAOH 20 wt% in water, Sigma-Aldrich), tetraethyl orthosilicate (TEOS 99%, Sigma-Aldrich), sodium chloride (NaCl, Fisher Chemical), ammonium nitrate (NH_4NO_3 98%, Acros Organics), sodium hydroxide (NaOH 97%, Fisher Chemical), hydrochloric acid (HCl 37%, Sigma-Aldrich), and methanol (≥99.9%, HPLC gradient grade, Fisher Chemical).

Some commercial zeolites were also tested as comparative studies, which are NH_4-ZSM-5 (Zeolyst CBV3020E) and H-ZSM-5 (Zeolyst CBV28014). It is worth noting that the ammonium form zeolite was pre-treated at 550 °C for 15 h with a heating ramp of 1 h to get to the H-ZSM-5 form.

As mentioned before, a commercial alkali lignin and several biomass materials have been selected to be added to the gel during the synthesis, which are oxidized lignin, sugarcane bagasse, ecoshell, spent coffee grounds, spent tea leaves and 3 types of algae. In this Thesis, the lignin extracted from wood waste (Kirov petrochemical plant, city of Kirov, Russia) has been treated by the group of Prof. Aleksander Vasilyev (Saint-Petersburg State University) to provide its oxidized form.[7] Moreover, the alkaline solution of oxidized hydrolyzed lignin (OHL) form was prepared according to the following protocol: an alkaline solution (3.6 g of NaOH in 0.5 L of H_2O) was replaced in a flask and 20 g of OHL were added under stirring. Then the temperature increased to 85 °C and continued for 1 h. Then, the solution was cooled and filtered. All the algae were provided by the Institute of Chemical Process Fundamentals (ICPF), Czech Republic. Among them, two samples of waste biomass based on freshwater algae (Trachydiscus minutus and Bracteacoccus bullatus) and the last sample consists of mixture of freshwater cyanobacterium.

2.1.2 Synthesis of zeolites

Before the methods can be determined, we need to make it clear that the hydrothermal

process of synthesis zeolites with biomasses is quite complex, which is affected by many factors, such as: reactant sources, Si/Al ratio, the type and the quantity of biomasses, hydrothermal time and temperature, calcination time and temperature, etc. Fortunately, based on the papers and the synthesis methods our group has performed before, we can mainly focus our study on the influence of biomass and hydrothermal duration on the synthesis of ZSM-5. As a result of this, a series of ZSM-5 zeolites with the assistance of oxidized lignin were prepared by optimizing the hydrothermal time from 2 to 7 days and the amount of oxidized lignin varied from 200, 300, to 500 mg. The specific results will be discussed later in the Thesis. Since impurities were generated in the products during the latter preparation (Z-LO method), the H_2O/Si ratio was adjusted to decrease the amount of water from 60 mL to 41 mL with other conditions remaining unchanged. According to the above research on the preparation conditions, the specific preparation routes are shown as follow. The biomass-assisted ZSM-5 was prepared by using the hydrothermal method with the following molar ratio: $NaAlO_2$: TEOS : TPAOH : NaCl : H_2O = 1.0 : 9.7 : 14.2 : 3.9 : 2140.0. Specifically, 0.125 g $NaAlO_2$ and 0.350 g NaCl was added in a 500 mL Erlenmeyer flask with 30 mL distilled water. After, 21.9 mL TPAOH was also mixed to the solution under stirring. Then, 11 mL deionized water was added to the solution. After, 3.1 mL TEOS was added dropwise to the solution under vigorous stirring (ca. 700 rpm). Finally, certain amount biomass (200, 300, or 500 mg) was added in the solution. Ageing and homogenization of the mixture were performed during 2 h. The gel was then transferred to a Teflon-lined stainless-steel autoclave (60 mL effective volume) and placed in an oven at 170 ^oC for 2 days. Herein, the above steps are called A method, and these samples are named A-biomass-(2d, 200), A-biomass-(2d, 300) and A-biomass-(2d, 500), respectively.

The B method also adopts hydrothermal synthesis for preparing ZSM-5 crystals but with different molar ratio: $NaAlO_2$: TEOS : TPAOH : NaCl : H_2O =1.0 : 43.2 :16.6 : 26.4 : 7692.3. The general synthesis methodology consisted in the dissolution of 0.038 g of $NaAlO_2$ and 0.705 g of NaCl in 30 mL distilled water. Then, 7.6 mL of TPAOH (20% in H_2O) and 30 mL of distilled water were added to the previous solution. After, 4.5 mL of TEOS (99%) was added dropwise to this solution under vigorous stirring.

Different masses of biomass were added right after (200, 300, and 500 mg). After 2 h stirring and aging at room temperature, the gel was introduced in a Teflon-lined autoclave for the hydrothermal treatment at 170 ^{o}C for 2 days.

After hydrothermal treatment for both A and B methods, the solution was filtered and washed with distilled water until pH = 7 and dried at 110 ^{o}C. After that, the obtained powder was calcined at 550 ^{o}C for 15 h in air to remove the structure directing agent and obtain Na-ZSM-5. The obtained white powder then was ion-exchanged three times with 30 mL NH_4NO_3 aqueous solution (1 M) per 200 mg of ZSM-5 at 80 ^{o}C under stirring for 1 h. The solution was then filtered and washed with deionized water followed by drying at 110 °C in an oven. The ammonium zeolite-form was calcined at 550 ^{o}C for 15 h to leave acidic H-ZSM-5 zeolite.

2.2 Characterization techniques

2.2.1 X-Ray Diffraction

X-ray powder diffraction (XRD) as a basic and rapid analysis technique, was primarily used for the identification of crystalline materials and could give the information of unit cell dimensions based on the specific diffraction patterns. It is widely applied now because it can reveal detailed and intrinsic information of solid materials' chemical composition, crystallographic structure and atomic spacing without sample destruction.

Crystals are a series of regular arrays of atoms arranged in three-dimension space to form the parallel planes. The distance, d, between different planes is determined by the nature of the materials; in other words, each solid owns its specific d-spacing. XRD is based on the constructive interference of monochromatic X-ray and a crystalline material. Herein, X-ray can be regarded as waves of electromagnetic radiation. The constructive interference will be produced when monochromatic X-ray beams are projected onto the sample's surface, as well as their path length difference equivalent to the integer number of their wavelength, as determined by Bragg's law:

$$n\lambda = 2dsin\theta \quad (1)$$

with d: spacing between diffracting planes in the atom lattice

θ: the incident angle, also called Bragg's angle

n: any integer number

λ: the incident beam wavelength

By scanning the powder through a range of 2θ angles, all possible diffraction directions of the lattice could be detected because of the random orientation of powdered materials. Finally, the crystalline structure of as-prepared materials can be determined by comparing the XRD pattern to the Joint Committee on Powder Diffraction Standards (JCPDS) files.

In this Thesis, all powder XRD patterns were recorded on Bruker AXS D8 Advance diffractometer and LynxEye detector, within the range of 2θ = 5-65° with a step size of 0.02° and a step time of 2 s. The analyses were performed with a source of X-ray (Cu Kα radiation, 1.5406 Å) and a power of 40 kV×40 mA. The patterns were processed with the software EVA (Bruker) and compared with the data base ICDD.

2.2.2 Scanning Electron Microscopy

Another "non-destructive" analysis technology, the scanning electron microscope (SEM) is used to observe the morphology of as-synthesized ZSM-5 crystals, including their particle size and shape, the degree of aggregation, and the content and distribution of each element. SEM technique involves a focused beam of electrons, accelerated by a 10 to 20 kV voltage, to generate a variety of signals with atoms at the surface of solid samples. These signals can contain large amount of information about the external topography and chemical composition of the materials, which include secondary electrons, back-scattered electrons, diffracted back-scattered electrons, photons, visible light and heat.[221] Secondary electrons (SE) as the most common SEM mode for imaging samples among them, can be explained that secondary electrons emitted by atoms excited by the electron beam are detected using a secondary electron detector.

The morphologies of different zeolites were observed using Zeiss Gemini SEM 500 microscope working at 9 kV accelerating voltage. Before observation, the samples were covered with a thin layer of Au for 60 s under Ar atmosphere to increase the electrical conductivity. Besides, the SEM can also perform the chemical compositions and distribution of elements of selected point locations on the materials in (semi)-

quantitatively determination by coupled with energy dispersive spectrometer (EDS) technique.

2.2.3 N_2 Adsorption-desorption

The Brunauer-Emmet-Teller (BET) theory consists in the physical adsorption of gas molecules to determine the surface area of the solid sample and its pore diameter on the basis of N_2 adsorption isotherm measurements at 77 K (liquid nitrogen). This theory is an extension of the Langmuir theory and assumes that multilayer adsorption occurs on the surface. The isotherms are obtained by following the adsorbed N_2 amount per gram of solid with an increase in the relative pressure as well as the reverse process. The equation (2) also presents some limits. For example, the linear relationship of this equation is only valid in the range of 0.05 to 0.35.

$$V = \frac{V_m pC}{(p_s - p)[1 - (p/p_s) + C(p/p_s)]} \times 100\% \quad (2)$$

with p: the equilibrium pressure, (Pa)

p_s: vapor pressure of the adsorbate at the measured temperature, (Pa)

V_m: vapor volume needed to completely recover the surface with a mono-molecular layer of adsorbate, (mL)

V: vapor volume adsorbed per gram of sample at pressure P, (mL)

C: constant of the studied gas-solid system

N_2 adsorption-desorption is one of the basic characterizations for porous materials, especially for cement, concrete, activated carbon, zeolites, etc. The technique was conducted by using an ASAP 2420 instrument (Micromeritics). N_2 adsorption-desorption isotherms were obtained after outgassing at 220 °C under vacuum overnight. The specific surface area (SSA) was calculated by the Brunauer-Emmett-Teller (BET) method in the range of relative pressure P/P_0 = 0.05-0.25. The pore volume and pore size distributions were determined by the Barrett-Joyner-Halenda (BJH) method.

2.2.4 NH_3 Adsorption

Temperature-programmed desorption (TPD) with ammonia is widely used for heterogeneous catalysts characterization, such as zeolites, revealing information on acid sites, like their concentration, strength and type (Brønsted or Lewis).[222, 223]

The analysis was performed in a chemisorption analyser AutoChem II from Micromeritics. Prior to the measurement, around 50 mg powder in a quartz U-tube were firstly activated under 500 ºC for 1 h to eliminate any adsorbed water or other impurities. Then, cooling down to 100 ºC and waiting for saturation under a continuous flow of 10% NH_3 for 30 min (30 mL/min). Physically adsorbed NH_3 can be removed by purging with He at the same temperature for 30 min. After that, the desorption process was performed by ramping the temperature from 100 ºC to 700 ºC at a rate of 10 ºC/min under He flow. During this process, a built-in thermal conductivity detector (TCD) monitored the concentration of the desorbed species.

2.2.5 Elemental microanalysis C, H, N

Microanalysis is an effective analysis mean for chemical identification and quantitative analysis of small amounts of samples and materials. To have a further understanding of several kinds of biomasses, simultaneous elemental microanalysis of the C, H and N were conducted by “Flash 2000” apparatus from ThermoFisher Scientific on about 1 mg of biomass powder. Besides, each sample was tested twice. This technique was performed at the Fédération de Chimie Le Bel.

2.2.6 Liquid chromatography-mass spectrometry

The extract of tea residues was analyzed by liquid chromatography-electrospray tandem mass spectrometry (LC-MS). The LC-MS instrument utilized was a Waters ACQUITY UPLC H-Class System equipped with a ACQUITY UPLC BEH C_{18} column (2.1 mm x 100 mm, 1.7 μm), and connected to a WatersXevoG2-XSQ-Tof mass spectrometer with electrospray ionization source. Elution was carried out at 30 °C, using a 0.1% (v/v) formic acid/water solution as mobile phase A, and a 0.1% (v/v) formic acid/methanol solution as mobile phase B. A flow rate of 0.3 mL/min was employed. The injection volume was 1.0 μL. The detection wavelength was 258 nm. The mass spectrometer was

operated in the positive ionization mode over a full scan range of 100-1000 m/z with the following settings: gas temperature of 450 °C, gas flow of 50 L/h, source temperature at 120 °C, and capillary voltage 3 kV.

2.3 Methanol-To-Olefins reaction

The MTO conversion over the zeolites was investigated using a fixed-bed reactor at atmospheric pressure. Prior to reaction, the catalysts were calcinated at 550 ^{o}C for 1 h under argon flow to remove impurities, after which the reactor temperature was decreased to 450 ^{o}C for the reaction. About 0.6 g catalyst powder was filled into the tubular quartz reactor and packed within two quartz wool plugs at both ends.

A determined constant argon flow was flown through a methanol saturator (ca. 0 ^{o}C) to achieve WHSV= 2.0 $g_{MEOH}/(g_{cat}.h)$. The products at the outlet were analysed every hour by GC equipped with a 50 m capillary column (PONA) and a flame ionization detector (FID). The GC program consisted in an isothermal at 40 ^{o}C for 7 min, followed by an increase of 20 ^{o}C/min until 280 ^{o}C and an isothermal at this temperature for 10 min. In the calculated methanol conversions and selectivities (wt%), dimethyl ether (DME) is considered as unconverted methanol.

The MTO reaction set-up used in our laboratory was shown in Figure 2.1.

The methanol conversion (X) over acid zeolite catalysts was defined in terms of methanol- and dimethyl ether-conversion, calculated from the difference between inlet and outlet concentration of methanol (DME being considered as a reactant). The selectivity was expressed as the ability to direct the reaction to give a particular product under the same reaction conditions. Here, the selectivity was considered as the mole ratio of each product referred to the moles of converted methanol and DME. The expressions of conversion and selectivity were shown in Equations (3) and (4). All the selectivities were expressed after 1 h on stream.

$$X = \frac{\text{n MeOH in - (n MeOH out + 2*n DME)}}{\text{n MeOH in}} * 100\% \quad (3)$$

$$S = \frac{\sum \alpha * \text{n (CH2)}}{\text{n MeOH in} - (\text{n MeOH out} + 2 * \text{n DME})} * 100\% \quad (4)$$

Where n represents the quantity of the desired fraction and α is the number of C-atoms in products, ∑ means the calculation of the selectivity towards light olefins (C_2-C_4 olefins).

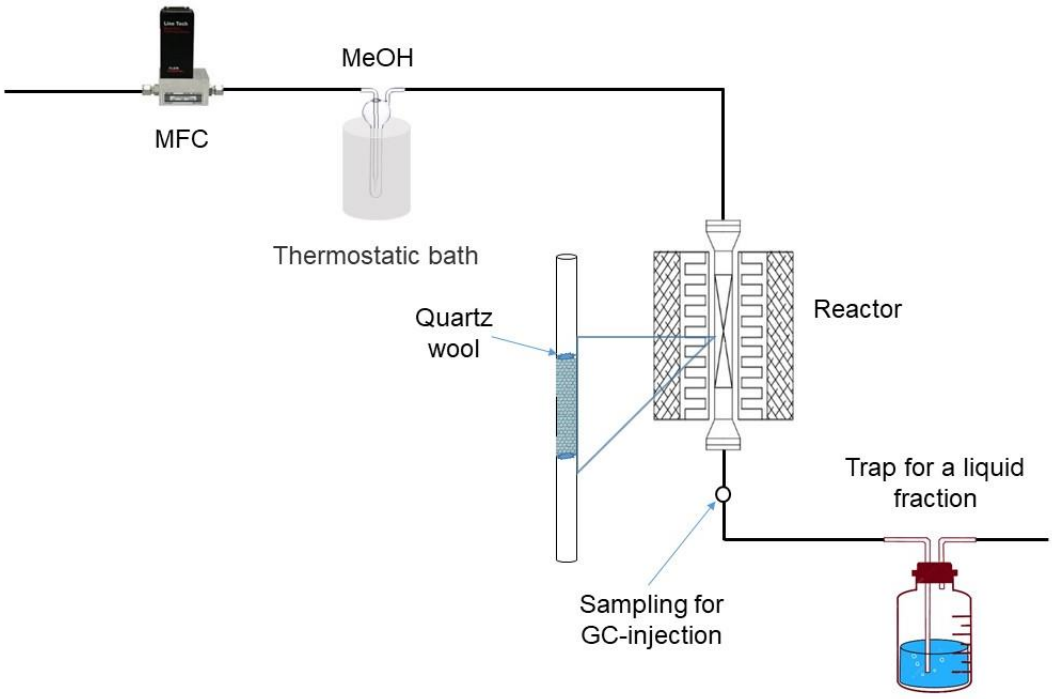

Figure 2.1 Experimental set-up for the MTO reaction.

Chapter 3. Synthesis and characterization of biomass-assisted zeolites

Abstract

The optimal hydrothermal duration and biomass composition and quantity were studied in this chapter for the synthesis of ZSM-5 zeolites. Indeed, several ZSM-5 zeolites were synthesized by changing the hydrothermal duration and testing three different reactant molar ratio. The later procedures were named as Z-LO method, A method and B method.

As-synthesized biomass-assisted ZSM-5 zeolites were characterized by XRD, SEM, BET, and NH_3-TPD techniques to investigate the effects of those biomasses extra-addition. The morphological, textural and surface acidic properties of those biomass-mediated ZSM-5 were significantly impacted by the presence of biomass.

Besides, the influence of the amount of TPAOH template was also investigated. Interestingly, some biomasses play a positive role as bio-sourced secondary templates (BSST) and facilitate the crystallization process of ZSM-5. This approach could therefore be a promising strategy to reduce the usage of expensive and toxic organic template, and hence to valorize this abundant bio-waste.

3.1 Introduction

It is widely known that zeolite synthesis is an intricate process which may be influenced by various factors, such as the composition of reactants, pH, temperature, agitation, synthesis duration, etc.,[224] as already mentioned in the previous chapter. Such understanding is still one of the major challenges in zeolite research and attract more people to further explore in this direction. Based on the previous research in our group, the synthesis recipe can be determined basically, by the reactant source and ratio, agitation, aging time, hydrothermal temperature. These specific parameters were presented in Chapter 2. ZSM-5 catalysts were prepared by using hydrothermal treatment using three different methods, which are Z-LO method, A method and B method. Their molar ratio are the following: $NaAlO_2$: TEOS : TPAOH : NaCl : H_2O = 1.0 : 9.7 : 14.2 : 3.9 : 2140.0 for **A method**; and $NaAlO_2$: TEOS : TPAOH : NaCl : H_2O =1.0 : 43.2 :16.6 : 26.4 : 7692.3 for **B method**. **Z-LO method** and A method involve similar ratio, only a decrease in the amount of water from 60 mL to 41 mL with other conditions unchanged. However, for the purpose of modification of zeolites and the valorization of bio-wastes, addition of biomass as potential secondary organic template will affect zeolite crystallization process, at the same time, the hydrothermal time also changes subsequently. In general, the synthesis process of a zeolite can be divided into four different stages: induction time, nucleation, crystal growth and Ostwald ripening stage. Enough time is therefore necessary to complete the four steps and form well-defined crystals. Because several metastable phases exist under specific conditions, the products are sometimes obtained as a mixture or amorphous matter. Therefore, to some extent, it seems that the longer the hydrothermal time, the more crystalline the zeolites should form. Whereas, from an industrial point of view, longer synthesis process means more running costs. Therefore, after comprehensive consideration of various factors, it is essential to select an optimal hydrothermal duration and biomass consumption, and characterize the effect of biomass on the crystallization process of as-synthesized zeolites.

Conventional organic templates such as tetrapropylammonium cations or amines (TPA^+) have typically been used for the preparation of ZSM-5 zeolites, which play an

important role in both structure-directing and micropore filling. However, the extensive and abundant use of templates has caused series of problems, such as (1) the high price that limits its implementation in industry, (2) their toxicity, (3) the removal of organic templates is normally after calcination at high temperature, causing a large number of polluting gases (*e.g.,* NO_x, and CO_2). Therefore, there is a growing research trend to reduce the use of organic templates and overcome their disadvantages, including synthesis with low-toxicity and cheap organic templates, synthesis with recyclable organic templates, as well as organotemplate-free routes (adjusting molar ratios, seed-assisted synthesis, zeolite crystal seed-directed synthesis), etc.[9, 225, 226] For instance, an organotemplate-free Beta zeolite was first synthesized by Okubo *et al.*,[227] however there are still many challenges for reducing the use of organic template.[228] For example, the synthesis method cannot be widely used in other zeolites (especially not easily for aluminophosphates and pure silica zeolites), and the hydrothermal time is relatively long, etc.[229, 230] In this chapter, we also investigate the influence of the amount of TPAOH template during the ZSM-5 synthesis and tried to reduce the use of template.

Furthermore, the organic structure-directing agents-based strategy was replaced by a novel green route involving a bio-sourced template, thus a biomass-derived template synthesis strategy. The bio-templates are commonly applied for the production of metal oxides, metal nanoparticles and mesoporous materials, but less explored in the synthesis of zeolites, which means that there's still a lot of potential in this field. Herein, our studies will present the use of some agricultural waste or domestic residue to guide the crystallization of ZSM-5 zeolites and their characterization in terms of structure, morphology and acidic properties, etc.

3.2 Influence of hydrothermal duration and biomass composition and quantity

Several zeolites were synthesized by conventional hydrothermal method for several days with different amounts of oxidized lignin, and summarized in Table 3.1.

Table 3.1 Evaluation of the hydrothermal time and the amount of biomass.

Days (d) \ Mass (g)	0.200	0.500	0.300
2	Z-LO-01	Z-LO-04	Z-LO-07
5	Z-LO-02	Z-LO-05	Z-LO-08
7	Z-LO-03	Z-LO-06	Z-LO-09

In order to shorten the hydrothermal time without affecting the zeolite properties and also select the proper mass of biomass, the time was varied between 2 and 7 days; the mass from 200, 300 to 500 mg were set. These samples were named Z-LO-01 to Z-LO-09.

Figure 3.1 shows the diffraction patterns of as-prepared samples after different durations and quantities of oxidized lignin after the calcination step and their corresponding blank samples without oxidized lignin, named as Z-LO-REF (2d), Z-LO-REF (5d) and Z-LO-REF (7d), respectively. The diffraction peaks correspond to ZSM-5 zeolite (JCPDS, PDF79-1638), which possess unit cell dimensions of a = 20.048 Å, b = 19.884 Å, c = 13.352 Å, and *Pnma* space group. However, the Bragg diffraction patterns also show a mixture of ZSM-5 and analcime (ANA), which chemical formula is $Na(AlSi_2O_6)(H_2O)$ (JCPDS, PDF86-2455), when the crystallization is not complete. As it can be seen from Z-LO-01 to Z-LO-03, Z-LO-04 to Z-LO-06 and Z-LO-07 to Z-LO-09, there was an appearance of diffraction peaks of ZSM-5 which became significantly stronger at longer hydrothermal times. Especially for Z-LO-03, and Z-LO-06, the (quasi)-sole presence of the MFI structure is exhibited and the peaks of impurity vanished. Compared with the reference samples, the effect of biomass is not very obvious based on these XRD patterns, and no biomass characterization peaks were observed. In addition, the intensities of the diffractions for zeolites produced with 300 or 500 mg oxidized lignin were stronger than zeolites with 200 mg oxidized lignin. Therefore, we infer that more biomass may promote the crystallization of zeolites. Besides, it can be seen that the addition of biomass did neither destroy the crystalline structure of the zeolite, nor contributed to the appearance

of oxidized lignin's phase.

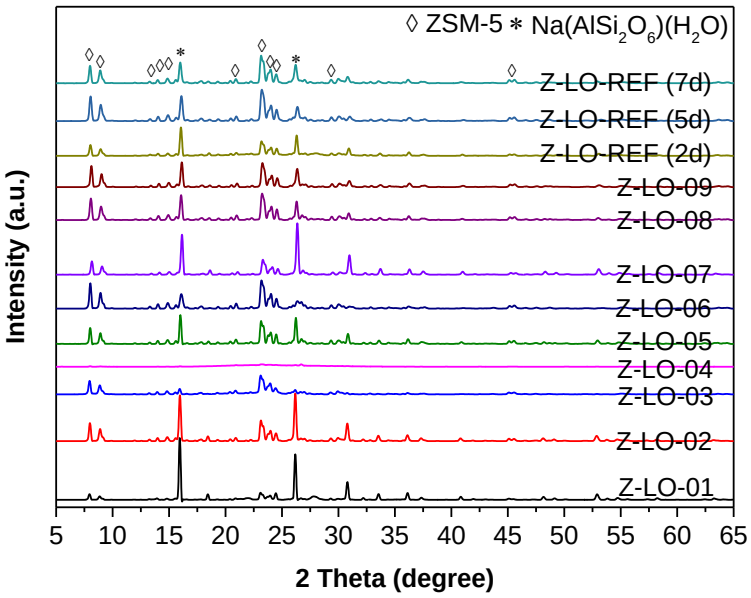

Figure 3.1 XRD patterns of the samples prepared at different times and with different masses of oxidized lignin.

SEM micrographs of each sample are shown in Figure 3.2 (a-i) and the results are in line with XRD patterns. The morphologies of the crystals found in Figure 3.2 (b, e-i) exhibited the characteristic coffin-shape, associated to ZSM-5 zeolite (MFI type) along with crystal sizes of 4-10 µm. Interestingly, the sample Z-LO-03 (Figure 3.2 (c)) exhibits small spherical crystals presenting a high surface roughness, and the same morphology can be found in our group's former studies. The classical morphology of the MFI crystals is replaced by spherical crystals similar in size in the presence of wood lignin.[6, 191] Figure 3.2 (a and d) did not show any crystal due to the short crystallization time, suggesting the presence of ANA and amorphous material, respectively. However, by combining with XRD results, it appears that zeolite crystals in Z-LO-07 samples (Figure 3.2 (g)), inferring that the proper amount of biomass is 300 mg under the same synthesis conditions.

In conclusion, it is found that the optimum amount of biomass is 300 mg and the longer hydrothermal time (7 days) is beneficial for the zeolite crystal growth.

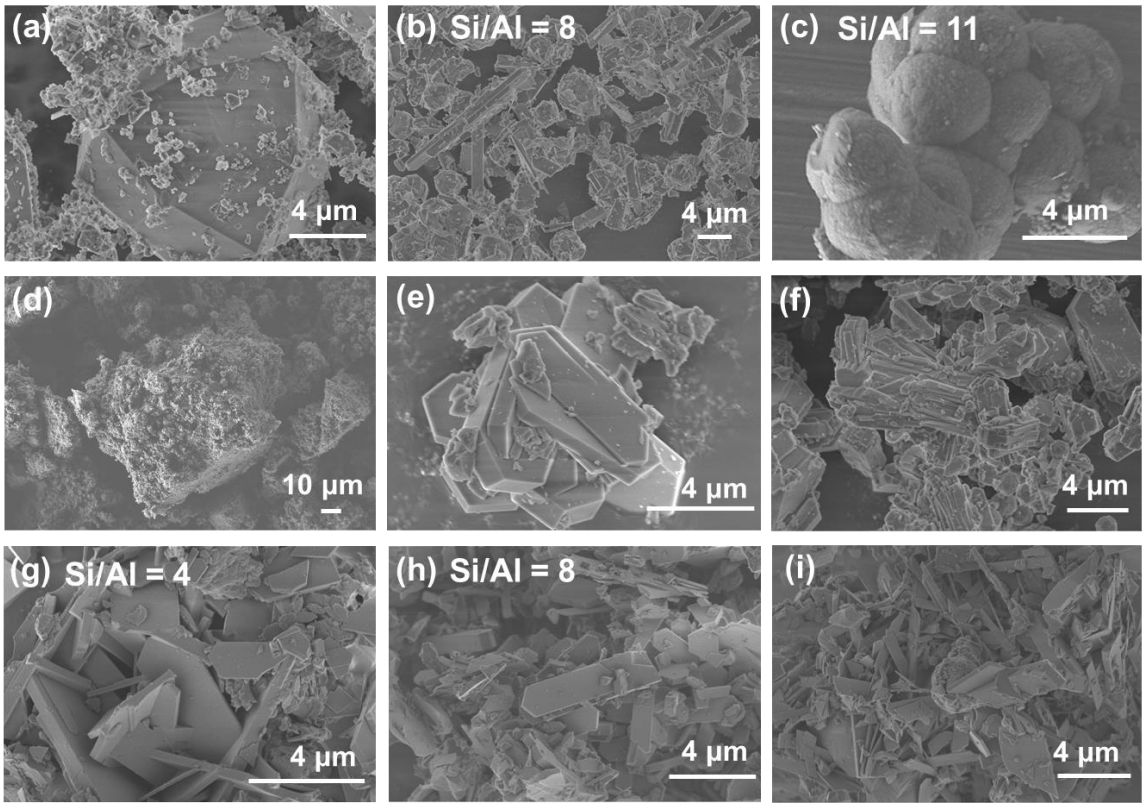

Figure 3.2 SEM images of (a-i) oxidized lignin-based ZSM-5 from Z-LO-01 to Z-LO-09.

3.3 Characterization of biomass-assisted zeolites

In order to obtain pure ZSM-5 crystals, the reactants ratio was adjusted to $NaAlO_2$: TEOS : TPAOH : NaCl : H_2O = 1.0 : 9.7 : 14.2 : 3.9 : 2140.0, and denoted as A method. The different zeolites synthesized by A method were characterized by X-ray diffraction. According to those patterns in Figure 3.3, it is possible to confirm that the sole presence of MFI structure can be obtained. It is worthy to mention that most biomasses-assisted zeolites exhibited higher intensities for the main reflections (101), (200), (501), (151), (313) when compared with A-REF sample. In other words, biomasses promoted the zeolite self-assembly process and well-defined crystals formation under the same synthesis conditions, as the bio-sourced secondary templates (BSST). Furthermore, it demonstrates that the BSST strategy plays a positive role in the synthesis of zeolites.

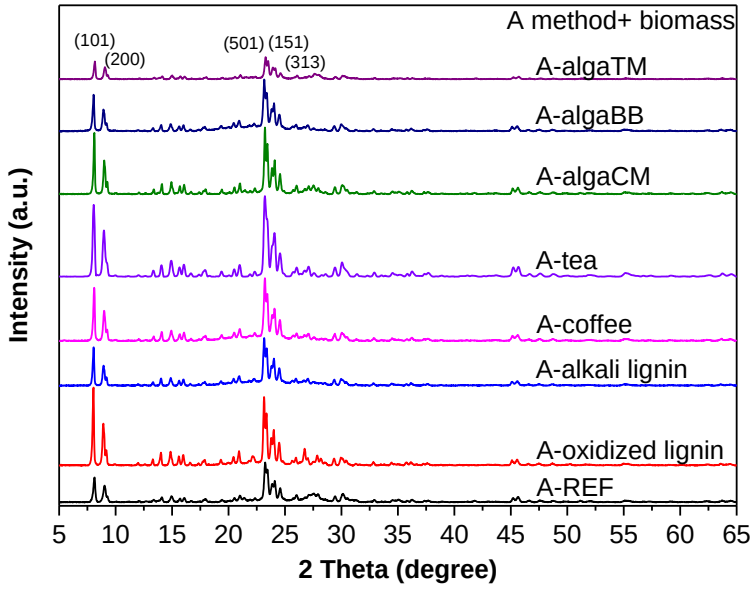

Figure 3.3 XRD patterns of the samples prepared by A method with different biomasses.

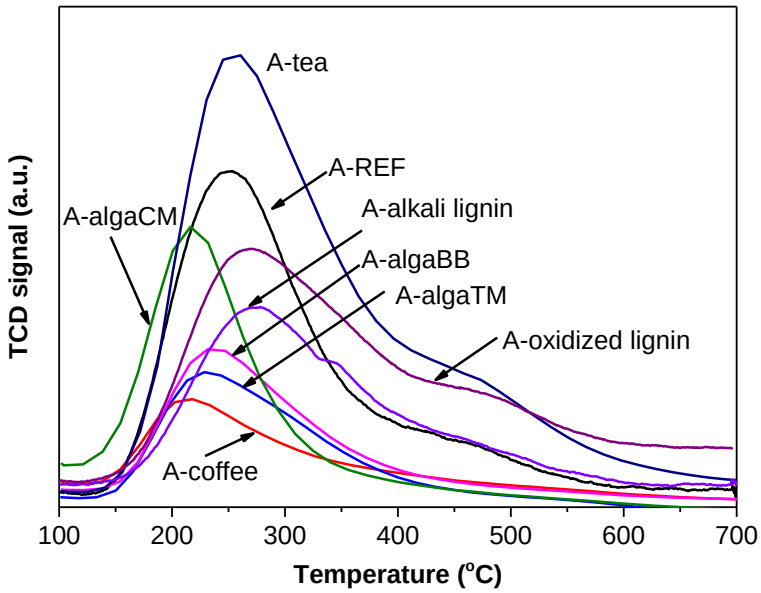

Figure 3.4 NH_3-TPD profiles of A method-ZSM-5 catalysts obtained with different biomasses.

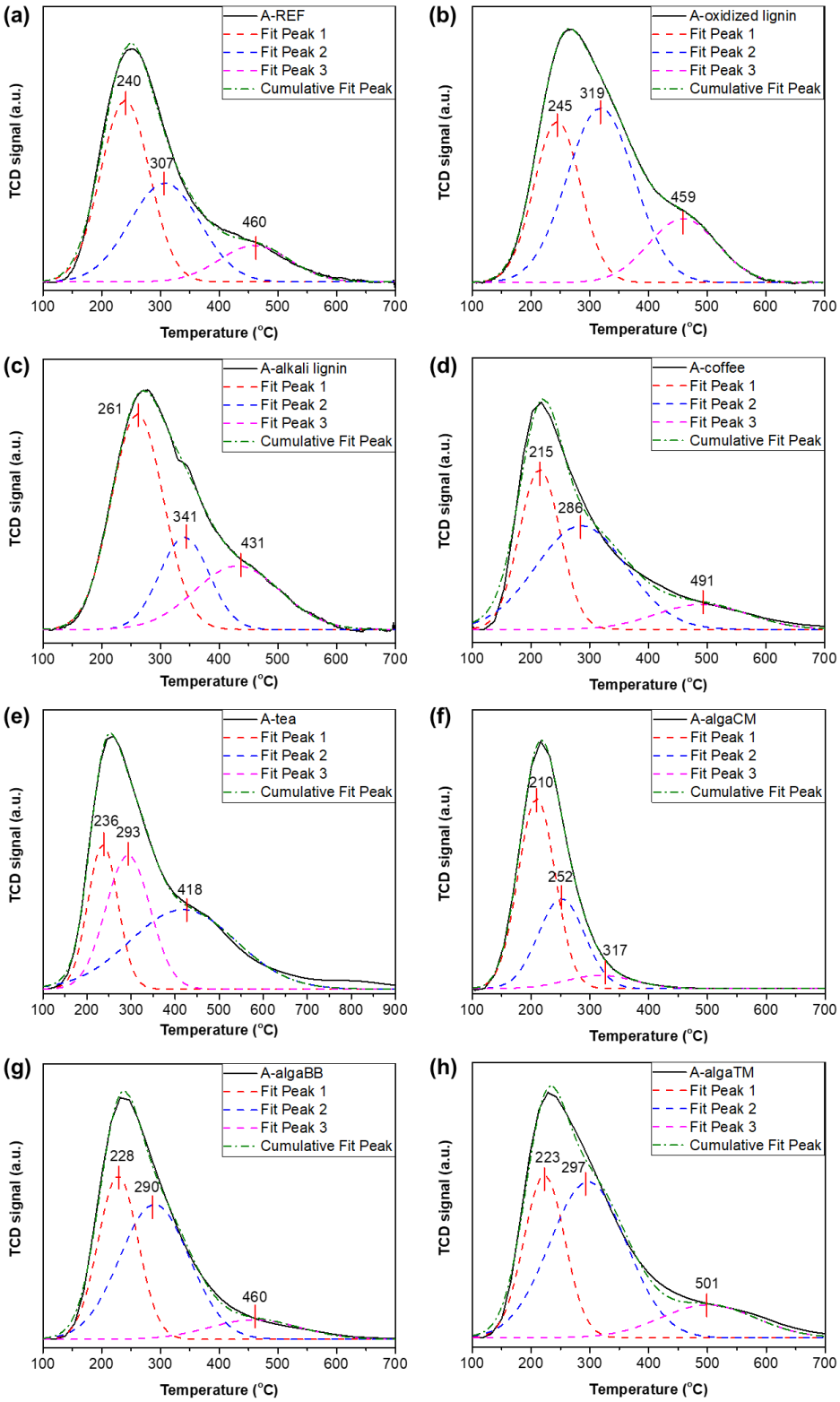

Figure 3.5 NH_3-TPD profiles and their corresponding deconvolution peaks into Gaussian peaks ($R^2 > 0.99$) of A method-ZSM-5 (a) without biomass, and with different biomasses: (b) oxidized lignin, (c) alkali lignin, (d) coffee, (e) tea, (f) algaCM, (g) algaBB, (h) algaTM.

The acidity of ZSM-5 and biomasses-derived ZSM-5 catalysts were determined by NH_3-TPD, as shown in Figure 3.4. In Figure 3.5, all curves were deconvoluted into three peaks by fitting experimental peaks according to the literature's method.[231] The peaks at temperatures <250 ºC, 250-350 ºC, and 350-500 ºC correspond to the desorption of NH_3 from weak acid, medium acid and strong acid types, respectively.[8] With these NH_3-TPD results in hand, it is possible to discriminate the acidic strength, indeed low temperature desorption corresponds to weak acid sites, whilst higher desorption can be regarded as strong Brønsted acid sites. Both weak acid sites and medium acid sites involve Lewis acidic sites, silanol groups, defects in the zeolite framework, etc., and strong acid sites are solely attributed to Brønsted acid sites that were formed by the bridged framework Al species.

Besides, the acid sites content (mmol/g) and specific peak positions (ºC) were summarized in Table 3.2. Eight samples showed different results in terms of their acidic properties thanks to the assistance of biomass. The acid sites distribution changed significantly after the BSST procedures. Although the total amount of acid sites decreased for most of the zeolites prepared with biomass, tea-assisted ZSM-5 still showed an increased total acid amount from 0.052 to 0.072 mmol/g, thus a 38% increase. A similar downward trend could be seen in former studies with zeolites prepared by glucose addition.[232] Among them, A-oxidized lignin and A-algaCM catalysts exhibited a relatively higher acid amount than other biomass-mediated zeolites, which were 0.035 and 0.046 mmol/g, respectively. Besides, A-alkali lignin, -coffee, -algaCM, -algaBB and -algaTM exhibited a decrease in the content of strong acid sites from 0.007 for reference ZSM-5 to 0.006, 0.001, 0.003, 0.002, and 0.001 mmol/g, respectively, while A-tea zeolite increased the strong acid sites content to 0.032 mmol/g due to an increase in framework aluminum species and (maybe) higher crystallinity. In addition, two samples, A-REF and A-algaCM, showed quite high content of weak acid sites, which were 0.025 and 0.027 mmol/g, respectively. The highest medium acid sites content was achieved over A-tea ZSM-5, which was 0.023 mmol/g. Because of the complexity of biomass topology, it is quite difficult to draw a conclusion how biomasses affect the acidity (at least so far).

Table 3.2 Acidity of A method-ZSM-5 and biomass modified ZSM-5 zeolites (2 days, 300 mg biomass).

Catalysts	Acid amount (mmol/g)	Acid sites content (mmol/g)			Peak position (°C)		
		Weak	Medium	Strong	Weak	Medium	Strong
A-REF	0.052	0.025	0.020	0.007	240	307	460
A-oxidized lignin	0.035	0.011	0.017	0.007	245	319	459
A-alkali lignin	0.022	0.012	0.005	0.006	261	341	431
A-coffee	0.010	0.004	0.005	0.001	215	286	491
A-tea	0.072	0.017	0.023	0.032	236	293	418
A-algaCM	0.046	0.027	0.016	0.003	210	252	317
A-algaBB	0.018	0.007	0.010	0.002	228	290	460
A-algaTM	0.006	0.002	0.003	0.001	223	297	501

As shown in Table 3.3, the relative crystallinity of A-REF ZSM-5 and biomass modified ZSM-5 zeolites were determined by using a standard Integrated Peak Area Method, which involves a comparison of the characteristic more intense peak $2\theta = 23^{o}$.[233] It can be seen that not all samples produced with biomass had an increase in their relative crystallinity, that only oxidized lignin, tea residue, algaCM and algaBB played a positive role in the zeolite crystal growth by A method. Obviously, the shorter hydrothermal duration is another reason for achieving an incomplete crystallization. Therefore, other biomasses, like alkali lignin and algaTM, did not improve the crystallization kinetics and promote self-assembly of ZSM-5 in a limited time. Because of the incomplete crystallization, those materials were not characterized further, but we tried to find a new method by changing the proportion of reactants to complete the crystallization process in a shorter time (2 days).

Even though several biomasses did not improve the relative crystallinity, A-tea ZSM-5 zeolite still exhibited outstanding properties in terms of relative crystallinity,

crystallization kinetics and acidic properties.

Table 3.3 Relative crystallinity of A method-ZSM-5 and biomass modified ZSM-5 zeolites.

Catalysts	Relative crystallinity (%)
A-REF-2d	69
A-oxidized lignin-2d-300	78
A-alkali lignin-2d-300	53
A-coffee-2d-300	67
A-tea-2d-300	86
A-algaCM-2d-300	76
A-algaBB-2d-300	72
A-algaTM-2d-300	48

As aforementioned, to synthesis well-defined zeolites in a limited time, the following new molar ratio were used: $NaAlO_2$: TEOS : TPAOH : NaCl : H_2O =1.0 : 43.2 :16.6 : 26.4 : 7692.3, and called as B method.

Figure 3.6 shows the XRD patterns of well-crystalline ZSM-5 zeolites synthesized via B method with the assistance of 7 types of biomasses (oxidized lignin, alkali lignin, coffee bagasse, spent tea leaves and three kinds of algae). All patterns exhibited the sole characteristic diffractions of MFI type materials, and the addition of biomasses did not contribute to the appearance of a new crystalline phase as observed with the A method.

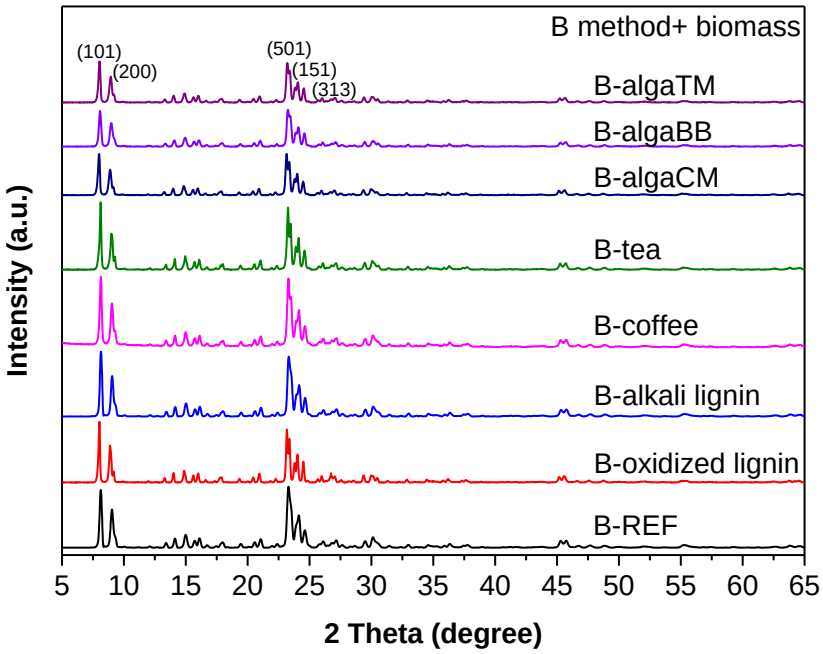

Figure 3.6 XRD patterns of pristine ZSM-5 (B-REF) and the ZSM-5 zeolites obtained with different biomasses.

The relative crystallinity of different biomasses-assisted ZSM-5 zeolites are presented in Table 3.4. It is noteworthy that the relative crystallinity of the samples significantly increased by shifting from A to B method. Thus, the synthesis of ZSM-5 by using B method seems to be a proper and cost-efficient way to shorten hydrothermal duration. In Table 3.4, the highest relative crystallinity of 95% was obtained for B-algaTM-2d-300 zeolite, and the relative crystallinity for all zeolites was improved in the presence of biomass.

Table 3.4 Relative crystallinity of B method-ZSM-5 and biomass modified ZSM-5 zeolites.

Catalysts	Relative crystallinity (%)
B-REF-2d	81
B-oxidized lignin-2d-300	83
B-alkali lignin-2d-300	88
B-coffee-2d-300	86

B-tea-2d-300	89
B-algaCM-2d-300	87
B-algaBB-2d-300	87
B-algaTM-2d-300	95

The microstructure of all catalysts was analyzed by SEM, as shown in Figure 3.7. Their morphologies appear different because of the effect of BSST and a bimodal crystallization was observed in Figure 3.7(a, c-e). According to Figure 3.7(a, c, and d), it can be seen that pristine ZSM-5 and ZSM-5 formed in the presence of alkali lignin and spent coffee bagasse exhibited a spherical aggregation with a particle size in the range of ca. 2 to 4 μm. Whilst in Figure 3.7(b, e-h), B-oxidized lignin, B-tea, B-algaCM, B-algaBB and B-algaTM zeolite crystals exhibited the characteristic coffin-shaped morphology associated to ZSM-5, without spherical crystals formation. These morphology changes can be attributed to the limited mono-directional b-axis crystal growth.

This was also observed for other zeolites produced after an addition of organic molecules, like urea,[234] or d-arginine (d-Arg) amino acid[4]. The intrinsic reason may be due to the formation of H-bond, van der Waals, or electrostatic interactions between biomass molecules and T-monomers in the zeolite precursors solution. The latter phenomenon appears rather similar to crystal growth inhibition of calcium oxalate monohydrate using hydroxycitrate from a fruit "garcinia cambogia"[235], suppression both in nucleation and crystal growth of barite by alginate (an acidic polysaccharide)[236] and modification of Ni-Al layered double hydroxide morphology by alginate[237]. The detailed study on the self-assembly mechanism of those biomass-assisted ZSM-5 zeolites will be discussed in Chapter 5.

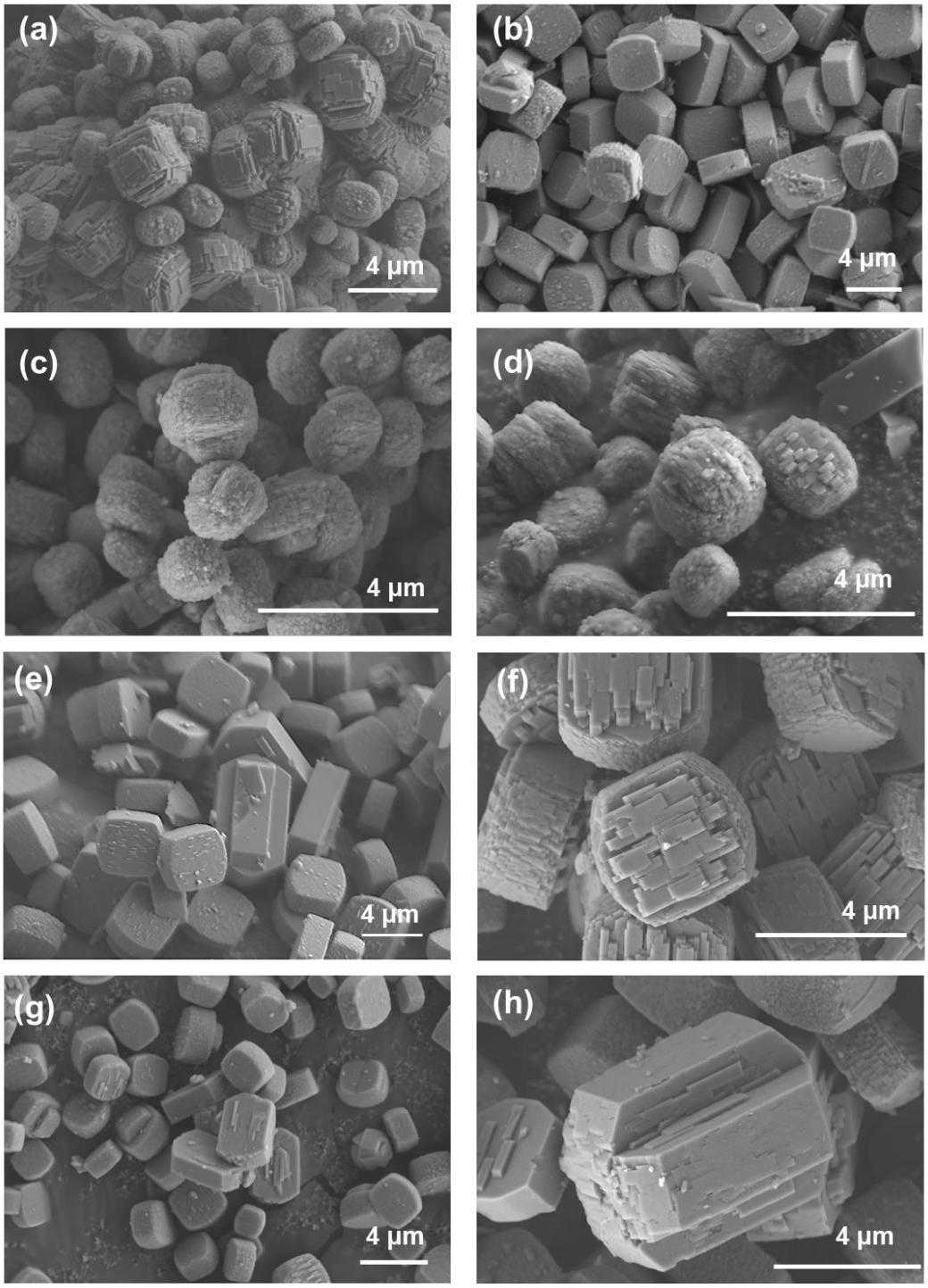

Figure 3.7 SEM images of (a) B-REF-2d, (b) B-oxidized lignin-2d-300, (c) B-alkali lignin-2d-300, (d) B-coffee-2d-300, (e) B-tea-2d-300, (f) B-algaCM-2d-300, (g) B-algaBB-2d-300, (h) B-algaTM-2d-300.

The textural properties of as-obtained biomass-modified ZSM-5 zeolites, such as BET surface areas, micropore surface area, external surface area, total pore volumes,

micropore volumes, external volumes and average pore diameters are listed in Table 3.5. It is worthy to highlight that the total surface areas of all zeolites raised significantly in the presence of biomass, especially for B-algaTM which was enhanced from 341 to 394 m^2/g, being roughly 16% higher than pristine ZSM-5. With the assistance of the biomasses, the microporous surface area was also increased to some extent. Here, the change in the external surface area was mainly due to an increase or decrease in the mesoporous range. Although with the addition of two kinds of lignin (oxidized lignin and alkali lignin), the mesopore surface area diminished slightly to 131 and 134 m^2/g, respectively, most of biomass-mediated zeolites exhibited a higher mesoporous surface area when compared to raw B-REF zeolite (143 m^2/g). Among them, B-algaCM zeolite exhibited the highest mesopore surface area of 184 m^2/g. Meanwhile, B-algaTM showed the maximum total pore volume, micropore volume, and mesopore volume, which were 0.21, 0.16 and 0.11 cm^3/g, respectively. Other zeolites just presented a slight increase in their total pore volume, microporous and mesoporous volumes than B-REF (0.18, 0.10 and 0.08 cm^3/g).

Table 3.5 Textural properties of biomass-modified ZSM-5 zeolites.

Sample	S_{BET} (m^2/g)	S_{micro} (m^2/g)	$S_{external}$ (m^2/g)	V_{pore} (cm^3/g)	V_{micro} (cm^3/g)	$V_{external}$ (cm^3/g)	Pore size (nm)
B-REF	341	198	143	0.18	0.10	0.08	2.1
B-oxidized lignin	355	224	131	0.18	0.11	0.08	2.0
B-alkali lignin	357	224	134	0.19	0.12	0.10	2.1
B-coffee bagasse	375	216	159	0.20	0.12	0.09	2.1
B-tea	372	207	164	0.19	0.10	0.09	2.1
B-algaCM	381	197	184	0.20	0.09	0.10	2.1
B-algaBB	372	213	159	0.19	0.10	0.07	2.1
B-algaTM	394	236	158	0.21	0.16	0.11	2.1

With the aim of studying the acidic properties of the catalysts, temperature programmed desorption of ammonia analysis was undertaken. The NH_3-TPD profiles of pristine and ZSM-5 zeolites obtained with the assistance of oxidized lignin, alkali lignin, coffee bagasse, tea waste, three kinds of algae, and their corresponding deconvolution peaks are shown in Figures 3.8 and 3.9.

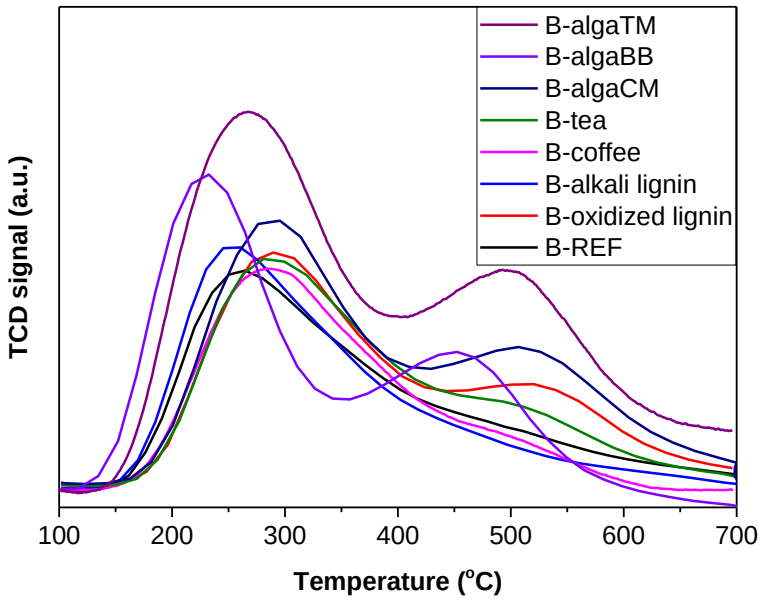

Figure 3.8 NH_3-TPD profiles of B method-ZSM-5 catalysts produced with different biomasses.

As shown in Figure 3.9, all zeolites exhibited three types of acid sites with different acid strength. With an addition of biomass, the quantities of total acid sites were increased for all samples. Interestingly, three kinds of algae (algaCM, algaBB and algaTM) depicted quite different experimental profiles than others, which revealed a noticeably higher amount of strong acid sites.

In order to get more detailed informations about the change in acidity: their numbers and strength, as well as the specific peak positions are listed in Table 3.6. It should be noted that 10% NH_3 was replaced by 2% NH_3 during the analysis of different samples, therefore, the NH_3-TPD analysis conditions of all as-synthesized zeolites

using B method were changed into adsorption of 2% NH_3 for 2 h. From the results, it can be observed that the total acid sites produced with algae were 1.33, 1.58 and 1.68 mmol/g, and strong acidic sites were 0.32, 0.54, and 0.44 mmol/g, much higher than pristine ZSM-5 (0.96 mmol/g of total acid sites and 0.13 mmol/g of strong acid sites). Besides, B-oxidized and B-tea zeolites also exhibited an increase of strong acidic sites with respect to pristine ZSM-5, being 0.26 and 0.27 mmol/g, respectively. In addition, B-alkali lignin exhibited the highest content of weak acid sites and medium acid sites (0.61 and 0.53 mmol/g), but the amount of strong Brønsted acid sites remained only 0.11 mmol/g. Moreover, all peak positions of strong acid sites shifted towards lower temperatures due to the effect of biomass.

In addition, it can be observed that as-prepared zeolites in the presence of biomasses exhibited diverse morphological, textural and surface acidic properties. Since the composition of biomass is quite complicated, and any small variation in the bio-template structure and/or functionality can lead to dramatic changes in their specificity or efficiency. It is rather difficult to draw a conclusion about the specific active components on each biomass.[238] In literature, some of the most effective bio-sourced secondary templates identified in synthetic crystallization are macromolecules such as polymers,[239] DNA,[240] proteins[241] and peptides,[242] which are rich in tea waste, algae and other biomass waste. The detailed discussion will be undertaken in Chapter 5.

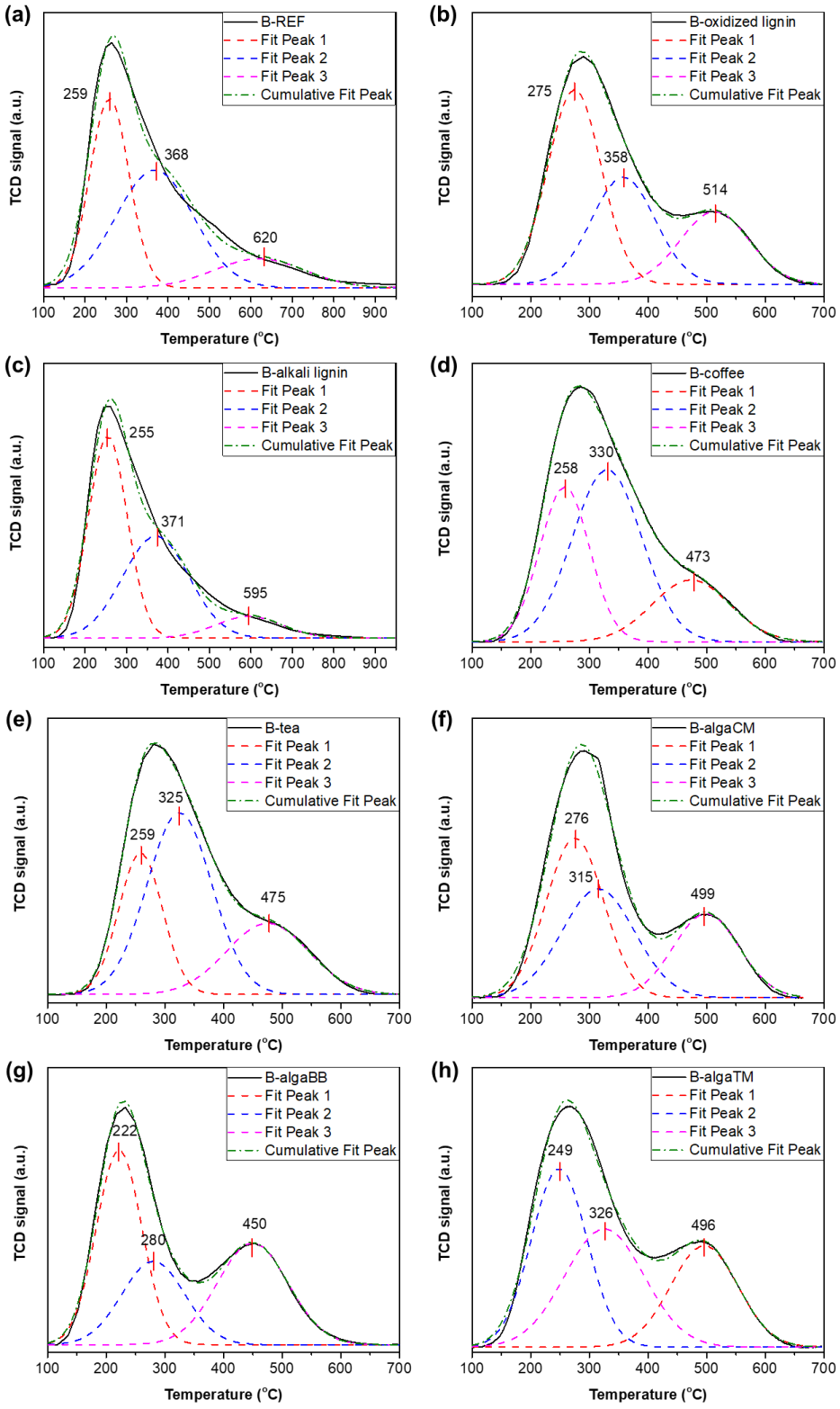

Figure 3.9 NH_3-TPD profiles and their corresponding deconvolution peaks into Gaussian peaks ($R^2 > 0.99$) of B method-ZSM-5 (a) without biomass, and with different biomasses: (b) oxidized lignin, (c) alkali lignin, (d) coffee, (e) tea, (f) algaCM, (g) algaBB, (h)algaTM.

Table 3.6 Acidity of B method-ZSM-5 and biomass modified ZSM-5 zeolites (2 days, 300 mg biomass).

Catalysts	Acid amount (mmol/g)	Acid sites content (mmol/g)			Peak position (℃)		
		Weak	Medium	Strong	Weak	Medium	Strong
B-REF	0.96	0.37	0.46	0.13	259	368	620
B-oxidized lignin	1.17	0.55	0.36	0.26	275	358	514
B-alkali lignin	1.26	0.61	0.53	0.11	255	371	595
B-coffee	1.02	0.32	0.50	0.20	258	330	473
B-tea	1.11	0.29	0.55	0.27	259	325	475
B-algaCM	1.33	0.54	0.47	0.32	276	315	499
B-algaBB	1.58	0.65	0.39	0.54	222	280	450
B-algaTM	1.68	0.64	0.60	0.44	249	326	496

As shown in Table 3.3, A-tea ZEM-5 possessed a higher relative crystallinity than other zeolites, which resulted in the excellent catalytic performance in the MTO reaction, shown in next chapter. Thanks to the discovery of the benefits of spent tea leaves, different amounts of tea waste ranging from 200 to 400 mg were chosen for the synthesis of ZSM-5, and detailed characterization by XRD, SEM, BET and NH_3-TPD will be given in coming section.

XRD diffraction patterns of all tea waste-mediated ZSM-5 zeolites after hydrothermal synthesis followed by thermal treatment at 550 ^oC are given in Figure 3.10. All samples exhibit characteristic diffraction peaks that are highly consistent with the MFI structure, assessing the formation of ZSM-5. As shown in Figure 3.10(a), it is important to point out that ZSM-5 zeolites obtained with the assistance of spent tea leaves exhibit much higher intensities for the main (101) and (200) crystalline plans in $2\theta = 7.9$ and 8.8^o doublet when compared to pristine ZSM-5 (without any tea residue) using A method. This phenomenon is not that obvious on the ZSM-5 synthesized by B method, but it can still be verified by comparing the intensities of B-tea300 and B-REF.

This corresponds to the shift from orthorhombic to monoclinic phase in the MFI topology.[243, 244] Focusing on MFI main reflections between 22.5-25.0º, extra-reflections are observed as shoulders at smaller 2θ angles, thus forming doublets in those peaks. These additional peaks can be indexed in the same *Pnma* space group but with slightly larger unit cell parameters. Interestingly, it was found that the peak intensity ratio of 2θ = 7.9 and 8.8º ($I_{8.8}/I_{7.9}$) is associated with samples' morphology as shown in Table 3.7 and Figure 3.11. The intensity ratio increased as the morphology shifted from cubic to planar shape or coffin-shape as reported by Jung et al.[245] However, further studies are needed to draw a definitive conclusion in establishing such correlations between them.

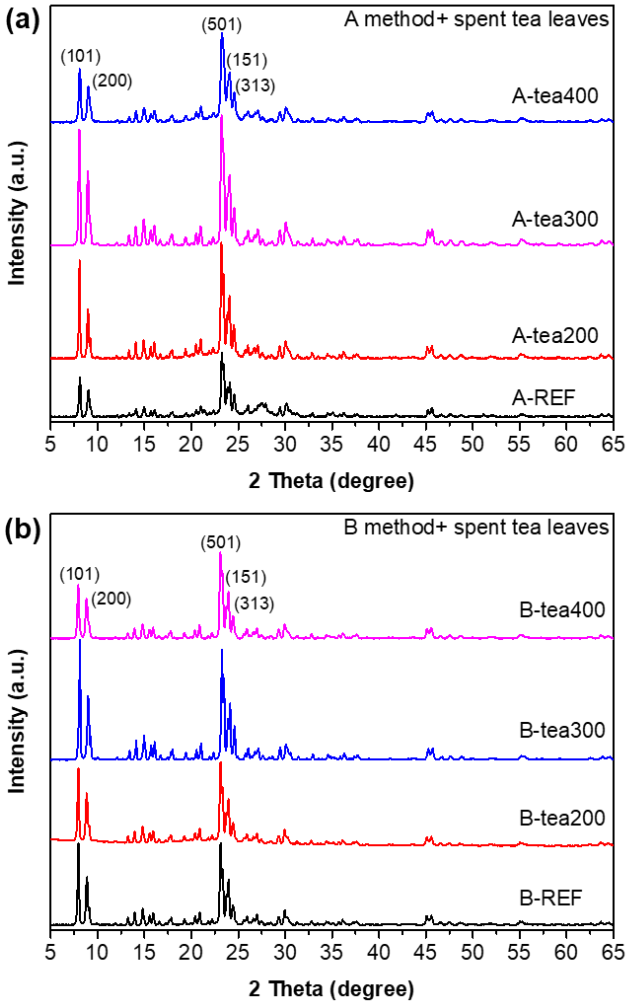

Figure 3.10 XRD patterns of ZSM-5-REF and ZSM-5 prepared in the presence of different amount of spent tea leaves (200, 300, 400 mg) under (a) A method and (b) B method.

Table 3.7 Intensity ratio of the peak at 8.8 and 7.9° 2θ of ZSM-5-REF and ZSM-5 with tea waste ($I_{8.8}/I_{7.9}$).

Sample	$I_{8.8}/I_{7.9}$	Sample	$I_{8.8}/I_{7.9}$
A-REF	0.86	**B-REF**	0.79
A-tea200	0.76	**B-tea200**	0.83
A-tea300	0.64	**B-tea300**	0.75
A-tea400	0.86	**B-tea400**	0.88

The morphology of as-synthesized tea waste-derived ZSM-5 zeolites and the reference ZSM-5 were examined by SEM analysis (Figure 3.11(a-h)). In regard with the zeolites produced by using A method, the A-REF exhibited a typical coffin-shape crystal associated to ZSM-5 topology with an average width of ca. 5 μm, a length of several-tenths of microns and a thickness of hundreds of nanometers. In contrast, tea waste-derived zeolites consist of cubic-shape particles with rough surface gradually with an increase in the spent tea leaves quantity. Herein, the spent tea leaves clearly act as a zeolite growth modifier (ZGM) inducing significant morphological changes. The concept of zeolite growth modifier (ZGM) was initially proposed by Rimer *et al.*, which involves a molecule able to select and bind to crystal faces with a specificity and hence alter the anisotropic rates of surface step growth.[238, 246, 247] In Figure 3.11(e-h), there is no obvious morphological or size changes in B-REF, B-tea200, and B-tea400 zeolites, where the spherical aggregation can be observed. By a careful observation, For B-tea300 ZSM-5, most of them exhibited the cubic particles with smooth surface or flat, coffin-like crystals.

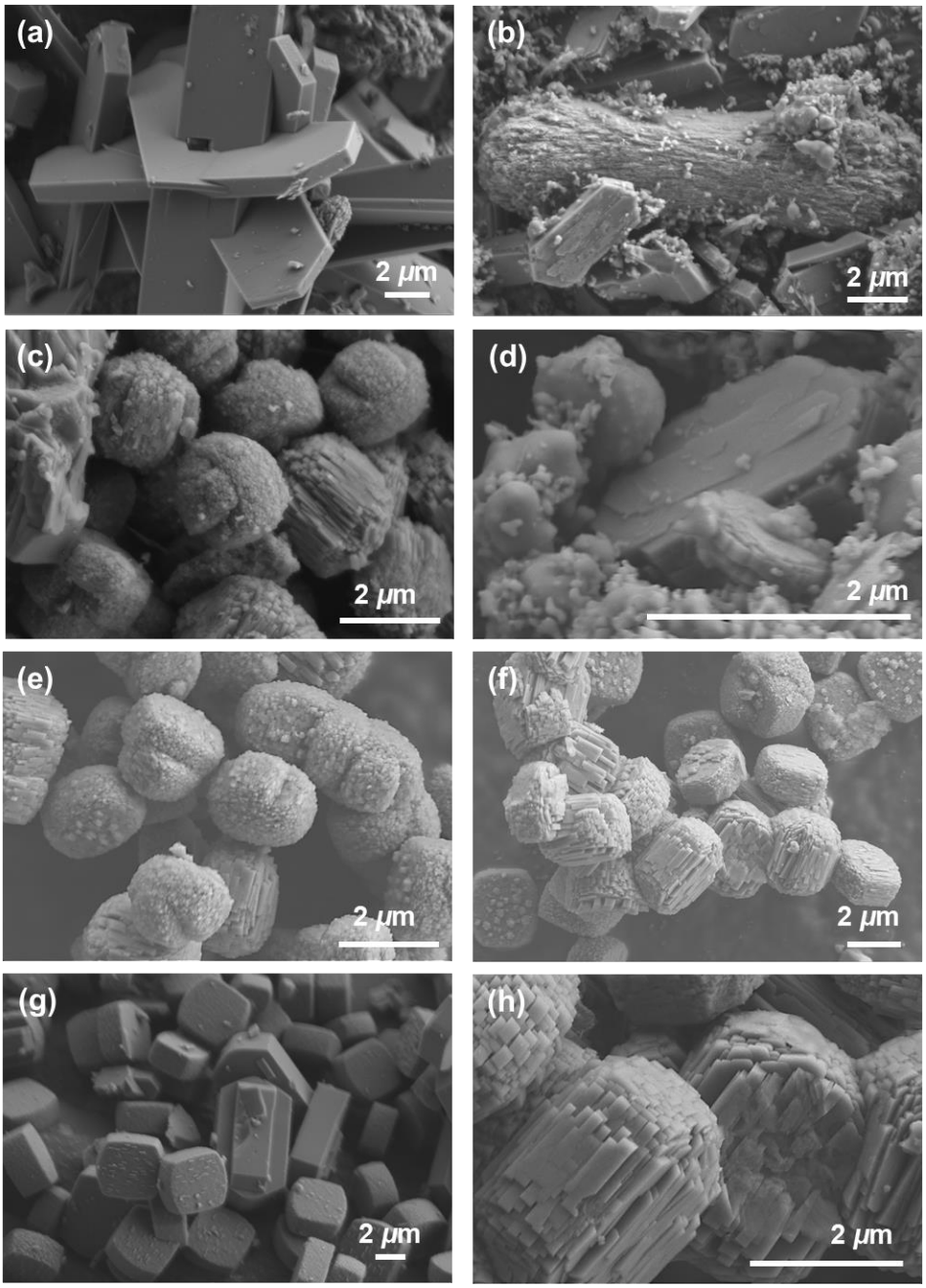

Figure 3.11 SEM images of ZSM-5 zeolites (a) A-REF, (b) A-tea200, (c) A-tea300, (d) A-tea400, (e) B-REF, (f) B-tea200, (g) B-tea300, (h) B-tea400.

The specific surface area, pore volume, and pore size of all ZSM-5 zeolites are summarized in Table 3.8. N_2 sorption/desorption results seem to support our hypothesis that spent tea leaves act as a bio-sourced secondary template (BSST) and impacts the zeolite crystallization process, thus consequently modifies its structure and properties. Regarding A method, the lower specific surface area of the reference ZSM-5 could be

due to the presence of amorphous SiO_2. The presence of spent tea leaves significantly shortened the hydrothermal time and allowed forming well-formed crystals. For instance, the specific surface area increased from 104 to 382 m^2/g after adding 300 mg tea waste. Therefore, it seems to be a wise strategy to get a double advantage for the valorization of biomass waste and reduction of synthesis time and economic cost. Likewise, the total surface area increased from 341 to 369, 372 and 385 m^2/g upon introduction of the tea waste from 0, 200, 300 and 400 mg in B method, being increased by 8%, 9%, and 13% with respect to reference ZSM-5. Besides, the external surface area was remarkably increased from 161 to 191 m^2/g. Meanwhile, the pore size did not change. It is can therefore be inferred that an increase in the external surface area is mainly due to the raise in the mesoporous range. It is well known that inducing mesoporosity in the zeolite catalysts has been regarded as a useful technology that improves diffusivity and catalyst lifetime. Recently, many efforts were devoted to introduce mesopores to form hierarchically structured zeolites through various approaches for mitigating some limitations of zeolite crystals and catalytic activity.[218] Fortunately, tea waste exhibited the capacity to generate more mesoporosity in the zeolite, thus to propose a facile and cheap approach able to avoid strong alkaline post-treatments or nucleation promoters. Tea waste is easier to acquire from our daily life. The presence of spent tea leaves and other biomasses induce textural changes as well as modify the zeolite surface properties.

Table 3.8 BET specific surface area, micropore area, external surface area, total pore volume, micropore volume, external volume and pore size of various ZSM-5 samples.

Sample	S_{BET} (m^2/g)	S_{micro} (m^2/g)	$S_{external}$ (m^2/g)	V_{pore} (cm^3/g)	V_{micro} (cm^3/g)	$V_{external}$ (cm^3/g)	Pore size (nm)
A-REF	104	79	25	0.06	0.04	0.02	2.24
A-tea200	160	113	47	0.09	0.06	0.03	2.24
A-tea300	382	204	178	0.21	0.10	0.11	2.17
A-tea400	153	110	43	0.09	0.05	0.04	2.23

B-REF	341	198	143	0.18	0.10	0.08	2.11
B-tea200	369	208	161	0.20	0.10	0.10	2.12
B-tea300	372	207	164	0.19	0.10	0.09	2.07
B-tea400	385	194	191	0.20	0.09	0.11	2.04

Besides, longer hydrothermal times (3d and 5d) were chosen to achieve a better crystallization of ZSM-5 without any biomass. Their textual properties (BET specific surface area, micropore surface area, external surface area, total pore volume, micropore volume, external volume, and pore size) are shown in Table 3.9. As speculated before, the synthesis duration led to a higher BET specific surface area. It also shows that through this preparation method, it takes a long time to complete the whole process of crystallization. However, on the bright side, we found that spent tea leaves can effectively accelerate the synthesis of zeolites and reduce the hydrothermal time. A complete framework structure can be formed in only 2 days when adding tea waste. The degree of crystallization appears better than the one achieved without biomass for 5 days.

Table 3.9 BET specific surface area, micropore surface area, external surface area, total pore volume, micropore volume, external volume, and pore size of reference ZSM-5 for different hydrothermal days and A-tea300-2d catalyst.

Sample	S_{BET} (m^2/g)	S_{micro} (m^2/g)	$S_{external}$ (m^2/g)	V_{pore} (cm^3/g)	V_{micro} (cm^3/g)	$V_{external}$ (cm^3/g)	**Pore size (nm)**
A-REF-2d	104	79	25	0.06	0.04	0.02	2.24
A-REF-3d	152	107	45	0.09	0.05	0.04	2.29
A-REF-5d	229	156	73	0.13	0.08	0.05	2.26
A-tea300-2d	382	204	178	0.21	0.10	0.11	2.17

To get more insights regarding the acidic properties of ZSM-5 samples with different amount of spent tea leaves, NH_3-TPD measurements were investigated and

the corresponding profiles are shown in Figure 3.12 and Figure 3.13. Likewise, most of samples exhibited three desorption peaks at <250 °C, 250-350 °C and more than 350 °C, which could be ascribed to the weak, medium and strong acid sites, respectively.[248]

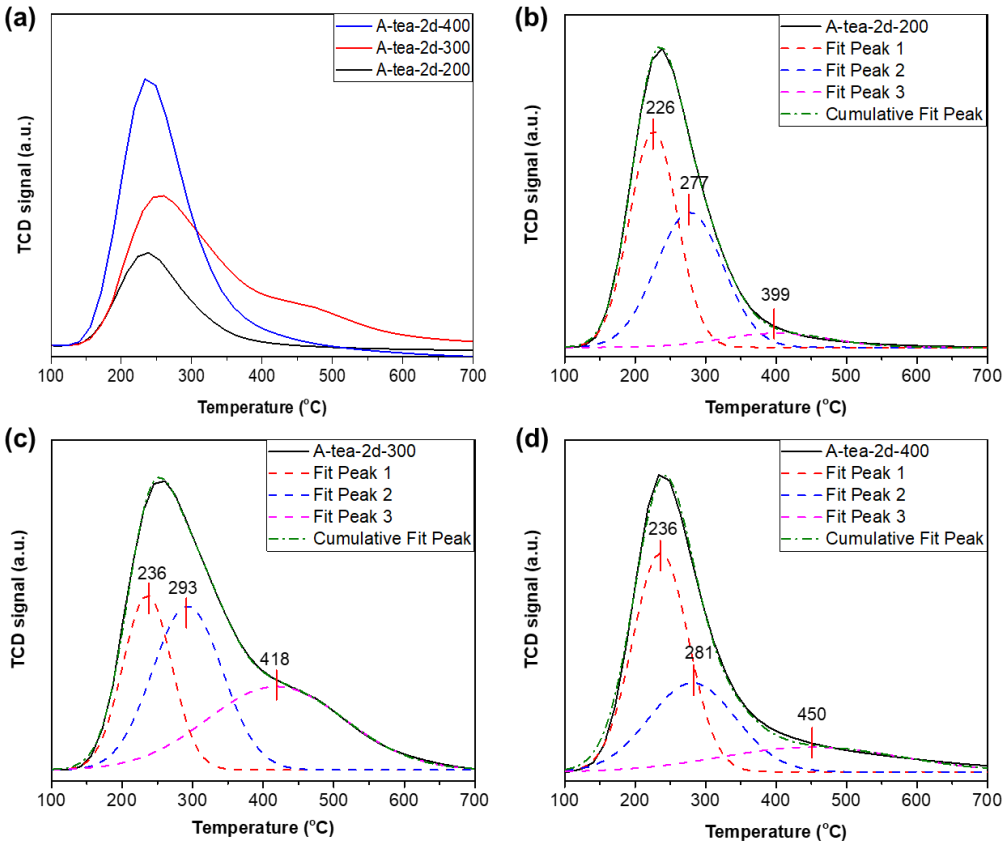

Figure 3.12 NH_3-TPD profiles and their corresponding deconvolution peaks into Gaussian peaks ($R^2 > 0.99$) of ZSM-5 by A method with different amount of tea waste.

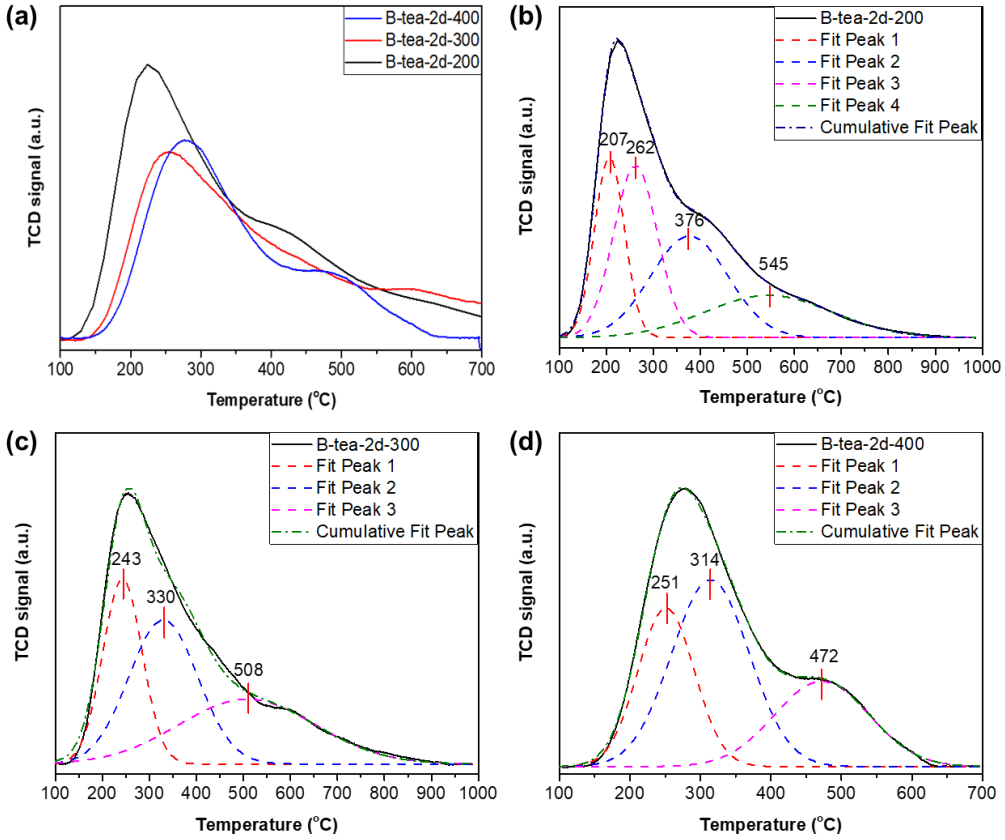

Figure 3.13 NH_3-TPD profiles and their corresponding deconvolution peaks (experiment and fit) of ZSM-5 by B method with different amount of tea waste.

In order to get precise information about the change of acidic properties, the acid sites content and the specific peak position (strength) are listed in Table 3.10. It should be mentioned that all samples shown in Table 3.10 were tested under 10% ammonia atmosphere for 1 h. With an increase in the amount of tea waste (200, 300, 400 mg), the numbers of acid sites for all A-tea ZSM-5 were increased from 0.03, 0.07 to 0.10 mmol/g, while the highest strong acid site was obtained by A-tea-2d-300 zeolite (0.032 mmol/g). The lower acid amount of A-tea-2d-200 may be due to the incomplete crystallization and the formation of amorphous SiO_2. For B method, B-tea-2d-200 had the highest content of total acid sites of 0.11 mmol/g. Interestingly, there were two strong acid sites can be observed for B-tea-2d-200 at 376 and 545 °C, respectively. As a result, the amount of strong acid sites was quite higher than other samples, and reached ca. 0.055 mmol/g. This may also be the reason for its better catalytic

performance, specific data shown in Chapter 4. Similar results can be found in glucose-modified ZSM-5, which showed numerous strong acid peaks in NH_3-TPD analysis.[232, 249]

Table 3.10 Acidity of ZSM-5 with different amount of tea waste.

Catalysts	Acid amount	Acid sites content (mmol/g)			Peak position (°C)		
	(mmol/g)	Weak	Medium	Strong	Weak	Medium	Strong
A-tea-2d-200	0.03	0.015	0.013	0.002	226	277	399
A-tea-2d-300	0.07	0.017	0.023	0.032	236	293	418
A-tea-2d-400	0.10	0.049	0.031	0.018	236	281	450
B-tea-2d-200	0.11	0.022	0.031	0.055	207	262	376/545
B-tea-2d-300	0.06	0.017	0.023	0.021	243	330	508
B-tea-2d-400	0.05	0.014	0.023	0.013	251	314	472

As a comparison, the XRD pattern of benchmark CBV 28014 (Zeolyst) is presented in Figure 3.14. It exhibits the sole characteristic diffraction reflections of MFI structure. In order to further compare the effects, the acidities between commercial ZSM-5 and as-prepared catalysts, ammonia desorption profiles over CBV 28014 zeolite measured are shown in Figure 3.15. The most obvious difference is that the commercial catalyst exhibits two desorption peaks at ca. 215 and 406 °C, related to weak and strong acid sites, respectively. However, zeolites prepared by A or B did not present two obvious desorption peaks, only B-oxidized lignin, B-algaCM, B-algaBB and B-algaTM had similar desorption profiles.

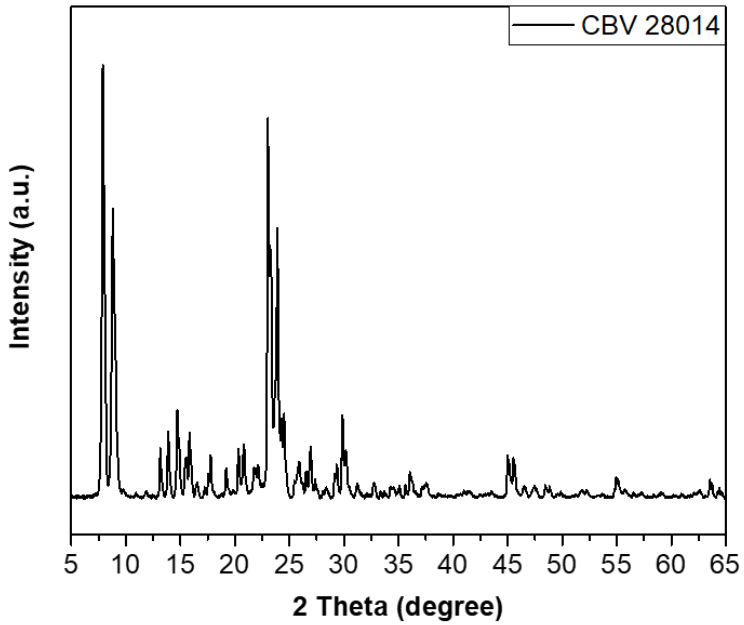

Figure 3.14 XRD patterns of pristine commercial ZSM-5 zeolite CBV 28014.

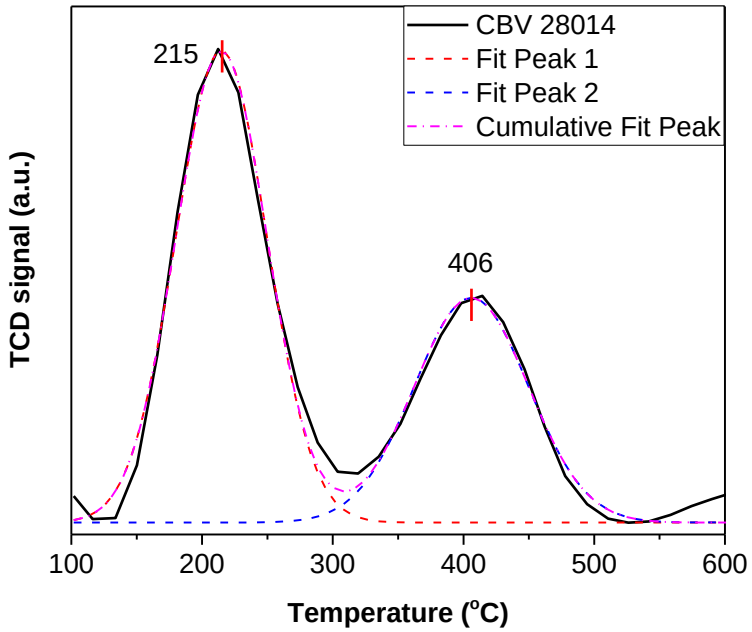

Figure 3.15 NH_3-TPD profile and its corresponding deconvolution peaks of commercial CBV 28014 zeolite. (Deconvolution of the NH_3-TPD curves into Gaussian peaks ($R^2 > 0.99$))

The acidic properties summary of A-tea ZSM-5 and benchmark zeolite CBV 28014 is shown in Table 3.11. It demonstrates that although a distinct desorption peaks of strong acid site can be observed at high temperature for CBV 28014, the total acid sites amount remains lower than as-synthesized A-tea-2d-300 zeolite. Therefore, the higher

weak, medium and strong acid amount of 0.017, 0.023 and 0.032 mmol/g were obtained, respectively, which may potentially lead to better catalytic performance in the MTO process.

Table 3.11 Comparison of acidity of representative A-tea ZSM-5 and benchmark zeolite CBV 28014.

Catalysts	Acid amount (mmol/g)	Acid sites content (mmol/g)			Peak position (°C)		
		Weak	Medium	Strong	Weak	Medium	Strong
A-tea-2d-300	0.072	0.017	0.023	0.032	236	293	418
CBV 28014	0.014	0.009	/	0.005	215	/	406

3.4 The influence of the amount of TPAOH template

In order to optimize the synthesis strategy and decrease the quantity of organic template (TPAOH), an attempt was first made in the synthesis of zeolite Z-LO-09. Here, the same synthesis method was undertaken while reducing the TPAOH by half, denoted Z-LO-09-1/2TPAOH. As shown in Figure 3.16, both of them exhibited the characteristic peaks observed at 7.9 º, 8.8 º, 23.1 º, 23.7 º and 24.5º, attributed to (101), (200), (501), (151) and (313) planes of the MFI framework. One could also notice that the intensity of $Na(AlSi_2O_6)(H_2O)$, ANA phase, diminished in Z-LO-09-1/2TPAOH than Z-LO-09 zeolite. However, the catalytic performance did not improve, but the lifetime decreased after reducing the template by half (as shown in Chapter 4).

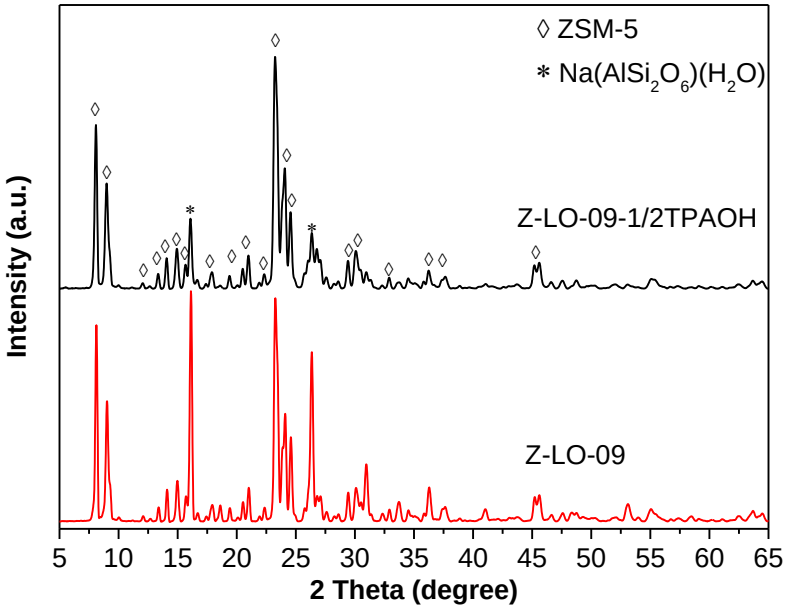

Figure 3.16 XRD patterns of ZSM-5 zeolite Z-LO-09 and Z-LO-09-1/2TPAOH.

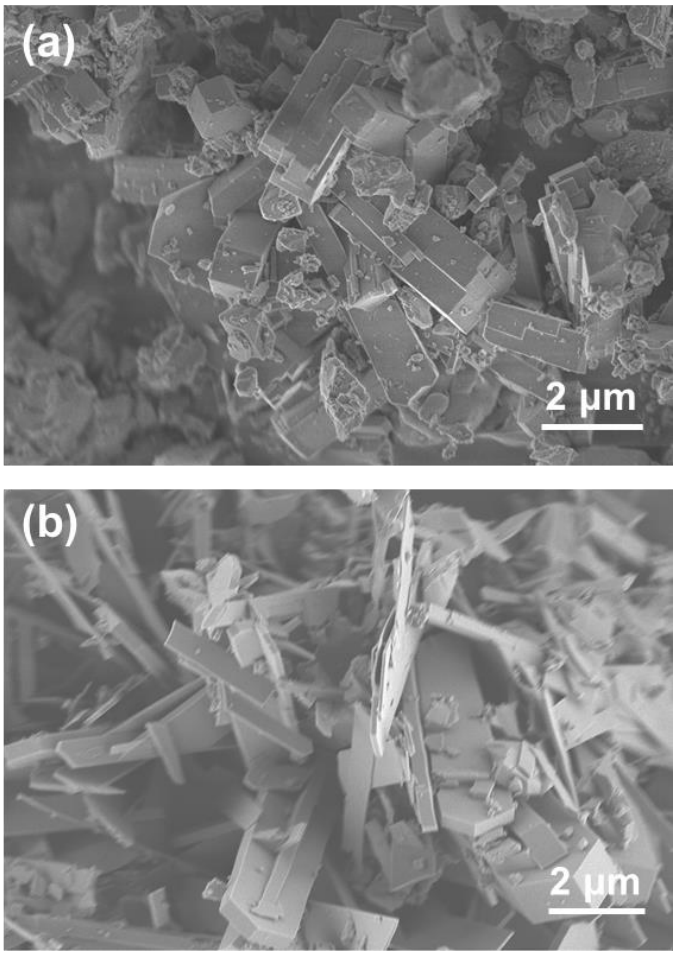

Figure 3.17 SEM image of (a) Z-LO-09-1/2TPAOH, and (b) Z-LO-09.

The morphologies were evaluated by SEM observations and presented in Figure 3.17. Z-LO-09 exhibited well-defined coffin shape crystals morphology of MFI-type with an average length of 2-4 μm and thin thickness. When the template amount was reduced, the thickness was significantly increased and the morphology changed thicker from flake.

Since A method requires longer crystallization duration, the crystal growth process can be better observed and compared with the difference before and after biomass addition. The XRD patterns of reference ZSM-5, A-REF-100%TPAOH, and 300 mg tea waste-assisted ZSM-5 with 0, 20, 50 and 100%TPAOH are displayed in Figure 3.18. First, it appears that characteristic peaks of the MFI framework are more intense with an increase in the template amount, after the same hydrothermal time (2 days). There is almost no crystallization occurring in A-tea-0%TPAOH with mainly amorphous phase formation. This indicates that the organic template is necessary for the guiding towards the MFI zeolite formation and cannot be fully replaced by biomass. Subsequently, small ZSM-5 characteristic peaks appeared with no other impurities in the product with 20% TPAOH template. When the amount reached 50%, the intensity of the peaks was higher than the reference zeolite with 100% TPAOH, which means that spent tea leaves allowed organizing amorphous phases into arrangements that are favorable for ZSM-5 particle nucleation and growth. Finally, the typical XRD pattern for crystalline ZSM-5 zeolite with no other impurities was obtained for A-tea-100%TPAOH. Although tea residues cannot completely replace the template, it can effectively promote the crystallization, while reducing the use of TPAOH and shorten the synthesis duration.

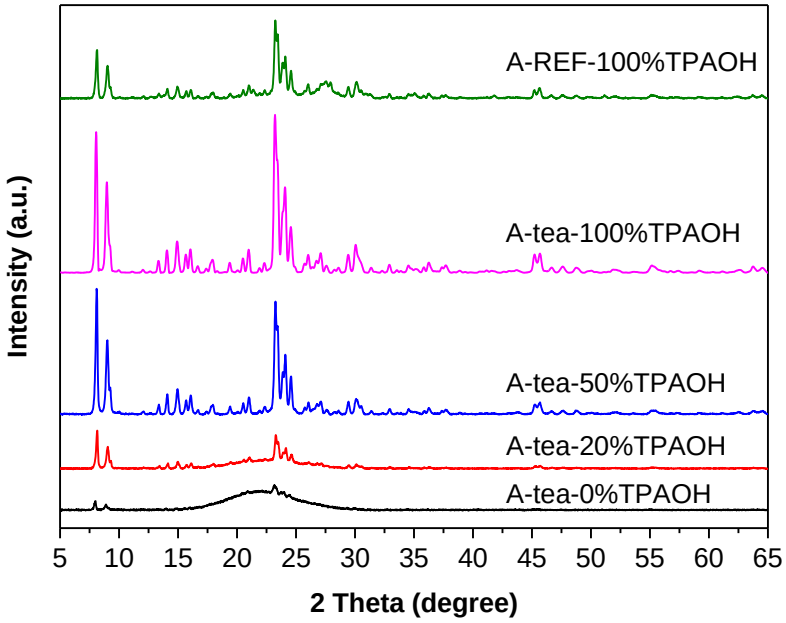

Figure 3.18 XRD patterns of parent ZSM-5 and A-tea zeolites with 0, 20, 50 and 100% TPAOH.

The SEM images of ZSM-5 catalysts (a) A-REF, (b-d) A-tea-2d-300 with 20, 50, and 100% TPAOH are shown in Figure 3.19. The SEM images assessed the crystal sizes, morphologies and aggregations for the different ZSM-5 catalysts. As already mentioned, A-REF-2d-100%TPAOH zeolite showed the MFI-typical hexagonal morphology with a mean length of 10 µm. Because there were only few crystals formed, it is difficult to observe any zeolite structure in Figure 3.19(b). For A-tea-50%TPAOH, particle morphologies typical for ZSM-5 crystals with ca. 2 µm aggregated crystallite slabs were observed. The morphology of A-tea-100%TPAOH can be described as ellipsoids with a size of 2-4 µm. It is noteworthy that the effect of spent tea leaves made a morphology change form flaky to spherical and ellipsoidal.

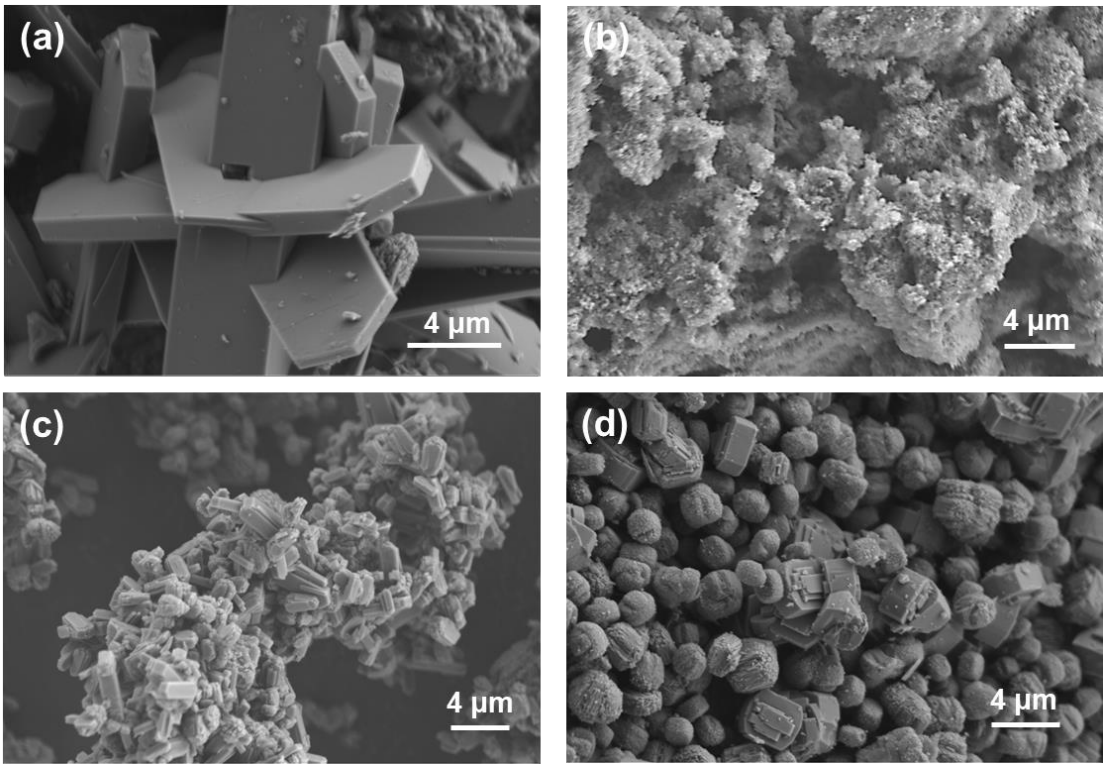

Figure 3.19 SEM image of (a) A-REF, (b-d) A-tea-2d-300 with 20, 50, and 100% TPAOH.

In Table 3.9, it is tentatively shown that the crystallinity may be effectively improved by increasing the hydrothermal time. Therefore, a hypothesis was made that A-tea-0%TPAOH (without template) is too slow to complete the crystallization process in 2 days. If the hydrothermal time is prolonged, do the initial small characteristic peaks become higher. Therefore, we compared the patterns of the two samples after 2 and 5 days of hydrothermal treatment. In Figure 3.20, by comparing the two patterns, the characteristic peak intensity hardly changed even if the hydrothermal time is prolonged. Therefore, we exclude the effect of insufficient hydrothermal time and proved that tea residues cannot solely act on the crystallization process.

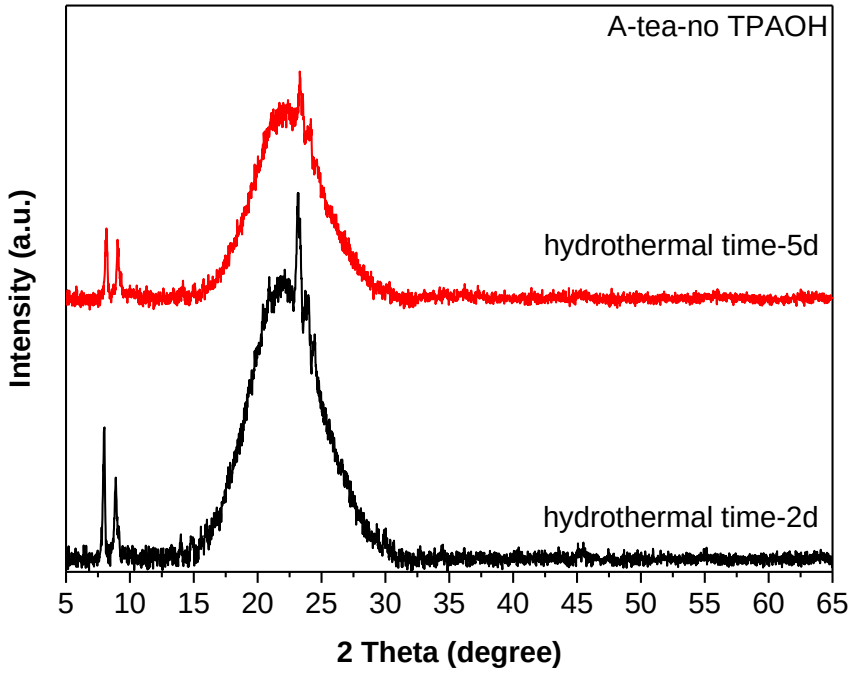

Figure 3.20 XRD patterns of A-tea zeolites without any TPAOH for different hydrothermal days (2 and 5 days).

The textural features of A-tea-ZSM-5 prepared using different amount of TPAOH as well as the A-REF-100%TPAOH are presented in Table 3.12. For reference sample, the values of BET specific surface area, micropore area, total pore volume, micropore volume, and pore size were 104 m^2/g, 79 m^2/g, 0.06 cm^3/g, 0.039 cm^3/g, and 2.24 nm, respectively. With a higher TPAOH amount, the BET specific surface area, micropore area increased considerably to 382 m^2/g and 204 m^2/g, respectively, and the average pore size diminished to 2.17 nm. The same phenomenon can be found both in XRD patterns and BET results that A-tea-50%TPAOH led to a better crystallization than pristine ZSM-5 without tea leaves.

Table 3.12 BET specific surface area, micropore area, total pore volume, micropore volume, and pore size of various ZSM-5 samples.

Sample	S_{BET} (m^2/g)	S_{micro} (m^2/g)	V_{pore} (cm^3/g)	V_{micro} (cm^3/g)	Pore size (nm)
A-REF-100%TPAOH	104	79	0.06	0.039	2.24

A-tea-0%TPAOH	52	9	0.18	0.004	13.77
A-tea-20%TPAOH	108	34	0.22	0.016	8.08
A-tea-50%TPAOH	236	152	0.14	0.075	2.43
A-tea-100%TPAOH	382	204	0.21	0.100	2.17

The desorption of NH_3 by an incremental increase in the temperature was performed in the tea leaves-assisted ZSM-5 syntheses with different amounts of template, as shown in Figure 3.21. As a priori expected, the acid intensity of A-tea-100TPAOH is much higher than the other two samples because it led to more complete crystallization. Regarding A-tea-100%TPAOH, the peaks were centered at 236, 293 and 418 °C, corresponding to the desorption of NH_3 from weak acid, medium acid and strong acid sites, respectively.

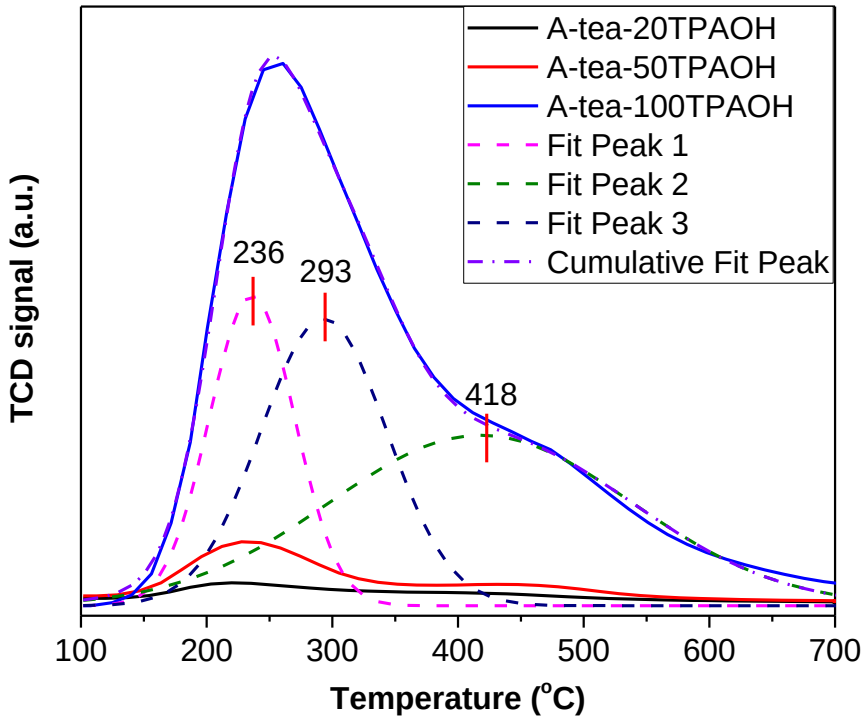

Figure 3.21 NH_3-TPD profiles of the tea leaves-assisted ZSM-5 catalysts with different amount of template and the corresponding deconvolution peaks of A-tea-100TPAOH. (Gaussian peaks ($R^2 > 0.99$))

3.5 Conclusions

In this Chapter, a series of ZSM-5 zeolites were synthesized with three different reactant molar ratios, hydrothermal time, biomass composition and quantity, amount of TPAOH. Besides, 8 kinds of biomasses (oxidized lignin, coffee bagasse, tea residues, algaCM, algaBB, algaTM, sugarcane bagasse, and ecoshell) and a commercial alkali lignin were evaluated as BSSTs involved in the zeolite crystallization process. Detailed characterizations by XRD, SEM, BET and NH_3-TPD techniques were conducted for all as-synthesized zeolites. It can be seen that the morphological, textural and surface acidic properties of those biomass-mediated ZSM-5 were significantly impacted by the presence of biomass.

Chapter 4. Conversion of methanol into light olefins over biomass-assisted ZSM-5 zeolites

Abstract

In this Chapter, we present a series of as-synthesized ZSM-5 zeolites by introduction of different kinds of biomass as secondary sacrificial template. It is the first time that the biomass nature impacted the catalytic performance of zeolites has been investigated. For comparison, three different preparation methods (Z-LO-07, A and B methods) were evaluated. Moreover, one promising biomass-assisted zeolite, tested in the methanol-to-olefins reaction, exhibited an excellent catalytic performance and was therefore compared with two benchmark zeolites.

4.1 Introduction

The methanol-to-olefins reaction (MTO) acts as one of the most successful non-petrochemical route, and has received great attention through the world, which can produce a large range of valuable chemical products, such as ethylene and propylene, primary blocks of plastics and polymers, from natural gas or coal.[250] Both light olefins (mainly C_2-C_4) and gasoline fractions have an increasing demand in the global energy market. The first commercialized MTG process was established in New Zealand in 1985 by Mobil Oil which discovered the methanol-to-hydrocarbons (MTH) process in 1977 by either converting methanol to olefins (MTO) or to gasoline (MTG).[251]

As just mentioned, the methanol conversion reaction is an effective manner to yield ethylene, propylene, butylenes, C_5^+ olefins, paraffins, naphthenes, up to aromatics.[252] In other words, the reaction takes place through a complicated "hydrocarbon pool" mechanism which allows to form numerous consecutive products. The tuning of the distribution of products, hence their "selectivity", remains of paramount important in the process. Likewise, the catalytic activity and stability are also key factors to evaluate catalyst materials in the MTO reaction. According to former studies,[253-255] the deactivation mechanism is due to coke deposition which influences both catalytic activity and selectivity.[256] Hence, the rational design of heterogeneous catalysts to optimize activity, selectivity and stability in the MTO is crucial and still remains a huge challenge in catalysis. Besides, a proper optimization of the balance between activity and stability remains a challenge because too strong acidity favors coke formation and therefore rapid deactivation. The main catalysts applied in the MTO are ZSM-5 (MFI structure) and SAPO-34 (CHA structure). ZSM-5 possesses crossed 10-member ring channels, with pore diameters of 5.1-5.6 Å pores. SAPO-34 has large cages and narrow pores with a diameter of 3.8 Å. Although the narrow channels can prevent the large aromatic hydrocarbons from escaping, producing mainly light olefins, the narrow opening favors coke accumulation and therefore accelerates catalysts deactivation when compared with ZSM-5. Since ZSM-5 acts as a key player in the MTO, this chapter will present various biomasses-derived ZSM-5 zeolites catalytic activity, selectivity and stability for this reaction.

4.2 Influence of hydrothermal time and biomass composition and quantity on catalytic performance

As-synthesized and characterized biomass@ZSM-5 zeolites, discussed in the former chapter, have been tested in the MTO reaction. All the catalytic reactions were performed in a quartz tubular fixed-bed reactor at atmospheric pressure. Before running the tests, ca. 60 mg catalyst was activated in flowing argon at 550 ºC for 1 h to remove adsorbed impurities and H_2O. After the temperature decreased to the reaction temperature of 450 ºC, a methanol stream (in Ar) was flown through the reactor at a weight hourly space velocity (WHSV) of 2 h^{-1}. The products were analyzed by a gas chromatograph, and the dimethyl ether (DME) found in the products was considered itself as a reactant.

Although many factors in the process of zeolite synthesis and different reaction conditions impact the catalytic performance, based on the previous research in our group,[257] this Thesis mainly focuses on the influence of hydrothermal duration and biomass composition/quantity on zeolites' catalytic activity, selectivity and stability. The MTO catalytic performance of Z-LO-01 to Z-LO-09 (details given in Table 3.1) and Z-LO-REF (2d, 5d and 7d) catalysts was investigated and the results are displayed in Figure 4.1. Z-LO-04 is not shown here, because this catalyst did not possess the MFI structure, and didn't exhibit any catalytic activity. By comparing several pairs of data (Z-LO-01, 02 and 03, or Z-LO-07, 08 and 09), it is easily observed that an increase in the hydrothermal synthesis time led to higher initial conversion. Meanwhile, because Z-LO-07, 08, and 09 exhibited higher activity and stability than other catalysts, 300 mg of biomass is considered to be an optimized amount. Besides, for most of the catalysts (Z-LO-01, 03, 05, 06 and 08), the tendency of conversion versus time-on-stream remained similar, exhibiting a gradual decreasing trend. The latter catalysts showed an initial stable conversion before a more or less drastic conversion drop, suggesting a reversed S-shaped curve. This can be explained by the autocatalytic nature of the reactions occurring during the MTO.[258] During the lifetime of the catalysts, the degree of conversion decrease is relatively slow. However, Z-LO-02, 07, 09 and Z-LO-REF

(5d), Z-LO-REF (7d) catalysts demonstrated a higher stability than other zeolites during ca. 30 h on stream, and specially, Z-LO-09 and Z-LO-REF (5d) zeolites with almost no drop and maintained close to 100% methanol conversion. Z-LO-REF (5d) exhibited a slight decline compared to Z-LO-09 after 20 h on stream. It is therefore to state here that Z-LO-09 and Z-LO-REF (5d) catalysts could be good candidates for the MTO reaction. We therefore turned our attention to other catalysts for saving time and improving efficiency. The catalytic performance of Z-LO-07 can meet our needs, which achieved an initial conversion of 93% which slightly declined to 68% after 29 h on stream.

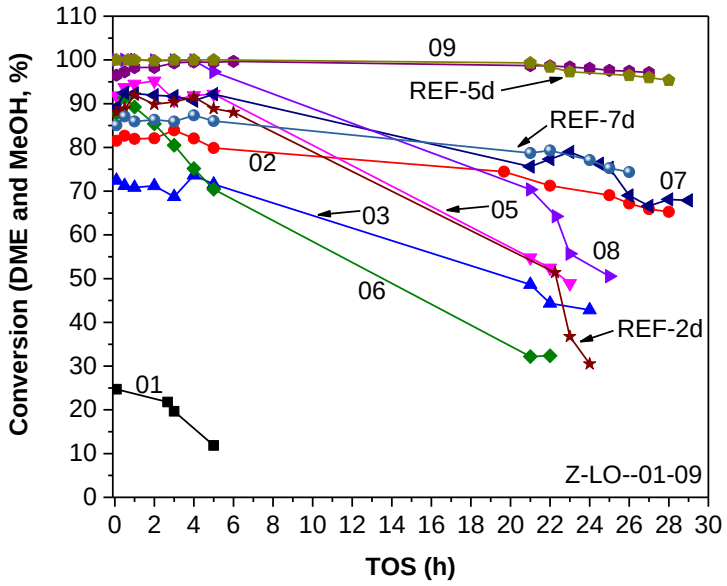

Figure 4.1 Methanol conversion with time-on-stream over the Z-LO-01 to 09 catalysts prepared with different hydrothermal time and biomass consumption, and three reference zeolites prepared with corresponding time. Reaction conditions: 450 °C, WHSV = 2 h^{-1}, catalyst weight = 60 mg.

In order to obtain the product distribution as a function of time-on-stream of the three Z-LO-07, 08 and 09 catalysts, the selectivities in methane, ethylene, propylene, isobutane, butylenes, and C_5^+ hydrocarbons are shown in Figure 4.2. It can be seen that methane and propylene selectivities were the lowest and highest, respectively over all

three zeolites. The selectivities towards ethylene and isobutane were slightly increased with time-on-stream over Z-LO-07 and Z-LO-08 samples, whereas the selectivity to isobutane slightly diminished over Z-LO-09. In particular, the selectivity in isobutane over Z-LO-08 increased more significantly than over the two other samples, from 10 to 26%. Moreover, the selectivity to C_5^+ hydrocarbons slightly dropped over all those catalysts especially during the first few hours on stream; the selectivity decrease towards C_5^+ hydrocarbons fraction contributes to an improvement in the catalyst's lifetime. The formation of saturated hydrocarbons and liquid heavy hydrocarbons (C_5^+ alkanes, larger alkenes or aromatics) can lead to coke formation and subsequently deactivation of the catalysts. According to the variations of selectivity (Figure 4.2), the order of stability may therefore be expressed as follows: Z-LO-09 > Z-LO-07 > Z-LO-08, which is also consistent with the experimental results presented in Figure 4.1.

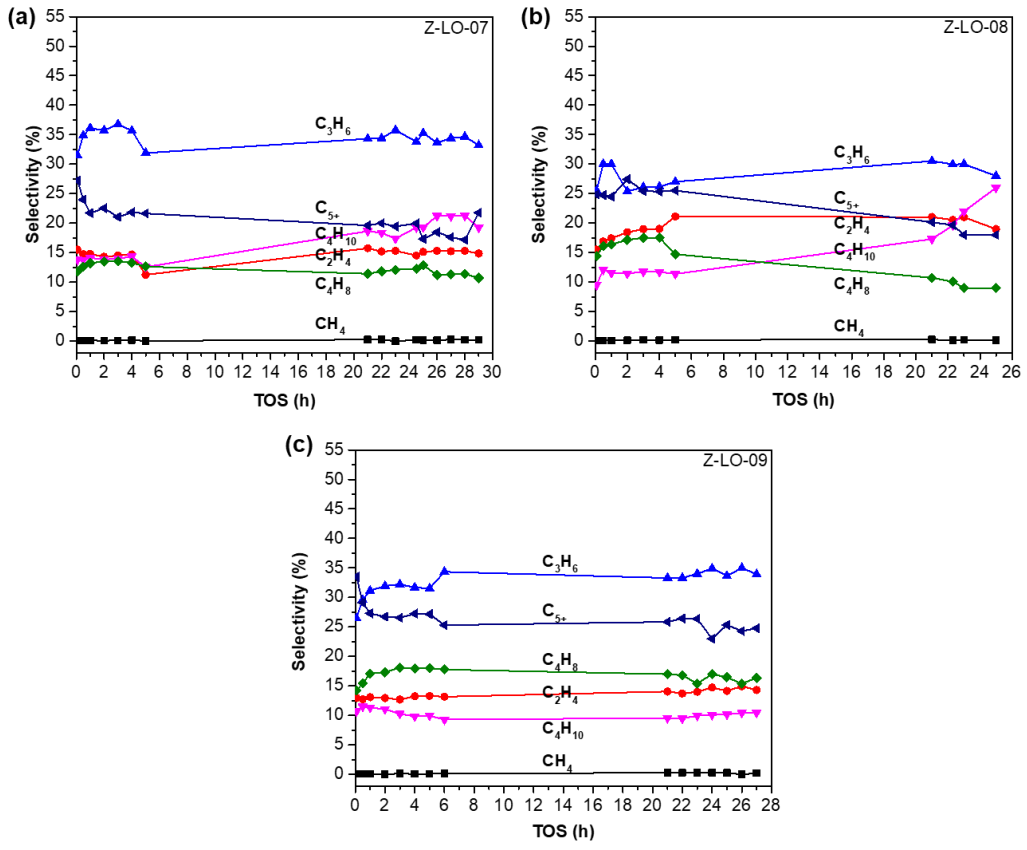

Figure 4.2 Variation of selectivities towards methane, ethylene, propylene, isobutane, butylenes, and C_5^+ with time-on-stream (TOS) over Z-LO-07, 08 and 09 catalysts. Reaction conditions: 450 °C, WHSV = 2 h^{-1}, catalyst weight = 60 mg.

The product distributions obtained over Z-LO-REF from 2 to 7 days and Z-LO-01 to Z-LO-09 catalysts are displayed in Figure 4.3. It is important to remind that the selectivity is defined as the mole fraction of one specific product per total mole fraction of all products formed. The Z-LO-REF (2d) catalyst exhibited a lower selectivity towards ethylene, propylene, isobutane, butylenes than other reference zeolites, and the main products detected were C_5^+ hydrocarbons. However, the selectivity towards light olefins and isobutane increased significantly thanks to the addition of oxidized lignin, especially for Z-LO-07 catalyst. Other catalysts did not show significant changes in the presence of biomass, therefore we infer that oxidized lignin or even other biomasses could promote the zeolite crystallization process and accelerated the zeolite crystal growth in rather short hydrothermal duration. Besides, a big difference can be observed for Z-LO-01 and other catalysts, since Z-LO-01 had a tendency to produce more i-C_4H_{10} instead of light olefins. It showed a selectivity towards isobutane of 50%, however the selectivities in ethylene, propylene and butylenes were only 11%, 19%, 5%, respectively. Besides, similar selectivities towards light olefins (C_2-C_4) were achieved over Z-LO-02 to Z-LO-09 zeolites. In terms of propylene selectivity, Z-LO-07 catalyst exhibited the highest value of 36%, while the highest ethylene selectivity (23%) was achieved over Z-LO-06 catalyst. Furthermore, the propylene/ethylene ratios are presented in Table 4.1, Z-LO-02, Z-LO-07 and Z-LO-09 still showed the highest ratio than other catalysts.

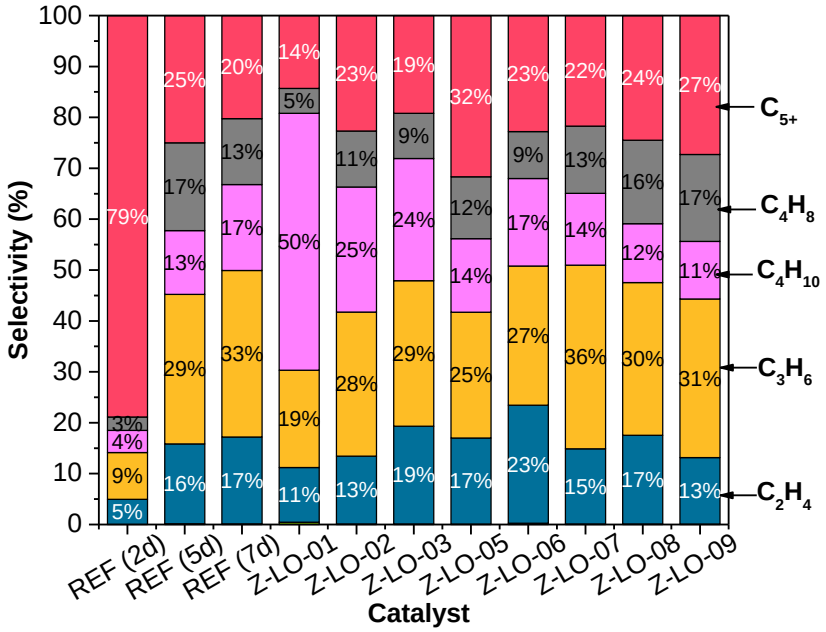

Figure 4.3 Product distributions during the MTO reaction over Z-LO-REF from 2 to 7 days and ZSM-5 zeolites from Z-LO-01 to Z-LO-09 at 450 ºC. Reaction conditions: WHSV = 2 h^{-1}, catalyst weight = 60 mg, TOS = 1 h.

Table 4.1 Propylene / Ethylene ratio achieved over Z-LO-01 to Z-LO-09 and their corresponding pristine ZSM-5 zeolites.

Catalyst	P/E	Catalyst	P/E
REF (2d)	1.8	**Z-LO-05**	1.5
REF (5d)	1.8	**Z-LO-06**	1.2
REF (7d)	1.9	**Z-LO-07**	2.4
Z-LO-01	1.7	**Z-LO-08**	1.8
Z-LO-02	2.2	**Z-LO-09**	2.4
Z-LO-03	1.5		

The selectivities towards light olefins (C_2-C_4) achieved over different ZSM-5 zeolites ranging from Z-LO-01 to Z-LO-09 and Z-LO-REF (2d) to Z-LO-REF (7d),

measured after 1 h time-on-stream, are given in Figure 4.4. Z-LO-REF (5d), Z-LO-REF (7d), Z-LO-07, 08, and 09 exhibited the higher selectivity, which were 62%, 63%, 64%, 64%, and 61%, respectively. High selectivities towards light olefins were already achieved over two parent zeolites Z-LO-REF (5d and 7d), so the addition of biomass did not further improve their selectivities. Whereas, the selectivity towards light olefins was increased from 17% to 35% and the highest 64% over Z-LO-REF (2d) and Z-LO-01, Z-LO-07 catalysts with the addition of oxidized lignin from 0 to 200, and 300 mg. It demonstrates that utilization of biomass can affect the selectivity in the MTO reaction, with a higher selectivity in light olefins reached with the catalyst prepared using 300 mg biomass (here oxidized lignin as an example).

By considering the classical tryptic in catalysis (activity, selectivity and stability), Z-LO-O7 is supposed to be selected as the appropriate catalyst, thus 2 days for hydrothermal reaction and 300 mg biomass were considered to be the optimized conditions for the synthesis of ZSM-5 zeolite.

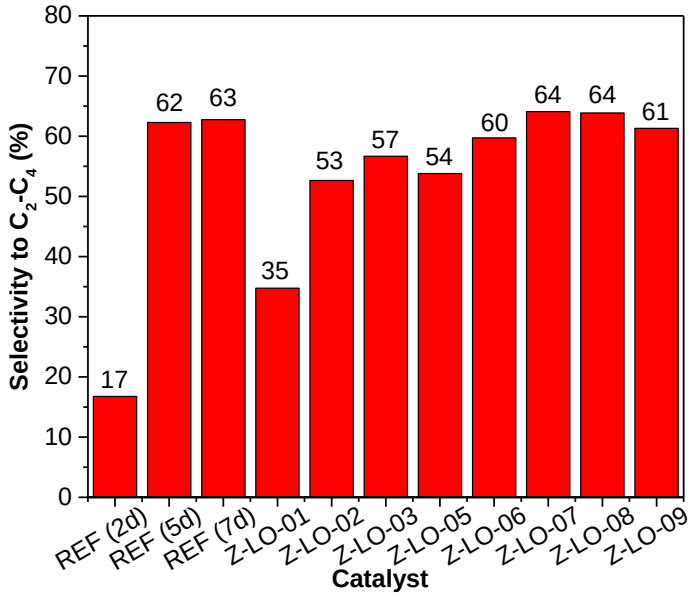

Figure 4.4 Selectivities in C_2-C_4 light olefins over different zeolites formed with Z-LO-REF (2d) to Z-LO-REF (7d), and Z-LO-01 to Z-LO-09. Reaction conditions: 450 °C, WHSV = 2 h^{-1}, catalyst mass = 60 mg, TOS = 1 h.

4.3 Influence of biomass nature on catalytic performance

As described in Chapter 3, analcime structure (ANA, $Na(AlSi_2O_6)(H_2O)$), formed and exhibit no catalytic activity.[259] Therefore, we adjusted the proportion of reactants in order to obtain a pure MFI structure, and denoted the new methods as A method and B method. The specific synthesis methods have been detailed in Chapter 2.

The conversion of methanol (and dimethyl ether, DME) over time-on-stream is shown in Figure 4.5. Significant differences in the catalytic performances could be observed. Z-LO-07-REF is obtained with same protocol than Z-LO-07 but without the utilization of oxidized lignin. The Z-LO-07-REF and A-method-REF zeolites showed a relatively high initial conversion (88% and 84%), whilst B-method-REF only exhibited a 65% conversion. Despite the lower activity of B-method-REF sample, it maintained a nearly constant conversion beyond 30 h, allowing a longer lifetime. However, other two catalysts showed a drastic conversion drop, for instance, Z-LO-07-REF only showed a stable conversion up to ca. 6 h and then strongly deactivated. In addition, it is worth noting that for Z-LO-07-REF (without biomass) the conversion declined to 50% after 22 h. However, at the same time, Z-LO-07 (with oxidized lignin) still maintained its activity at approximately 80% (Figure 4.1), showing a higher resistance to deactivation in the presence of oxidized lignin.

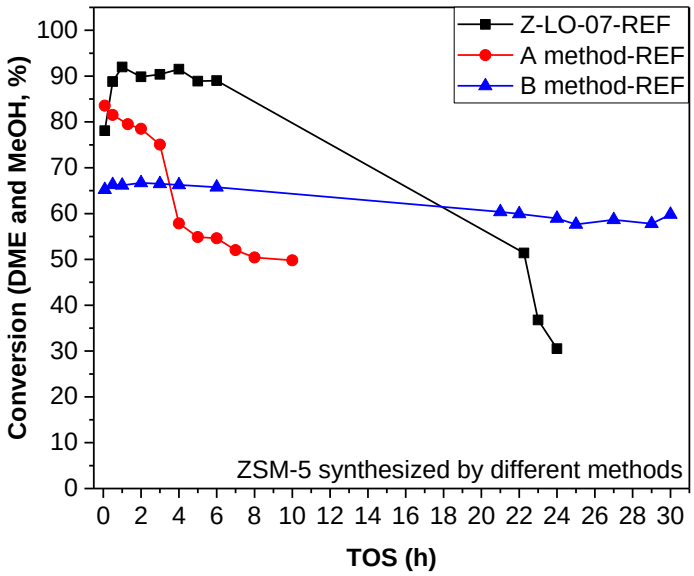

Figure 4.5 Methanol conversion versus time-on-stream (TOS) over pristine ZSM-5 zeolites synthesized by three different methods. Reaction conditions: 450 ºC, WHSV = 2 h^{-1}, catalyst weight = 60 mg.

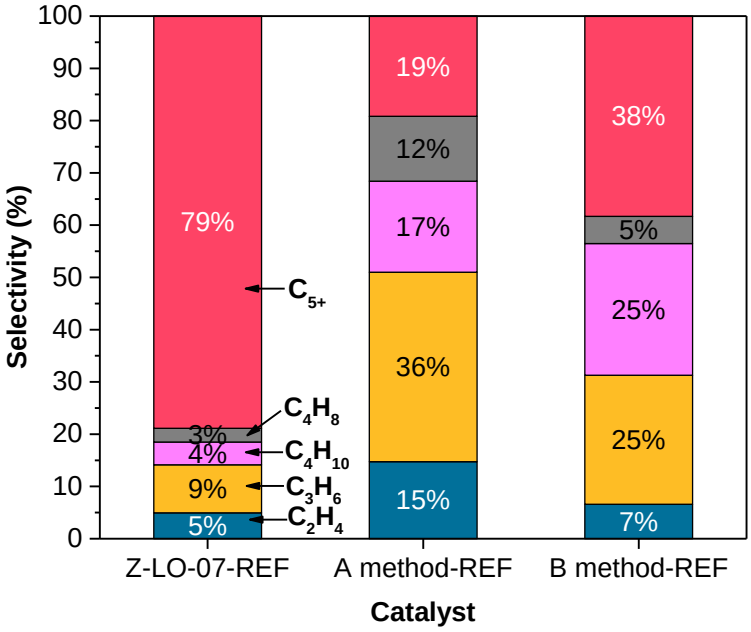

Figure 4.6 Selectivity in the different products during the methanol conversion over three different zeolites. Reaction conditions: 450 ºC, WHSV = 2 h^{-1}, catalyst weight = 60 mg, TOS = 1 h.

Figure 4.6 shows the selectivity in the different hydrocarbons over the three zeolites. One can notice that without using oxidized lignin in the preparation, the selectivity to ethylene, propylene, isobutane, butylenes of Z-LO-07-REF decreased sharply, and selectivity to C_5^+ hydrocarbons increased up to 79%. Although the stability of A method is not outstanding, its selectivity remained obviously better than other two methods, being 36% for propylene and 15% for ethylene.

Furthermore, the catalytic selectivities towards C_2-C_4 olefins were exposed in Figure 4.7. The results are consistent with those discussed above, and the selectivities in light olefins over three reference ZSM-5 catalysts (Z-LO-07-REF, A method-REF, and B method-REF) were 17%, 63% and 36%, respectively. It can therefore be seen that the three methods led to completely different catalytic performance, with Z-LO-7-REF showing the highest initial conversion, A method-REF displaying the highest selectivity to light olefins, and B method-REF leading to longer lifetime.

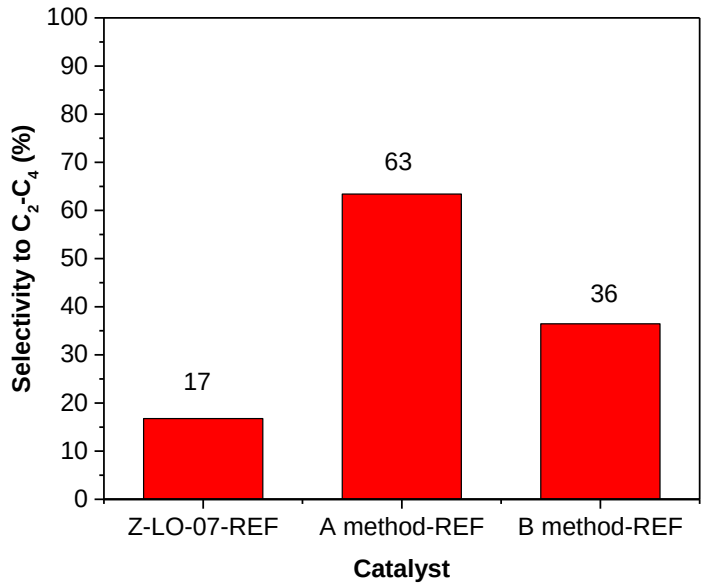

Figure 4.7 Selectivities to light olefins (C_2-C_4) over three reference ZSM-5 catalysts. Reaction conditions: 450 °C, WHSV = 2 h^{-1}, catalyst weight = 60 mg, TOS = 1 h.

Starting with Z-LO-07-REF samples, we synthesized a series of H-ZSM-5 zeolites in the presence of various biomasses, which are oxidized lignin, Russian lignin, sugarcane, ecoshell, coffee, tea residues and a commercial Kraft lignin, denoted as alkali lignin. All these biomasses acted as bio-sourced secondary templates (BSST) for modifying the zeolite crystal growth and morphology. However, how do they participate in the crystallization of zeolite is not clear and a better understanding of the BSST strategy should be further discovered. Our target is to assess the catalytic performance of zeolites by using several kinds of biomasses, and compare their differences in terms of activity, selectivity and stability at the same time. While choosing one or more promising catalysts for MTO reaction, we also attempt to explain their structure-activity relationships as a function of the biomass nature.

The catalytic performances of biomasses-derived H-ZSM-5 catalysts were evaluated in the methanol conversion (MTO) at 450 ºC, and the results of the different samples are given in Figure 4.8. It can be directly noticed that there were huge differences in the data among the samples prepared with 7 types of biomasses. The zeolites prepared in the presence of spent tea leaves, oxidized lignin and coffee bagasse exhibited an enhanced methanol conversion compared with their pristine counterparts, whereas a faster deactivation occurred for the sample prepared with Russian lignin, alkali lignin, ecoshell, and sugarcane bagasse.[260] In particularly, the zeolites prepared with alkali lignin, Russian lignin and coffee bagasse led to a decreased conversion. The use of alkali lignin, Russian lignin, ecoshell, sugarcane bagasse seriously diminished the zeolite lifetime. Surprisingly, the tea, oxidized lignin or coffee bagasse-assisted ZSM-5 catalysts exhibited good stability and kept the initial conversion more than ca. 20 h. It is noteworthy that in the prensence of tea residues, the conversion obviously remained >95% during roughly 24 h of reaction. Beyond that, it was also observed that the methanol conversion over some samples (e.g. Z-LO-07-REF, -alkali lignin, -Russian lignin and -coffee bagasse) presented a trend of rising first and then deactivating with time-on-stream. The reason for such initial conversion increase at the initial stage of the reaction might be due transient behavior on the catalyst surface, prior to steady-state conditions.[261]

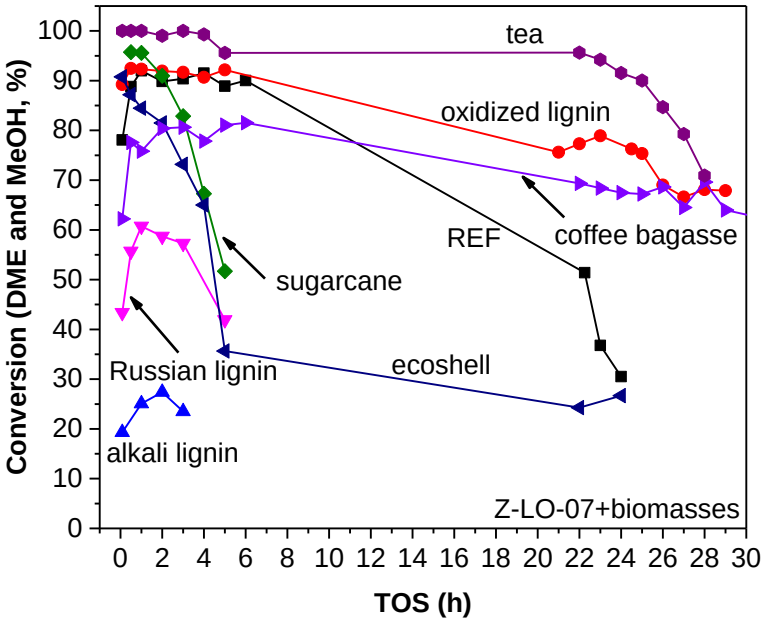

Figure 4.8 Long term stability in the MTO reaction of as-synthesized ZSM-5 zeolites with 300 mg of various biomasses. Reaction conditions: 450 °C, WHSV = 2 h^{-1}, catalyst weight = 60 mg.

Figure 4.9 shows the distribution of different hydrocarbons over Z-LO-07-REF zeolites produced with different kinds of biomass. Almost every catalysts showed an improved selectivity towards light olefins under the influence of biomass, except alkali lignin-assisted zeolite. H-ZSM-5 in the presence of alkali lignin led to the highest selectivity towards isobutane (56%). Besides, the production of methane can be detected in the presence of sugarcane bagasse and ecoshell. Note that despite the significant changes in the products distribution, the ratio of propylene to ethylene for reference catalyst remains similar to the tea-assisted catalyst, as shown in Table 4.2.

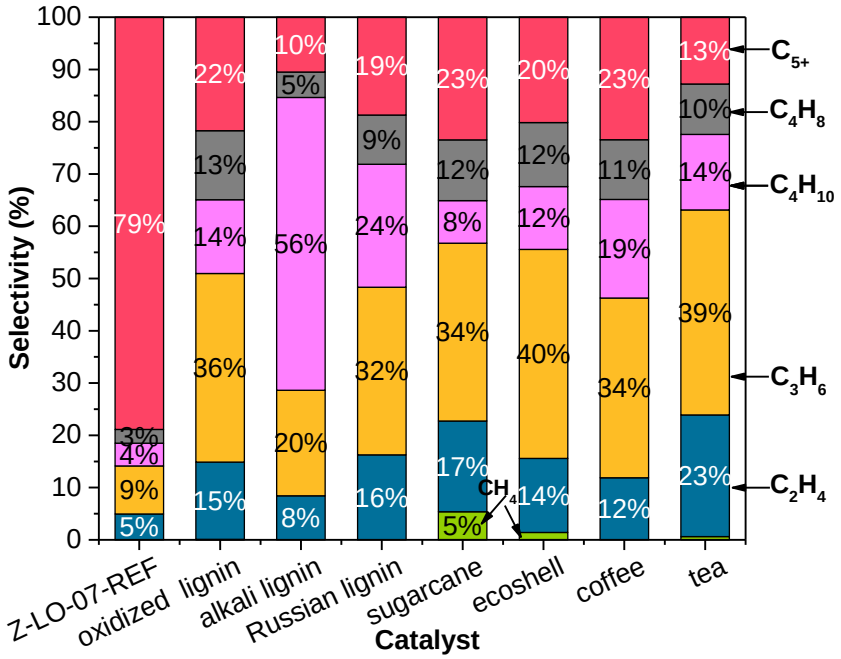

Figure 4.9 Selectivity to different hydrocarbons over Z-LO-07 zeolites with different kinds of biomass (oxidized lignin, alkali lignin, Russian lignin, sugarcane, ecoshell, coffee and tea residues).

Table 4.2 Propylene / Ethylene ratio over Z-LO-07-biomasses.

catalyst	REF	oxidized lignin	alkali lignin	Russian lignin	Sugar-cane	ecoshell	coffee	tea
P/E	1.8	2.4	2.5	2	2	2.9	2.8	1.7

Biomass-modified samples demonstrated much higher selectivity to light olefins with lower contribution of heavier hydrocarbons (C_5^+) and aromatics, as displayed in Figure 4.10. For example, Z-LO-07-oxidized lignin and Z-LO-07-tea had almost 3.8 and 4.3 times higher selectivity to light olefins and 3.6 and 6.1 times lower selectivity to heavier hydrocarbons (C_5^+) fraction, respectively. Therefore, by comprehensively considering the catalyst activity, stability and selectivity, tea waste and oxidized lignin are obviously beneficial for improving the performance in the MTO. Moreover, even compared with two benchmark zeolites CBV 28014 and CBV 3020E (Figure 4.21), the

selectivities in light olefins of tea waste- and oxidized lignin-ZSM-5 are still higher than the benchmark zeolites (58% for CBV 28014 and 37% for CBV 3020E).

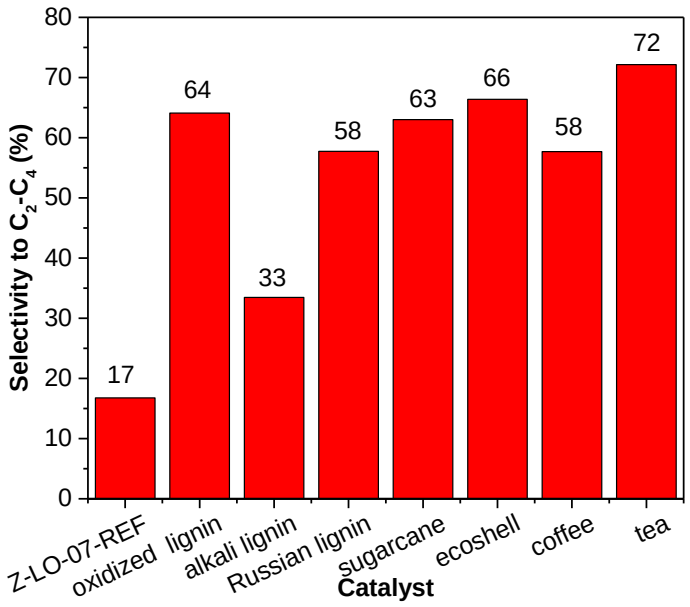

Figure 4.10 Selectivities in light olefins (C_2-C_4) over Z-LO-07-REF and Z-LO-07 zeolites with different kinds of biomass (300 mg).

For the A method, we also performed several catalytic tests at 450 ºC and WHSV = 2 h^{-1}. From Figure 4.11, it appears that the three curves followed almost the same trend and exhibited a similar long lifetime even if their hydrothermal time were increased from 3, 5, to 7 days. In contrast, A-REF-2d exhibited an initial methanol conversion of around 84%, which then diminished to 50% after 10 h on stream. Because of the above research, it is found that some biomass materials can effectively improve the activity and stability of catalysts, such as tea leaves. We have chosen A-REF-2d zeolites as a reference material, acting as a control group for further study.

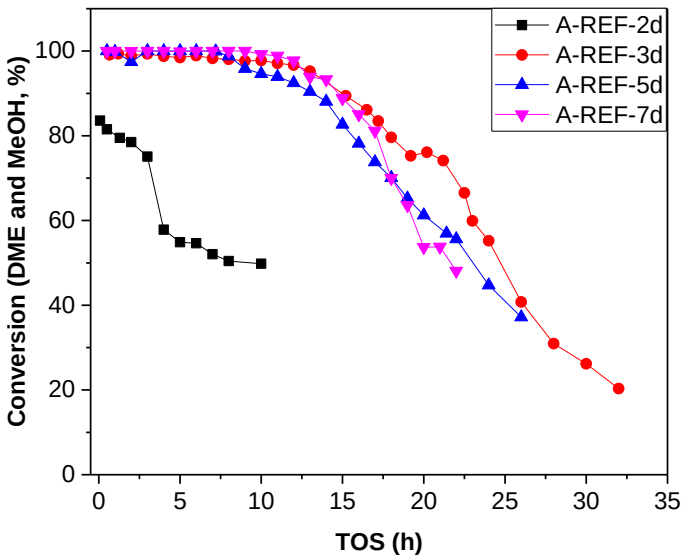

Figure 4.11 Comparison of methanol conversion results with time-on-stream over ZSM-5 synthesized by A method at different hydrothermal times (2, 3, 5 and 7 days). Reaction conditions: 450 ºC, WHSV = 2 h^{-1}, catalyst weight = 60 mg.

Regarding selectivity towards the different hydrocarbons, no significant change could be seen among the four samples obtained after different synthesis durations (Figure 4.12). All of them showed high selectivities to ethylene, propylene, and butylenes, thus the light olefins selectivity was increased slightly from 63% to 77% with the prolongation of the hydrothermal time from 2 to 7 days (Figure 4.12(b)).

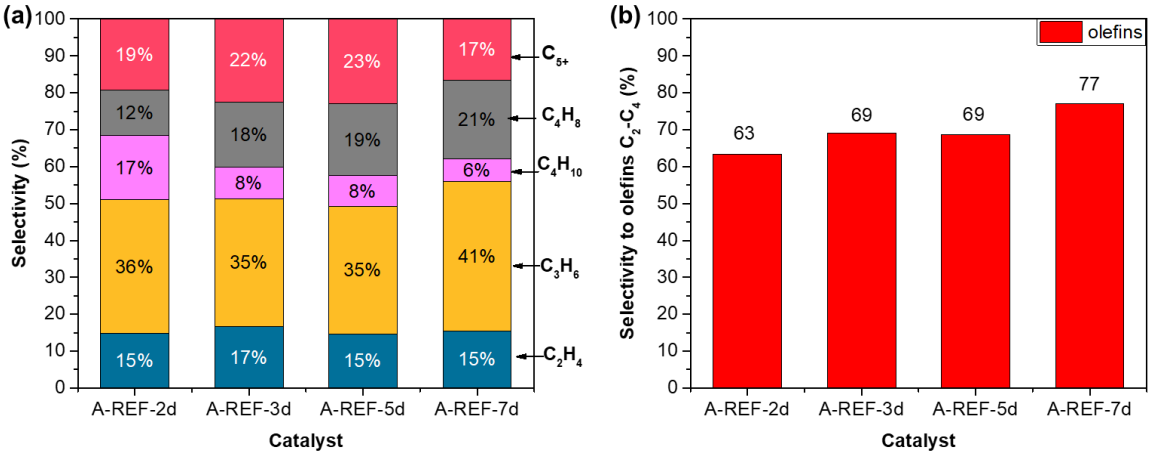

Figure 4.12 Selectivities towards (a) ethylene, propylene, isobutane, butylenes, and C_5^+ and (b) light olefins (C_2-C_4) over catalysts synthesized by A method at different hydrothermal durations (2, 3, 5 and 7 days).

Seven types of biomasses originated from different countries, which were oxidized lignin, alkali lignin, coffee bagasse, tea waste, mixture of freshwater cyanobacterium (algaCM), freshwater algae Bracteacoccus bullatus (algaBB) and another freshwater algae Trachydiscus minutus (algaTM), were selected to add into the alkali solutions as bio-sourced secondary templates for the synthesis of several zeolites. The catalytic activity of these zeolites was evaluated in the methanol-to-olefins reaction, as shown in Figure 4.13. It can be noticed that an obvious deactivation occurred for the samples prepared with biomasses, but the zeolites obtained in the presence of spent tea leaves behave completely different and demonstrated an outstanding catalytic performance among other catalysts. Indeed, the initial activity reached approximately 100% and remained constant for more than 50 h on stream, and then only slightly dropped to 97% after 60 h. The activity and stability of A-tea-ZSM-5 was noticeably improved with respect to the reference sample without biomass. In addition, a careful comparison revealed that some zeolites in the presence of biomass, such as oxidized lignin, algaCM, algaBB, exhibited an improvement in their initial methanol conversion with respect to A-REF zeolite. Due to the insufficient crystallization process of the zeolite, or the addition of some biomasses did not have a significant contribution as a zeolite growth modifier, the catalytic activity and stability for some samples, such as A-alkali lignin, A-coffee and A-algaTM, did not promote greatly.

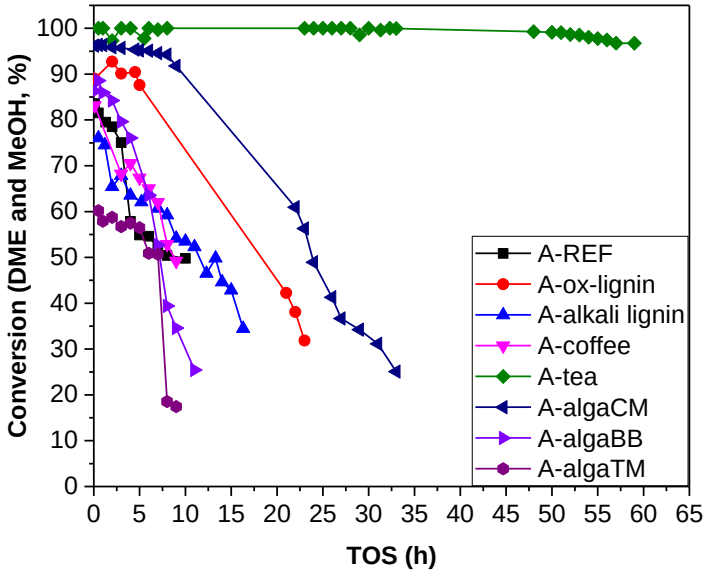

Figure 4.13 Methanol conversion with time-on-stream over A-REF and different biomasses-derived ZSM-5 by using A method. (biomasses: oxidized lignin, alkali lignin, coffee and tea residue and three kinds of algae).

Although A method led to achieve good selectivity toward light olefins in comparison with the other two methods, it is still surprising to see that the selectivity to ethylene and propylene was improved further by the addition of tea leaves. Specifically, the selectivity to ethylene and propylene were 22% and 49% over A-tea zeolite sample (Figure 4.14), which increased to 47% and 36%, respectively, compared to the blank control group A-REF zeolite (15%, 36%). For other catalysts, even though their activities differed significantly, all of them exhibited high selectivity to light olefins and did not change significantly with an addition of biomass. The highest selectivity which we were able to reach was 83% for A-tea zeolite, and other catalysts also maintained it above 60%, as shown in Figure 4.15.

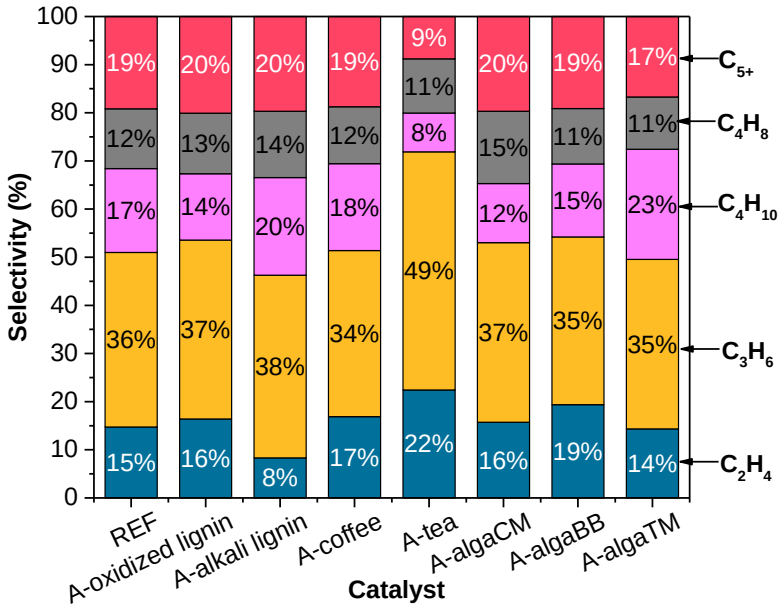

Figure 4.14 Selectivities towards ethylene, propylene, isobutane, butylenes, and C_5^+ hydrocarbons over A-REF and biomass-derived ZSM-5 by using A method.

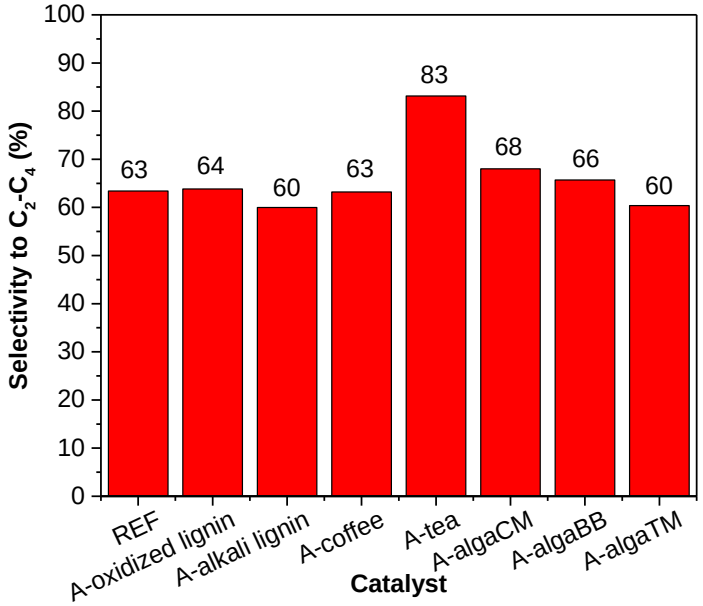

Figure 4.15 Selectivities towards light olefins (C_2-C_4) over A-REF and biomass-derived A-ZSM-5. Reaction conditions: 450 °C, WHSV = 2 h^{-1}, catalyst weight = 60 mg, TOS = 1 h.

Further optimization of the A-tea catalyst by changing the biomass content from

200, 300 to 400 mg. The lifetime results showed a trend of increasing first and then decreasing with a raise in the weight of spent tea leaves, as displayed in Figure 4.16. All tea-assisted ZSM-5 started with a 100% methanol conversion in the initial reaction stage and longer lifetime than A-REF sample.

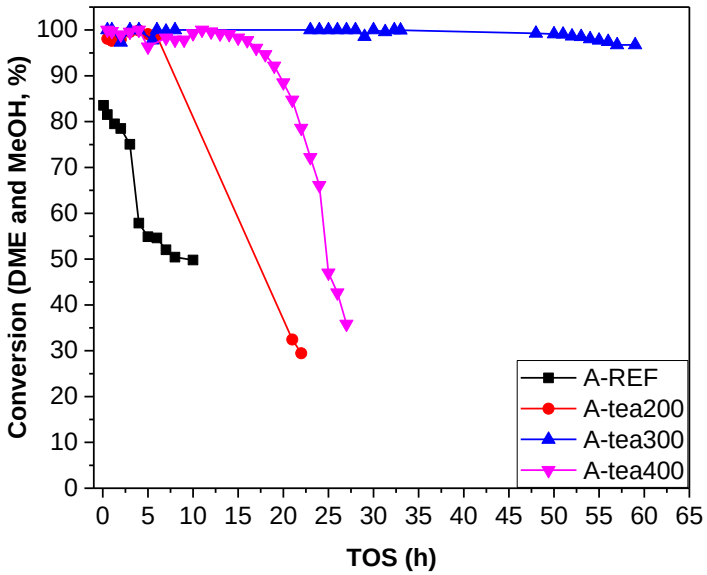

Figure 4.16 Methanol (and dimethyl ether) conversion over A-REF and ZSM-5 prepared by A method with different amounts of tea waste (200, 300 and 400 mg).

The products selectivity of those samples was presented in Figures 4.17 and 4.18. The selectivity to isobutane diminished while the selectivity in propylene increased, which may be due to an increase in the amount of tea waste. As a result of this, the selectivity toward light olefins of 83% and 74% after 1 h on stream over A-tea300 and A-tea400, respectively.

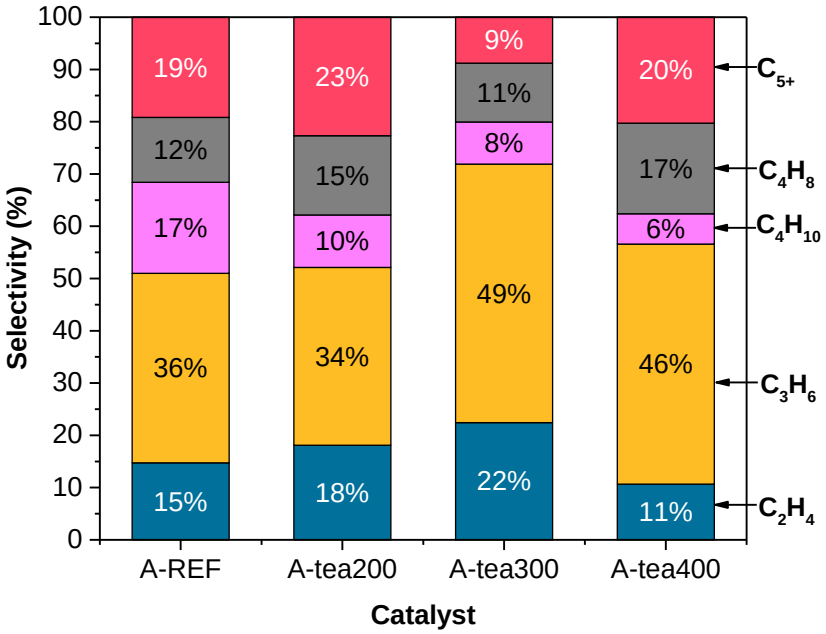

Figure 4.17 Selectivity to different hydrocarbons over A-REF and ZSM-5 prepared by A method with different amounts of tea waste (200, 300 and 400 mg).

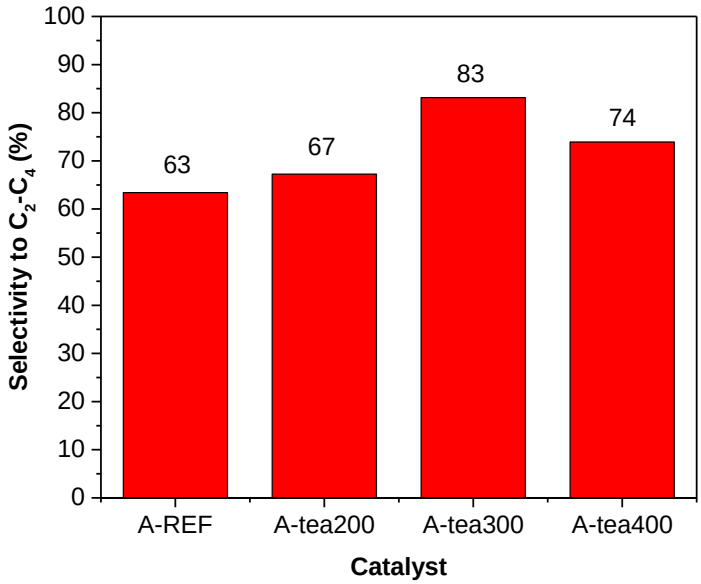

Figure 4.18 Selectivities in light olefins over A-REF and tea leaves-derived A-ZSM-5.

A-tea300 catalyst was tested in the MTO reaction and its performance was compared with CBV 28014 and CBV 3020E commercial zeolites provided by Zeolyst

(Figure 4.19). CBV 3020E has a SiO_2/Al_2O_3 mole ratio of 30 and specific surface area of 368 m^2/g, and it has therefore similar textural properties as the ZSM-5 zeolites that we prepared. CBV 28014 has a higher SiO_2/Al_2O_3 mole ratio of 280 with a specific surface area of 400 m^2/g. It is worth noting that A-tea300 catalyst exhibited a longer lifetime regarding commercial zeolite, CBV 3020E, which maintained a conversion at 100% for 15 h, significantly lower than the 50 h of A-tea300 zeolite under the same conditions. Likewise, CBV 28014 demonstrated a considerable stability while maintaining its initial catalytic activity for more than 60 h. However, the methanol conversion over CBV 28014 remained lower (80%) than A-tea300 (100%) under the same test conditions. Fortunately, our catalyst is really competitive with respect to these two benchmark catalysts.

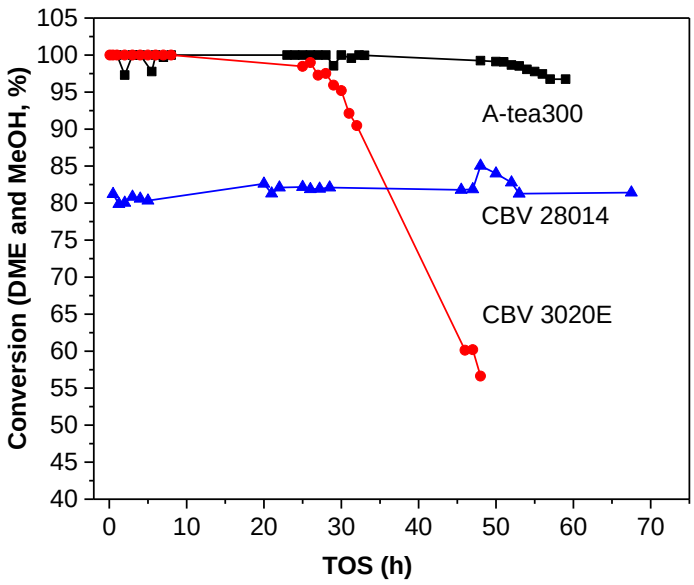

Figure 4.19 Comparison of methanol (and dimethyl ether) conversion over as-synthesized A-tea300 catalyst and two commercial zeolites (CBV 28014, and CBV 3020E). Reaction conditions: 450 ºC, WHSV = 2 h^{-1}, catalyst weight = 60 mg.

Interestingly, observing the selectivity in methane, ethylene, propylene, isobutane, butylenes and hydrocarbons with 5 C or more (including aromatics) represented in Figures 4.20 and 4.21, it is worthy to mention that ethylene formed in much lower

quantities over the two commercial zeolites than over A-tea300 zeolite. Indeed, ethylene selectivity was only 2% for the two former zeolites. In stark contrast, 23% and 31% of isobutane selectivity and 19% and 30% of C_5^+ selectivity were achieved over CBV 28014 and CBV 3020E, respectively. Therefore, a higher selectivity toward light olefins could be obtained over as-synthesized A-tea300 catalyst, close to 80% with respect to 58% and 37% C_2-C_4 olefins selectivity obtained over CBV 28014 and CBV 3020E, respectively.

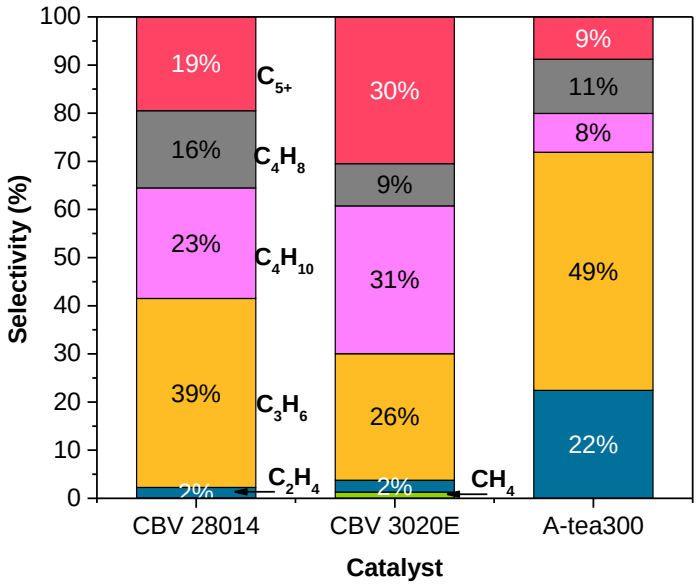

Figure 4.20 Selectivity in the MTO reaction over A-tea300 zeolites and CBV28014 and CBV 3020E zeolites: 450 ºC, WHSV = 2 h^{-1}, catalyst weight = 60 mg, TOS = 1 h.

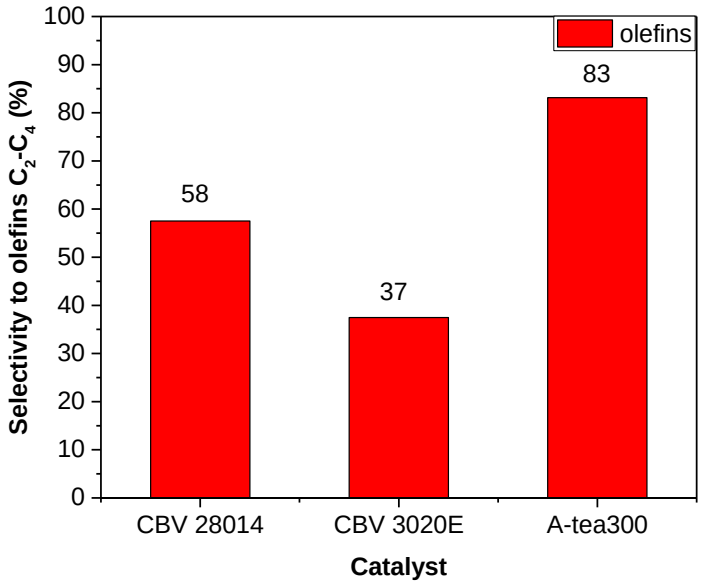

Figure 4.21 Selectivities towards ethylene, propylene and butylenes over A-tea300 and CBV 28014 and CBV 3020E zeolites at 450 ºC.

The dependence between selectivity and time-on-stream in the fixed bed reactor is shown in Figure 4.22. The changes in selectivity over time-on-stream towards the different products were diverse over A-tea300, CBV 28014 and CBV 3020E catalysts. Regarding A-tea300 sample, almost half of the methanol converted into propylene during the reaction. The selectivity towards other light olefins, ethylene and butylenes, also presented relatively high values of 25% and 11%, respectively. At longer reaction duration, the slope of the selectivty toward ethylene and proylene slightly decreased whereas the selectivity in C_5^+ hydrocarbons increased obviously from 8% to about 15%. Similar to A-tea300 sample, the selectivity in propylene for CBV 28014 remained also higher than other hydrocarbons which was 40% at the reaction start and then maintained at ca. 35% after a slight drop. While the selectivities towards ethylene and butylene were both lower than isobutane and C_5^+ hydrocarbons, providing values of 2% and 16%, respectively. Moreover, the selectivity toward C_5^+ hydrocarbons steadily increased from about 17% to 23% during 100 h on stream. Regarding CBV 3020E catalyst, the selectivity in isobutane and C_5^+ hydrocarbons always predominated the product

distribution, even the ethylene selectivity promoted from 2% to 13% by extending the reaction duration, this light olefins selectivity on CBV 3020E remained however the lowest among the three catalysts.

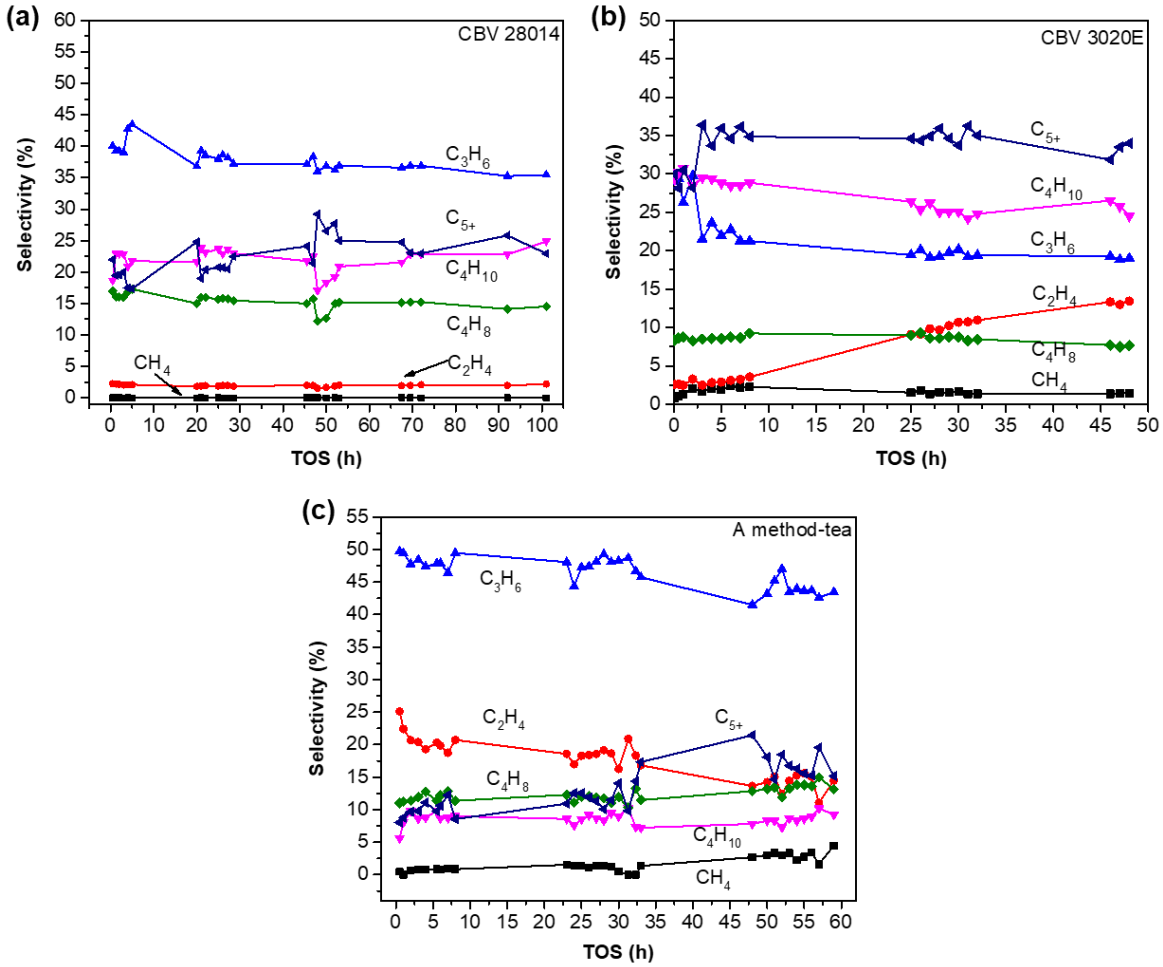

Figure 4.22 Variation in the selectivities in methane, ethylene, propylene, isobutane, butylenes, and C_5^+ with the time-on-stream (TOS) over A-tea300, CBV 28014 and CBV 3020E catalysts.

It is well known that there are always several reactions occurring simultaneously, and these reactions may affect each other in a sophisticated way in the course of the MTO reaction. Usually, we hold an opinion that most of the propylene is formed through an olefin cycle according to the hydrocarbon pool mechanism, and no induction period is required for the olefin cycle once the first C–C bond is formed, which explains

why the selectivity towards propylene is less affected with time-on-stream.[262] However, the production of ethylene differs from propylene. Through chain growth, olefin oligomerization, aromatization, and hydrogen transfer between the aromatic intermediates and light olefins, diverse products, light olefins, aromatics and paraffins, are produced. In the aromatic-based cycle, aromatics are repeatedly methylated and dealkylated to form light alkenes. Lighter methylbenzenes such as dimethylbenzene and trimethylbenzene in the aromatic-based cycle favor ethylene formation by β-scission.[263, 264] Thus, it can be seen that the formation of ethylene would take some time as observed in the ethylene selectivity change over CBV 3020E with time-on-stream (Figure 4.22(b)).

A-tea300 catalyst exhibited comparable methanol conversion and light olefins selectivity as the commercial zeolites under the same conditions. Meanwhile, it was also compared with other representative biomass-derived ZSM-5 catalysts for the MTO reaction, and their specific surface area, SiO_2/Al_2O_3 mole ratio, test conditions and catalytic performance are shown in Table 4.3. It can be seen from Table 4.3 that the different kinds of biomass, like lignin, vanillin, coumaric acid, sugarcane bagasse, and fly ash, were used to guide the self-assembly of zeolite nanocrystals as a growth modifier at temperatures ranging from 350 to 450 ºC, WHSV ranging from 1 to 2. In the case of MFI zeolites, different catalytic activities, selectivities and stabilities were achieved in the methanol conversion to light olefins. For example, by using South African coal fly ash for the synthesis of ZSM-5 zeolite, the catalyst exhibited a 35% propylene selectivity and 66% light olefins (C_2-C_4) selectivity at full methanol conversion after 1 h on stream. Besides, Gomes *et al*. prepared a catalyst in the presence of sugarcane bagasse, which exhibited a light olefins selectivity only 8%, but showed an unexpected selectivity toward C_5^+ gasoline fraction (MTG) of ca. 90%.[191] Also using sugarcane bagasse for ZSM-5 zeolite synthesis, the selectivity towards light olefins can vary from 8% to 61%, and propylene selectivity increased from 9% to 34% by changing the synthesis conditions. Even so, A-tea300 catalyst still presented an excellent catalytic activity, selectivity and long lifetime when compared to other biomass-derived ZSM-5 zeolites.

Table 4.3 Summary of several representative biomass-derived ZSM-5 catalysts for the MTO reaction

Catalyst	S_{BET} (m^2/g)	SAR	TOS (h)	Conversion (%)	Stability (h) (50%)	Selectivity to C_2-C_4 olefins (%)	Selectivity to propylene (%)	P/E[a]	T (^oC)	WHSV (h^{-1})	ref.
ZSM-5 SAR8	392	8.5	1	99	19	<40	13	1	400	1.1	[193]
ZSM-5R	320	25	0.08	99	31	56	27	1.8	350	1.8	[200]
ZSM-5N	345	19	0.08	100	>50	48	23	1.6	350	1.8	[200]
ZSM-5MS	453	43	0.08	99	>50	60	30	2.5	350	1.8	[200]
ZSM-5F	305	53	0.08	98	>50	66	36	5.5	350	1.8	[200]
ZSM-5/reference	330	/	1	100	25	58	33	2.8	400	1.12	[191]
ZSM-5/lignin	451	/	1	100	<25	56	26	1.2	400	1.12	[191]
ZSM-5/vanillin	308	/	1	97	18	56	28	1.6	400	1.12	[191]
ZSM-5/coumaric acid	427	/	1	100	ca.12	61	26	1.2	400	1.12	[191]
ZSM-5/SCB(sugarcane bagasse)	/	13	1	100	22	8	/	/	400	1.12	[191]
ZSM-5/SCBH(sugarcane bagasse)	/	18	1	100	ca.35	17	/	/	400	1.12	[191]

H-ZSM-5_{PL2}(fly ash)	328	5.8	1	58	5	41	20	1.2	450	1.12	[192]
H-ZSM-$5_{PL2\text{-}OA}$(fly ash)	/	6.3	1	100	ca.23	66	35	2.1	450	1.12	[192]
H-ZSM-5_{5524}(commercial)	480	25	1	100	> 25	44	19	1.6	450	1.12	[192]
ZSM-A(sugarcane bagasse)	239	7.6	1	98	ca.25	21	9	1.1	400	1.1	[190]
ZSM-B(sugarcane bagasse)	360	29	1	99	ca.55	61	34	2	400	1.1	[190]
ZSM-C(sugarcane bagasse)	242	9.4	1	96	/	26	9	0.9	400	1.1	[190]
ZSM-D(sugarcane bagasse)	289	14.8	1	95	ca.30	42	17	1	400	1.1	[190]
A-tea leaves	382	28	1	100	more than 65	83	50	2.2	450	2	/

a: P/E = selectivity toward propylene / selectivity toward ethylene.

The changes in the methanol conversion using the different kinds of biomasses modified ZSM-5 zeolites under ca. 145 h time-on-stream are presented in Figure 4.23. As already mentioned above, B-REF exhibited longer lifetime but lower activity than Z-LO-07-REF and A-REF catalysts. Therefore, our aim was to design a catalyst whose activity can be efficiently improved by the presence of biomass. The seven types of biomasses are oxidized lignin, alkali lignin, coffee and tea residue and three kinds of algae. From 4.23(a), we could find that zeolites' initial conversion were increased from 66% in different degree in the presence of biomass. It is worthy to mention that ZSM-5 zeolites by using three algae (algaCM, algaBB and algaTM) showed prolonged lifetime and 50% methanol conversion at ca. 75, 134, and 94 h, respectively.

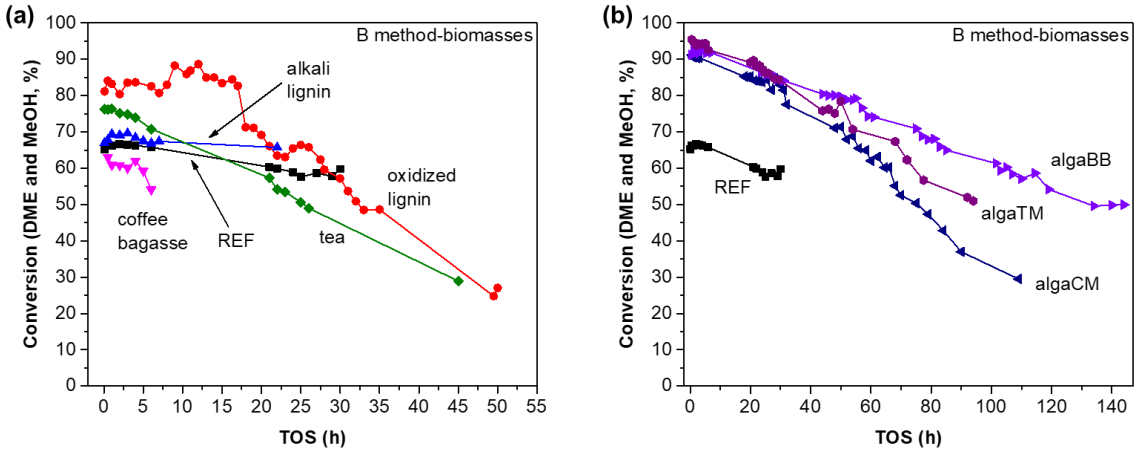

Figure 4.23 Methanol (and dimethyl ether) conversion over B-REF and ZSM-5 prepared by B method with different kinds of biomasses (oxidized lignin, alkali lignin, coffee and tea residues and three kinds of algae).

Besides, their selectivities at 1 h for each catalyst are presented in Figure 4.24 and Figure 4.25. For all cases, the ethylene, propylene and butylenes selectivities increased while the formation of saturated alkanes and aromatics decreased after the addition of biomass. The selectivity in light olefins increased from 36% to maximum 63% over B-oxidized lignin zeolite. Even for B-alkali lignin, the light olefins selectivity was 52% and increased by about 43% with respect to reference zeolite.

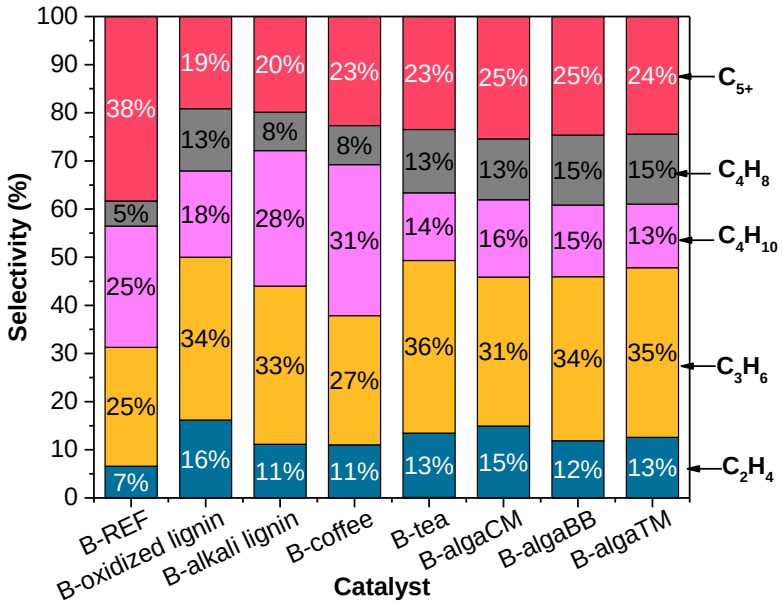

Figure 4.24 Selectivities in methane, ethylene, propylene, isobutane, butylenes, and C_5^+ hydrocarbons over B-REF and biomass-derived ZSM-5 using B method. Reaction conditions: 450 °C, WHSV = 2 h^{-1}, catalyst weight = 60 mg, TOS = 1 h.

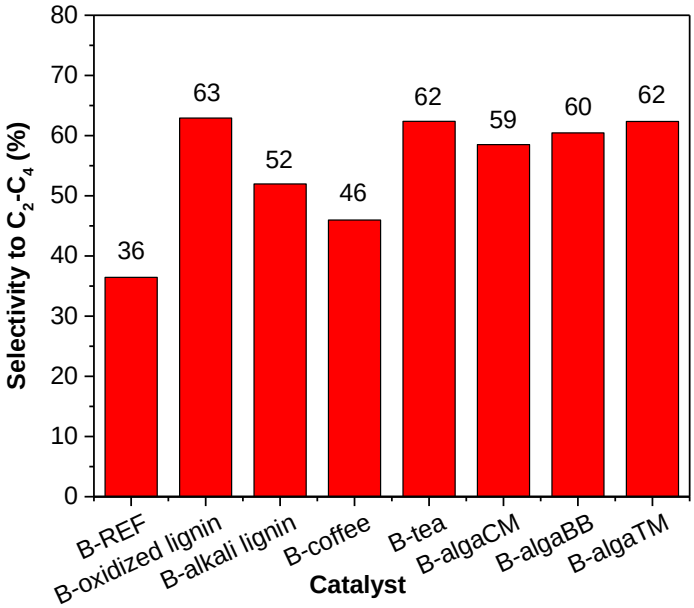

Figure 4.25 Selectivities in light C_2-C_4 olefins over B-REF and 300 mg biomass-derived B-ZSM-5.

In addition, the effects of different amounts of tea leaves on catalytic performance

were also compared for B method. Methanol (and dimethyl ether) conversion over B-REF and ZSM-5 prepared by B method with different weights of tea waste (200, 300 and 400 mg) is shown in Figure 4.26. Unlike previous results of A-tea200, A-tea300 and A-tea400, a significant increase in their activity raised the problem of rapid deactivation. B-tea400 allowed reaching an initial full methanol conversion, which decreased to half conversion in ca. 17 h.

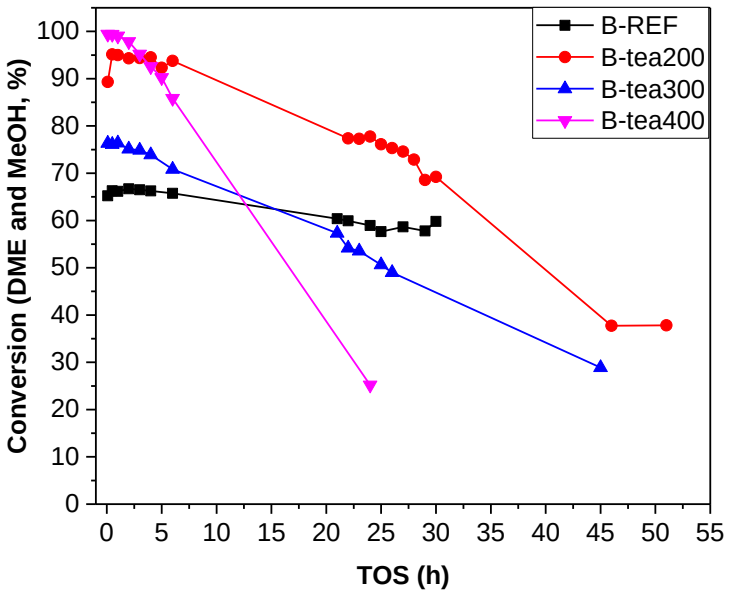

Figure 4.26 Methanol (and dimethyl ether) conversion over B-REF and ZSM-5 prepared by B method with different amount of tea waste (200, 300 and 400 mg).

The selectivity distribution was found to be influenced by the amount of biomass added during the synthesis. Those selectivities to different hydrocarbons were collected in Figure 4.27 and Figure 4.28. Clearly, the presence of spent tea leaves in the catalysts had a promoting effect towards the unsaturated hydrocarbons production and diminished the production of saturated hydrocarbons and aromatics. By NH_3-TPD analysis, it was shown that the number of acid sites in B-REF, B-tea200, 300 and 400 was 0.96, 0.11, 0.06 and 0.05 mmol/g, respectively. For the parent samples, the differences found in product distribution of unsaturated and saturated hydrocarbons may be initially explained in terms of the less density of available Brønsted and Lewis

sites in tea-assisted-ZSM-5 samples which hinder hydrogen transfer reactions, leading to the formation of a lower amount of hydrogen rich molecules (such as alkanes).[265] Therefore the addition of tea waste seems to inhibit hydrogen transfer steps and promote dehydrogenation reaction, and then increasing the selectivity of light olefins rather than isobutane and other saturated hydrocarbons. It can be seen from the results that the selectivities in light olefins was enhanced from 36% to 62%, 62% and 75% over B-REF, B-tea200, 300 and 400 catalysts, which increased 69%, 71% and 100% than reference sample.

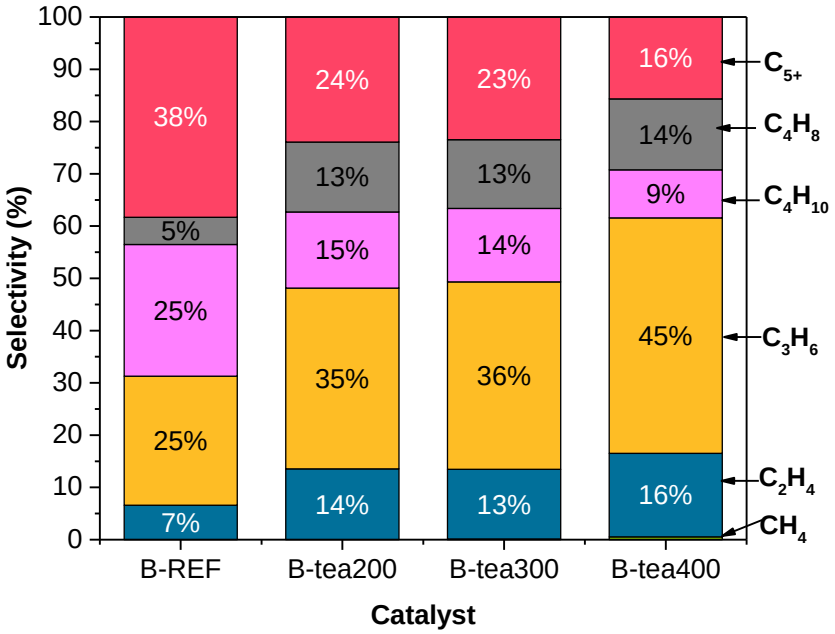

Figure 4.27 Selectivity distribution of methanol to different hydrocarbons over B-REF and ZSM-5 prepared by B method with different amount of spent tea leaves (200, 300 and 400 mg).

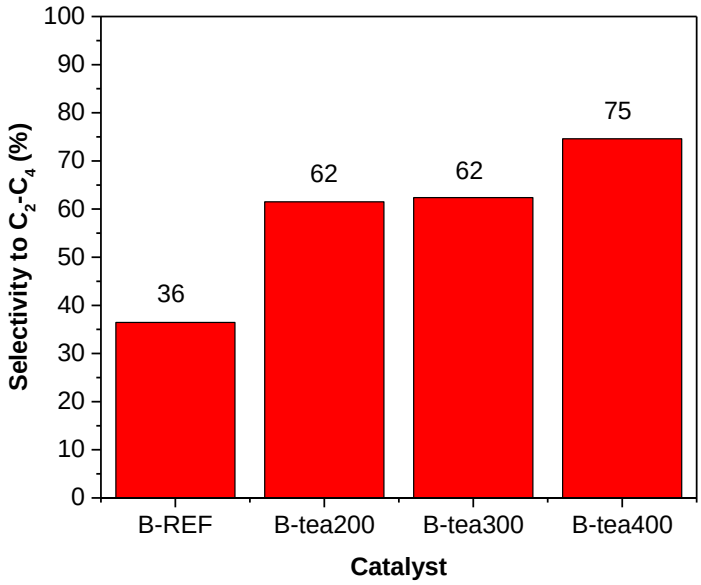

Figure 4.28 Selectivities toward light olefins over B-REF and different amount tea leaves-derived B-ZSM-5.

4.4 Influence of TPAOH on catalytic performance

To evaluate the influence of TPAOH organic template on the catalysts performance, Z-LO-09 and Z-LO-09 prepared with half TPAOH template (Z-LO-09-1/2TPAOH) were tested as catalysts in the MTO reaction at 450 ^{o}C. Under those conditions, two samples can reach high initial conversion of oxygenates (methanol and DME). After, the conversion dropped sharply for the sample with lower TPAOH content, but Z-LO-09 sample maintained almost full conversion beyond 27 h. These results also explained why we selected Z-LO-09 sample for further research even Z-LO-09-1/2TPAOH catalyst exhibited purer MFI crystals and less ANA phase.

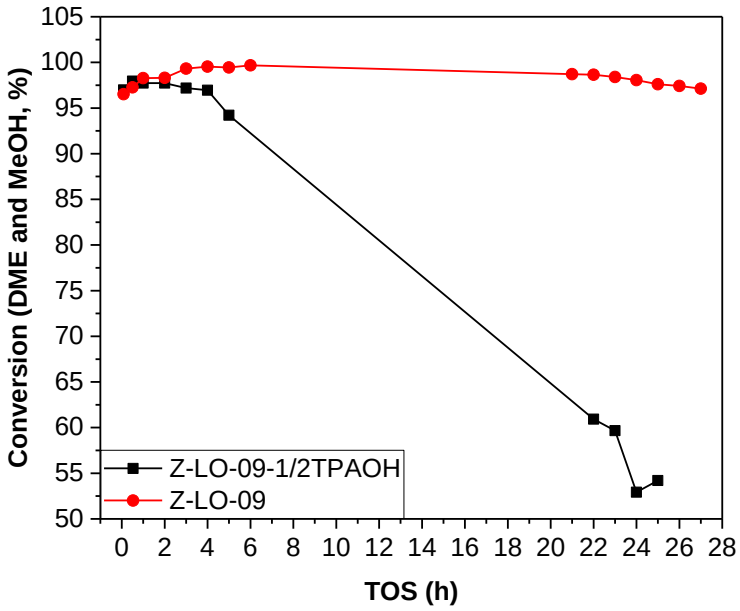

Figure 4.29 Methanol (and dimethyl ether) conversion over Z-LO-09 and Z-LO-09 prepared with half TPAOH template (Z-LO-09-1/2TPAOH).

To further investigate the effect of organic template on catalytic activity, selectivity, and stability over ZSM-5 zeolite, A-tea300 sample with excellent catalytic properties was selected, and synthesized by reduced TPAOH template consumption to 20%, and 50% during the synthesis process. The conversion of methanol in the various products versus time-on-stream over the four catalysts is shown in Figure 4.30. These four catalysts exhibited quite different activities and lifetimes. The obvious decrease in the catalytic activity and lifetime could be attributed to the lower quantity of TPAOH template over A-tea-100%TPAOH, A-tea-50%TPAOH and A-tea-20%TPAOH catalysts. However, it was notable that when the template is reduced to half, the activity and stability of A-tea-50%TPAOH sample were still higher than that of reference sample with the full amount of template added (A-REF-100%TPAOH). It can be therefore be mentioned that the biomass-assisted synthesis method provides a cheap and sustainable way of preparing competitive MTO catalysts with significantly reduced template utilization.

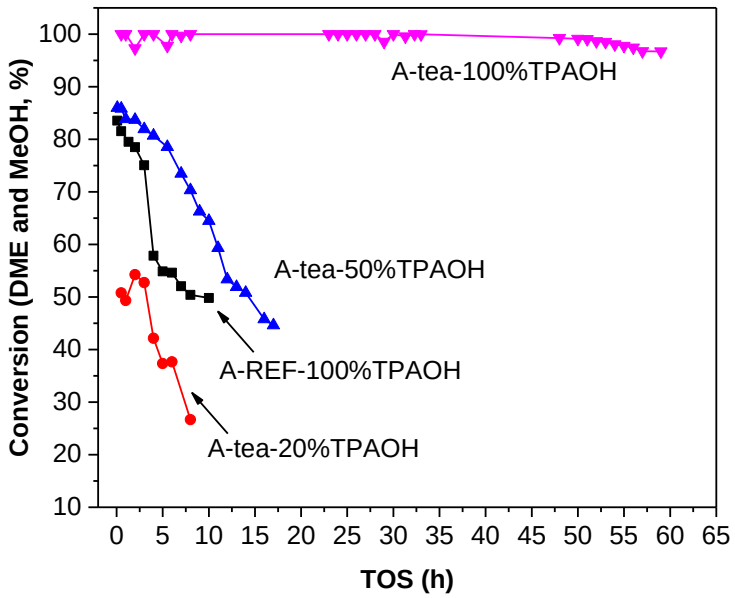

Figure 4.30 Comparison of methanol (and dimethyl ether) conversion over A-REF-100%TPAOH, A-tea-20%, 50% and 100% TPAOH.

Figure 4.31 expresses the selectivities toward methane, ethylene, propylene, isobutane, butylenes and C_5^+ and light olefins (C_2-C_4) over the four H-ZSM-5 zeolites. Propylene was the main product obtained over the four catalysts, being 36%, 31%, 33% and 49% over A-REF-100%TPAOH, A-tea-20%, 50% and 100%TPAOH catalysts, respectively. Isobutane selectivity reached over A-tea-20%TPAOH was as high as propylene selectivity. The ethylene and propylene selectivities and total selectivity for C_2-C_4 light olefins were enhanced with an increase of TPAOH. In addition, both A-tea-50%TPAOH catalyst and reference sample exhibited similar properties in terms of activity, selectivity and stability. In other words, the consumption of expensive TPAOH template can be effectively reduced by adding biomass materials such as tea residues. Besides, it can also contribute to the biomass waste valorization at the same time.

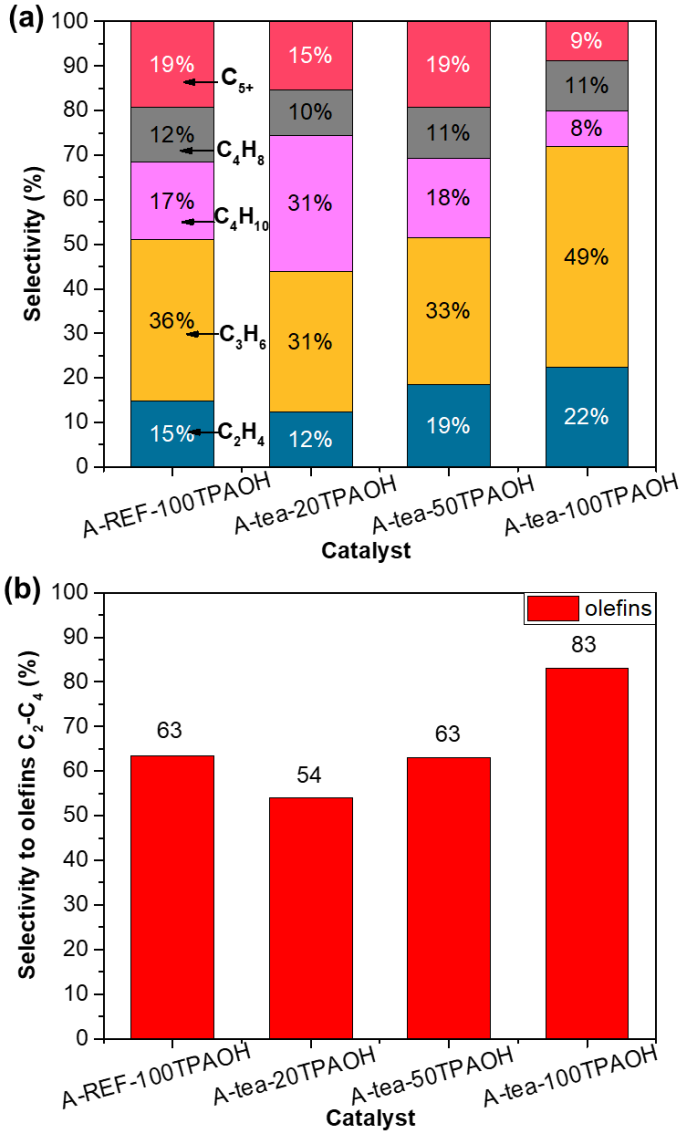

Figure 4.31 Selectivities in (a) methane, ethylene, propylene, isobutane, butylenes and C_5^+ and (b) C_2-C_4 light olefins over A-REF-100%TPAOH, A-tea-20%, 50% and 100%TPAOH catalysts. Reaction conditions: 450 ºC, WHSV = 2 h^{-1}, catalyst weight = 60 mg, TOS = 1 h.

4.5 Conclusions

In this chapter, the incorporation of different kinds of biomasses (oxidized lignin, alkali lignin, Russian lignin, sugarcane, ecoshell, coffee bagasse, tea residues and three algae) during the zeolite synthesis was presented. This is also the first report to summarize and compare the effects of various biomasses on the catalytic performance in the MTO

reaction. First, the hydrothermal time and biomass nature and quantity were determined by a series of catalysts from Z-LO-01 to Z-LO-09 samples. Then, we compared the similarities and differences of the three methods (Z-LO-07, A method and B method) and the changes in the catalytic performance after biomass addition. The addition of several kinds of biomasses effectively enhanced the catalytic activity, selectivity and stability in the MTO process. Among them, A-tea300 zeolite exhibited close to full methanol, excellent stability and C_2-C_4 light olefins selectivity of 83%; its catalytic performance being even higher than CBV 28014 and CBV 3020E commercial zeolites. In addition, three B method-prepared zeolites in the presence of algae (algaCM, algaBB and algaTM) showed remarkable prolonged lifetimes from about 45 h to ca. 75, 134 and 94 h, respectively at the methanol conversion of 50%. Besides, the effect of expensive TPAOH template consumption was investigated by decreasing its amount from 100% to 50% and 20% over A-tea300 sample. The results suggested that the consumption of expensive TPAOH template can be effectively replaced by biomass addition such as spent tea leaves. Besides, it can also contribute to the biomass waste valorization.

Chapter 5. Investigation of the mechanism(s) of bio-sourced secondary templates (BSST) impact on zeolite crystal formation

Abstract

This chapter mainly focuses on the alkaline hydrolysates of biomass used as bio-sourced secondary templates (BSST) and how they interact with soluble silicate or aluminate species (T-monomers). Hence, we also investigate how the BSST species modify the zeolite and further impact the catalytic performance in the MTO reaction. Indeed, saccharides and amino acids are the main hydrolysates of lignin, cellulose, hemicellulose and algae, respectively. Herein, we propose a tentative mechanism while exploring the interaction of hydroxyl, carboxyl and amino functional groups of BSST with aluminates and silicates. Effective bio-templates closely mimic crystal surface features and may orientate in solute vacancies by H-bonding or electrostatic interactions. We found that BSST acted both as “inhibitor” for the crystal growth in the b-axis direction and as “promoter” to accelerate the kinetics of crystallization.

By correlating the relative length of b-axis with catalytic performance, it can be clearly seen that the both activity and selectivity towards light olefins (and stability) were improved with a decrease in b-oriented channel length. This may be due sufficient accessibility to the acid sites, rapid diffusion of reactants and products which hindered coke formation. Through the discussion of a tentative self-assembly mechanism, we suggest therefore that the MTO catalytic performance enhancement can be achieved by the judicious selection of BSST nature.

Finally, from the perspective of environmental protection, the synthesis of zeolites in the presence biomass is a facile, cheap and green strategy, and could allow a smart valorization of bio-wastes.

5.1 Introduction

Zeolites are crystalline microporous aluminosilicates, with uniform micropores, tunable acidities and high thermal stability, being important shape-selective catalysts in the petrochemical industry and fine-chemical synthesis.[266, 267] However, the formation of coke in conventional H-ZSM-5 catalysts could reduce their catalytic performance and lead to faster deactivation. Moreover, the microporous structure of zeolite often goes hand-in-hand with diffusion limitations that also affects catalytic performance.

The problem can be overcome by controlling the zeolite morphology and cutting the thickness of the zeolite channels, which could effectively reduce diffusion path lengths and hence improve molecular diffusion. This can be realized by the design of hierarchical micro-mesoporous zeolites through several strategies.[232, 268-270] Rimer et al. proposed the smart concept of "zeolite growth modifiers" (ZGMs) considering organic molecules interacting with soluble silicate or aluminate species (monomers) during the self-assembly process and limiting their growth.[246] Our group developed a related strategy, named as "bio-sourced secondary templates" (BSST) for the synthesis of zeolites. Herein, we report the use of numerous biomasses (oxidized lignin, sugarcane bagasse, ecoshell, coffee bagasse, tea residues, algaCM, algaBB, algaTM and commercial alkali lignin) as BSST to synthesize ZSM-5 crystals exhibiting controllable b-axis channel length.

In this study, the hydrolysates of biomasses obtained through alkaline and hydrothermal treatments were preliminary foreseen to alter the growth of zeolite crystals as illustrated in former studies.[6, 191] We have to recognize that a critical challenge remains in identifying the composition of bio-sourced secondary templates and BSST-zeolite crystal molecular recognition due to the complexity of organic matter, suffering hydrolysis process and insufficient in-situ characterization techniques. Through summarizing existing zeolite nucleation/growth theories and based on our experiment results, a tentative self-assembly mechanism was proposed herein involving biomass templates not only as a "inhibitor" to hinder the b-oriented crystal growth, but also facilitating the kinetics of zeolite crystallization.

5.2 Characterization of various biomasses

Biomass is the matter derived from plants or microbial that use sunlight to grow which include plant and animal material, material left over from agricultural and forestry cultures. For most of the plant biomass, they are mainly consisting of three organic compounds, which are lignin, cellulose and hemicellulose components.[271]

Lignin, as a key part comprising roughly 15% of all terrestrial biomass, is one of the most recalcitrant of all natural polymers.[168] Lignin supports plant with polysaccharides, cellulose and hemicellulose.[272] The major elements in biomass are commonly C, O, H, and still have some inorganic elements, like N, Ca, K, Si, Mg, Al, S, Fe, P, Cl, Na, Mn and Ti. The biomass chemical composition is significantly different from the type and geographical origins.[273]

Besides, algae have enormous diversity and represent an almost untapped resource. Algae are one of the most common organisms inhabiting the Earth, which normally include carotenoids, antioxidants, fatty acids, enzymes, polymers, peptides, toxins and sterols.[274, 275] Table 5.1 listed the basic elements, C, H, N, and their content for each biomass selected. The obvious N content in coffee, and three kinds of algae can be attributed to the presence of enzymes, amino acids, or proteins.

Table 5.1 Microanalysis of C, H, and N elements over selected biomasses.

Biomass type	C (%)	H (%)	N (%)
oxidized lignin	56.7	5.1	0
alkali lignin	46.5	5.0	0
coffee	48.7	6.9	2.2
tea	47.1	6.0	6.7
algaCM	44.7	7.0	3.9
algaBB	51.3	8.0	3.1
algaTM	41.5	6.4	3.5
sugarcane	44.8	5.8	0.2
ecoshell	47.6	6.1	0.2

Biomass pretreatment (BPs) technologies (chemical, physical or biological) change structural and compositional constraints to promote hydrolysis rate and increase yields of saccharides from lignin, cellulose, and hemicellulose and amino acids from algae.[276] Treatment methods can be divided as follow: (1) acid hydrolysis (concentrated acid and dilute acid hydrolysis), (2) hydrothermal pretreatment, (3) wet oxidation, (4) alkaline treatment, (5) delignification pretreatment.[277] Mansouri et al. evaluated the effects of temperature from 116 to 180 ºC and reaction time on lignin in an alkaline medium, led to an increase in the content of the various functional groups, like phenolic-hydroxyl and aliphatic-hydroxyl, and decreased the ash content.[278] It was suggested that the main hydrolysis products of lignocellulosic materials are mainly classified into saccharides and phenolic compounds in alkaline medium under hydrothermal conditions.[279-281] Algae waste was normally used as bio-sorbent for heavy metals removal, thus being helpful in environmental protection.[282] Pearsall and Fogg have discussed the possibility of using algae due to their amino-acids composition of such algal proteins.[283] Mišurcová *et al*. established the amino acid groups of algal products from diverse groups (Cyanophyceae, Chlorophyta, Rhodophyta and Phaeophyta) after acidic and alkaline hydrolyses. The determination in the content of various amino acids, such as aspartic acid, threonine, serine, glutamic acid, proline, glycine, alanine, valine, isoleucine, was summarized in their study.[284]

5.3 Interactions between zeolite and biomass-templates during crystal formation

The morphology of all synthesized biomass-ZSM-5 using B method was examined by SEM, as shown in Figure 3.7 (already described in Chapter 3). Herein, we intend to highlight the changes of b-axis thickness, thanks to the presence of biomass, in the zeolite crystals. It can be seen that ZSM-5 zeolites obtained without any biomass addition, B-alkali lignin-2d-300 and B-coffee-2d-300 samples (which exhibited relatively poor catalytic performance) exhibited a rough surface and spherical morphology with an average diameter of ca. 4 μm, and some smaller particles with a size of 2 μm (Figure 3.7a, c and d). Yet, the H-ZSM-5 catalysts produced via the addition of oxidized lignin, tea waste, algaCM, algaBB and algaTM, showed improved

activity, stability and prolonged lifetime, exhibit a typical coffin-shaped morphology with smooth surface and uniform sizes in the range of ca. 3-5 μm. Moreover, the statistical analysis of specific thickness for b-axis and the diagonal length of (010) plane of eight samples were presented in Figures 5.1 to 5.8, and the corresponding mean and variance were also shown in those Figures. The average lengths of b-axis, and a/c aspect ratio of the corresponding zeolites were counted by statistics of 50 crystals. Because the different sizes of the particles will also affect the b-axis length, we introduced a/c aspect ratio as another comparison criterion. The detailed values were summarized in Table 5.2. It further proves that the catalyst which possesses a shorter b-axis channel length / diagonal ratio, led to the higher catalytic performance in the MTO reaction. Oxidized lignin-, tea-, algaCM-, algaBB- and algaTM-assisted zeolites presented the b-axis channel length / diagonal ratio in the range of 0.38 to 0.51, but B-REF ZSM-5, alkali lignin-, and coffee-mediated ZSM-5 showed ratios of 0.57, 0.56 and 0.60, respectively. The results were also consistent with the peak intensity ratio ($I_{8.8}/I_{7.9}$).

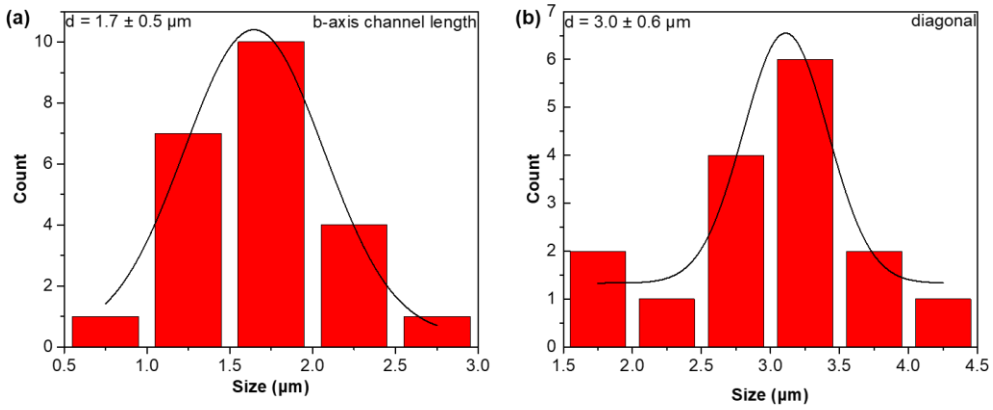

Figure 5.1 (a) Thickness of b-axis and (b) diagonal length of (010) plane over B-REF-2d zeolite.

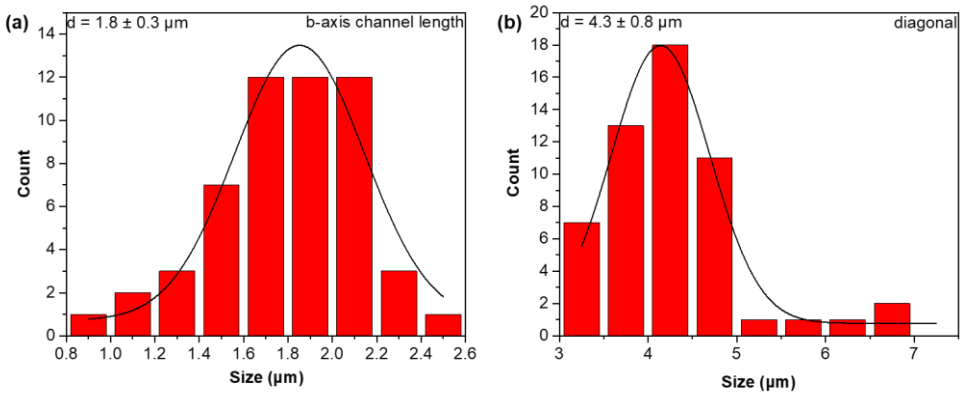

Figure 5.2 (a) Thickness of b-axis and (b) diagonal length of (010) plane over B-oxidized lignin-2d-300 zeolite.

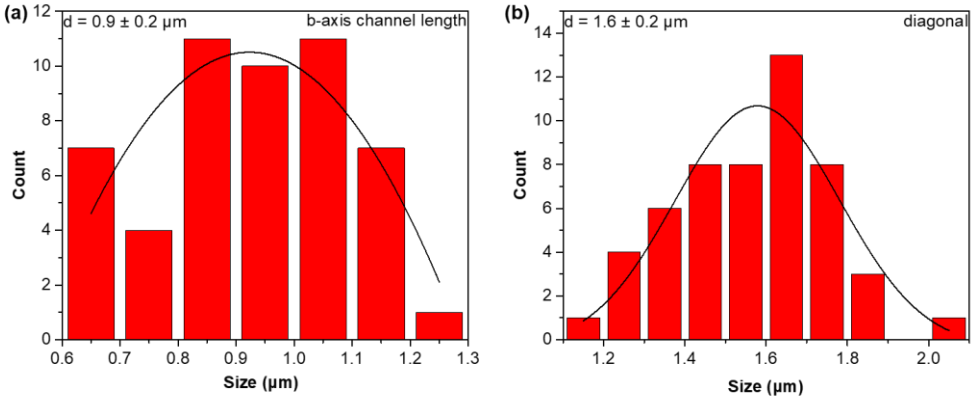

Figure 5.3 (a) Thickness of b-axis and (b) diagonal length of (010) plane over B-alkali lignin-2d-300 zeolite.

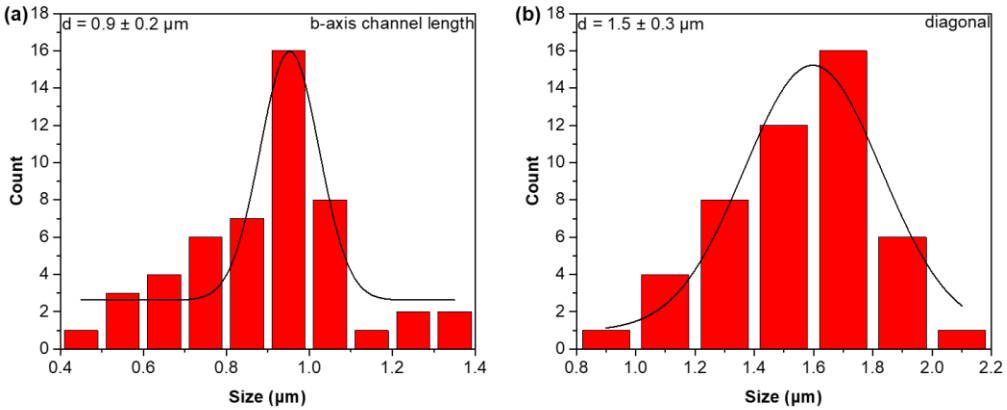

Figure 5.4 (a) Thickness of b-axis and (b) diagonal length of (010) plane over B-coffee-2d-300 zeolite.

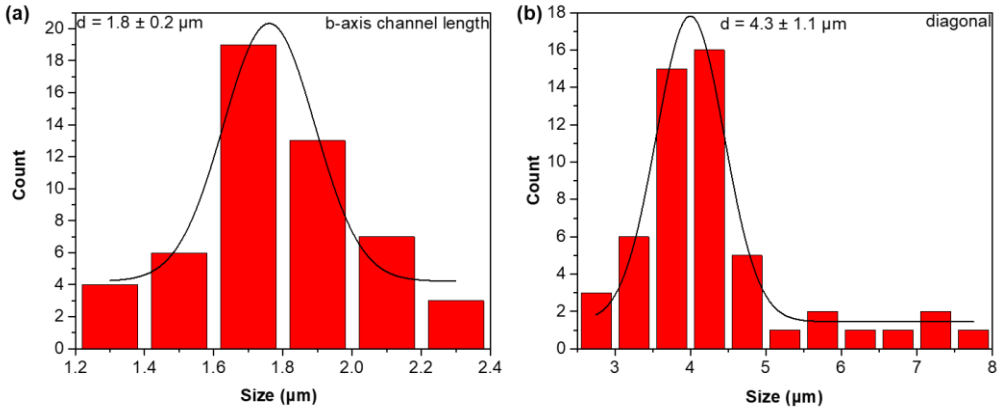

Figure 5.5 (a) Thickness of b-axis and (b) diagonal length of (010) plane over B-tea-2d-300 zeolite.

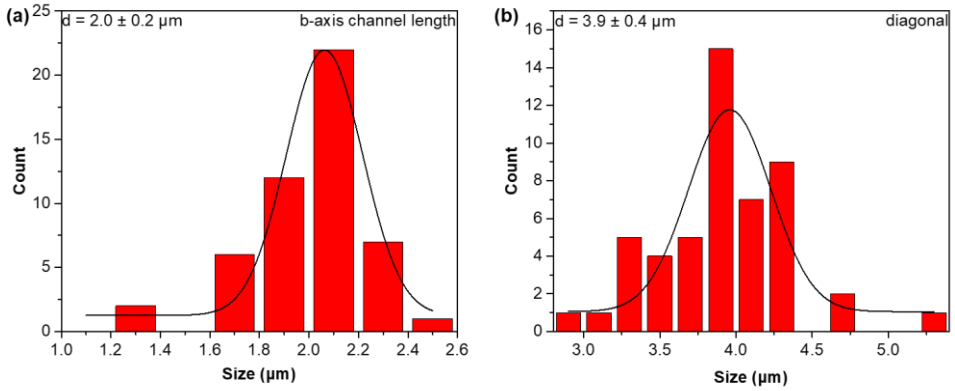

Figure 5.6 (a) Thickness of b-axis and (b) diagonal length of (010) plane over B-algaCM-2d-300 zeolite.

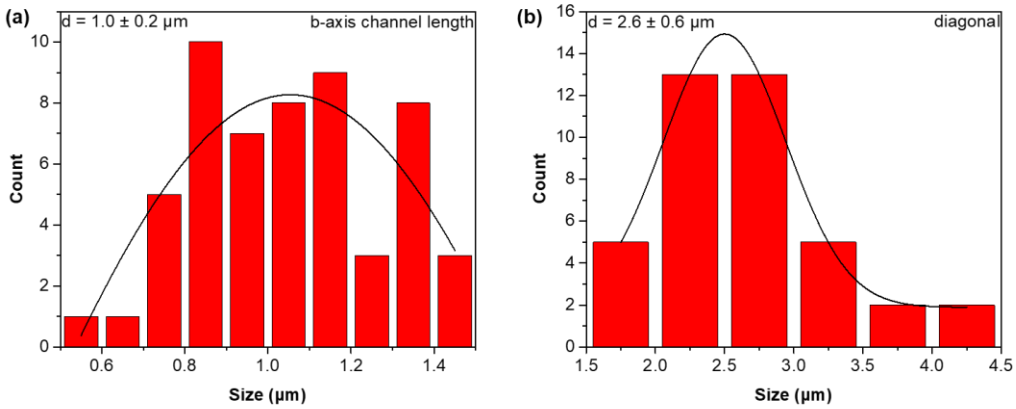

Figure 5.7 (a) Thickness of b-axis and (b) diagonal length of (010) plane over B-algaBB-2d-300 zeolite.

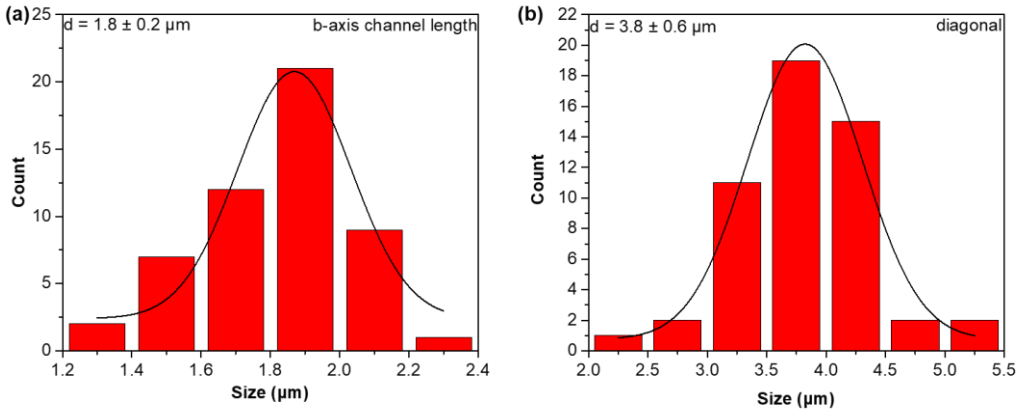

Figure 5.8 (a) Thickness of b-axis and (b) diagonal length of (010) plane over B-algaTM-2d-300 zeolite.

Table 5.2 Zeolite morphology parameters of different biomass-assisted ZSM-5 catalysts and their intensity ratio of characteristic diffraction peak $2\theta = 8.8^{o} / 7.9^{o}$.

catalysts	**b-axis channel length (μm)**	**Diagonal (μm)**	**b-axis channel length / diagonal**	$\mathbf{I_{8.8}/I_{7.9}}$
B-REF	1.7	3.0	0.57	0.56
B-oxidized lignin	1.8	4.3	0.42	0.62
B-alkali lignin	0.9	1.6	0.56	0.54
B-coffee	0.9	1.5	0.60	0.55
B-tea300	1.8	4.3	0.42	0.61
B-algaCM	2.0	3.9	0.51	0.60
B-algaBB	1.0	2.6	0.38	0.65
B-algaTM	1.8	3.8	0.47	0.62

In Figure 5.9 (a and b), the relationship between initial conversion (1 h on stream) or selectivity toward light olefins (1 h on stream), and the b-axis channel length / diagonal ratio over different catalysts were well elaborated, respectively. It was shown that the initial conversion and selectivity towards light olefins increased following the reduction of relative length of b-axis channel. Specifically, B-REF zeolite and two as-

prepared ZSM-5 catalysts with alkali lignin and coffee bagasse, exhibited rather poor methanol conversion and selectivity towards light olefins, and accordingly possessed longer b-axis channels. In stark contrast, five ZSM-5 zeolites (B-oxidized lignin, B-tea and B-algaCM, B-algaBB and B-algaTM) with shorter b-axis channel lengths led to much better activities and selectivities towards C_2-C_4 olefins. This interesting study presents a close relationship between the morphology and activity, selectivity of the catalyst, and gives an effective approach to reduce b-axis length and further improve the catalytic performance with the assistance of biomass.

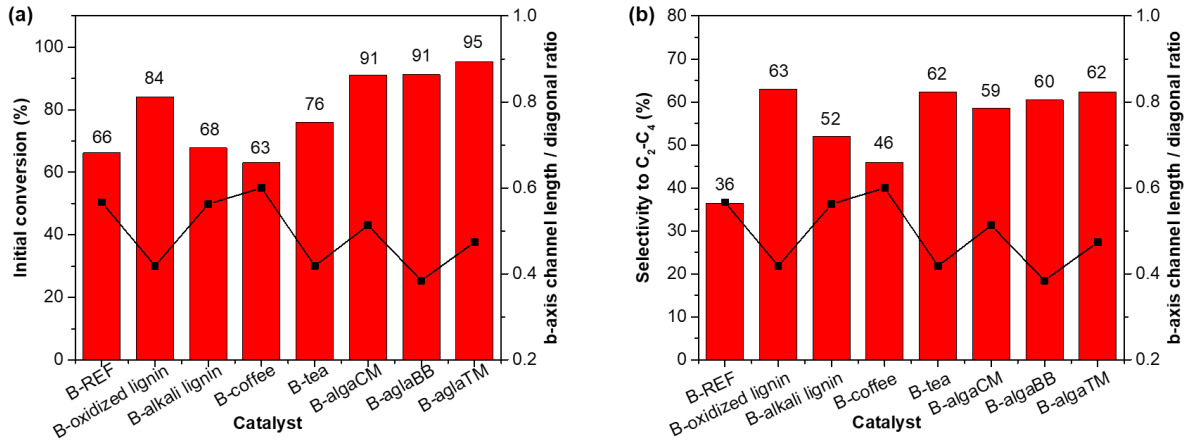

Figure 5.9 Relationships between (a) initial conversion (1 h TOS) and the b-axis channel length / diagonal ratio, and (b) selectivity toward light olefins (1 h TOS) and the b-axis channel relative length over different catalysts.

ZSM-5 zeolite exhibits an anisotropic framework growth with two intersecting 10-membered rings channels, which are straight channels parallel to b-axis and sinusoidal channels parallel to a-axis.[4, 285] During the MTO reaction, these two kinds of channels limit guest molecule access within the pores and extend the internal path length for molecular diffusion.[235] The molecules like methanol and methane can diffuse randomly throughout the network, but as the size of molecules further increases during the olefins-based cycle and aromatics-based cycle, the effective diffusions of alkanes, alkenes and aromatics within the zeolite pores become diverse in the different channels, and be associated with the activity, selectivity, and stability of zeolite catalysts.[286] Besides, long channel lengths will favor the accumulation of carbonaceous species, thus facilitating coke formation. As such, the strategy relies on proper tailoring of the ZSM-

5 zeolite morphology using bio-sourced secondary templates and attempt to explore their self-assembly process(es).

As we mentioned earlier, during hydrolysis in highly concentrated alkaline solutions, the presence of nucleophilic hydroxyl anions led to lignin, cellulose, and hemicellulose fragmentation and solubilization reactions, which caused an increase in the content of various functional groups, such as aliphatic-hydroxyl, phenolic-hydroxyl, carboxyl groups.[161, 271, 278] Therefore, the products of biomass hydrolysis are polysaccharides, which further convert into common furanoses and pyranoses, like glucose, xylose, fructose, sorbose, etc.[280, 287]

It is commonly known that monosaccharides, the simplest carbohydrates, are aldehydes or ketones with two or more hydroxyl groups, and usually form five-membered and six-membered rings, in which the C_1 stereochemistry can be either α or β.[288] Some of the research has focused on the effects of adding various organic solutes to aqueous silicate solutions in order to "simulate" more accurately the conditions of actual zeolite synthesis. It has been reported that six-coordinate Si complexes are formed when silicon is chelated by catechol, 2-hydroxypyridine N-oxide, tropolone or their respective analogues.[289] Lambert *et al*. evidenced that sugars can react with basic silicic acid to form silicate complexes.[288] Then, Kästele *et al*. also proved that saccharides are able to interact with xylose as a chelating molecule to expand the silicate tetra-coordination sphere to penta-coordinated by ^{29}Si NMR analysis.[290] It is worth noting that the chelation reaction occurs under highly basic conditions that are needed for the preparation of such compounds.[291] The reported solution pH values are generally between 11 and 13, and under acidic conditions the complexes will hydrolyze.

We suggest that the chelation effect between BSST and T-monomers creates a more stabilized environment than T-OH species, and T-entities prior to coordination with BSST species in strongly alkaline medium. At this time, large number of T-monomers gathered around the biomass molecules, and consequent aggregation of TPA^+ template cations. However, when the biomass is continuously hydrolyzed, the pH value decreased and the coordination groups of T-BSST were re-dissolved. A large number of gathered silicon or aluminum precursors can be condensed and nucleated rapidly

around TPA^+ templates.

It is also important to note that simple saccharides can barely be chelated to form silicate / aluminate complexes, like glucose, mannose, galactose and sucrose since they do not meet the chelated criteria and failed to form complexes.[288] Therefore, the reasonable choice of biomass nature becomes an important step for the design of an optimized catalyst.

An experiment of different biomasses hydrolysis in strong alkaline medium was conducted and shown in Table 5.3. 600 mg biomass were added to 50 mL aqueous solution with 0.02 g NaOH, and stirred for 1 h at room temperature. The initial pH of each solution was 12.0. Then the solution was transferred to a Teflon-lined stainless-steel autoclave and heated at 170 ^oC for 24 h to mimic the zeolite crystallization process. The chosen hydrothermal time of 24 h is lower than real reactions (48 h), since the biomass mainly plays a role in the nucleation and crystallization stages, not the ripening stage. It was observed that the pH values decreased after an addition of the biomasses. The final pH varied between 4.5 (ecoshell) and 8.5 (alkali lignin). It is interesting to mention that biomass-assisted ZSM-5 catalysts, which have excellent catalytic performance, their corresponding biomasses' aqueous solutions are slightly acidic water (pH = 5.0 - 6.9). These may imply some affinities towards dissolved biomass species or quantity and catalytic performance. Rimer described the decrease in the pH as a switch that changes the predominant growth species during the zeolite crystallization process.[292] Moreover, we found that there was one order of magnitude difference between the mass of hydrolyzed alkali lignin and other hydrolysates. Since lignin is a polymer derived from some monolignol precursors that crosslink in diverse ways, which are paracoumaryl alcohol, coniferyl alcohol, and sinapyl alcohol (Figure 5.10). Alkali lignin is a commercial lignin (Sigma-Aldrich) which possesses only a coniferyl alcohol-based structure. This lignol structure can be totally degraded under hydrothermal treatment, causing a significant mass reduction of alkali lignin.

Table 5.3 pH values and mass changes of different biomasses hydrolysis in strong alkaline aqueous solution.

biomass	pH	mass (g)
none	12.0	/
oxidized lignin	6.7	0.42
alkali lignin	8.5	0.02
coffee	4.8	0.28
tea residue	6.1	0.20
algaCM	5.7	0.27
algaBB	5.1	0.25
algaTM	6.5	0.22
sugarcane	4.6	0.30
ecoshell	4.5	0.37

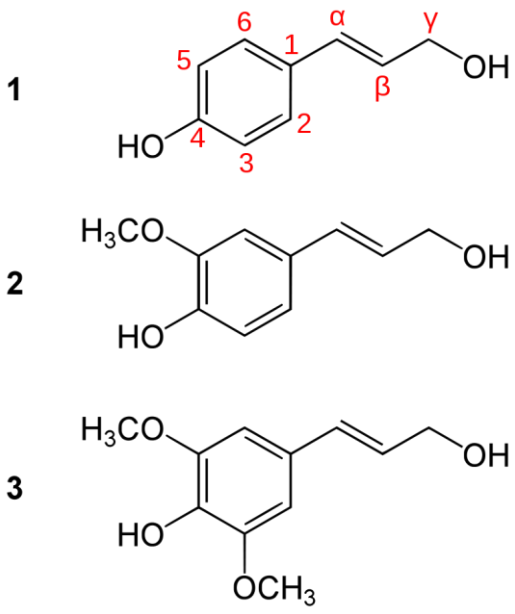

Figure 5.10 The three common monolignols: (1) paracoumaryl alcohol, (2) coniferyl alcohol and (3) sinapyl alcohol.

In order to decipher the chemical composition of biomass dissolved matter in this alkaline solution, tea extracts as an example were analyzed by LC-MS, as shown in

Figure 5.11. It can clearly be seen that the dominant peak appears at 3.64 min and corresponds to major ions in ESI-MS at *m/z* 195 attributed to the molecular mass of 7-tetradecenoic acid. Another dominant peak at about 16.07 min corresponds to the molecule of coronaric acid with major ions at *m/z* 279. Mass spectrum of the peak at 11.20 min with the ions in ESI-MS at *m/z* 261 was indicative of 9α-hydroxysophoramine.[293, 294] The main identified compounds are summarized in Table 5.4. This finding suggests that there were a large number of organic acids, amides and saccharides in this tea hydrolysate.

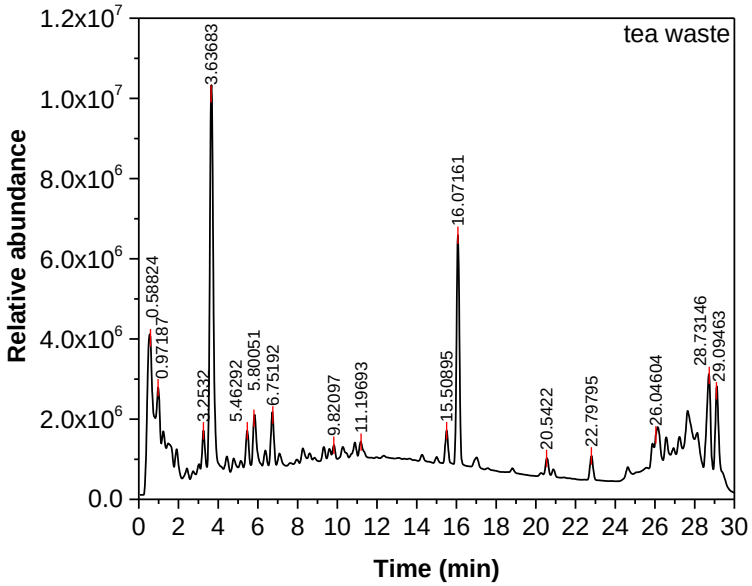

Figure 5.11 LC-MS analysis of spent tea leaves.

Table 5.4 Liquid chromatography-mass spectrometry (LC-MS) analysis of identified compounds found in tea alkaline solution.

Compounds	Time (min)	Fragments m/z
hydrocinnamic acid	0.98	166
n-Butyl α-D-fructofuranoside	0.59	237
cyclo(L-Pro-L-Val-)	3.26	197
7-tetradecenoic acid	3.64	195

nodakenetin	6.75	247
9α- Hydroxysophoramine	11.20	261
γ-linolenic Acid	15.51	279
coronaric acid	16.07	279
bufotalinin	22.80	415
N-isobutyl-2E,4E-octadecadienamide	28.25	336
hyodeoxycholic Acid	28.60	393

Besides, some organic macromolecules with carboxyl groups also appeared during the alkaline hydrothermal pre-treatment process, such as p-coumaric acid (Figure 5.12). The abundant negative charged -COO^- groups could provide coordination sites for positive ions, like tetrapropylammonium cations (TPA^+), in aqueous solution through electrostatic attraction and accelerate self-assembly to form crystals.[295, 296] Afterwards, basic silicic derived from the hydrolysis of TEOS may react with the phenolic hydroxyl groups of p-coumaric acid to form complexes. The nucleation process happens near the biomass and the kinetics of nucleation can be promoted by the biomass assistance.[297] This can be inferred from A-REF and A-tea zeolites. The relative crystallinity (or percentage of crystallinity) of zeolite A-REF ZSM-5 and A-tea-assisted ZSM-5 were determined by using a standard Integrated Peak Area Method, which involves a comparison of the integrated peak areas in the range of $2\theta = 23^o$.[233, 298] Other synthesis conditions were consistent for these two samples. The relative crystallinities of A-REF and A-tea were 68% and 88%, respectively. It confirms that some biomass species are able to accelerate the crystallization process and promote the catalytic performance in the MTO.

Besides, microalgae also represent an almost untapped resource. Over 15000 novel compounds originating from algal biomass, including chlorophyll, carotenoids, antioxidants, fatty acids, enzymes, polymers, peptides, toxins and sterols, were determined. As a result, a numerous amino acids hydrolyze in the alkaline solution, such as arginine, leucine, glutamate, ….[299]

It was reported that ZSM-5 nanocrystals with short b-axis length were prepared by using urea as additive, and urea also became an important mean to tune b-axis length of ZSM-5 crystals.[234, 300-302] However, most of them mainly focus on the preparation of ZSM-5 with different morphologies or comparison of catalytic performances with different b-axis thickness. Few studies have systematically explained the mechanism of suppression of b-oriented growth in the presence of urea or other organic molecules. Urea as an organic compound possesses two -NH_2 groups linked by a carbonyl functional group, which is similar to amino acids. Through the formation of amorphous silica exoskeletons of diatomites in the presence of amine-rich proteins, Rimer *et al*. prepared silicalite-1 zeolites (MFI structure) using zeolite growth modifiers (ZGMs) analogues.[4] They found that spermine ($C_{10}H_{26}N_4$) modifier, with the similar structure to triethylenetetramine (TETA, $C_6H_{18}N_4$) organic template but with more carbonyl groups, exhibited a much more effective inhibition of b-oriented growth than TETA. It also demonstrates that how subtle changes in the organic template structure can cause large differences in the results, and further highlight the difficulty of distinguishing the effect of biomass on morphological control. Yu *et al*. achieved a L-lysine-assisted MFI-type nano-zeolite by using two-step crystallization process. Among the synthesis process, L-lysine acted as a crystal growth inhibitor to limit the crystal growth of zeolites and formed hexagonal prism morphology.[266, 303] Inhibitors which range from small ions and molecules to large macromolecules, are very common and used for slowing or interfering with a chemical action.[235]

A simplified mechanism of ZSM-5 zeolite self-assembly involving amino acids is shown in Figure 5.12 (middle part). Carboxylate-based compounds are the required use of caustic (highly alkaline) solutions to dissociate acidic groups for an improved efficacy. Like p-coumaric acid, carboxyl groups may adsorb tetrapropylammonium cations (TPA^+ ions) through electrostatic attraction. In the meantime, the assembly occurred through H-bonds between the tail amino groups of amino acids and the oxygens from $Si(OH)_xO_y^-$ or $Al(OH)_xO_y^-$ precursors. Similar mechanism was studied by Rimer and his group by means of umbrella sampling molecular dynamics (USMD) simulations.[292] The results indicated that (R)-ornithine-lactam (R-OL), obtained from

the decomposition of D-arginine (D-Arg) during hydrothermal treatment in alkaline media (pH > 11), adsorbed with the hydrophobic group (partially formed pores) and exposed its hydrophilic amine and carboxyl groups to generate H-bonds with surface silanol groups. Moreover, the narrow width of (010) plane facilitated confinement and interaction between amine and carboxyl functional groups and soluble silicate or aluminate species. This study is consistent with our experiment results that the b-axis length of ZSM-5 zeolites was drastically reduced in the presence of biomass.

As zeolite growth near equilibrium conditions can be described by a layer-by-layer model, and the increase of surfaces is implemented by the addition of growth units to step sites.[4] Zeolites follow an anisotropic growth along a-, b-, and c-axes, with exposed facets of (100), (010), (101). It is reported that organic molecules prefer to interact on (010) plane because this surface is the most energetically favorable orientation among the three surfaces.[300] Therefore, various biomasses acted as inhibitors and were effective to limit the crystal growth along the b-oriented direction. However, the reason for such growth hindering may not be simply due to the formation of weak bonds with basal surface, but an inherent ability of the BSST to impede the attachment of growth units, attributing to a slower rate of growth in the (010) direction.[292]

In addition, a diffusion-limited growth and reaction-limited growth are two disctinct mechanisms. Normally, due to the slow diffusion rate in solution, the diffusion-limited process is the rate-determining step. However, it is probably because T-monomers surrounding the organic modifiers to form condensates rather than dispersed throughout the solution, and equivalent to concentration effect to some extent, the diffusion rate is reduced. Accordingly, the BSST not only served as a crystal inhibitor but also accelerate the aggregation of growth units as a promoter.

In the MTO reaction, b-axis channels play a critical role in the diffusion of reactants and products. As the results of shorter b-axis channel length of biomass-assisted H-ZSM-5 catalysts, led to superior catalytic performance, probably due to a favored accessibility to active acid sites. Likewise, the higher selectivity towards light olefins and prolonged lifetime may be linked to the rapid diffusion of products, thus reducing coke formation.

In summary, the putative self-assembly mechanism of ZSM-5 zeolite involving biomass as BSST is presented in Figure 5.12.

Herein, we present a facile and sustainable route to design ZSM-5 zeolites with significantly promoted catalytic activity, selectivity and stability for the MTO reaction. This strategy opens the door for the design of other zeolites (and other materials) with controllable morphology and intrinsic properties. It is also worth noting that biomass waste can be utilized and valorized as useful BSST in materials synthesis by this cost-effective and green approach.

Additionally, it should be noticed that due to the complexity of elucidating the composition of biomass hydrolysates in alkaline solution after hydrothermal treatment and the role of bio-template in the zeolite crystals self-assembly, our proposed mechanism may not be appear as a dogma, but rather as a reasonable starting point for in-depth investigations. To this end, further studies are required to come closer to the whole understanding of bio-sourced secondary templates' modification in zeolite crystallization.

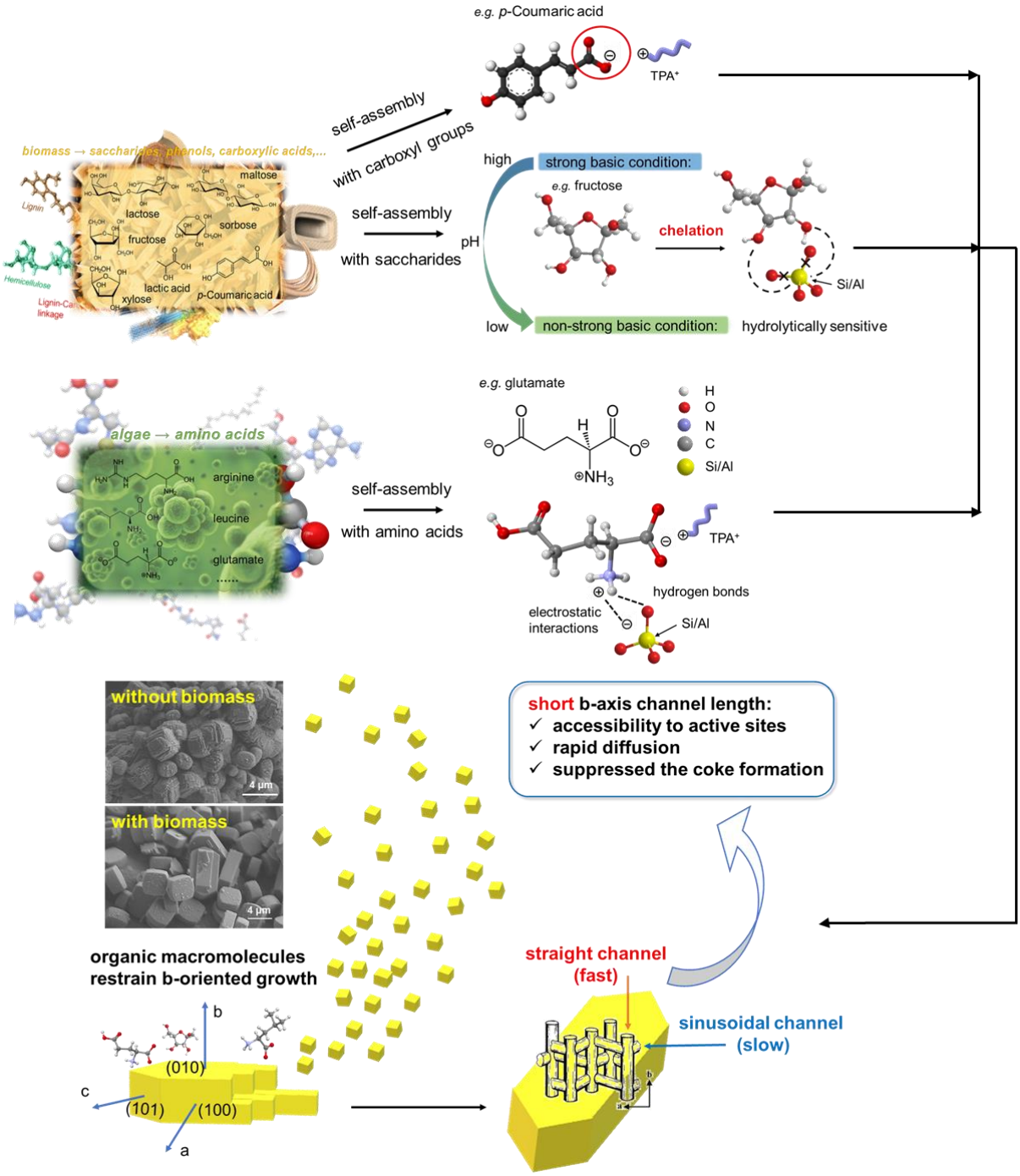

Figure 5.12 Tentative self-assembly mechanism of ZSM-5 zeolite crystals involving biomass as bio-sourced secondary template (BSST).

Chapter 6. Catalytic performance of layered double hydroxides (LDHs) derived materials in gas-solid methanol conversion reactions

Abstract

Novel layered double hydroxides (LDHs) were prepared by a co-precipitation method and characterised by X-ray diffraction (XRD), Fourier transformed infrared spectroscopy (FT-IR), thermogravimetric analysis (TGA) and scanning electron microscopy (SEM). As-prepared LDH derived catalysts were first evaluated in the gas-phase conversion of methanol. The results indicate that LDH derived materials act as selective catalysts towards dimethyl ether (DME), methane or light olefins formation, depending on their chemical composition. For instance, $CuAlO_x$ showed a high selectivity in DME up to 88%, whilst $CuCoO_x$ converted methanol to CH_4 and DME. $NiFeO_x$ allowed achieving a full methanol conversion selectively into CH_4 during at least 30h on stream.

6.1 Introduction

Layered double hydroxides (LDHs), known as hydrotalcite-like compounds (HTLcs) or synthetic anionic clays, are a family of ionic lamellar materials, consisting of positively charged brucite-like layers, charge compensating anions and water molecules within the interlayer spaces.[131, 304, 305] The metal cations occupy the centers of an octahedral structure, whose vertexes contain hydroxide anions; these octahedra are connected by sharing edges to form an infinite sheet.[306, 307] The general chemical formula is $[M^{2+}_{1-x}M^{3+}_{x}(OH)_2]\ A^{n-}_{m/n}\cdot yH_2O$, where $M^{2+} = Mg^{2+}$, Zn^{2+}, Ni^{2+} etc.… and $M^{3+} = Al^{3+}$, Mn^{3+}, Fe^{3+}…, respectively. A is a non-framework charge compensation anion with charge n, $A^{n-} = CO_3^{2-}$, Cl^-, NO_3^- etc., n is normally comprised between 0.17 and 0.33, as shown in Figure 6.1.[308-312]

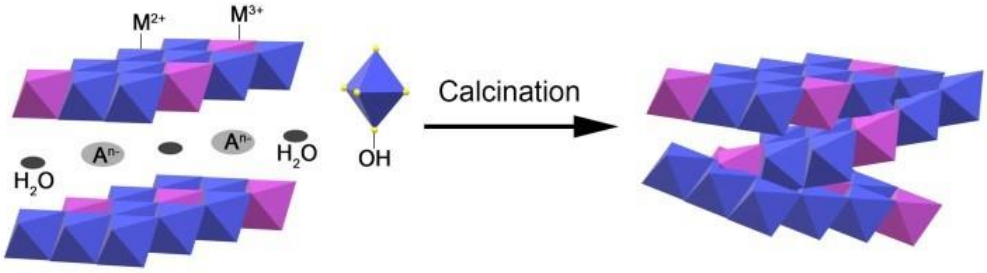

Figure 6.1 Schematic structure of LDH and its change to layered double oxides (LDO) upon calcination.

Due to their controllable chemical composition, LDHs show a wide range of structures / properties and present a high potential for a wide range of applications such as water decontamination,[313, 314] flame retardant,[315, 316] medicinal chemistry[317, 318] and adsorbents.[129, 319] After thermal treatment, LDH loses its layered structure and turns into layered double oxides (LDOs) as shown in Figure 6.1. LDO structure possesses three kinds of active sites: (i) weak Brønsted basic sites (OH^- groups on the surface), (ii) medium strength Lewis sites (both $Mg^{2+} – O^{2-}$ and $Al^{3+} – O^{2-}$ acid-base pairs), and (iii) strong Lewis basic sites (O^{2-} anions).[320] This renders LDOs promising catalysts for numerous acid-base reactions.

Besides, methanol is one of the topmost raw chemicals used in industry attracting more and more attention as it can be easily obtained from natural resources. For its proper utilisation, methanol can be selectively transformed to valuable products such as olefins,[321, 322] dimethyl ether,[323, 324] dimethoxymethane,[325] formaldehyde,[326] etc.

ZSM-5 zeolites, possessing MFI framework type have been deeply investigated, and several ZSM-5 catalysts have already been tested in the methanol conversion reaction as shown in previous Chapters. However, as composition tailorable multifunctional materials, LDHs based catalysts for methanol conversion were scarcely reported. The work reported herein aims to present a comprehensive study of catalytic behaviour of different kinds of LDHs. LDHs were prepared by a conventional co-precipitation method with different M^{2+} (Mg, Cu, Ni, Zn) and M^{3+} (Al, Fe, Co) cations. All synthesized LDHs were thoroughly characterised using X-ray diffraction (XRD), thermogravimetric analysis (TGA), scanning electron microscopy (SEM), Fourier transform infrared spectroscopy (FT-IR) and nitrogen adsorption-desorption measurements. Finally, their catalytic performances were evaluated in the methanol conversion into hydrocarbons.

6.2 Preparation and characterization of LDHs

6.2.1 Synthesis of LDHs

A series of LDHs with different M^{2+} / M^{3+} cations composition was prepared by using the co-precipitation method, M^{2+} / M^{3+} was set to 3.[327] All chemicals were purchased from Acros Organics, VWR and Sigma-Aldrich. Briefly, an aqueous salt solution containing a mixture of 0.075 mol M^{2+} precursor [i.e., $Mg(NO_3)_2$, $Cu(NO_3)_2$, $Ni(NO_3)_2$, and $Zn(NO_3)_2$ and $Al(NO_3)_3$] and 0.025 mol M^{3+} precursor [i.e., $Al(NO_3)_3$, $Fe(NO_3)_3$, and $Co(NO_3)_3$] was added dropwise to an alkaline solution (100 mL) containing 0.25 mol Na_2CO_3. The pH of the precipitation solution was kept constant at 10 by addition of NaOH (4M) solution. The resulting mixture was aged at room temperature overnight under continuous stirring. The aged mixture was then filtered and washed with deionized water followed by drying at 100 ºC in an oven.

6.2.2 Characterization of LDHs

In order to perform an in-depth investigation of the influence of the cation nature, present within the LDHs structure, on its activity, M^{2+}Al-type LDHs with various divalent cations, like Mg, Ni, Cu and Zn, and CuCo, CuFe, NiFe and ZnFe were synthesized. All the samples were prepared by conventional co-precipitation method, and the pH of the solution was kept at 10. Figure 6.2 presents the XRD patterns of as-synthesized samples. For ZnAl and MgAl, pure LDHs phase were successfully obtained with characteristic peaks at 11.7º, 23.7º, 34.7º and 39.3º, corresponding to the basal planes of (003), (006), (009) and (015) reflections.[328] NiAl, NiFe, CuCo and CuAl also exhibited the typical reflections at 2θ = 11º and 23º, ascribed to LDH structure with poor crystallinity. In contrast, CuFe failed to form LDH under those co-precipitation conditions and appeared to produce $Cu(OH)_2$ and $Fe_2O_3 \cdot H_2O$ phases (JCPDS 13-0420, JCPDS 13-0092). This result is in line with CuFe LDH reported formation at lower pH = 5.[329]

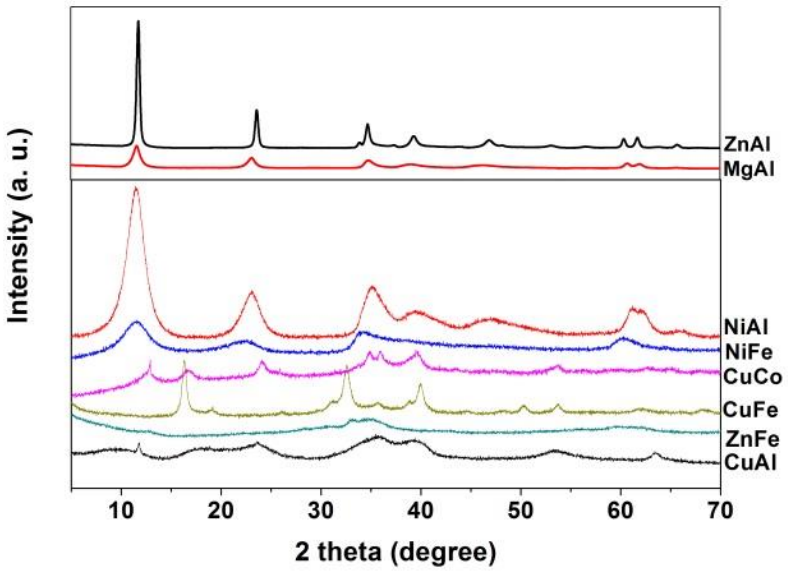

Figure 6.2 XRD patterns of as-prepared LDH samples.

The FT-IR spectra of the samples are presented in Figure 6.3. It is important to highlight that most of the materials exhibit the characteristic vibrations of LDH. All

spectra contain a broad and strong absorption band between 3383 and 3566 cm^{-1} associated with the superposition of hydroxyl stretching band (–OH), arising from hydroxyl groups of brucite-like layers, and hydrogen-bonded interlayer water molecules.[130, 330] A weak vibration band at approximately 1631 cm^{-1} can also be observed in the samples, attributed to the vibration of interlayer water molecules.[331] It can be clearly seen that CuFe did not exhibit any vibration at 1631 cm^{-1}, thus suggesting the absence of interlayer water molecules. This result confirms that CuFe failed to crystallise in the LDH structure, as suggested by XRD data (Figure 6.2). In addition, the vibration present at 1382 cm^{-1} can be attributed to the charge compensation carbonate anions, whilst for CuFe, no carbonate species could be detected, confirming the absence of CO_3^{2-} in this sample.

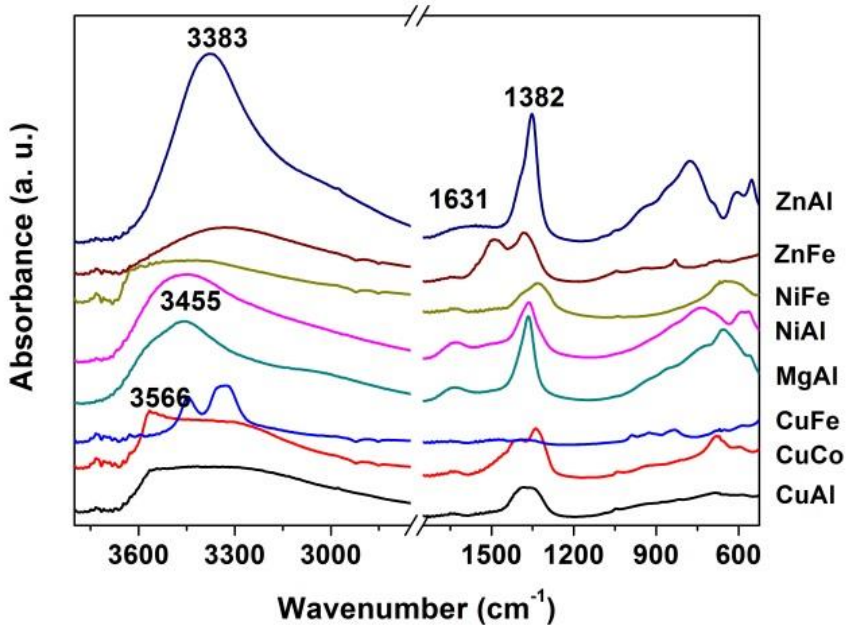

Figure 6.3 FTIR spectra of as-prepared LDH samples.

The structure evolution of each material as a function of the temperature raise was examined by TGA, as shown in Figure 6.4. All the samples presented an obvious two-stage weight loss in the temperature range from 50 ºC to 700 ºC, which is typical for LDHs. The initial weight loss stopped between 190 ºC and 250 ºC, due to the loss of interlayer water. Again, CuFe presented a different first stage of weight loss that stopped

around 300 ºC, probably due to the loss of crystalline water in $Fe_2O_3 \cdot H_2O$. For the majority of as-synthesized samples, the initial weight losses were between 15 and 20 wt%, in agreement with former reports.[332] In contrast for NiAl LDH, the decrease in weight upon heating from 40 to 200 °C was limited to 3%. Its second weight loss appeared in the temperature range 250-450 ºC, probably due to dehydroxylation of octahedral layers, as well as decarbonation of interlayer charge compensating anions. CuFe sample exhibited a relatively higher thermal stability, with its second weight loss ending at ca. 550 ºC. For all remaining LDHs, this latter loss ended at around 400 ºC.

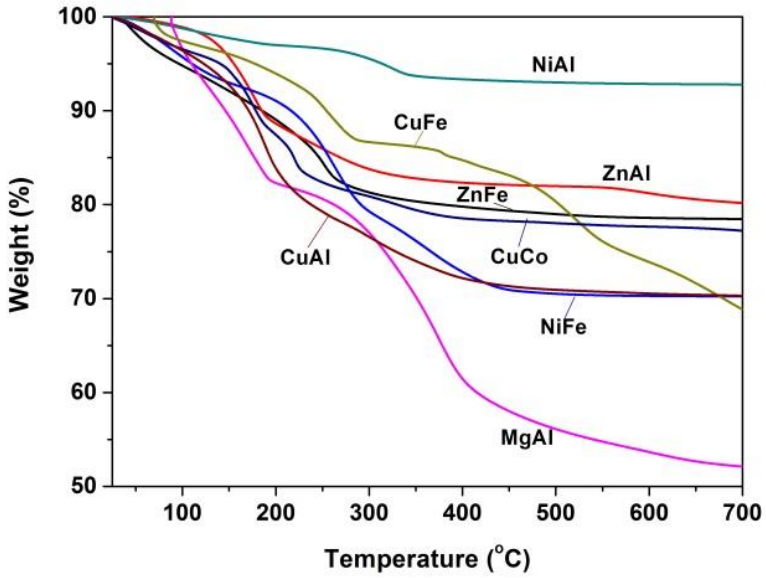

Figure 6.4 TGA analysis of as-prepared LDH samples. The y-axis represents the relative weight of the different materials.

The morphologies of LDH samples were observed by SEM (Figure 6.5). CuFe, CuAl, CuCo, NiAl and ZnFe exhibit rather aggregated nanoparticles. NiFe LDH grew in a "stone"-like morphology with no obvious pore structure. ZnAl exhibits another typical LDH morphology, aggregating into flake-like particles. The thickness of a plate is roughly 20 nm and its size is around 100 nm. As a representative hydrotalcite, MgAl LDH exhibits a typical spheroidal sand rose morphology (Figure 6.5(h)) with a size of spheroidal roses around 400-500 nm and a thickness of the petals around 15 nm, similar to the size of ZnAl LDH reported elsewhere.[333]

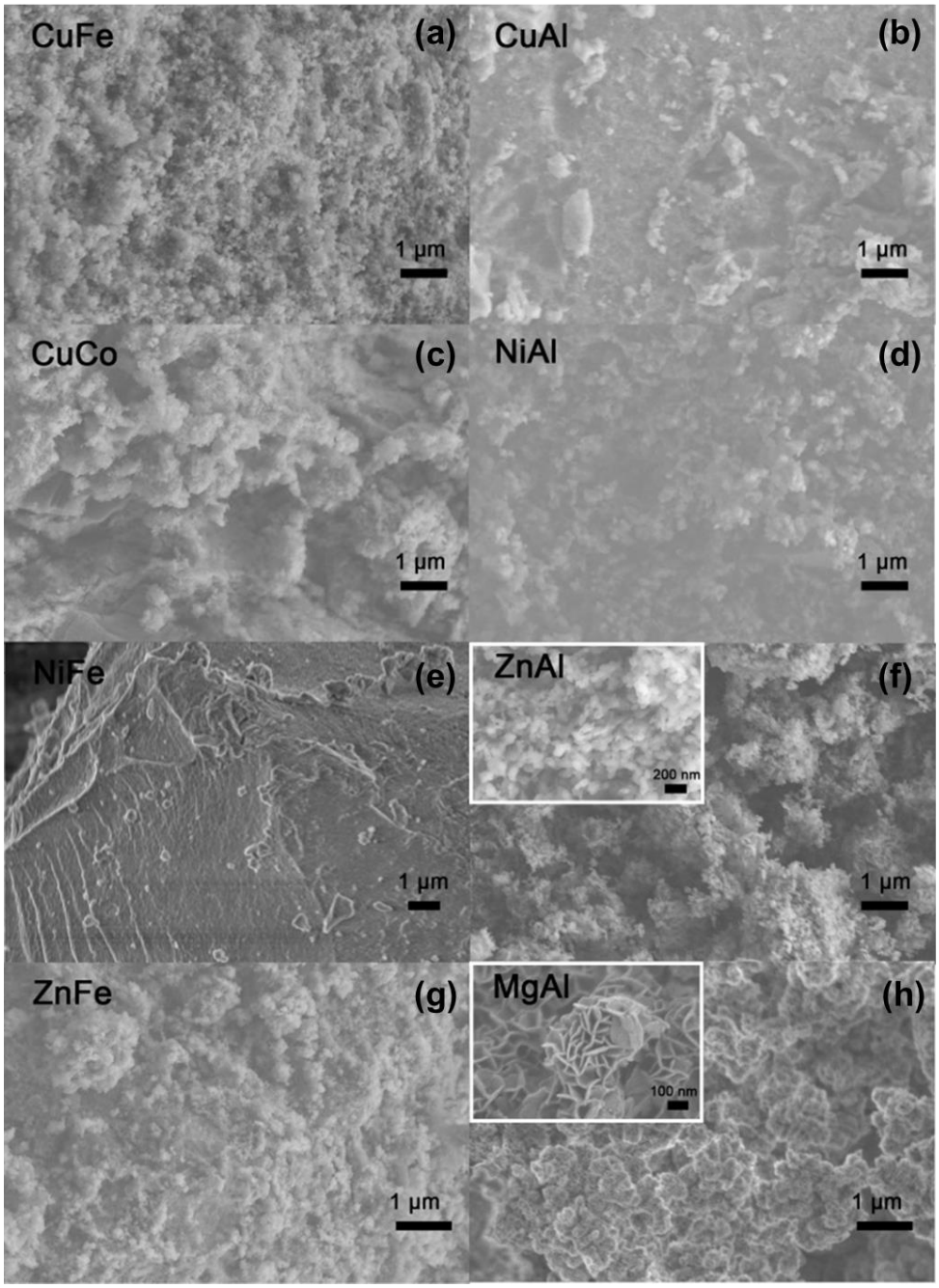

Figure 6.5 SEM images of as-prepared LDHs. (a) CuFe, (b) CuAl, (c) CuCo, (d) NiAl, (e) NiFe, (f) ZnAl, (g) ZnFe and (h) MgAl.

Since the LDH derived catalysts need to be activated upon thermal treatment, XRD patterns were also recorded after calcination. It is known that LDH usually loses its layered structure, turning into layered double oxides (LDOs) which possess three types of active sites. The structure and composition changes are the most important features

for further catalytic purposes. As shown by TGA analysis (Figure 6.4), LDH first lost its interlayer water during calcination. Afterwards, when the temperature reached 250 ^{o}C, dehydroxylation of the octahedral layers and decarbonation of interlayer charge compensating carbonate anions process started and lasted up to 450 ^{o}C. Based on this inwardness, all the samples were calcined at 450 ^{o}C for 1 h. As shown in Figure 6.6, all the materials lost their original structure and changed to a mixed-metal oxide phase. CuCo, CuAl and CuFe exhibited well-crystallised CuO structure according to the sharp peaks at 35.5^{o} and 38.7^{o}. In addition, depending on the composition of the different mixed-metal oxides such as Al_2O_3, Fe_2O_3 and $Cu_{0.92}Co_{2.08}O_4$, characteristic peaks could be observed, respectively.

For NiAl, NiFe and ZnNi, ZnFe, XRD patterns indicate the presence NiO or ZnO as main phases with neither aluminum nor iron oxides detected, suggesting a well dispersion of amorphous aluminum and iron oxides within the samples. In contrast, MgAl LDH turned into $MgAl_2O_4$ as main phase with small peaks corresponding to Al_2O_3.

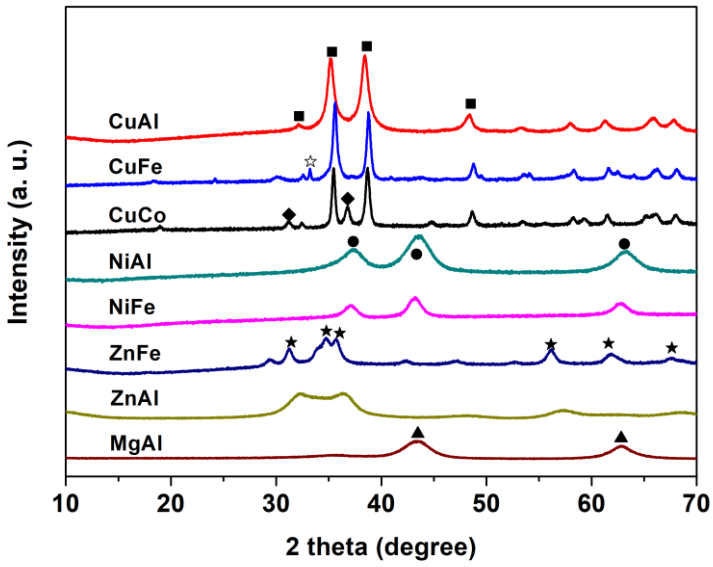

Figure 6.6 XRD patterns of calcined samples. (■) CuO, (●) NiO, (◆) $Cu_{0.92}Co_{2.08}O_4$ (JCPDS 37-0878), (▲) $MgAl_2O_4$ (JCPDS 33-0853), (★) ZnO and (☆)Fe_2O_3.

Nitrogen adsorption–desorption isotherms for all LDOs were obtained after activation at 450 ºC for 1 h and outgassing at 220 ºC under vacuum overnight. The specific surface area was calculated by the Brunauer–Emmett–Teller (BET) method. The pore volume and pore size distributions were determined by the Barrett–Joyner–Halenda (BJH) method. The textural properties are presented in Table 6.1. As a priori expected, it appears that the LDH composition greatly affects the specific surface area (SSA), pore size and pore volume. MgAl LDH derived $MgAlO_x$ exhibited the largest BET surface area of 224 m^2/g and pore volume (0.74 cm^3/g) owing to its "sand rose" microstructure which allows the presence of numerous accessible pores between "petals" and maintains a high SSA upon thermal treatment. Besides, CuFe and CuCo, ZnAl and ZnFe, NiAl and NiFe exhibited similar SSA values amongst all as-prepared LDHs. However, Al-containing LDHs exhibited the largest SSA values. It can therefore be concluded that the composition has a great effect on the morphology and surface area of LDHs which may induce an influence on the catalytic performance of these LDO catalysts.

Table 6.1 BET specific surface area, pore size, and pore volume of calcined samples.

Samples	S_{BET} (m^2/g)	BJH pore size (Å)	V_{pore} (cm^3/g)
$CuAlO_x$	122	10.2	0.37
$CuFeO_x$	30	19.7	0.15
$CuCoO_x$	26	15.9	0.10
$NiAlO_x$	197	7.1	0.38
$NiFeO_x$	108	4.9	0.19
$ZnAlO_x$	57	10.9	0.13
$ZnFeO_x$	48	8.7	0.09
$MgAlO_x$	224	13.3	0.74

6.3 Methanol conversion reaction over LDO catalysts

The experimental setup and reaction conditions for the methanol conversion reaction over LDHs are similar to those of the aforementioned zeolites. Prior to use, catalysts were calcined at 450 °C for 1 h under argon flow. About 60 mg of catalyst was placed in a tubular quartz reactor and packed between two quartz wool plugs. A constant nitrogen flow was fed through a methanol saturator, cooled to 0 °C, to set WHSV= 1.2 $g_{methanol}$ / (g_{cat}.h). The reactant was subsequently fed to the reactor containing the catalyst at 450 °C. The products at the outlet were analyzed by GC equipped with a 50 m capillary column (PONA) and a flame ionization detector (FID). The methanol conversion was calculated from the difference between inlet and outlet concentrations of methanol. The selectivity was obtained by the mole ratio of each product referred to the moles of converted methanol. It is worthy to mention that DME was considered as a product.

The catalytic performance of each calcined LDHs was then evaluated. Figure 6.7 presents the conversion of methanol over Al-based LDO catalysts at 450 °C. For $CuAlO_x$, the initial methanol conversion taken after 5 min time-on-stream was 100%. The methanol has therefore been entirely converted into DME and CH_4. Afterwards, the conversion gradually diminished from 100% to 80% after 2 h, and so did the methane selectivity (Figure 6.7a). The DME selectivity increased along with the reaction time and achieved its highest value at 60 min (79%). Unfortunately, a drastic decline in the conversion was observed probably due to coke formation.

In stark contrast, the methanol conversion and DME selectivity remained very low over $MgAlO_x$ catalyst (Figure 6.7b), probably due to the absence of acid sites. Surprisingly, the methanol conversion remained complete and stable during 25h on stream over $NiAlO_x$ and DME presence could not be detected. Indeed, methanol converted selectively into CH_4 over $NiAlO_x$. For an industrial point of view, the reverse reaction CH_4 to methanol would be economically interesting. However, according to the micro-reversibility principle in catalysis, a catalyst can be potentially used in both sides of a chemical reaction. One may therefore expect the possible design of $NiAlO_x$ catalyst to convert methane into methanol. For $ZnAlO_x$ (Figure 6.7d), a rapid decline

in the conversion could be observed, from 40% (initial conversion) down to 7% after 3 h on stream. However, the initial DME yield remained higher than over $MgAlO_x$ catalyst. Along with the reaction time, both methanol conversion and DME selectivity diminished to low levels, accompanied by the appearance of light olefins (mainly butylenes).

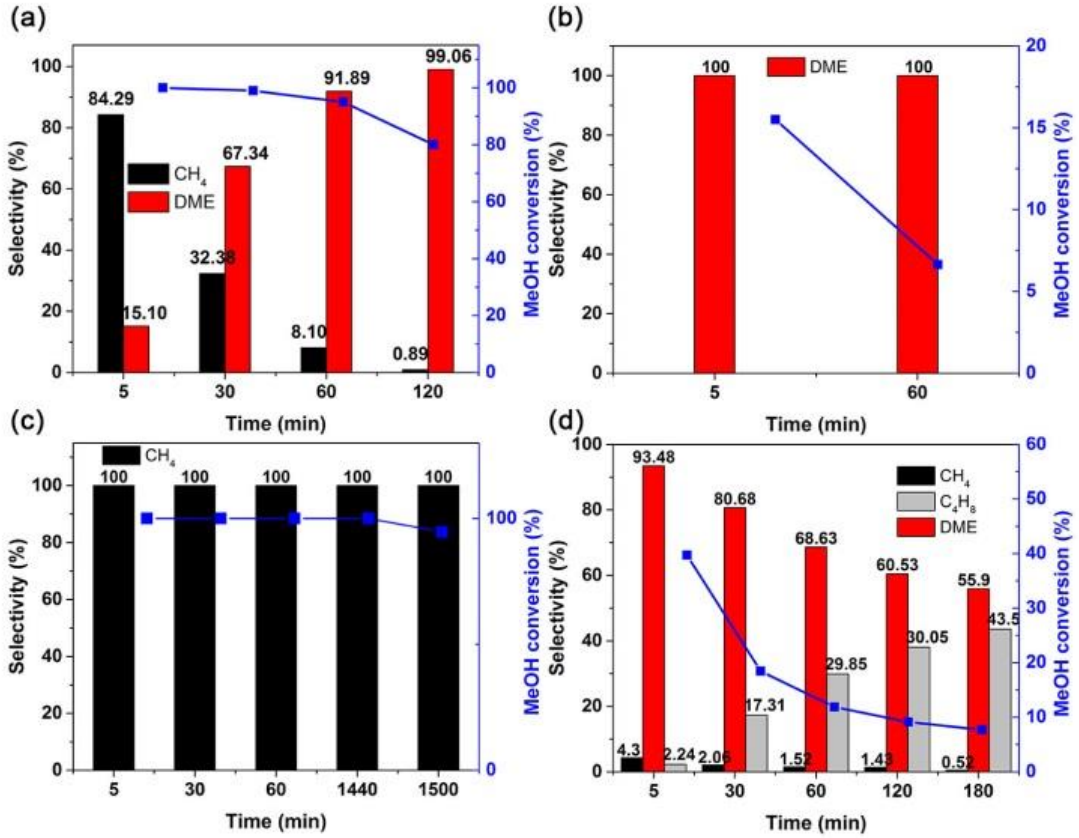

Figure 6.7 Methanol conversion over LDO catalysts as well as selectivities towards the different products [%] obtained over (a) $CuAlO_x$, (b) $MgAlO_x$, (c) $NiAlO_x$ and (d) $ZnAlO_x$.

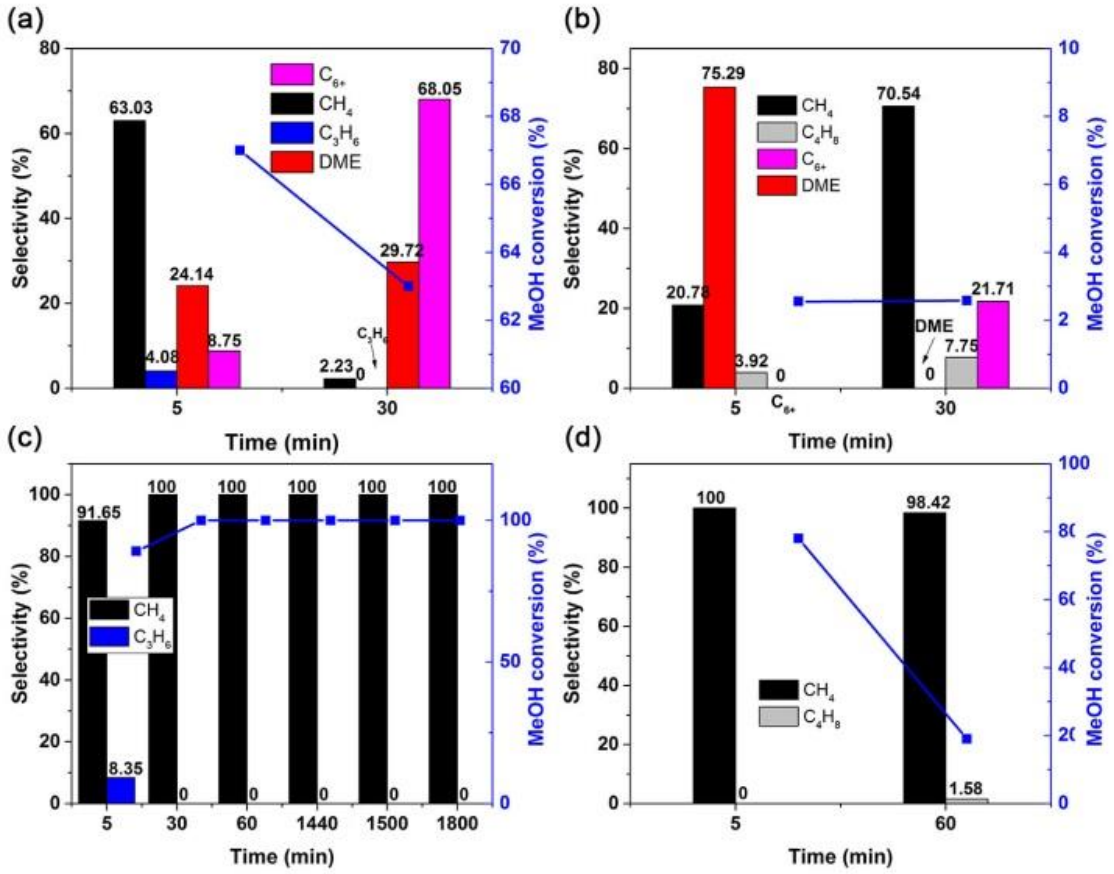

Figure 6.8 Methanol conversion as well as selectivities towards the different product obtained over LDO catalysts. (a) $CuCoO_x$, (b) $CuFeO_x$, (c) $NiFeO_x$ and (d) $ZnFeO_x$.

As aforementioned, $CuAlO_x$ exhibited a high selectivity to DME after 60 min when compared to other catalysts. $NiAlO_x$ showed high selectivity and stability towards CH_4. For a better understanding, CuCo, CuFe, NiFe and ZnFe LDHs were also tested and the results are presented in Figure 6.8. $CuCoO_x$ exhibited a 63% conversion after 30 min into a wide distribution of products: CH_4, C_3H_6, DME and C_6^+ fraction. As the reaction time increased from 5 to 30 min, CH_4 fraction at the reactor outlet diminished from 43% to 1.4% at the benefits of C_6^+ gasoline fraction which was enhanced from 6% to 43%. By comparison with $CuAlO_x$, DME selectivity remained lower over $CuCoO_x$, being in the range of 16-18%. $CuFeO_x$ almost did not exhibit any catalytic activity (Figure 6.8b). Likewise, to $NiAlO_x$, $NiFeO_x$ catalyst led to a complete and stable methanol to CH_4 conversion: *i.e;* CH_4 selectivity and methanol conversion maintained 100% even after 30 h on stream (Figure 6.8c). To investigate the effect of Fe in the matrix, $ZnFeO_x$ was

tested under the same conditions (Figure 6.8d). Behaving significantly differently than $ZnAlO_x$, the methanol converted mainly into CH_4 rather than DME. However, $ZnAlO_x$ and $ZnFeO_x$ exhibited both poor stability and conversion during the progress of the reaction. In spite of having the highest SSA (224 m^2/g, Table 6.1), $MgAlO_x$ exhibited bad performance in the methanol conversion, probably because of its large amount of basic sites. Active LDH catalysts for this gas-phase reaction probably exhibit a sufficient acidity for catalysing the methanol dehydration at 450 °C. Unfortunately, $NiAlO_x$ and $NiFeO_x$ did not exhibit significant methanol conversion at 280 °C, neither methane nor DME could be detected.

TGA was performed under air for $NiFeO_x$ and $NiAlO_x$ LDO samples. Figure 6.9 shows the relative weight versus temperature for the later NiAl material (both materials exhibited the same profile). The first weight decrease corresponds to the water loss (samples were kept for several days before analysis); then the weight increase is probably due to Ni oxidation. Importantly, the last weight decrease can be attributed to coke oxidation into carbon dioxide (above 400 ºC). The amount of carbon present on the catalyst surface could be estimated to 4 wt% after 25 h on stream.

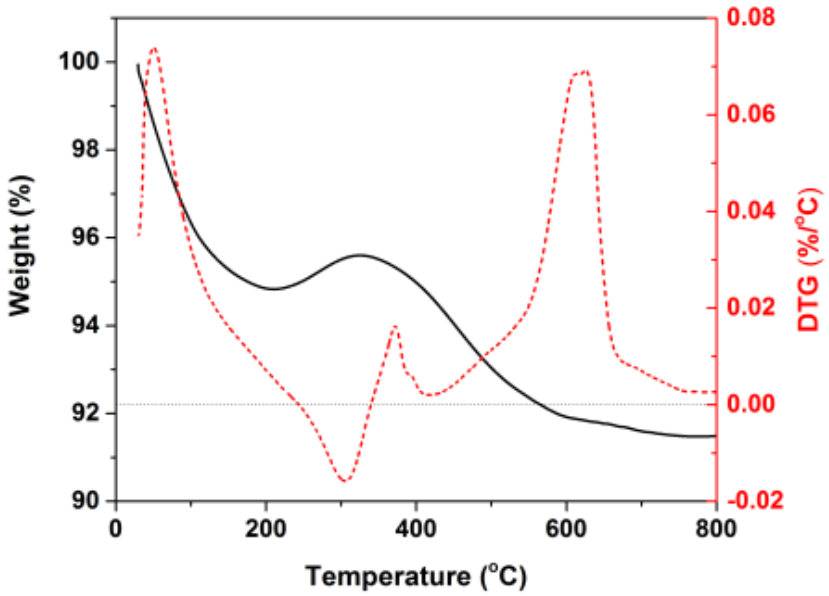

Figure 6.9 TGA under air of aged $NiAlO_x$ LDO catalyst after 25 h on stream at 450 °C. The y-axis represents the relative weight of the different materials.

6.4 Conclusions

Novel LDH derived LDO catalysts were prepared and successfully tested in the gas-phase methanol conversion. By using a conventional co-precipitation method, a series of LDHs were synthesized and thoroughly characterised. After thermal activation, all the samples turned into a mixture of metal oxide or bimetal oxide which exhibited a decent to significant catalytic activity.

SEM images confirmed drastic changes in the materials morphology: ZnAl consisted of small nanoplates, MgAl formed typical sand rose morphology, NiFe grew in a stone-like morphology and the others rather formed aggregated nanoparticles.

While $CuAlO_x$ demonstrated a high selectivity in DME, $NiFeO_x$ showed a 100% selectivity to CH_4 at full conversion and a high stability (superior to 30 h), suggesting that $NiFeO_x$ could be a potential candidate for the timely reversible CH_4 to methanol reaction.

General conclusions and future prospects

This Thesis includes several studies involving the design of zeolites in the presence of biomass, their applications in the methanol-to-olefins (MTO) reaction and investigation of the mechanism(s) of bio-sourced secondary templates (BSST) impact on the zeolite formation.

In **Chapter 1**, an overview on the zeolite history, nature, and applications was presented, particularly focus was given to the ZSM-5 zeolite studied in this Thesis. Besides, an insight on biomass and biomass role as a BSST in the zeolite synthesis was also given. Besides a brief introduction on the MTO chemistry was presented, which is the catalytic application studied in this work.

All the zeolite synthesis methods (Z-LO method, A and B methods) and procedures were detailed in **Chapter 2**, along with a brief description of the techniques used to characterize the materials. The catalytic set-up and test conditions are also presented.

First, the optimal hydrothermal duration and biomass composition and quantity were investigated and set in **Chapter 3** for the synthesis of ZSM-5 zeolites. Secondly, several zeolites were synthesized by hydrothermal reaction with three different reactant molar ratios, which were named as Z-LO method, A method and B method. In our studies, 8 kinds of biomasses (oxidized lignin, coffee bagasse, tea residues, algaCM, algaBB, algaTM, sugarcane bagasse, and ecoshell) and a commercial alkali lignin were evaluated as BSSTs involved in the zeolite crystallization process. As-synthesized biomass-assisted ZSM-5 zeolites were further characterized by XRD, SEM, BET and NH_3-TPD techniques. From these results, it can be seen that the morphological, textural and surface acidic properties of those biomass-mediated ZSM-5 were significantly impacted by the presence of biomass. By comparing with the pristine ZSM-5, we found that the crystallization kinetics also increased via biomass addition. Lastly, the influence of the amount of TPAOH template was also investigated. It is worth mentioning that the use of expensive and toxic organic template could be reduced by an addition of cheap biomasses and it is also a smart strategy to valorize this abundant bio-waste. Moreover, our research systematically pursued numerous samples, and will provide a

reference database for future investigations of BSST strategy in the zeolite nucleation and growth.

The different as-synthesized zeolites were tested in the MTO reaction and a significant improvement of the catalytic performance, *i.e.,* activity, selectivity and stability in the presence of biomass, were shown in **Chapter 4**. For example, tea-mediated ZSM-5 catalysts exhibited high catalytic performance, one of them could maintain almost full methanol conversion for more than 50 h, and achieve a selectivity towards light olefins of 83%, higher than two benchmark zeolites CBV 28014 and CBV 3020E (58% and 37%, respectively) and other reported biomass-assisted zeolites. Besides, ZSM-5 zeolites using three algae (algaCM, algaBB and algaTM) showed prolonged lifetime and 50% methanol conversion at ca. 75, 134, and 94 h, respectively. In a word, this synthetic strategy involving biomass provides a facile, cheap and green route to produce effective ZSM-5 catalysts for the MTO reaction.

Although the ZSM-5 catalysts with high catalytic performance were already obtained, the mechanism of BSST impact on zeolite formation still kept awake our great curiosity. Therefore, **Chapter 5** mainly focuses on how the BSSTs interact with soluble silicate and aluminate species and further impact the catalytic performance in the MTO reaction. We propose a tentative mechanism with BSST interacting with hydroxyl-, carboxyl- and amino functional groups by H-bonding, or electrostatic interactions, thus acting both as “inhibitor” for the growth in b-axis direction and as “promoter” to accelerate the kinetics of crystallization. Biomass-assisted zeolite with shorter b-axis channel exhibited higher catalytic activity, selectivity towards light olefins and longer lifetime may be due to a high accessibility towards the acid sites, hence hindering coke formation. Therefore, we hope this study could inspire the next research on BSST-mediated zeolite synthesis and give some help for future zeolite design.

In addition, **Chapter 6** relates the preparation of layered double hydroxides (LDHs) and their application in the methanol conversion reaction. Series of detailed characterization were conducted over as-prepared LDHs. The results indicate that LDH derived materials act as selective catalysts towards dimethyl ether (DME), methane or light olefins formation, depending on their chemical composition. For instance, $CuAlO_x$

exhibited a high selectivity in DME up to 88%, whilst $CuCoO_x$ converted methanol to CH_4 and DME. $NiFeO_x$ allowed achieving a full methanol conversion selectively into CH_4 during at least 30 h on stream.

As final remarks, it is known that research is an endless job. This work is far from being completed and I risk saying that more questions have been raised by the end of this Thesis, especially in the mechanism study.

From my point of view, most of biomasses we used were raw materials, without any treatment, thus one may expect differences in the zeolite synthesis process when adding biomass after acid or alkali treatment. However, an experiment devoted to the synthesis of ZSM-5 by adding tea waste treated by HCl was conducted, but there no obvious difference could be stated. This new catalyst exhibited similar catalytic performance to the tea-assisted ZSM-5 without any treatment. Besides, coke formation can be evaluated by TGA and further correlate the relationship between crystal b-axis length and coke formation.

Regarding to the mechanism study, the exact composition of different biomass alkaline solutions should be further determined by several techniques (especially NMR) to explain the differences in the zeolite structures, acidic properties and catalytic performances. Furthermore, it can also help us to recognize the active ingredient in the biomass for a tailored zeolite self-assembly and guide the selection of BSST species. Moreover, this BSST strategy could be applied to synthesize other type of zeolites, since it is a facile, cost-effective strategy.

References

1. M. Yang, B. Li, M. Gao, S. Lin, Y. Wang, S. Xu, X. Zhao, P. Guo, Y. Wei, M. Ye, P. Tian and Z. Liu, *ACS Catal.*, 2020, **10**, 3741-3749.
2. J. Han, Z. Liu, H. Li, J. Zhong, W. Zhang, J. Huang, A. Zheng, Y. Wei and Z. Liu, *ACS Catal.*, 2020, **10**, 8727-8735.
3. T. Biligetu, Y. Wang, T. Nishitoba, R. Otomo, S. Park, H. Mochizuki, J. N. Kondo, T. Tatsumi and T. Yokoi, *J. Catal.*, 2017, **353**, 1-10.
4. A. I. Lupulescu and J. D. Rimer, *Angew. Chem. Int. Ed.*, 2012, **51**, 3345-3349.
5. J. D. Rimer, R. F. Lobo and D. G. Vlachos, *Langmuir.*, 2005, **21**, 8960-8971.
6. B. Louis, E. S. Gomes, P. Losch, G. Lutzweiler, T. Coelho, A. Faro, J. F. Pinto, C. S. Cardoso, A. V. Silva and M. M. Pereira, *ChemCatChem*, 2017, **9**, 2065-2079.
7. O. Zaitceva, B. Louis, V. Beneteau, P. Pale, S. Shanmugam, E. I. Evstigneyev and A. V. Vasiliev, *Catal. Today*, 2021, **367**, 111-116.
8. Q. Che, M. Yang, X. Wang, Q. Yang, L. R. Williams, H. Yang, J. Zou, K. Zeng, Y. Zhu, Y. Chen and H. Chen, *Bioresour. Technol.*, 2019, **278**, 248-254.
9. X. Meng and F. S. Xiao, *Chem. Rev.*, 2014, **114**, 1521-1543.
10. G. Wu, X. Wang, Y. Yang, L. Li, G. Wang and N. Guan, *Microporous Mesoporous Mater.*, 2010, **127**, 25-31.
11. G. A. Olah, *Angew. Chem.*, 2005, **44**, 2636-2639.
12. P. Tian, Y. Wei, M. Ye and Z. Liu, *ACS Catal.*, 2015, **5**, 1922-1938.
13. J. Weitkamp, *Solid State Ion.*, 2000, **131**, 175-188.
14. A. F. Cronstedt, *Akad. Handl.*, 1756, **18**, 120-130.
15. E. Erdem, N. Karapinar and R. Donat, *J. Colloid. Interf. Sci.*, 2004, **280**, 309-314.
16. A. S. Nizami, O. K. M. Ouda, M. Rehan, A. M. O. El-Maghraby, J. Gardy, A. Hassanpour, S. Kumar and I. M. I. Ismail, *Energy*, 2016, **108**, 162-171.
17. H.Ghobarkar, O.Schäf and U.Guth, *Prog. Solid State Chem.*, 1999, **27**, 29-73.
18. R. M. Barrer, *J. Chem. Soc.*, 1948, 2158-2163.
19. R. M. Barrer and D. W. Riley, *J. Chem. Soc.*, 1948, 133-143.
20. C. S. Cundy and P. A. Cox, *Chem. Rev.*, 2003, **103**, 663-702.
21. R. M. Barrer, *J. Chem. Soc.*, 1948, 127–132.
22. R. M. Barrer, *Zeolites*, 1981, **1**, 130-140.
23. *U. S. Patent*, 2,882,243, 1959.
24. J. A. Rabo and M. W. Schoonover, *Appl. Catal. A: Gen.*, 2001, **222**, 261-275.
25. R. M. Barrer, *Pure Appl. Chem.*, 1979, **51**, 1091-1100.
26. E. L. Wu, S. L. Lawton, D. H. Olson, A. C. Rohrman and G. T. Kokotailo, *J. Phys. Chem.*, 1979, **83**, 2777-2781.
27. W. M. Meier and C. Baerlocher, in *Structures and Structure Determination*, Springer-Verlag, Berlin, Heidelberg, 1999, vol. 2, pp. 141-161.
28. Z. Wang, Y. Jiang, O. Lafon, J. Trebosc, K. Duk Kim, C. Stampfl, A. Baiker, J. P. Amoureux and J. Huang, *Nat. Commun.*, 2016, **7**, 13820.
29. W. Loewenstein, *Am. Mineral.*, 1954, **39**, 92-96.
30. W. Mozgawa, M. Król and K. Barczyk, *Chemik*, 2011, **65**, 667-674.
31. J. A. Boscoboinik, X. Yu, B. Yang, S. Shaikhutdinov and H.-J. Freund, *Microporous Mesoporous Mater.*, 2013, **165**, 158-162.

32. C. Baerlocher, L. B. McCusker and D. H. Olson, *Atlas of Zeolite Framework Types*, 6th revised edn., Elsevier B.V., 2007.
33. M. Daramola, E. Aransiola and T. Ojumu, *Materials*, 2012, **5**, 2101-2136.
34. P. Vinaches, K. Bernardo-Gusmao and S. B. C. Pergher, *Molecules*, 2017, **22**.
35. M. Moliner, T. Willhammar, W. Wan, J. Gonzalez, F. Rey, J. L. Jorda, X. Zou and A. Corma, *J. Am. Chem. Soc.*, 2012, **134**, 6473-6478.
36. F. J. Chen, Y. Xu and H. B. Du, *Angew. Chem.*, 2014, **53**, 9592-9596.
37. C. Zhang, E. Kapaca, J. Li, Y. Liu, X. Yi, A. Zheng, X. Zou, J. Jiang and J. Yu, *Angew. Chem.*, 2018, **57**, 6486-6490.
38. M. E. Davis, C. Saldarriaga, C. Montes, J. Garces and C. Crowdert, *Nature*, 1988, **331**, 698-699.
39. R. M. Dessau, J. L. Schlenker and J. B. Higgins, *Zeolites*, 1990, **10**, 522-524.
40. R. Martinez-Franco, M. Moliner, Y. Yun, J. Sun, W. Wan, X. Zou and A. Corma, *Proc. Natl. Acad. Sci. U. S. A.*, 2013, **110**, 3749-3754.
41. C. C. Freyhardt, M. Tsapatsis, R. F. Lobo, K. J. B. Jr and M. E. Davis, *Nature*, 1996, **381**, 295-298.
42. M. Yoshikawa, P. Wagner, M. Lovallo, K. Tsuji, T. Takewaki, C.-Y. Chen, L. W. Beck, C. Jones, M. Tsapatsis, S. I. Zones and M. E. Davis, *J. Phys. Chem. B* 1998, **102**, 7139-7147.
43. A. K. Cheetham, H. Fjellvg, T. E. Gier, K. O. Kongshaug, K. P. Lillerud and G. D. Stucky, *Stud. Surf. Sci. Catal.*, 2001, **135**, 158.
44. A. Burton, S. Elomari, C. Y. Chen, R. C. Medrud, I. Y. Chan, L. M. Bull, C. Kibby, T. V. Harris, S. I. Zones and E. S. Vittoratos, *Chem. Eur. J.*, 2003, **9**, 5737-5748.
45. T. Willhammar, A. W. Burton, Y. Yun, J. Sun, M. Afeworki, K. G. Strohmaier, H. Vroman and X. Zou, *J. Am. Chem. Soc.*, 2014, **136**, 13570-13573.
46. K. G. Strohmaier and D. E. W. Vaughan, *J. Am. Chem. Soc.*, 2003, **125**, 16035-16039.
47. A. Corma, M. J. Diaz-Cabanas, F. Rey, S. Nicolopoulus and K. Boulahya, *Chem. Commun.*, 2004, 1356-1357.
48. R. Bai, Q. Sun, N. Wang, Y. Zou, G. Guo, S. Iborra, A. Corma and J. Yu, *Chem. Mater.*, 2016, **28**, 6455-6458.
49. M. V. Opanasenko, W. J. Roth and J. Čejka, *Catal. Sci. Technol.*, 2016, **6**, 2467-2484.
50. M. E. Davis and R. F. Lobo, *Chem. Mater.*, 1992, **4**, 756-768.
51. V. R. R. Marthala, M. Hunger, F. Kettner, H. Krautscheid, C. Chmelik, J. Kärger and J. Weitkamp, *Chem. Mater.*, 2011, **23**, 2521-2528.
52. M. Matsukata, N. Nishiyama and K. Ueyama, *Micropor. Mater.*, 1996, **7**, 109-117.
53. G. Pál-Borbély, Á. Szegedi and H. K. Beyer, *Microporous Mesoporous Mater.*, 2000, **35-36**, 573-584.
54. G. Pál-Borbély, H. K. Beyer, Y. Kiyozumi and F. Mizukami, *Microporous Mesoporous Mater.*, 1998, **22**, 57-68.
55. P. Wei, X. Zhu, Y. Wang, W. Chu, S. Xie, Z. Yang, X. Liu, X. Li and L. Xu, *Microporous Mesoporous Mater.*, 2019, **279**, 220-227.
56. B. Marler, N. Ströter and H. Gies, *Microporous Mesoporous Mater.*, 2005, **83**, 201-211.
57. H. Xu, J. Zhu, L. Zhu, E. Zhou and C. Shen, *Molecules*, 2020, **25**.
58. S. Shimizu and H. Hamada, *Angew. Chem. Int. Ed.*, 1999, **38**, 2725-2727.
59. S. Che, T. Du, S. Zhu, X. Fang and Y. Wang, *J. Ceram. Soc. Jpn.*, 2019, **127**, 606-611.
60. C. Belviso, *Prog. Energy Combust. Sci.*, 2018, **65**, 109-135.

61. A. Chaisena and K. Rangsriwatananon, *Mater. Lett.*, 2005, **59**, 1474-1479.
62. B. Lu, T. Tsuda, H. Sasaki, Y. Oumi, K. Itabashi, T. Teranishi and T. Sano, *Chem. Mater.*, 2004, **16**, 286-291.
63. V. Sazonova, Y. Yaish, H. Ustunel, D. Roundy, T. A. Arias and P. L. McEuen, *Nature*, 2004, **431**, 284-287.
64. C. E. A. Kirschhock, S. P. B. Kremer, P. J. Grobet, P. A. Jacobs and J. A. Martens, *J. Phys. Chem. B*, 2002, **106**, 4897-4900.
65. R. M. Barrer and P. J. Denny, *J. Chem. Soc.*, 1961, 971-982.
66. G. T. Kerr and G. T. Kokotailo, *J. Am. Chem. Soc.*, 1961, **83**, 4675.
67. *U.S. Patent*, 3702886, 1972.
68. S. Sang, F. Chang, Z. Liu, C. He, Y. He and L. Xu, *Catal. Today*, 2004, **93-95**, 729-734.
69. S. L. Burkett and M. E. Davis, *J. Phys. Chem. A*, 1994, **98**, 4647-4653.
70. J. Kecht, S. Mintova and T. Bein, *Chem. Mater.*, 2007, **19**, 1203-1205.
71. K. Lillerud and H. Robson, *Verified Synthesis of Zeolitic Materials*, Elsevier, Amsterdam, the Netherlands, 2001.
72. Y. Kamimura, K. Itabashi and T. Okubo, *Microporous Mesoporous Mater.*, 2012, **147**, 149-156.
73. B. Louis and L. Kiwi-Minsker, *Microporous Mesoporous Mater.*, 2004, **74**, 171-178.
74. J. L. Guth, H. Kessler, J. M. Higel, J. M. Lamblin, J. Patarin, A. Seive, J. M. Chezeau and R. Wey, in *Zeolite Synthesis*, American Chemical Society, 1989, vol. 398, pp. 176-195.
75. S. Mintova, J. P. Gilson and V. Valtchev, *Nanoscale*, 2013, **5**, 6693-6703.
76. C. S. Cundy and P. A. Cox, *Microporous Mesoporous Mater.*, 2005, **82**, 1-78.
77. K. S. Walton, M. B. Abney and M. Douglas LeVan, *Microporous Mesoporous Mater.*, 2006, **91**, 78-84.
78. R. Barrer and B. Coughlan, *Soc. Chem. Ind.*, 1968, 141.
79. Y. Sun, Q. Fang, J. Dong, X. Cheng and J. Xu, *Desalination*, 2011, **277**, 121-127.
80. C. Yan, H. Cheng, Z. Yuan and S. Wang, *Environ. Technol.*, 2015, **36**, 169-177.
81. T. Ikeda, T. Nagase, N. Hiyoshi and Y. Oumi, *Microporous Mesoporous Mater.*, 2012, **163**, 42-50.
82. R. R. Sharma, *Enzyme Inhibition: Mechanisms and Scope*, INTECH Open Access Publisher, Rijeka, Croatia, 2012.
83. H. Khanmohammadi, B. Bayati, J. Rahbar- Shahrouzi, A.-A. Babaluo and A. Ghorbani, *J. Environ. Chem. Eng.*, 2019, **7**, 103040.
84. L. Ćurković, Š. Cerjan-Stefanović and T. Filipan, *Water Res.*, 1997, **31**, 1379-1382.
85. N. Herron, G. D. Stucky and C. A. Tolman, *Chem. Commun.*, 1986, 1521-1522.
86. T. W. van Deelen, C. Hernández Mejía and K. P. de Jong, *Nat. Catal.*, 2019, **2**, 955-970.
87. X. Pan and X. Bao, *Acc. Chem. Res.*, 2011, **44**, 553-562.
88. B.-Z. Zhan, M. A. White, T.-K. Sham, J. A. Pincock, R. J. Doucet, K. V. R. Rao, K. N. Robertson and T. S. Cameron, *J. Am. Chem. Soc.*, 2003, **125**, 2195-2199.
89. I. Iskandar, A. Kristiani, S. Sudiyarmanto, F. Aulia, L. Nurul Hidayati, H. Abimanyu, S. Ismadji, T. E. Agustina, I. Yani, L. N. Komariah and S. Hasyim, *Mater. Web. Conf.*, 2017, **101**, 01001.
90. H. Wang, L. Wang and F. S. Xiao, *ACS Cent. Sci.*, 2020, **6**, 1685-1697.
91. A. Feliczak-Guzik, *Microporous Mesoporous Mater.*, 2018, **259**, 33-45.
92. Y. Sasaki, T. Suzuki, Y. Takamura, A. Saji and H. Saka, *J. Catal.*, 1998, **178**, 94-100.
93. R. Chal, C. Gérardin, M. Bulut and S. van Donk, *ChemCatChem*, 2011, **3**, 67-81.

94. R. A. Beyerlein, C. Choi-Feng, J. B. Hall, B. J. Huggins and G. J. Ray, *Top. Catal.*, 1997, **4**, 27-42.
95. R. Giudici, H. W. Kouwenhoven and R. Prins, *Appl. Catal. A: Gen.*, 2000, **203**, 101-110.
96. M. Müller, G. Harvey and R. Prins, *Microporous Mesoporous Mater.*, 2000, **34**, 135-147.
97. L. Aouali, J. Jeanjean, A. Dereigne, P. Tougne and D. Delafosse, *Zeolites*, 1988, **8**, 517-522.
98. R. López-Fonseca, B. de Rivas, J. I. Gutiérrez-Ortiz, A. Aranzabal and J. R. González-Velasco, *Appl. Catal. B: Environ.*, 2003, **41**, 31-42.
99. A. Feng, Y. Yu, L. Mi, Y. Cao, Y. Yu and L. Song, *Microporous Mesoporous Mater.*, 2019, **280**, 211-218.
100. G. Agostini, C. Lamberti, L. Palin, M. Milanesio, N. Danilina, B. Xu, M. Janousch and J. A. van Bokhoven, *J. Am. Chem. Soc.*, 2010, **132**, 667-678.
101. E. F. T. Lee and L. V. C. Rees, *Faraday Trans.*, 1987, **1**, 1531-1537.
102. S. Moreno and G. Poncelet, *Micropor. Mater.*, 1997, **12**, 197-222.
103. C. Zhang, Q. Liu, Z. Xu and K. Wan, *Microporous Mesoporous Mater.*, 2003, **62**, 157-163.
104. N. Dudovich, D. Oron and Y. Silberberg, *Nature*, 2002, **418**, 512-514.
105. X. Jin, Y. Millot, C. Sayag, J. Blanchard and P. P. Man, *ChemistrySelect*, 2020, **5**, 2489-2495.
106. H. K. Beyer, I. M. Belenykaja, F. Hange, M. Tielen, P. J. Grobet and P. A. Jacobs, *Faraday Trans.*, 1985, **81**, 2889-2901.
107. C. S. Triantafillidis, A. G. Vlessidis and N. P. Evmiridis, *Ind. Eng. Chem. Res.*, 2000, **39**, 307-319.
108. L. Cherif, F. Z. El-Berrichi, A. Benguedach, P. Tougne and J. Fraissard, *Colloid. Surface. A*, 2003, **220**, 83-89.
109. A. Feng, Y. Yu, L. Mi, Y. Cao, Y. Yu and L. Song, *Microporous Mesoporous Mater.*, 2019, **290**, 109646.
110. G. T. Kerr, *J. Phys. Chem.*, 1969, **73**, 2780-2782.
111. C. D. Chang, C. T. W. Chu, J. N. Miale, R. F. Bridger and R. B. Calvert, *J. Am. Chem. Soc.*, 1984, **106**, 8143-8146.
112. Z. Zhang, X. Liu, Y.Xu and R.Xu, *Zeolites*, 1991, **11**, 232-238.
113. J. Weitkamp and L. Puppe, *Catalysis and Zeolites: Fundamentals and Applications*, Springer, Berlin Heidelberg, 1999.
114. H. van Bekkum, E. M. Flanigen and J. C. Jansen, *Introduction to Zeolite Science and Practice*, Elsevier B.V., 1991.
115. D. W. Breck and G. W. Skeels, in *Proceedings of the 5th International Conference on Zeolites*, Heyden, London, 1980, p. 335.
116. J. C. Vega-Vila, J. W. Harris and R. Gounder, *J. Catal.*, 2016, **344**, 108-120.
117. J. Dijkmans, M. Dusselier, W. Janssens, M. Trekels, A. Vantomme, E. Breynaert, C. Kirschhock and B. F. Sels, *ACS Catal.*, 2015, **6**, 31-46.
118. M. Hunger, J. Kärger, H. Pfeifer, J. Caro, B. Zibrowius, M. Bülow and R. Mostowicz, *Faraday Trans.*, 1987, **83**, 3459-3468.
119. G. D. Yadav, *Catal. Surv. from Asia*, 2005, **9**, 117-137.
120. Y. Li, L. Li and J. Yu, *Chem*, 2017, **3**, 928-949.
121. V. Van Speybroeck, K. Hemelsoet, L. Joos, M. Waroquier, R. G. Bell and C. R. Catlow, *Chem. Soc. Rev.*, 2015, **44**, 7044-7111.
122. A. R. Loiola, J. C. Andrade, J. M. Sasaki and L. R. da Silva, *J. Colloid Interf. Sci.*, 2012, **367**,

34-39.
123. M. R. Abukhadra, S. M. Ali, E. A. Nasr, H. A. A. Mahmoud and E. M. Awwad, *ACS Omega.*, 2020, **5**, 14656-14668.
124. T. Kobayashi, M. Ohshiro, K. Nakamoto and S. Uchida, *Ind. Eng. Chem. Res.*, 2016, **55**, 6996-7002.
125. P. Bosch, D. Caputo, B. Liguori and C. Colella, *J. Nucl. Mater.*, 2004, **324**, 183-188.
126. A. Olmos, S. Rigolet, B. Louis and P. Pale, *J. Phys. Chem. C*, 2012, **116**, 13661-13670.
127. S. Chassaing, V. Bénéteau and P. Pale, *Catal. Sci. Technol.*, 2016, **6**, 923-957.
128. M. Djaeni, P. Bartels, J. Sanders, G. van Straten and A. J. B. van Boxtel, *Dry. Technol.*, 2007, **25**, 225-239.
129. Q. Wang, J. Luo, Z. Zhong and A. Borgna, *Energy Environ. Sci.*, 2011, **4**, 42-55.
130. L. Huang, J. Wang, Y. Gao, Y. Qiao, Q. Zheng, Z. Guo, Y. Zhao, D. O'Hare and Q. Wang, *J. Mater. Chem. A*, 2014, **2**, 18454-18462.
131. Q. Wang and D. O'Hare, *Chem. Rev.*, 2012, **112**, 4124-4155.
132. T. S. Frantz, W. A. Ruiz, C. A. da Rosa and V. B. Mortola, *Microporous Mesoporous Mater.*, 2016, **222**, 209-217.
133. L. Grajciar, J. Cejka, A. Zukal, C. Otero Arean, G. Turnes Palomino and P. Nachtigall, *ChemSusChem*, 2012, **5**, 2011-2022.
134. M. Katoh, T. Yoshikawa, T. Tomonari, K. Katayama and T. Tomida, *J. Colloid. Interf. Sci.*, 2000, **226**, 145-150.
135. A. Corma, *Chem. Rev.*, 1995, **95**, 559-614.
136. J. Liang, Z. Liang, R. Zou and Y. Zhao, *Adv. Mater.*, 2017, **29**.
137. A. Primo and H. Garcia, *Chem. Soc. Rev.*, 2014, **43**, 7548-7561.
138. J. Weitkamp, *Solid State Ionics*, 2000, **131**, 175-188.
139. A. Corma, *J. Catal.*, 2003, **216**, 298-312.
140. I. Fechete, Y. Wang and J. C. Védrine, *Catal. Today*, 2012, **189**, 2-27.
141. Z. Xue, T. Zhang, J. Ma, H. Miao, W. Fan, Y. Zhang and R. Li, *Microporous Mesoporous Mater.*, 2012, **151**, 271-276.
142. M. F. Alotibi, B. A. Alshammari, M. H. Alotaibi, F. M. Alotaibi, S. Alshihri, R. M. Navarro and J. L. G. Fierro, *Catal. Surv. from Asia*, 2019, **24**, 1-10.
143. J. Cejka, H. v. Bekkum, A. Corma and F. Schueth, *Introduction to Zeolite Molecular Sieves*, Elsevier Science, 2007.
144. B. Yilmaz and U. Müller, *Top. Catal.*, 2009, **52**, 888-895.
145. B. Jha and D. N. Singh, *J. Mater. Educ.*, 2011, **33**, 65-132.
146. R. Bingre, B. Louis and P. Nguyen, *Catalysts*, 2018, **8**, 163.
147. E. T. C.Vogt, G. T. Whiting, A. D. Chowdhury and B. M.Weckhuysen, in *Advances in Catalysis*, 2015, vol. 58, pp. 143-314.
148. G. Song, L. Shen and J. Xiao, *Ind. Eng. Chem. Res.*, 2011, **50**, 9758-9766.
149. A. Tursi, *Biofuel Res. J.*, 2019, **6**, 962-979.
150. C. C. Xu, B. Liao, S. Pang, L. Nazari, N. Mahmood, S. H. K. Mohammad, T. A. Dutta and M. B. Ray, in *Comprehensive Energy Systems*, ed. I. Dincer, Elsevier, 2018, vol. 1, pp. 770-794.
151. S. Chandrasekhar, K. G. Satyanarayana, P. N. Pramada and P. Raghavan, *J. Mater. Sci.*, 2003, **38**, 3159-3168.
152. R. Rajamma, R. J. Ball, L. A. Tarelho, G. C. Allen, J. A. Labrincha and V. M. Ferreira, *J. Hazard*

Mater., 2009, **172**, 1049-1060.
153. S. Wang, A. Miller, E. Llamazos, F. Fonseca and L. Baxter, *Fuel*, 2008, **87**, 365-371.
154. S. V. Vassilev, D. Baxter, L. K. Andersen and C. G. Vassileva, *Fuel*, 2010, **89**, 913-933.
155. S. V. Vassilev, D. Baxter, L. K. Andersen and C. G. Vassileva, *Fuel*, 2013, **105**, 40-76.
156. F. G. Gemechu, *Trends Food Sci. Technol.*, 2020, **104**, 235-261.
157. N. Yang, C. Liu, X. Liu, T. K. Degn, M. Munchow and I. Fisk, *Food Chem.*, 2016, **211**, 206-214.
158. A. Chowdhury, S. Sarkar, A. Chowdhury, S. Bardhan, P. Mandal and M. Chowdhury, *Indian J. Sci. Technol.*, 2016, **9**.
159. C.-F. Chen, C.-Y. Hu, M.-L. Liou, C.-C. Wu, Y.-S. Su and C.-J. Liu, *Sustainability*, 2014, **6**, 6985-6997.
160. N. S. Trivedi, S. A. Mandavgane, S. Mehetre and B. D. Kulkarni, *Environ. Sci. Pollut. Res. Int.*, 2016, **23**, 20243-20256.
161. M. Danish and T. Ahmad, *Renew. Sust. Energ. Rev.*, 2018, **87**, 1-21.
162. S. Nizamuddin, H. A. Baloch, G. J. Griffin, N. M. Mubarak, A. W. Bhutto, R. Abro, S. A. Mazari and B. S. Ali, *Renew. Sust. Energ. Rev.*, 2017, **73**, 1289-1299.
163. A. T. Hoang, X. L. Bui and X. D. Pham, *Energ. Source. Part A*, 2018, **40**, 929-939.
164. C. Yeretzian, A. Glöss, S. Petrozzi, L. D'Ambrosio, K. Knöpfli-Lengweiler, F. Wieland, A. F. Wild and R. Anliker, in *New Food*, Russell Publishing Ltd., U.K., 2010, vol. 13, pp. 10-17.
165. X. Jiang, C. Abbati de Assis, M. Kollman, R. Sun, H. Jameel, H.-M. Chang and R. Gonzalez, *Green Chem.*, 2020, **22**, 7448-7459.
166. J. Pu, T.-S. Nguyen, E. Leclerc, C. Lorentz, D. Laurenti, I. Pitault, M. Tayakout-Fayolle and C. Geantet, *Appl. Catal. B: Environ.*, 2019, **256**, 117769.
167. A. Rahimi, A. Ulbrich, J. J. Coon and S. S. Stahl, *Nature*, 2014, **515**, 249-252.
168. N. M. Stark, D. J. Yelle and U. P. Agarwal, in *Lignin in Polymer Composites*, eds. O. Faruk and M. Sain, Elsevier, Oxford, 2016, pp. 49-66.
169. L. Donaldson, B. Nanayakkara and J. Harrington, in *Applied Plant Sciences*, eds. B. Thomas, B. G. Murray and D. J. Murphy, Elsevier, 2017, vol. 1, pp. 203-210.
170. G. Bochmann, in *Substitute Natural Gas from Waste: Technical Assessment and Industrial Applications of Biochemical and Thermochemical Processes*, eds. M. Materazzi and P. U. Foscolo, Elsevier, 2019, vol. 4, pp. 49-62.
171. Carla S. G. P. Queirós, S. Cardoso, A. Lourenço, J. Ferreira, I. Miranda, M. J. V. Lourenço and H. Pereira, *Biomass Convers. Bior.*, 2019, **10**, 175-188.
172. M. R. Barr, L. Forster, C. D'Agostino and R. Volpe, *Appl. Surf. Sci.*, 2022, **571**, 151253.
173. K. Bilba, M.-A. Arsene and A. Ouensanga, *Cem. Concr. Compos.*, 2003, **25**, 91-96.
174. I. M. Nwajiaku, J. S. Olanrewaju, K. Sato, T. Tokunari, S. Kitano and T. Masunaga, *Inter. J. Recycl. Organic Waste Agri.*, 2018, **7**, 269-276.
175. T. Zhao, Z. Chen, X. Lin, Z. Ren, B. Li and Y. Zhang, *Carbohydr. Polym.*, 2018, **184**, 164-170.
176. X. Lin, Z. Chen, Y. Zhang, W. Luo, H. Tang, B. Deng, J. Deng and B. Li, *Food Chem.*, 2015, **173**, 432-440.
177. L. F. Ballesteros, J. A. Teixeira and S. I. Mussatto, *Food Bioproc. Tech.*, 2014, **7**, 3493-3503.
178. C.-H. Weng, Y.-T. Lin, D.-Y. Hong, Y. C. Sharma, S.-C. Chen and K. Tripathi, *Ecol. Eng.*, 2014, **67**, 127-133.
179. X. Song, X. Ma, Y. Li, L. Ding and R. Jiang, *Appl. Surf. Sci.*, 2019, **487**, 189-197.

180. P. Rani and R. Srivastava, *Chem. Rec.*, 2020, **20**, 968-988.
181. A. S. Priya, K. R. S. Devi, K. Karthik and S. Sugunan, *Waste Biomass Valori.*, 2019, **11**, 4809-4819.
182. N. S. Caetano, V. F. M. Silva and T. M. Mata, *Chem. Eng. Trans.*, 2012, **26**, 1-6.
183. K. Kante, C. Nieto-Delgado, J. R. Rangel-Mendez and T. J. Bandosz, *J. Hazard. Mater.*, 2012, **201-202**, 141-147.
184. R. Pode, *Renew. Sust. Energ. Rev.*, 2016, **53**, 1468-1485.
185. C. Santasnachok, W. Kurniawan, C. Salim and H. Hinode, *J. Adv. Agric. Technol.*, 2014, **1**.
186. Y. Li, G. Liang, L. Chang, C. Zi, Y. Zhang, Z. Peng and W. Zhao, *Energ. Source. Part A*, 2019, **43**, 1745-1758.
187. E.-P. Ng, J.-H. Chow, R. R. Mukti, O. Muraza, T. C. Ling and K.-L. Wong, *Mater. Chem. Phys.*, 2017, **201**, 78-85.
188. B. Zhang, S. A. Davis, S. Mann and N. H. Mendelson, *Chem. Commun.*, 2000, 781-782.
189. V. Valtchev, F. Gao and L. Tosheva, *New J. Chem.*, 2008, **32**, 1331.
190. E. S. Gomes, D. A. G. Aranda, M. M. Pereira and B. Louis, *Microporous Mesoporous Mater.*, 2018, **263**, 251-256.
191. E. S. Gomes, G. Lutzweiler, P. Losch, A. V. Silva, C. Bernardon, K. Parkhomenko, M. M. Pereira and B. Louis, *Microporous Mesoporous Mater.*, 2017, **254**, 28-36.
192. R. N. M. Missengue, P. Losch, G. Sedres, N. M. Musyoka, O. O. Fatoba, B. Louis, P. Pale and L. F. Petrik, *C. R. Chim.*, 2017, **20**, 78-86.
193. M. M. Pereira, E. S. Gomes, A. V. Silva, A. B. Pinar, M.-G. Willinger, S. Shanmugam, C. Chizallet, G. Laugel, P. Losch and B. Louis, *Chem. Sci.*, 2018, **9**, 6532-6539.
194. W. Koch, W. Kukula-Koch, L. Komsta, Z. Marzec, W. Szwerc and K. Glowniak, *Molecules*, 2018, **23**.
195. D. Li, Y. Chen, J. Hu, B. Deng, X. Cheng and Y. Zhang, *Appl. Catal., B*, 2020, **270**, 118881.
196. K. Amakawa, Y. V. Kolen'ko, A. Villa, M. E. Schuster, L.-I. Csepei, G. Weinberg, S. Wrabetz, R. Naumann d'Alnoncourt, F. Girgsdies, L. Prati, R. Schlögl and A. Trunschke, *ACS Catal.*, 2013, **3**, 1103-1113.
197. M. Hävecker, S. Wrabetz, J. Kröhnert, L.-I. Csepei, R. Naumann d'Alnoncourt, Y. V. Kolen'ko, F. Girgsdies, R. Schlögl and A. Trunschke, *J. Catal.*, 2012, **285**, 48-60.
198. R. Naumann d'Alnoncourt, L.-I. Csepei, M. Hävecker, F. Girgsdies, M. E. Schuster, R. Schlögl and A. Trunschke, *J. Catal.*, 2014, **311**, 369-385.
199. T. Weissenberger, B. Reiprich, A. G. F. Machoke, K. Klühspies, J. Bauer, R. Dotzel, J. L. Casci and W. Schwieger, *Catal. Sci. Technol.*, 2019, **9**, 3259-3269.
200. F. L. Bleken, S. Chavan, U. Olsbye, M. Boltz, F. Ocampo and B. Louis, *Appl. Catal. A: Gen.*, 2012, **447-448**, 178-185.
201. L. Meng, X. Zhu, W. Wannapakdee, R. Pestman, M. G. Goesten, L. Gao, A. J. F. van Hoof and E. J. M. Hensen, *J. Catal.*, 2018, **361**, 135-142.
202. M. Firoozi, M. Baghalha and M. Asadi, *Catal. Commun.*, 2009, **10**, 1582-1585.
203. M. DeLuca, C. Janes and D. Hibbitts, *ACS Catal.*, 2020, **10**, 4593-4607.
204. J. Li, Y. Wei, G. Liu, Y. Qi, P. Tian, B. Li, Y. He and Z. Liu, *Catal. Today*, 2011, **171**, 221-228.
205. H.-J. Chae, Y.-H. Song, K.-E. Jeong, C.-U. Kim and S.-Y. Jeong, *J. Phys. Chem. Solids*, 2010, **71**, 600-603.
206. P. Losch, A. B. Pinar, M. G. Willinger, K. Soukup, S. Chavan, B. Vincent, P. Pale and B. Louis,

J. Catal., 2017, **345**, 11-23.
207. W. Dai, G. Wu, L. Li, N. Guan and M. Hunger, *ACS Catal.*, 2013, **3**, 588-596.
208. M. Dyballa, U. Obenaus, M. Blum and W. Dai, *Catal. Sci. Technol.*, 2018, **8**, 4440-4449.
209. H. Khezri, A. Izadbakhsh and A. A. Izadpanah, *Fuel Process. Technol.*, 2020, **199**, 106253.
210. I. A. Bakare, O. Muraza, M. Yoshioka, Z. H. Yamani and T. Yokoi, *Catal. Sci. Technol.*, 2016, **6**, 7852-7859.
211. D. R. Dubois, D. L. Obrzut, J. Liu, J. Thundimadathil, P. M. Adekkanattu, J. A. Guin, A. Punnoose and M. S. Seehra, *Fuel Process. Technol.*, 2003, **83**, 203-218.
212. Y. Ji, H. Yang and W. Yan, *Catalysts*, 2017, **7**, 367.
213. H. U. Hambali, A. A. Jalil, S. Triwahyono, S. F. Jamian, N. A. A. Fatah, A. A. Abdulrasheed and T. J. Siang, *Int. J. Hydrog. Energy*, 2019.
214. F. Mohammadparast, R. Halladj and S. Askari, *Chem. Eng. Commun.*, 2014, **202**, 542-556.
215. P. Losch, M. Boltz, C. Bernardon, B. Louis, A. Palčić and V. Valtchev, *Appl. Catal. A: Gen.*, 2016, **509**, 30-37.
216. S. Ivanova, B. Louis, B. Madani, J. P. Tessonnier, M. J. Ledoux and C. Pham-Huu, *J. Phys. Chem. C*, 2007, **111**, 4368-4374.
217. Z. Liao, T. Xu, Y. Jiang, B. Jiang, J. Wang, Y. Yang, Y. Jiao, Z. Yang and J. Zhang, *Ind. Eng. Chem. Res.*, 2018, **58**, 27-33.
218. S. Kim, G. Park, M. H. Woo, G. Kwak and S. K. Kim, *ACS Catal.*, 2019, **9**, 2880-2892.
219. N. Cui, H. Guo, J. Zhou, L. Li, L. Guo and Z. Hua, *Microporous Mesoporous Mater.*, 2020, **306**, 110411.
220. P. Losch, T. Hoff, J. Kolb, C. Bernardon, J.-P. Tessonnier and B. Louis, *Catalysts*, 2017, **7**, 225.
221. H. Kim, M. M. Murata, H. Chang, S. H. Lee, J. Kim, J. H. Lee, W. Y. Rho and B. H. Jun, in *Nanotechnology for Bioapplications*, ed. B.-H. Jun, springer nature, Singapore, 2021, vol. 12.
222. M. D. Romero, J. A. Calles, A. Rodríguez and A. d. Lucas, *Micropor. Mater.*, 1997, **9**, 221-228.
223. L. Rodríguez-González, F. Hermes, M. Bertmer, E. Rodríguez-Castellón, A. Jiménez-López and U. Simon, *Appl. Catal. A: Gen.*, 2007, **328**, 174-182.
224. T. Wakihara and T. Okubo, *Chem. Lett.*, 2005, **34**, 276-281.
225. H. Awala, J. P. Gilson, R. Retoux, P. Boullay, J. M. Goupil, V. Valtchev and S. Mintova, *Nat. Mater.*, 2015, **14**, 447-451.
226. E.-P. Ng, J.-M. Goupil, A. Vicente, C. Fernandez, R. Retoux, V. Valtchev and S. Mintova, *Chem. Mater.*, 2012, **24**, 4758-4765.
227. Y. Kamimura, K. Iyoki, S. P. Elangovan, K. Itabashi, A. Shimojima and T. Okubo, *Microporous Mesoporous Mater.*, 2012, **163**, 282-290.
228. Y. Wang, Q. Wu, X. Meng and F.-S. Xiao, *Engineering*, 2017, **3**, 567-574.
229. T. Tang, L. Zhang, H. Dong, Z. Fang, W. Fu, Q. Yu and T. Tang, *RSC Adv.*, 2017, **7**, 7711-7717.
230. Y. Huang, K. Wang, D. Dong, D. Li, M. R. Hill, A. J. Hill and H. Wang, *Microporous Mesoporous Mater.*, 2010, **127**, 167-175.
231. A. Zheng, Z. Zhao, S. Chang, Z. Huang, H. Wu, X. Wang, F. He and H. Li, *J. Mol. Catal. A: Chem.*, 2014, **383-384**, 23-30.
232. R. Feng, X. Yan, X. Hu, Y. Zhang, J. Wu and Z. Yan, *Appl. Catal. A: Gen.*, 2020, **594**, 117464.
233. G. Winé, J.-P. Tessonnier, S. Rigolet, C. Marichal, M.-J. Ledoux and C. Pham-Huu, *J. Mol. Catal. A: Chem.*, 2006, **248**, 113-120.
234. Y. Ma, N. Wang, W. Qian, Y. Wang, J. Zhang and F. Wei, *RSC Adv.*, 2016, **6**, 81198-81202.

235. J. Chung, I. Granja, M. G. Taylor, G. Mpourmpakis, J. R. Asplin and J. D. Rimer, *Nature*, 2016, **536**, 446-450.
236. X. Geng, R. D. Sosa, M. A. Reynolds, J. C. Conrad and J. D. Rimer, *Mol. Syst. Des. Eng.*, 2021, **6**, 508-519.
237. H. Wang, G. Fan, C. Zheng, X. Xiang and F. Li, *Ind. Eng. Chem. Res.*, 2010, **49**, 2759-2767.
238. R. Li, A. Smolyakova, G. Maayan and J. D. Rimer, *Chem. Mater.*, 2017, **29**, 9536-9546.
239. L. Qi, H. Cölfen and M. Antonietti, *Chem. Mater.*, 2000, **12**, 2392-2403.
240. A. Cai, A. Guo, Y. Chang, Y. Sun, S. Xing and Z. Ma, *Mater. Lett.*, 2013, **111**, 158-160.
241. Y.-C. Liou, A. Tocilj, P. L. Davies and Z. Jia, *Nature*, 2000, **406**, 322-324.
242. S. Farmanesh, J. Chung, R. D. Sosa, J. H. Kwak, P. Karande and J. D. Rimer, *J. Am. Chem. Soc.*, 2014, **136**, 12648-12657.
243. F. Jin, X. Wang, T. Liu, L. Xiao, M. Yuan and Y. Fan, *Chin. J. Chem. Eng.*, 2017, **25**, 1303-1313.
244. Y. Jiao, X. Fan, M. Perdjon, Z. Yang and J. Zhang, *Appl. Catal. A: Gen.*, 2017, **545**, 104-112.
245. J. H. Jung, J. K. Lee, J. K. Kim and H. K. Rhee, *Korean J. Chem. Eng.*, 2000, **17**, 461-467.
246. A. I. Lupulescu, M. Kumar and J. D. Rimer, *J. Am. Chem. Soc.*, 2013, **135**, 6608-6617.
247. K. N. Olafson, R. Li, B. G. Alamani and J. D. Rimer, *Chem. Mater.*, 2016, **28**, 8453-8465.
248. P. Sadeghpour, M. Haghighi and K. Khaledi, *Mater. Chem. Phys.*, 2018, **217**, 133-150.
249. R. Feng, X. Yan, X. Hu, J. Wu and Z. Yan, *Microporous Mesoporous Mater.*, 2020, **302**, 110246.
250. Y. Liang, B. Gao, L. Zhou, X. Yang, T. Lu, H. Yao and Y. Su, *J. Mater. Chem. A*, 2021, **9**, 1859-1867.
251. C. D. Chang and A. J. Silvestri, *J. Catal.*, 1977, **47**, 249-259.
252. Pau Ferri, C. Li, R. Millán, J. Martínez-Triguero, M. Moliner, M. Boronat and A. Corma, *Angew. Chem.*, 2020, **59**, 19708–19715.
253. S. Müller, Y. Liu, M. Vishnuvarthan, X. Sun, A. C. van Veen, G. L. Haller, M. Sanchez-Sanchez and J. A. Lercher, *J. Catal.*, 2015, **325**, 48-59.
254. F. L. Bleken, T. V. W. Janssens, S. Svelle and U. Olsbye, *Microporous Mesoporous Mater.*, 2012, **164**, 190-198.
255. H. Schulz, *Catal. Today*, 2010, **154**, 183-194.
256. D. Chen, K. Moljord and A. Holmen, *Microporous Mesoporous Mater.*, 2012, **164**, 239-250.
257. R. Bingre, C. M. Sayago, P. Losch, L. Huang, Q. Wang, M. M. Pereira and B. Louis, *Inorg. Chim. Acta*, 2019, **487**, 379-386.
258. M. Stocker, *Microporous Mesoporous Mater.*, 1999, **29**, 3-48.
259. P. Losch, M. Boltz, K. Soukup, I. H. Song, H. S. Yun and B. Louis, *Microporous Mesoporous Mater.*, 2014, **188**, 99-107.
260. B. Louis, E. S. Gomes, T. Coelho, G. Lutzweiler, P. Losch, A. V. Silva, A. C. Faro, T. Romero, M. B. Osman, A. Balanqueux, C. Bernardon and M. M. Pereira, *Nanosci. Nanotech. Let.*, 2016, **8**, 917-923.
261. L. Qi, J. Li, Y. Wei, L. Xu and Z. Liu, *Catal. Sci. Technol.*, 2016, **6**, 3737-3744.
262. J. Zhang, L. Ren, Y. Mi, P. Luo, H. Xu, Y. Guan, H. Peng, S. Song, W. Song, H. Wu, M. He and P. Wu, *Catal. Sci. Technol.*, 2021, **11**, 6234-6247.
263. S. Kim, G. Park, S. K. Kim, Y. T. Kim, K.-W. Jun and G. Kwak, *Appl. Catal. B: Environ.*, 2018, **220**, 191-201.
264. M. Hu, C. Wang, X. Gao, Y. Chu, G. Qi, Q. Wang, G. Xu, J. Xu and F. Deng, *ACS Catal.*, 2020, **10**, 4299-4305.

265. I. Pinilla-Herrero, E. Borfecchia, J. Holzinger, U. V. Mentzel, F. Joensen, K. A. Lomachenko, S. Bordiga, C. Lamberti, G. Berlier, U. Olsbye, S. Svelle, J. Skibsted and P. Beato, *J. Catal.*, 2018, **362**, 146-163.
266. Q. Zhang, A. Mayoral, O. Terasaki, Q. Zhang, B. Ma, C. Zhao, G. Yang and J. Yu, *J. Am. Chem. Soc.*, 2019, **141**, 3772-3776.
267. M. Choi, K. Na, J. Kim, Y. Sakamoto, O. Terasaki and R. Ryoo, *Nature*, 2009, **461**, 246-249.
268. L. H. Chen, M. H. Sun, Z. Wang, W. Yang, Z. Xie and B. L. Su, *Chem. Rev.*, 2020, **120**, 11194-11294.
269. X. Wang, H. Chen, F. Meng, F. Gao, C. Sun, L. Sun, S. Wang, L. Wang and Y. Wang, *Microporous Mesoporous Mater.*, 2017, **243**, 271-280.
270. F. Liu, S. Zuo, C. Wang, J. Li, F.-S. Xiao and C. Qi, *Appl. Catal. B: Environ.*, 2014, **148-149**, 106-113.
271. J. Sadhukhan, E. Martinez-Hernandez, M. A. Amezcua-Allieri, J. Aburto and J. A. Honorato S, *Bioresour. Technol. Rep.*, 2019, **7**, 100230.
272. H. Nishimura, A. Kamiya, T. Nagata, M. Katahira and T. Watanabe, *Sci. Rep.*, 2018, **8**, 6538.
273. S. V. Vassilev, D. Baxter, L. K. Andersen, C. G. Vassileva and T. J. Morgan, *Fuel*, 2012, **94**, 1-33.
274. S. Scieszka and E. Klewicka, *Crit. Rev. Food Sci. Nutr.*, 2019, **59**, 3538-3547.
275. Y. I. Maltsev, I. A. Maltseva, S. Y. Maltseva and M. S. Kulikovskiy, *Russ. J. Plant Physl.*, 2020, **67**, 185-193.
276. F. Carvalheiro, L. C. Duarte and F. M. Gírio, *J. Sci. Ind. Res.*, 2008, **67**, 849-864.
277. T. Lan, R. An, Z. Liu, K. Li, J. Xiang and G. Liu, *J. Colloid Interf. Sci.*, 2018, **532**, 331-342.
278. C. Mancera, F. Ferrando, J. Salvadó and N. E. El Mansouri, *Biomass Bioenerg.*, 2011, **35**, 2072-2079.
279. H. Li and A. G. McDonald, *Ind. Crops Prod.*, 2014, **62**, 67-76.
280. I. Pavasars, J. Hagberg, H. Borén and B. Allard, *J. Polym. Environ.*, 2003, **11**, 39-47.
281. K. Li, S. Liu and X. Liu, *Int. J. Energ. Res.*, 2014, **38**, 965-977.
282. D. Bulgariu and L. Bulgariu, *J. Clean. Prod.*, 2016, **112**, 4525-4533.
283. L. Fowden, *Nature*, 1951, **167**, 1030-1031.
284. L. Misurcova, F. Bunka, J. Vavra Ambrozova, L. Machu, D. Samek and S. Kracmar, *Food Chem.*, 2014, **151**, 120-125.
285. X. Liu, J. Shi, G. Yang, J. Zhou, C. Wang, J. Teng, Y. Wang and Z. Xie, *Commun. Chem.*, 2021, **4**, 1-10.
286. L. Zhang, Y. Song, G. Li, Q. Zhang, S. Zhang, J. Xu, F. Deng and Y. Gong, *RSC Adv.*, 2015, **5**, 61354-61363.
287. E. G. Menezes, J. R. do Carmo, J. G. Alves, A. G. Menezes, I. C. Guimaraes, F. Queiroz and C. J. Pimenta, *Biotechnol. Prog.*, 2014, **30**, 451-462.
288. J. B. Lambert, G. Lu, S. R. Singer and V. M. Kolb, *J. Am. Chem. Soc.*, 2004, **126**, 9611-9625.
289. S. D. Kinrade, K. J. Maa, A. S. Schach, T. A. Sloan and C. T. G. Knight, *Dalton. Trans.*, 1999, 3149-3150.
290. X. Kastele, P. Klufers, F. Kopp, J. Schuhmacher and M. Vogt, *Chemistry*, 2005, **11**, 6326-6346.
291. A. Samadi-Maybodi, R. K. Harris, S. Naser Azizi and A. M. Kenwright, *Magn. Reson. Chem.*, 2001, **39**, 443-446.
292. W. Qin, A. Agarwal, M. K. Choudhary, J. C. Palmer and J. D. Rimer, *Chem. Mater.*, 2019, **31**,

3228-3238.
293. B. Esmaeelian, K. Benkendorff, M. R. Johnston and C. A. Abbott, *Mar. Drugs*, 2013, **11**, 3802-3822.
294. S. Suleman Ismail Abdalla, H. Katas, J. Y. Chan, P. Ganasan, F. Azmi and M. Fauzi Mh Busra, *RSC Adv.*, 2020, **10**, 4969-4983.
295. J. Jiang, S. Ji, C. Duanmu, Y. Pan, J. Wu, M. Wu and J. Chen, *Particuology*, 2017, **33**, 55-62.
296. M. Fujiwara, A. Sakamoto, K. Shiokawa, A. K. Patra and A. Bhaumik, *Microporous Mesoporous Mater.*, 2011, **142**, 381-388.
297. Y. Zhang, K. Zhu, X. Duan, P. Li, X. Zhou and W. Yuan, *RSC Adv.*, 2014, **4**, 14471-14474.
298. X. Ou, S. Xu, J. M. Warnett, S. M. Holmes, A. Zaheer, A. A. Garforth, M. A. Williams, Y. Jiao and X. Fan, *Chem. Eng. J.*, 2017, **312**, 1-9.
299. S. K. Ratha and R. Prasanna, *Appl. Biochem. Micro.*, 2012, **48**, 109-125.
300. Z. Shan, H. Wang, X. Meng, S. Liu, L. Wang, C. Wang, F. Li, J. P. Lewis and F. S. Xiao, *Chem. Commun.*, 2011, **47**, 1048-1050.
301. B. A. Qureshi, X. Lan, M. T. Arslan and T. Wang, *Ind. Eng. Chem. Res.*, 2019, **58**, 12611-12622.
302. Y. Liu, X. Zhou, X. Pang, Y. Jin, X. Meng, X. Zheng, X. Gao and F.-S. Xiao, *ChemCatChem*, 2013, **5**, 1517-1523.
303. Q. Zhang, G. Chen, Y. Wang, M. Chen, G. Guo, J. Shi, J. Luo and J. Yu, *Chem. Mater.*, 2018, **30**, 2750-2758.
304. U. Sharma, B. Tyagi and R. V. Jasra, *Ind. Eng. Chem. Res.*, 2008, **47**, 9588-9595.
305. N. D. Hutson and B. C. Attwood, *Adsorption*, 2008, **14**, 781-789.
306. H. J. Jang, C. H. Lee, S. Kim, S. H. Kim and K. B. Lee, *ACS Appl. Mater. Inter.*, 2014, **6**, 6914-6919.
307. G. Hu, N. Wang, D. O'Hare and J. Davis, *Chem. Commun.*, 2006, 287-289.
308. S. Britto, G. S. Thomas, P. V. Kamath and S. Kannan, *J. Phys. Chem. C*, 2008, **112**, 9510-9515.
309. J. P. Thiel, C. K. Chiang and K. R. Poeppelmeier, *Chem. Mater.*, 1993, **5**, 297-304.
310. A. V. Besserguenev, A. M. Fogg, R. J. Francis, S. J. Price and D. O'Hare, *Chem. Mater.*, 1997, **9**, 241-247.
311. A. M. Fogg, G. R. Williams, R. Chester and D. O'Hare, *J. Mater. Chem.*, 2004, **14**, 2369-2371.
312. Z. Yong and A. E. Rodrigues, *Energy Convers. Manag.*, 2002, **43**, 1865-1876.
313. M. S. San Román, M. J. Holgado, C. Jaubertie and V. Rives, *Solid State Sci.*, 2008, **10**, 1333-1341.
314. X. Liu, L. Ge, W. Li, X. Wang and F. Li, *ACS Appl. Mater. Inter.*, 2015, **7**, 791-800.
315. Q. Wang, J. P. Undrell, Y. Gao, G. Cai, J.-C. Buffet, C. A. Wilkie and D. O'Hare, *Macromolecules*, 2013, **46**, 6145-6150.
316. Q. Yan, Z. Zhang, Y. Zhang, A. Umar, Z. Guo, D. O'Hare and Q. Wang, *Eur. J. Inorg. Chem.*, 2015, **2015**, 4182-4191.
317. C. J. Wang and D. O'Hare, *J. Mater. Chem.*, 2012, **22**, 23064.
318. F. Lv, L. Xu, Y. Zhang and Z. Meng, *ACS Appl. Mater. Inter.*, 2015, **7**, 19104-19111.
319. M. K. R. Reddy, Z. P. Xu, G. Q. M. Lu and J. C. D. d. Costa, *Ind. Eng. Chem. Res.*, 2006, **45**, 7504-7509.
320. J. Kuljiraseth, A. Wangriya, J. M. C. Malones, W. Klysubun and S. Jitkarnka, *Appl. Catal. B: Environ.*, 2019, **243**, 415-427.
321. X.-D. Chen, X.-G. Li, H. Li, J.-J. Han and W.-D. Xiao, *Chem. Eng. Sci.*, 2018, **192**, 1081-1090.

322. Q. Peng, G. Wang, Z. Wang, R. Jiang, D. Wang, J. Chen and J. Huang, *ACS Sustainable Chem. Eng.*, 2018, **6**, 16867-16875.
323. I. Banu, R. Ganea, G. Vasilievici, A. Anghel, V. Gogulancea, G. Isopencu and G. Bozga, *Energ. Fuel.*, 2018, **32**, 8689-8699.
324. M. Migliori, E. Catizzone, A. Aloise, G. Bonura, L. Gómez-Hortigüela, L. Frusteri, C. Cannilla, F. Frusteri and G. Giordano, *J. Ind. Eng. Chem.*, 2018, **68**, 196-208.
325. K. Ftouni, L. Lakiss, S. Thomas, M. Daturi, C. Fernandez, P. Bazin, J. El Fallah and M. El-Roz, *J. Phys. Chem. C*, 2018, **122**, 29359-29367.
326. M. Sukumar and L. J. Kennedy, *J. Nanosci. Nanotechnol.*, 2019, **19**, 826-832.
327. J. Yu, Q. Wang, D. O'Hare and L. Sun, *Chem. Soc. Rev.*, 2017, **46**, 5950-5974.
328. M. Climent, *J. Catal.*, 2004, **225**, 316-326.
329. T. Xue, R. Li, W. Gao, Y. Gao, Q. Wang and A. Umar, *J. Nanosci. Nanotechnol.*, 2018, **18**, 3381-3386.
330. M. R. Othman, N. M. Rasid and W. J. N. Fernando, *Chem. Eng. Sci.*, 2006, **61**, 1555-1560.
331. Q. Wang, Z. Wu, H. H. Tay, L. Chen, Y. Liu, J. Chang, Z. Zhong, J. Luo and A. Borgna, *Catal. Today*, 2011, **164**, 198-203.
332. P. Sahoo, S. Ishihara, K. Yamada, K. Deguchi, S. Ohki, M. Tansho, T. Shimizu, N. Eisaku, R. Sasai, J. Labuta, D. Ishikawa, J. P. Hill, K. Ariga, B. P. Bastakoti, Y. Yamauchi and N. Iyi, *ACS Appl. Mater. Inter.*, 2014, **6**, 18352-18359.
333. Q. Wang, H. H. Tay, D. J. Ng, L. Chen, Y. Liu, J. Chang, Z. Zhong, J. Luo and A. Borgna, *ChemSusChem*, 2010, **3**, 965-973.

Publications

5) **Qianwen Zheng**, Liang Huang, Ziyi Zhong, Benoît Louis, Qiang Wang, Synthesis of $K_xNa_{2-x}TiO_3$ as a novel CO_2 sorbent for high-temperature CO_2 sorption with fast sorption rate, ***Chem. Eng. J.***, 380(2020)122444.
6) Liang Huang, Cristina Megías-Sayago, Rogeria Bingre, **Qianwen Zheng**, Qiang Wang*, Benoit Louis*, Catalytic performance of layered double hydroxides (LDHs) derived materials in gas-solid and liquid-solid phase reactions, ***ChemCatChem***, 11(2019)3279-3286.
7) Wanlin Gao, Shuyu Liang, Rujie Wang, Qian Jiang, Yu Zhang, **Qianwen Zheng**, Bingqiao Xie, Cui Ying Toe, Xuancan Zhu, Junya Wang, Liang Huang, Yanshan Gao, Zheng Wang, Changbum Jo, Qiang Wang, Lidong Wang, Yuefeng Liu, Benoit Louis, Jason Scott, Anne-Cecile Roger, Rose Amal, Hong He, Sang-Eon Park, Industrial carbon dioxide capture and utilization: State of the art and future challenges, ***Chem. Soc. Rev.***, 49(2020)8584-8686.
8) Qiang Wang, Liang Huang, **Qianwen Zheng**. A carbon dioxide adsorption material and its preparation method, Chin. Pat. Appl. Publ., (2020) No. ZL201710239197.8.

Communications

1. Recent progress in the biomass-mediated synthesis of porous materials, (oral presentation), ICPEES - Department of Catalysis and Materials (C&M), 3rd C&M Scientific Day, **Qianwen Zheng**, Benoit Louis, ECPM, 14th October 2021.
2. Biomass-assisted ZSM-5 synthesis for methanol conversion into olefins, (oral presentation), Journée des Doctorants en Chimie 2020, **Qianwen Zheng**, Benoit Louis, online, 12th November 2020.
3. Design of porous materials for CO_2 conversion into olefins, (oral presentation), ICPEES - Department of Catalysis and Materials (C&M), 1st C&M Scientific Day, **Qianwen Zheng**, Benoit Louis, ECPM, 6th November 2018.
4. Biomass-assisted ZSM-5 synthesis for methanol conversion into olefins, (Poster), 36ème Réunion Annuelle du Groupe Français des Zéolithes, **Qianwen Zheng**, Benoit Louis, cancalled due to the COVID-19, 31th March-2nd April 2020.

Qianwen Zheng

Design of porous materials with biomass for the methanol conversion into olefins

Résumé

Les zéolithes sont des catalyseurs de grande importance pour les industries chimiques en raison de la topologie spécifique de leur structure et de leurs propriétés uniques. En outre, leur grande capacité d'adaptation, grâce à leur structure métastable, pendant le processus d'auto-assemblage en fait des candidats prometteurs pour diverses réactions catalytiques. Parallèlement, notre groupe a proposé une stratégie originale qui fait appel à la biomasse bon marché comme agent structurant secondaire bio-sourcé (BSST) pour la synthèse de zéolithes.

Par conséquent, l'objectif de cette thèse est de concevoir à façon une zéolithe avec de la biomasse pour la conversion du méthanol en oléfines. Une série de zéolithes ZSM-5 a été synthétisée avec trois différents rapports molaires de réactifs, temps hydrothermique, composition et quantité de biomasse, quantité de TPAOH et des caractérisations détaillées en termes de texture, morphologie, et propriétés acides ont été effectuées pour toutes les zéolithes. Ces catalyseurs ont été évalués dans la réaction du MTO et comparés à deux zéolithes de référence. Sur la base des résultats expérimentaux, le(s) mécanisme(s) provisoire(s) de l'impact du BSST sur la cristallisation des zéolithes ont été proposés.

En résumé, cette étude a permis d'obtenir des candidats ayant des performances catalytiques plus élevées, et de donner des indications pour adapter la synthèse des zéolithes par la stratégie BSST.

Mots clés : zéolithe, stratégie BSST, mécanisme, réaction MTO

Abstract

Zeolites are aluminosilicate catalysts of great importance for chemical industries due to their specific framework topology and unique properties. Besides, the versatile tunability thanks to their meta-stable state during self-assembly process also renders them promising candidates for various catalytic reactions. Meanwhile, a smart strategy was proposed by our group which involves cheap biomass as bio-sourced secondary templates (BSST) for the synthesis of several zeolite structures.

Therefore, the aim of this Thesis was to rationally design zeolites with biomass for the methanol conversion into olefins. A series of ZSM-5 zeolites were synthesized with three different reactant molar ratios, hydrothermal time, biomass composition and quantity, amount of TPAOH and detailed characterizations in terms of textural and acidic properties were conducted for all as-synthesized zeolites. These catalysts were evaluated in the MTO reaction and compared with two benchmark zeolites. Based on the experimental results, a tentative mechanism(s) of BSST impact on zeolite crystallization was proposed.

In summary, this study led to obtain some potential candidates exhibiting a higher catalytic performance, and gave some hints for tailoring zeolite synthesis by conducting the BSST strategy.

Keywords: zeolite, BSST strategy, mechanism, MTO reaction